Mechanisms of glial cell specification in the mammalian neurogenic niche by DNA replication regulators

Gonzalo Ortiz Álvarez

▶ **To cite this version:**

Gonzalo Ortiz Álvarez. Mechanisms of glial cell specification in the mammalian neurogenic niche by DNA replication regulators. Neuroscience. Université Paris sciences et lettres, 2020. English. NNT : 2020UPSLE048 . tel-03587630

HAL Id: tel-03587630

https://theses.hal.science/tel-03587630v1

Submitted on 24 Feb 2022

HAL is a multi-disciplinary open access archive for the deposit and dissemination of scientific research documents, whether they are published or not. The documents may come from teaching and research institutions in France or abroad, or from public or private research centers.

L'archive ouverte pluridisciplinaire **HAL**, est destinée au dépôt et à la diffusion de documents scientifiques de niveau recherche, publiés ou non, émanant des établissements d'enseignement et de recherche français ou étrangers, des laboratoires publics ou privés.

PSL UNIVERSITÉ PARIS

THÈSE DE DOCTORAT
DE L'UNIVERSITÉ PSL

Préparée à l'Institut de Biologie de l'Ecole Normale Supérieure de Paris, FRANCE

Mechanisms of glial cell specification in the mammalian neurogenic niche by DNA replication regulators

Mécanismes de spécification des cellules gliales dans la niche neurogénique mammifère par des régulateurs de la réplication de l'ADN

Soutenue par
Gonzalo ORTIZ ÁLVAREZ
Le 04 septembre 2020

Ecole doctorale n° 158
Cerveau, Cognition et Comportement

Spécialité
Neurosciences

Composition du jury :

M. Arturo LONDOÑO VALLEJO DR, Institut Curie, PSL	*Président*
Mme. Laure BALLY-CUIF DR, Institut Pasteur	*Rapporteur*
Mme. Isabel FARIÑAS DR, Ciberned, Universidad de Valencia	*Rapporteur*
M. Travis STRACKER DR, Institute for Research in Biomedicine	*Examinateur*
Mme. Nathalie SPASSKY DR, Institut de Biologie de l'ENS	*Directeur de thèse*

ENS | PSL

A mis padres.

Gracias por mi educación,

pues en ella, soy libre.

Acknowledgments / Agradecimientos

I would like to express my deepest gratitude to Nathalie Spassky, my mentor and supervisor for the past five years. This has been an incredibly meaningful experience for me and I am deeply thankful to you for letting me join your team, but not just that. Thank you, Nathalie, for keeping your door always open, for sharing your very intellect with me in the form of so many ideas and for asking my opinion about the ways we should follow our research. It made me feel more competent and even smarter talking to you. I have the proof that this was an awesome experience, and it is the fact that I woke up every morning excited to go to the lab.

Thank you, Nathalie and Alice, for your (almost) infinite wisdom, for your helpful discussions and willingness to help me when stuck. Marion, you are one of the kindest souls I have ever met and seeing you smile every day in the lab was a fortune. Thank you Pauline, Ayush, Aurélien, Solène and Marie Clémence for your hard work that has made my PhD a successful one, as well as for your good mood. Olivier, Raphaël and Alexia, you are wonderful people who bring a wonderful mood wherever you go. Thanks for all the laughter. Thanks to all the people that I have crossed in the Spassky lab, for more or less time, who have helped me or just cheered me up and contributed to these joyful years: Adel, Elise, Amélie Rose, Benoît, Michella.

Marie, you have been a perfect lab partner and friend. As a co-author on our first paper, you made my PhD what it is, and I thank you. As a friend, you have given me so much more. Your loyalty, kindness and all the “happy hour” souvenirs make you one of my dearest friends in Paris.

I would like to thank all the members of the Brunet, Garel and Morin teams, because you have made our workplace welcoming, and so many times you have helped me with my doubts or shared with me the lunch table.

The IBENS platforms are also full of professional and excellent people. I would like to thank the Administration, as well as the Informatics, Imaging and Animal facilities, whose work has contributed so much to this part of my career. A special thank you goes to Caroline, for teaching me how to do an animal surgery, and Eléonore and Amandine, for being so efficient in the care of our animals.

The main reason why Paris has become my second home is, of course, the wonderful encounters and friendships. Thank you Abdoul, Akindé, Alciades, Cécile, Hugues, Orthis for all the hours at *La Montagne*. I cannot think of a funnier crew. Thank you, Kamal, for being one of the most generous people I know and always being there. Filippo, you have been my partner in *La Maison du Brésil* and shared so many laundries. We have had so much fun together. My dear Laure and Eloïse, thank you for that smile you always receive me with, your kind words. You two made it difficult the choice to not stay in your lab for my thesis. Thank you for not forgetting me and still welcoming me in your afterwork drinks.

Thank you, Alex. You are that British friend that everyone should have. Fun, easygoing, a true *Friends* lover. In all, legend. Fan Di, Didi, for all the dinner "dates", your precious advice, for being a good listener and better friend, I miss you in Paris. Franck and Ioana, what can I say. My partners in crime thank you for sharing this PhD with me, because we have all lived the ups and downs of our respective projects and life in the lab as if it was one big awesome PhD. Thanks for all the spontaneous "do you want to go for a drink" after work, our confidences, the joy and laughter, so much laughter. For being those two wonderful people forever associated to my PhD and life in Paris.

Thank you Stephen. I could say I am angry you came to my Paris adventure so late. But instead I will say I am thankful to have met you and I am glad that our adventure continues. Sometimes the best parts come at the end.

Isa, coincidimos durante demasiado poco tiempo en París. Pero te convertiste en una persona importantísima en mi vida y, si puedo decir que mi primer año en París fue de los mejores, fue en buena parte gracias a ti. Espero que coincidamos en alguna ciudad, quizás a la orilla del mar, muy pronto, y que sigas ofreciéndome tu amistad y que sigas siendo para mí un referente y estímulo científico. Gracias a ti también, Lucía, mi otro "salvavidas" español en París, por acogerme con esa magnífica sonrisa cuando llegué a esta ciudad y no conocía a nadie.

Una estancia en el extranjero siempre es mejor cuando en casa te espera buena gente. A mi maestro, Alex, por ser parte de una de mis primeras y decisivas experiencias científicas y haberte convertido en un estupendo amigo, te doy las gracias. A Ana, Elena, Ange y demás gente del instituto, gracias por los buenísimos ratos que pasamos cada vez que vuelvo. Por

hacer que tantos años parezcan que no han pasado (tanto). A mi grupo de la facultad, que sois lo mejor, que siempre espero con ganas nuestro próximo encuentro en Sevilla. Julia, Luis, Lau, Selu, Hele, Miguel, Ana. Gracias por seguir en mi vida y recibirme con una bella sonrisa, alguna que otra carcajada, y muchos besos y abrazos.

Por último, quiero transmitir mi mayor afecto a mi familia, porque crecer con vosotros ha sido una suerte, por todo el amor que me habéis brindado, porque soy quien soy gracias a vosotros. Primos/as, tíos/as, abuelos/as en Granada, San Fernando o Galicia, gracias. Un especial reconocimiento a mis tíos Rafael y Gonzalo, siempre interesados por mi carrera, siempre dispuestos a apoyarme, siempre ahí. A mi "cuñao", Dani, porque eres una persona maravillosa, gracias por haberte unido a la familia. Y gracias por todos los maravillosos momentos que hemos pasado durante el confinamiento de este año, por abrirme las puertas de tu casa.

Gracias a mis hermanos, Ana y Óscar, por ser la esencia de mi infancia, por haber crecido junto a mí. Os quiero y estoy tan orgulloso de vosotros como creo que vosotros lo estáis de mí. Gracias Ana por apoyarme como me apoyas, por extrañarme como me extrañas. Gracias Óscar porque cuando vuelvo a casa, puedo volver a hacer payasadas contigo como cuando éramos pequeños.

Y, por último, mis padres, a quienes dedico este trabajo. Gracias a mi padre, Miguel Ángel, a quien extraño cada día. Tu forma de ser me inspiró y me sigue inspirando, tu forma de amar la vida, la libertad. Gracias por darme la mejor educación que supiste. Soy lo que soy gracias a ella. Gracias a mi madre, Teresa, que siempre me ha apoyado en mi decisión de estudiar en el extranjero, aunque ello te entristeciera en parte. Tu sincera alegría cada vez que conseguía una plaza fuera me ha permitido hacer lo que he hecho sin pesadumbre ni arrepentimiento. Si he podido hacerlo, ha sido gracias a ti y tu incondicional apoyo. Os quiero a ambos.

Thesis summary

The adult mouse brain retains a capability to produce new neurons from discrete neurogenic regions throughout life. One of them is localized in the subventricular zone of the lateral ventricle and is composed of two types of glial cells: astrocytes (adult neural stem cells) and multiciliated ependymal cells. The latter are highly specialized cells that present an apical patch of centrioles that nucleate motile cilia, whose coordinated beating is at the root of functions key to adult neurogenesis, in particular, and brain homeostasis in general. Among these, the cerebrospinal fluid circulation for trophic support, waste removal and neuronal migration guidance are of high importance. Therefore, understanding the processes that establish the neurogenic niche composition is of high value to tackle some of the most severe brain malignancies, such as hydrocephalus, neurodegenerative diseases or even tumors generated in the germinal regions.

In the present doctoral research, we have used a fate mapping technique to determine that ependymal progenitors do not migrate. This knowledge was necessary to use state-of-the-art clonal analysis techniques. Thus, a high-throughput analysis of large cohorts of neurogenic niche clones visualized with the *Brainbow* technique, as well as single-cell resolution of the ependymal progenitor division patterns via the Mosaic Analysis with Double Markers transgenic animals, has revealed that: (i) ependymal and adult neural stem cells share a common lineage, (ii) they can both arise through symmetric or asymmetrical cell divisions and (iii) their fate is modulated by DNA replication regulators, Geminin and GemC1, which favor a stem or an ependymal cell fate, respectively.

We have consequently elucidated the cellular and molecular mechanisms by which GemC1 triggers an ependymal fate. This protein, initially discovered as being a DNA replication-licensing factor, generates an arrested cell cycle-like phenotype at the same time that it promotes centriole amplification. Ependymal progenitors that express GemC1 halt their cell cycle and thus inhibit entry into mitosis. Upon looking at the specific mechanisms that could trigger such an arrest, we found that GemC1 generates the simultaneous expression of centriole amplification, ciliary growth, cell cycle progression and arrest genes, as well as the induction of a replicative stress, although strikingly, all this only in cycling cells. The occurrence of such stress translates to a higher presence of telomere dysfunction induced foci, this is, telomeres that co-localize with DNA damage signals. Furthermore, when we over-expressed the telomerase, the enzyme responsible for telomere length maintenance, we observed a bias towards the neural stem cell fate. This suggests that damage to the telomeres or its protection could be at the source of the terminal ependymal differentiation or the stem cell fate, respectively.

Together, this work sheds some light into the specific mechanisms that lead to an ependymal fate against the stem cell one, with some unexpected roles of cell cycle actors, damage pathways and telomere dynamics, that are usually associated to cycling or quiescent cells, but rarely to differentiation.

Résumé de la thèse

Le cerveau adulte des souris conserve une capacité à produire de nouveaux neurones tout au long de la vie, à partir de niches neurogéniques. Une d'entre elles est localisée dans la zone sous-ventriculaire et est composée de deux types de cellules gliales : les astrocytes (cellules souches neurales) et les cellules épendymaires multiciliées. Celles-ci sont des cellules fortement spécialisées qui présentent un groupe apical de centrioles à la base des cils motiles, dont le battement coordonné est à l'origine de fonctions indispensables pour la neurogenèse adulte, en particulier, et l'homéostase du cerveau, de façon générale. Parmi ces fonctions essentielles, la circulation du liquide céphalorachidien pour support trophique, l'enlèvement des déchets ou guider la migration des neurones sont d'une grande importance. Donc, la compréhension des procès qui établissent la niche neurogénique est d'une grande valeur pour aborder quelques maladies du cerveau d'entre les plus sévères, comme l'hydrocéphalie, les affections neurodégénératives ou même les tumeurs engendrées dans les régions germinales.

Mon travail de recherche doctorale a consisté à utiliser une technique de suivi du destin cellulaire et à déterminer que les progéniteurs épendymaires ne migrent pas. Cette connaissance était nécessaire pour l'utilisation de techniques de pointe d'analyse clonal. Alors, l'analyse à haute résolution d'un grand nombre de clones de la niche neurogénique visualisés avec la technique *Brainbow*, ainsi que la résolution au niveau cellulaire des modes de division des progéniteurs épendymaires, en utilisant les animaux transgéniques *Mosaic Analysis with Double Markers*, nous a révélé que : (i) les cellules épendymaires et les cellules souches neurales adultes appartiennent à un même lignage, (ii) elle sont nées via des divisions symétriques ou asymétriques, (iii) leur destin est modulé par des facteurs de la réplication de l'ADN, Geminin et GemC1, qui favorisent le destin souche ou épendymaire, respectivement.

Nous avons ensuite élucidé les mécanismes cellulaires et moléculaires par lesquels GemC1 déclenche le destin épendymaire. Cette protéine, initialement décrite comme un facteur de promotion de la réplication de l'ADN, génère un phénotype d'arrêt de cycle au même temps que l'amplification centriolaire. Les progéniteurs épendymaires qui expriment GemC1 pausent leur cycle et inhibent ainsi leur entrée en mitose. Lors de la recherche d'un mécanisme qui pourrait déclencher cet arrêt, nous avons décrit comment GemC1 génère l'expression simultanée de gènes d'amplification centriolaire et croissance ciliaire, de progression et arrêt de cycle, et aussi un stress réplicatif mais, étonnamment, tout ça uniquement dans des cellules cyclantes. La présence de ce stress se traduit dans une plus haute fréquence de télomères dysfonctionnels, c'est-à-dire, des télomères colocalisés avec des signaux de dommage à l'ADN. De plus, lorsque nous avons surexprimé la télomérase, l'enzyme responsable du maintien de la longueur des télomères, nous avons observé un biais vers le destin de cellule souche adulte. Cela suggère que le dommage aux télomères ou leur protection pourrait être à la source de la différentiation terminal épendymaire ou un destin de cellule souche, respectivement.

Ce travail permet de clarifier les mécanismes qui mènent à un destin épendymaire ou de cellules souches, avec des rôles inattendus des acteurs du cycle, les voies de signalisation de dommage cellulaire et la dynamique des télomères, qui sont habituellement associés aux cellules en cycle ou quiescentes, mais rarement à la différentiation.

List of abbreviations

Chapter 1. On the complexity and development of the Central Nervous System

CNS: Central Nervous System

E: Embryonic Day

BMP: Bone Morphotenetic Protein

NP: Neural Plate

FGF: Fibroblast Growth Factor

NT: Neural Tube

LGE: Lateral Ganglionic Eminence

MGE: Medial Ganglionic Eminence

CGE: Caudal Ganglionic Eminence

LGE: Lateral Ganglionic Eminence

Shh: Sonic Hedgehog

INM: Interkinetic Nuclear Migration

PSE: Pseudostratified Epithilium

NEC: Neuroepithelial Cell

VZ: Ventricular zone

MZ: Marginal zone

RGC: Radial Glial Cell

GLAST: glutamate astrocyte-specific transporter

BLBP: brain lipid-binding protein

GFAP: glial fibrillary acidic protein

SVZ: Subventricular zone

aRGCs: apical Radial Glial Cells

bRGCs: Basal Radial Glial Cells

IL-6: Interleukin 6

CNTF: ciliary neurotrophic factor

LIF: leukemia inhibitory factor

CT-1: cardiotrophin 1

Ngn-1: Neurogenin 1

NFI: Nuclear Factor 1

N-CoR: nuclear receptor co-repressor

KO: Knock-out

ER: Estrogen Receptor

Hsp90: heatshock protein 90

NSC: Neural Stem Cell

MADM: Mosaic Analysis with Double Markers

tdT: Tandem dimer Tomato

IUE: *In utero* electroporation

KD: Knock-down

Chapter 2. On the composition of the neurogenic niche and its regulators

MCC: Multiciliated Cell

CSF: Cerebrospinal Fluid

PCP: Planar Cell Polarity

TEM: Transmission Electron Microscopy

BrdU: Bromodeoxyuridine

PCD: Primary Ciliary Dyskenesia

GemC1: Geminin coiled-coil domain-containing protein 1

NICD: Notch Intracellular Domain

V-SVZ: Ventricular-Subventricular Zone

RMS: Rostral Migratory Stream

SGZ: Subgranular Zone

DCX: Doublecortin

Pre-RC: Pre-replication complex

GemC1: Geminin coiled-coil domain-containing protein 1

Chapter 3. On the cellular and molecular mechanisms of ependymal cell specification and differentiation

CDK: Cyclin-dependent kinase

CKI: Cyclin-dependent kinase inhibitor

R: Restriction point

pRb: Retinoblastoma

ORC: Origin recognition complex

APC/C: Anaphase-promoting complex

DSB: Double strand break

ATM: Ataxia-telangiectasia mutated

ATR: Ataxia-telangiectasia and Rad3-related

ssDNA: single-stranded DNA

RPA: Replication protein A

DDR: DNA damage response

NHEJ: Non-Homologous End Joining

HR: Homologous Recombination

TIF: Telomere Dysfunction Induced Foci

FISH: Fluorescent *in situ* hybridization

Table of contents

Table of figures

Chapter 1. On the complexity and development of the Central Nervous System

Chapter 2. On the composition of the neurogenic niche and its regulators

Chapter 3. On the cellular and molecular mechanisms of ependymal cell specification and differentiation

Chapter 4. Concluding remarks and perspectives

CHAPTER 1. GENERAL INTRODUCTION. ON THE COMPLEXITY AND DEVELOPMENT OF THE CENTRAL NERVOUS SYSTEM

The origin and development of the Nervous System relies on an extremely complex morphogenetic program. It involves the participation of a vast number of molecules and gene circuits in a perfectly orchestrated manner in order to engineer one of the most sophisticated systems created in evolution. It includes the generation of a wide array of cell types and the establishment of necessary relationships among each other, for their own survival and the proper function of this complicated machine as a whole. Errors in this tightly regulated process are at the onset of neurological and psychiatric disorders (Silbereis et al., 2016).

This system, present throughout the entire Animal Kingdom, is responsible for some of the most primitive actions, like sensory and motor functions, in the relationship of the environment with the individual (Catala and Kubis, 2013). Nonetheless, the nervous system is also the root of the highest cognitive abilities, such as autobiographical memory, conceptual learning, abstract thinking, language or self-awareness. They set primate identity, and more notably humans', apart from other vertebrate clades. These functions allow us to formulate the very question of why we are what we are as a species, since the dawn of mankind, but are also at the base of its answer, for they are the characteristics that make us human (Sousa et al., 2017).

The source of these high cognitive skills is in the Central Nervous System (CNS), composed of the brain and the spinal cord. A testimony of its complexity lies in its myriad numbers. Recent studies of total neuron and glia count range from 70 to 100 billion neurons in the brain alone and roughly as many glial cells (von Bartheld et al., 2016). These astronomical figures do not end here, since all these cells are nothing without taking its connectivity and necessary relationships into account. Around 164 trillion synapses only in the neocortex (several hundred trillion to more than a quadrillion in the entire CNS, though number differs between studies) have been reported (Silbereis et al., 2016; Sousa et al., 2017). Also speaking for its intricacy, the CNS takes over two decades to build in humans. Thus, although most neurogenesis is finalized during gestation, processes such as astrogliogenesis,

oligodendrogenesis, synaptogenesis and myelination continue well beyond infancy (Silbereis et al., 2016).

1.1. Embryonic origin of the CNS: from the three germ layers to the neural tube

Following fertilization, the egg undergoes a series of quick cell divisions until it forms a structure called the blastocyst, with an inner cell mass of pluripotent stem cells, able to generate all somatic and germline cells. A subset of cells within, the epiblast, which conserves its pluripotent potential, starts acquiring an epithelial morphology and preparing for gastrulation, this is, the formation of the three germ layers. This process starts around embryonic day (E) 6.5 in the mouse and the third week of human gestation. The three germ layers specified during this process are the endoderm, the mesoderm and the ectoderm. The entire nervous system is derived from the latter. The specification of the definitive ectoderm within the gastrula is a result of the secretion of Nodal, Wnt and Bone Morphogenetic Proteins (BMP) signaling inhibitors that prevent it to undergo epithelial-to-mesenchymal transitions, differentially from the nascent mesoderm and endoderm (Muhr and Ackerman, 2020; Shparberg et al., 2019).

The definitive ectoderm is bipotential as it generates the neuroectoderm or neural plate (NP), precursor of the nervous system, and the superficial ectoderm, from which the skin derives. Both diverge from each other due to the presence of a gradient of BMP signaling, in such a way that low levels specify the neuroectoderm and high levels, the superficial ectoderm. Attenuated BMP signaling, along with Fibroblast Growth Factor (FGF) and Wnt ligands lead to the origin of a border between the two, a strip of cells that forms the neural crest, which is at the origin of the peripheral nervous system (Gammill and Bronner-Fraser, 2003; Schille and Schambony, 2017; Shparberg et al., 2019).

Once the NP and neural crest, this is, the border between the NP and the superficial ectoderm, are specified, the formation of the neural tube (NT), the primordium of the CNS, begins. As the NP grows, it invaginates inwards and the depressed midline region forms the neural groove. As it invaginates even further, the neural crests elevate to form the neural folds. These converge by approaching the midline until they meet and fuse, closing the NT. The rest of the ectoderm body closes with it, as it lies dorsal to the submerged NT. The

transformation of the NP into the NT is called primary neurulation (Figure 1) (Nieuwenhuys et al., 2008; Silbereis et al., 2016).

The closure of the NT is primed at several points and it varies among species. In amphibians, for instance, it closes at the same time all along the rostrocaudal axis, whereas in teleost fish, such as the zebrafish, there is no closure per se, since the NT opens within the NP. In mice, there are three closure points: one at the border between the future spinal cord and brain, one at the future forebrain/midbrain boundary and one at the rostral end. Humans, in contrast have only two of the mentioned closure points, as they do not present the one in the forebrain/midbrain boundary. Closure beyond these areas proceeds bidirectionally in a "zipper-like" movement, rostrally and caudally, except for the rostral-most closure point, where it only advances caudally. The NT is fully sealed by E10 in mice and the end of the fourth gestation week in humans. By the end of neurulation, the NT encloses a cavity running all along the rostrocaudal axis, which precedes the ventricular system of the adult organism. Such cavity is lined by a highly proliferative neuropithelium (Greene and Copp, 2009; Nikolopoulou et al., 2017).

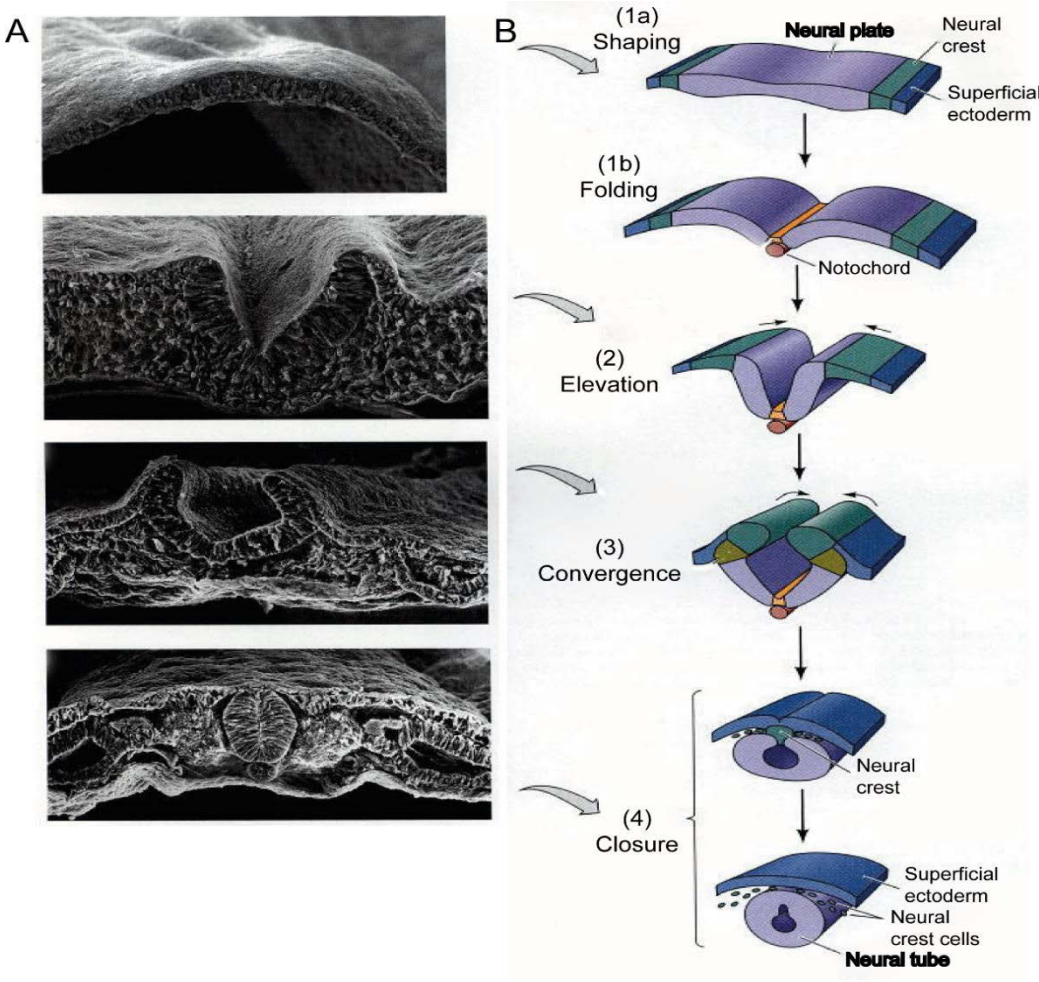

Figure 1. Primary neurulation in vertebrates. (A) Scanning electron micrograph of the neural tube formation process in the chicken embryo. (B) Illustrative representation of the process. After the induction of the neural plate or neuroectoderm on the definitive ectoderm (1a), it begins to fold along the midline, causing the invagination of the tissue (1b). This process leads to the elevation of the neural folds (2), which then converge (3) and travel towards the midline as they meet and fuse to close the neural tube (4). This structure remains ventral to the dorsal superficial ectoderm that will generate the epidermis. Adapted from Gilbert, 2000.

1.2. Embryonic origin of the CNS: from the neural tube to the forebrain

Once that primary neurulation has come to an end, three rostrocaudally disposed enlargements arise, the primary brain vesicles. These are the predecessors of the prosencephalon or forebrain, the mesencephalon or midbrain and the rhombencephalon or hindbrain, from rostral to caudal, the three main parts of a developed brain. By E9.5 in mouse and during the fourth week of human gestation, in the rostral-most vesicle, the prospective forebrain, two buds start to evaginate as the precursors of the brain hemispheres, which together form the telencephalon. As a consequence of this process of evagination, the inner cavity of the NT enlarges to form two ventricular cavities (one per hemisphere) that become the lateral ventricles in the adult (Figure 2) (Chen et al., 2017; Nieuwenhuys et al., 2008).

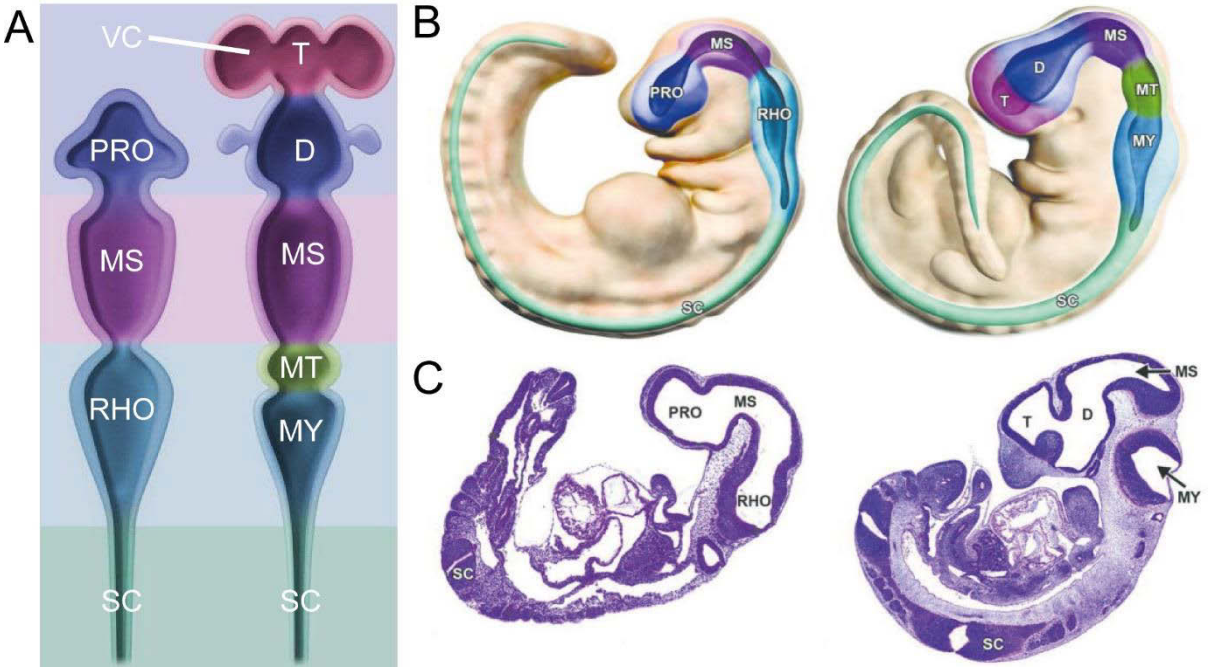

Figure 2. Formation of the brain vesicles. (A) Schematic representation of a dorsal view of the brain vesicles evaginating from the recently closed neural tube in the mouse. Firstly (E9.0), three brain vesicles are formed (PRO or prosencephalon, MS or mesencephalon and RHO or rhombencephalon), followed by a further subdivision of PRO and RHO to form five secondary brain vesicles (E11.5). T (Telencephalon) and D (Diencephalon) form in the PRO and MT (metencephalon) and MY (myelencephalon) arise from the RHO, all rostral to the SP (spinal cord) and enclosing the VC (ventricular cavity). (B) 3D view of the brain vesicles within

the developing mouse embryo. (C) Lateral view of a hematoxylin and eosin staining of a sagittal section of the mouse embryo. The big hollow within PRO, MS and RHO (later within T, D, MS and MY) gives rise to the ventricular system during development. Adapted from Chen *et al.*, 2017.

Each brain hemisphere is constituted of a ventral and a dorsal part, namely, the subpallium and pallium, respectively. Between E10 and E12 in the mouse developing brain (from the second month in human gestation), the neuroepithelium of the subpallium undergoes massive proliferation and generates two intraventricular protrusions: the lateral and medial ganglionic eminences (LGE and MGE, respectively), which fuse caudally in the telencephalon into one caudal ganglionic eminence (CGE) (Chen et al., 2017; Nieuwenhuys et al., 2008).

Within each particular section of the incipient CNS, a regionalization takes place via transient signaling centers that generate diffusible cues. The particular exposure to these extracellular and intracellular signals in each region translates into a specific combination of transcription factors in recipient cells that help shape cellular identities. One of the most prominent examples is the specification of a posterior identity by Wnt, FGF and retinoid signaling. On the other hand, the presence of inhibitors of these pathways, such as Cerberus, Dickkopf or Tlc, a Frizzled-related protein, contribute to establishing an anterior identity and, the ulterior formation of the telencephalon (brain hemispheres) (Figure 3A) (Rallu et al., 2002a).

As crucial as the anteroposterior patterning is the establishment of regional identities along the dorsoventral axis. Sonic hedgehog (Shh) is expressed before the onset of neurogenesis in the ventral telencephalon as an important determinant of ventral fate. On the opposite pole, Gli3 gene expression, which modulates Hedgehog signaling, is essential to maintain dorsal markers (Figure 3B) (Rallu et al., 2002a). These are two important mutually repressing factors whose over-expression or loss of function can lead to the acquisition of dorsal or ventral identities in an ectopic location (Rallu et al., 2002b). This is the case as well for Wnt signaling, a promoter of pallial (dorsal) fates (Figure 3B) whose defects in expression cause an invasion of ventral identity cells and its upregulation leads to a decrease of subpallial (ventral) markers (Backman et al., 2005). Evidently, this interplay of gene circuits generates a dorsoventral patterning of the telencephalon.

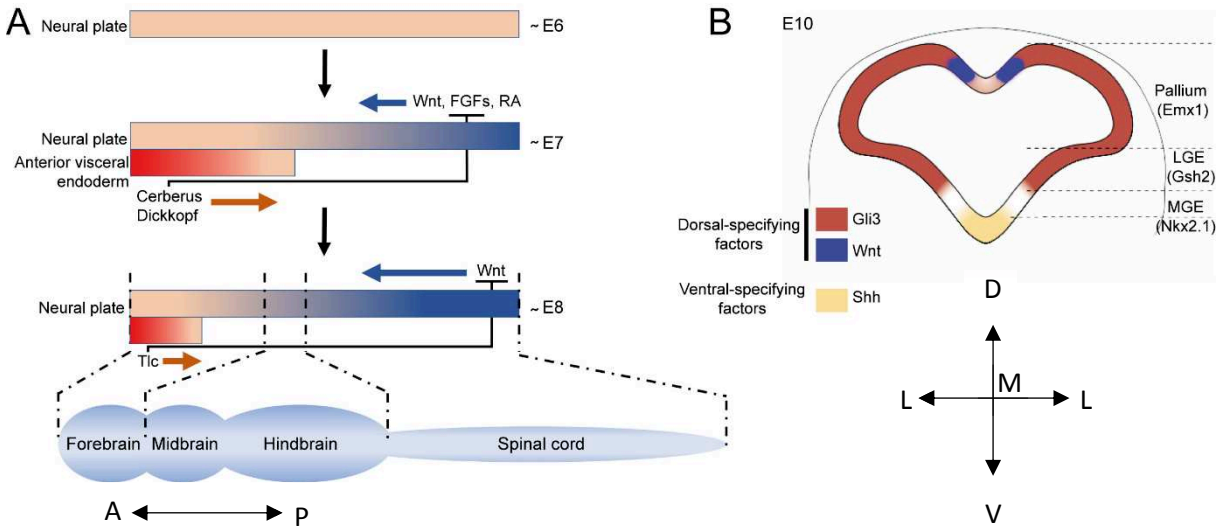

Figure 3. CNS arealization along the anteroposterior and dorsoventral axes in response to extracellular cues. (A) The polarization of the CNS along the anteroposterior axis is the result of signaling molecule gradients from the Wnt, FGF and retinoic acid (RA) pathways. A decrescent influence of these pathways on the region closer to the future head is promoted by inhibitors of the said molecules, such as Cerberus, Dickkopf and Tlc. These are in turn produced in extra-ectodermal structures like the anterior visceral endoderm generated during gastrulation. The result is the formation of the brain vesicles (forebrain, midbrain, hindbrain) on the anterior pole of the CNS and the spinal cord on the posterior portion. (B) An important patterning of the CNS also takes place along the dorsoventral axis. Molecules such as Wnt and Gli3 contribute to the specification of dorsal fates, whereas Shh is essential on the ventral-most part to generate the correct ventral structures. Although only the telencephalon is shown, a similar patterning takes place in the spinal cord, but this is not the subject of discussion for the present work. On the right, the different anatomical temporary embryonic structures are depicted (pallium, LGE and MGE), as well as one key transcription factor (in brackets) characteristic of each of them, which have had an importance for fate mapping strategies (see below). A: Anterior; P: Posterior; D: Dorsal; V: Ventral, L: Lateral; M: Medial. Adapted from Rallu, Corbin and Fishell, 2002 and Backman *et al.*, 2005.

In response to the patterning of the telencephalon, specific regional transcription factor networks are activated and discreate telencephalic territories are formed. Consequently, the above-discussed pallium, LGE and MGE can be distinguished not only by anatomical criteria, but also by genetic expression. Among the most important transcription factors activated in each zone, we can find Pax6 or Emx1 in the pallium, Gsh2 in the LGE and MGE or Nkx2.1 in the MGE alone (Nord et al., 2015). Some of these factors regulate the expression of each other, such as Pax6 and Gsh2 who repress one another (Rallu et al., 2002b, 2002a).

This transcriptional regionalization of the developing telencephalon has a prominent role in the generation of specific neurons from determined territories, but it has also been used to genetically engineer reporter lines that have allowed fate mapping of various cell types. In our study, we have profited from a fate-mapping technique relying on this territorial

gene expression to determine the spatial origin of ependymal cells (Refer to Chapter 2 – Published work *Neuron*, 2019, Figure 1).

1.3. Stem cell proliferation and differentiation in the CNS

1.3.1. Interkinetic Nuclear Migration

In 1935, F.C. Sauer firstly observed in the NP of the chick that proliferating cells possessed processes attaching to both free surfaces, this is, the apical and the basal side of the epithelium. However, the nuclei were organized on different layers. Besides he described how mitoses always took place on the apical end (Sauer, 1935). This was the first milestone to establish what would later be known as the Interkinetic Nuclear Migration (INM).

The proliferating cells of the developing CNS form a pseudostratified epithelium (PSE), from the NP to the telencephalon. In this particular histological organization, cells display an apicobasal polarity, elongated morphology, with densely packed nuclei located in various layers, and apical and basal processes that span from a few micrometers (like in the NP) to distances in the millimeter order of magnitude (like in the primate neocortex). The location of the nuclei at different apicobasal levels is a direct consequence of the INM. During this phenomenon, after mitosis and during the G1 phase of the cell cycle, nuclei migrate basal-wards, undergo S phase on the basal side, move back apical-wards during G2 and complete the cell cycle by completing mitosis on the apical or ventricular surface (Figure 4A) (Kulikova et al., 2011; Nieuwenhuys et al., 2008; Norden, 2017; Saade et al., 2018). Pseudostratification has been described as a highly efficient way for progenitor cells to replicate. This is because a desynchronized location of the nuclei, the bulkiest part of the cell, allows for more cells to exist in a defined volume, hence increasing the total mitotic output (Figure 4B) (Miyata et al., 2015). Furthermore, the differential exposure to apical cues, such as Notch signaling, necessary to maintain the stem-like state of progenitors (Mizutani et al., 2007), which can be regulated by INM duration variations, is a potent modulator of neurogenesis (Del Bene et al., 2008).

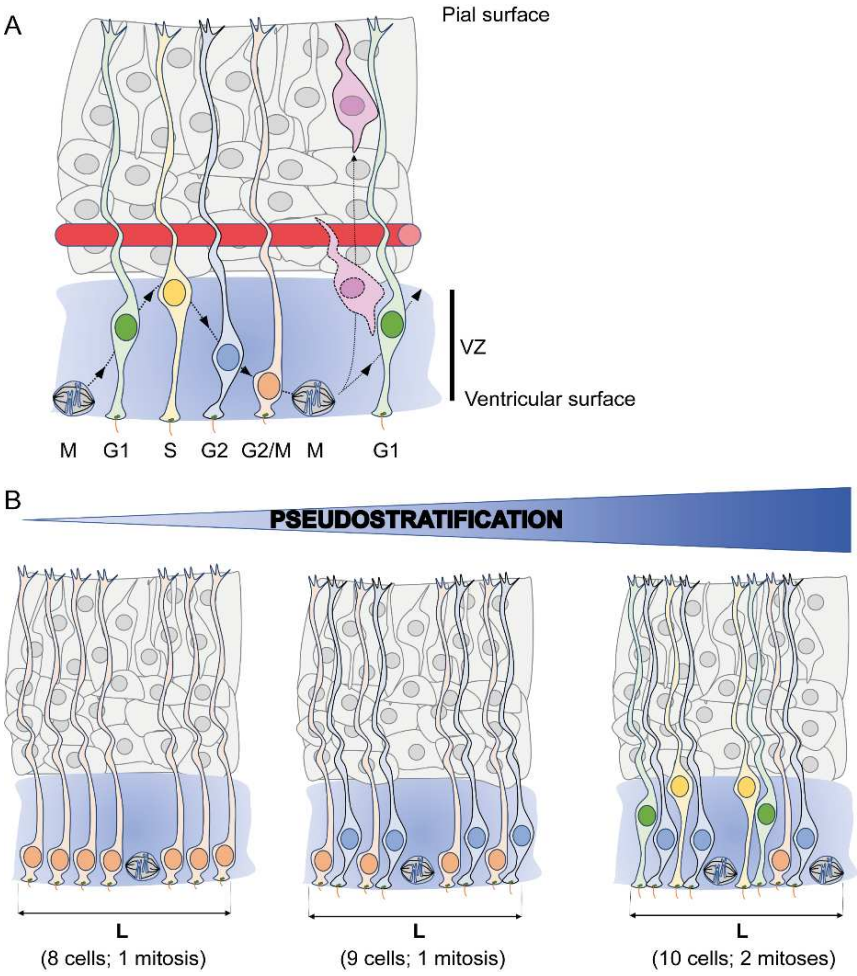

Figure 4. Interkinetic nuclear migration in a pseudostratified epithelium. (A) Apical Radial Glial Cells undergo mitosis on the ventricular (apical) surface and then their nuclei perform a cell cycle-coupled movement from the apical to the basal pole of the Ventricular Zone (VZ). During G1 (green cell) they migrate basal-wards and when they reach the basal side, they replicate their DNA during the S phase (yellow cell). Afterwards, during G2, they migrate towards the apical surface again (blue cell) and, upon arrival during G2/M (orange cell) they complete mitosis again (grey cell) and start a new cell cycle. Progenitors during neurogenesis divide asymmetrically to self-renew and generate one postmitotic neuronal precursor or neuroblast (pink cell) that migrates out of the proliferative area. The red rod represents a blood vessel with which progenitors establish physical contact. (B) Higher degrees of pseudostratification confer a greater amount of mitosis per unit time. Considering an epithelium of constant length, L, (and area, considering apical contacts of the same size) and the same mitotic rate, more cells and more mitoses fit in the same volume with higher pseudostratification, since the voluminous cell body can be accommodated at different levels along the apicobasal axis. For instance, considering a mitotic rate of one in five cells, only one mitosis and seven more cells fit in the given distance L, when no pseudostratification is present (all nuclei at the same level). If a higher level of pseudostratification is considered (cell bodies arranged throughout two levels), one more cell can fit. Finally, if the pseudostratification is even more complex (four levels as shown in the scheme), up to ten progenitor cells can fit, two of which would be in a mitotic stage. Adapted from Miyata *et al.*, 2015.

As for the biological reason as to why mitosis takes place on the apical surface, several explanations have been proposed. The equal inheritance of apical attachments in a rapidly proliferative tissue or the exposure to Notch signaling are among them (Miyata et al., 2015; Saade et al., 2018). Besides, since the centrosome is located apically to act as the basal body of a primary cilium, which serves as a cellular antenna capable of sensing and integrating extracellular information, it is plausible that the nucleus would have to migrate apically to meet it for mitosis. Nonetheless, this theory was put to the test by Strzyz et al. in zebrafish retinal neuroepithelium, where they show that INM is centrosome-independent. They claim

INM is important rather to maintain epithelial integrity, for apical mitoses help daughter cells reintegrate into the tissue (Strzyz et al., 2015).

The components of the cytoskeleton play a key role in this cell cycle-coupled migration. Both movements, away and from the ventricular surface, have been described as active processes that rely on actin and its associated motor protein myosin, and/or microtubules and their coupled motor partners, dyneins and kinesins. Although some controversy is found (Schenk et al., 2009), actin-based movements are found in shorter neuroepithelia, such as the NT or retina, whereas microtubule-based actions take place in thicker ones, such as the rodent telencephalon (Tsai et al., 2010). Interestingly, the basal-wards movement that takes place during G1 has also been proposed to present an important, although not exclusive, passive, non-autonomous components. Kosodo et al. suggest that after mitosis, free, mobile nuclei during G1 in a densely-packed tissue are displaced by apical-wards moving G2 nuclei (Kosodo et al., 2011).

1.3.2. The constitution of the ventricular and subventricular zones and lineage of its cells

A type of neural progenitor cell called neuroepithelial cell (NEC) constitutes the NP and early NT. Upon cell division in the NT, they form a densely packed zone where nuclei reside. This is called the ventricular zone (VZ) and contains the precursor cells to all neurons and macroglia of the CNS. The outer marginal zone (MZ) contains all the cytoplasmic processes that span the length of the NT (Nieuwenhuys et al., 2008).

There is a first period during CNS development when symmetrical proliferative divisions prevail. In it, one progenitor NEC generates two equal daughter cells in order to increase the progenitor pool. Concomitant with the onset of neurogenesis, between E9 and E10 in mice (around the fourth week in human gestation, shortly after the closure of the NT), NECs transition into another type of progenitor, called Radial Glial Cell (RGC). The onset of neurogenesis is a consequence of the switch from symmetrical proliferative divisions of NECs to the asymmetric neurogenic ones of RGCs (Gaiano et al., 2000; Martynoga et al., 2012).

NECs transition into RGCs happens upon the thickening of the developing telencephalon (as well as in the other regions of the CNS) in order to maintain contact with the free surfaces, the apical ventricular surface and the basal pial surface. Thus, they keep

forming a PSE. Therefore, they display a strong apicobasal polarity like NECS, with a short apical process and large endfoot, and a long basal process. Similar to NECs, they undergo INM and present a primary cilium that protrudes into the ventricular cavity. Finally, the expression of progenitor markers, such as Nestin, an intermediate filament protein, or region-specific transcription factors like Pax6 is also common to both cell types. Nonetheless, they differ in that RGCs present astroglial markers like the glutamate astrocyte-specific transporter (GLAST), the brain lipid-binding protein (BLBP) or the glial fibrillary acidic protein (GFAP), among other features (Alvarez-Buylla et al., 2001; Namba and Huttner, 2017).

RGCs were initially described as the precursors of glial cells (Alvarez-Buylla et al., 2001). However, this paradigm shifted in the early 2000s when it was proven that they were also the precursors of neurons both *in vitro* (Malatesta et al., 2000) and *in vivo*, using a combination of time-lapse microscopy and neuronal marker immunolabeling (Miyata et al., 2001; Noctor et al., 2001; Tamamaki et al., 2001). These studies revealed that RGCs divided apically in an asymmetric manner to generate a daughter neuron and another progenitor that remains within the VZ. These and later publications lead to the current prevailing paradigm: that RGCs are the precursor cells to all neurons (except for a few directly deriving from NECs at the onset of neurogenesis) and glia (except for microglia) of the entire CNS (Anthony et al., 2004).

The VZ is ubiquitous in the CNS, from the spinal cord to the brain. However, only in the developing brain, a second proliferative layer emerges towards the middle of cortical neurogenesis, the subventricular zone (SVZ). Its progenitors divide *in situ*, this is, they do not undergo INM, and it remains in the adult organism. The absence of an INM in the SVZ claims a redefinition of what RGCs are or, at least, a much broader classification of progenitors in the telencephalon. Indeed, over the past two decades progenitor cells that do not divide on the apical surface, but on more basal or subapical zones have been discovered (Haubensak et al., 2004; Pilz et al., 2013). This has led to a new classification of progenitors in the CNS based on the location of their mitoses, their cell polarity (presence of basal and/or apical processes, as well as plasma membrane basolateral or apical-specific markers) and their proliferative capacity (number of cell divisions). Besides the already discussed apical RGCs (aRGCs), subapical progenitors and basal RGCs (bRGCs) have been described, based on the mitosis location. The latter are mostly responsible for the formation and enlargement of the SVZ and they derive from aRGCs. Both aRGCs and bRGCs are characterized by the potential to perform

several divisions and the fact that they can be symmetric proliferative (two daughter cells equal to the mother), symmetric consumptive (two equal daughter cells different from the mother cell) or asymmetric self-renewing (only one daughter cell is equal to the mother). Furthermore, they both generate not only neurons, but other types of progenitors, like intermediate progenitors or transit amplifying progenitors, which are able to divide once or multiple times, respectively, hence increasing the total final output of neurons (Taverna et al., 2014).

As a highly interesting fact, the presence of bRGCs in the SVZ has been extendedly studied due to its direct correlation with the neocortex evolutionary expansion and higher neuronal numbers, especially in primates. Along with an increase of the neurogenic period, they are actually the principal source of neurons in this clade and the reason for their distinct higher brain capabilities (Namba and Huttner, 2017; Wilsch-Bräuninger et al., 2016). This greater capacity of proliferation has been linked to differences in coding genes, regulatory elements and copy number variations of genes, which translate into larger division rates, namely more symmetric proliferative divisions (Florio et al., 2017).

The postmitotic neuroblasts resulting from asymmetric and symmetric consumptive cell divisions migrate radially or tangentially out of the germinal layers to colonize the incipient cortical plate (CP), the precursor of the neocortex. There they differentiate and thicken it to form the cortical layers in an “inside-outside” fashion, meaning the inner layers are formed first and then the outer ones are generated subsequently (layers VI to II in decrescent order). This process lasts until E19 in the mouse (the twenty-sixth week of human gestation), with the end of cortical neurogenesis (Dehay and Kennedy, 2007; Nieuwenhuys et al., 2008).

1.3.3. The neurogenesis to gliogenesis switch

During embryogenesis, neurons and stem cells are not the only cell types that are born. The neuroglia is another important set of cells generated during this period and, as discussed before, they end up equaling neurons in number in the adult CNS.

Rudolf Virchow firstly described glia or neuroglia in 1846 as a homogeneous population of cells that supports neuronal activity. Although the last decades of research have proven that this population is anything but homogeneous, they are indeed essential for proper CNS

homeostasis and functions. Two major groups of these cells have been described: the mesoderm-derived microglia, which possess roles in immune response and other homeostasis-keeping functions (out of the scope of this work), and the ectoderm-derived macroglia, which comprises oligodendrocytes, astrocytes and ependymal cells (Molofsky and Deneen, 2015; Rowitch and Kriegstein, 2010).

Oligodendrocytes are cells whose primary function is to wrap neuronal axons with extensions of their cell membrane to form the myelin sheaths. These lipid-rich structures insulate the nerve fibers in order to increase the speed of electrical impulses across the nervous system (Frisén, 2016). Astrocytes are a much more heterogeneous set of cells that hence participate in a wide range of functions: (i) They synthesize extracellular matrix proteins, adhesion molecules and morphogens to ensure neuronal maturation and synapses formation. (ii) They play a key role in angiogenesis and the formation of the blood-brain-barrier and its maintenance. (iii) They buffer extracellular ion concentrations, specially potassium ions, an action which is necessary for the proper electrical activity of neurons. (iv) Astrocytes can participate in neurotransmitter uptake as well, to ensure proper synaptic function. (v) These cells can provide with trophic support to other cells, like neurons and (vi) perform detoxifying roles. (vii) Finally, a very interesting function of astrocytes in the adult is to serve as neuronal precursors in what is called adult neurogenesis (Wang and Bordey, 2008). This function and the special kind of astrocytes that support it are treated latter on the present work (see Chapter 2 – 2.2. The neurogenic niche, adult neural stem cells and adult neurogenesis).The third type of neuroglia, ependymal cells, is also extendedly assessed further on this reading, as they constitute the type of cell on whose developmental mechanisms our work is focused.

1.3.3.1. Glial cell lineage

The origin of glial cells, also known as gliogenesis, takes place after neurogenesis, which does not exclude for some neuron and glial cells to be generated at the same time. Like neurons, glia's precursor cells are RGCs of the VZ and SVZ (Rash et al., 2019). The question remains though, since the discovery that RGCs could generate both neurons and glia, is whether there exists a bipotent progenitor, or if, by the contrary, there are glia-restricted and

neuron-restricted RGCs. The previous conception on the origin of the CNS cells was the latter. However, over the past two decades, evidence has piled up to support the existence of neuron-restricted and bipotent progenitor cells since early in development (the onset of neurogenesis). In order to find glia-restricted RGCs, later developmental stages must be assessed (Figure 5). However, these glia-restricted progenitor cells come from the asymmetric self-renewing cell divisions that earlier on generated neuron precursors (Costa et al., 2009).

In vitro and *in vivo* studies evidence the existence of progenitors of neurons, glia or both. When brain progenitors are isolated and plated from early embryonic stages, they give rise at first to purely neuronal clones. Only when these cells are allowed to divide further and when they are isolated from late embryonic stages, some of these generate glia in mixed neuron-glia and glia-restricted clones, respectively (Anthony et al., 2004; Costa et al., 2009; Malatesta et al., 2000). As for the *in vivo* evidence, Gao *et al.* proved that, in a first moment, only neurons are formed from a common progenitor in "quanta" or discrete packages of 8 to 9 neurons through successive asymmetric divisions, but later on, at the end of these rounds of divisions, around 1:6 of the RGCs generate glia. They proved that glia were contained within neurogenic clones and confirmed that the first were born after a series of neurogenic divisions, this is, neurogenesis precedes gliogenesis (Gao et al., 2014). Mimicking the *in vitro* paradigm, only when RGCs are transduced with a reporter-coding retrovirus at later stages of development *in vivo*, glia-restricted clones are detected (Costa et al., 2009). Although the numbers of glia-restricted clones found by Gao *et al.* seem to not go in accordance with the total final number of glia cells discussed before (as much glia as neurons, von Bartheld, Bahney and Herculano-Houzel, 2016), it is noteworthy that up to 90% of all non-neuronal cells in the adult are produced during the second to third postnatal week in rodents (Bandeira et al., 2009). Both astrocyte and oligodendrocyte precursor cells are able to divide and increase their numbers postnatally (Figure 5). In the case of astrocyte precursors, these are generated via asymmetric divisions from RGCs, and then migrate to their final destination where they can

once again proliferate via symmetric divisions to generate more astrocytes (Bergles and Richardson, 2016; Tien et al., 2012).

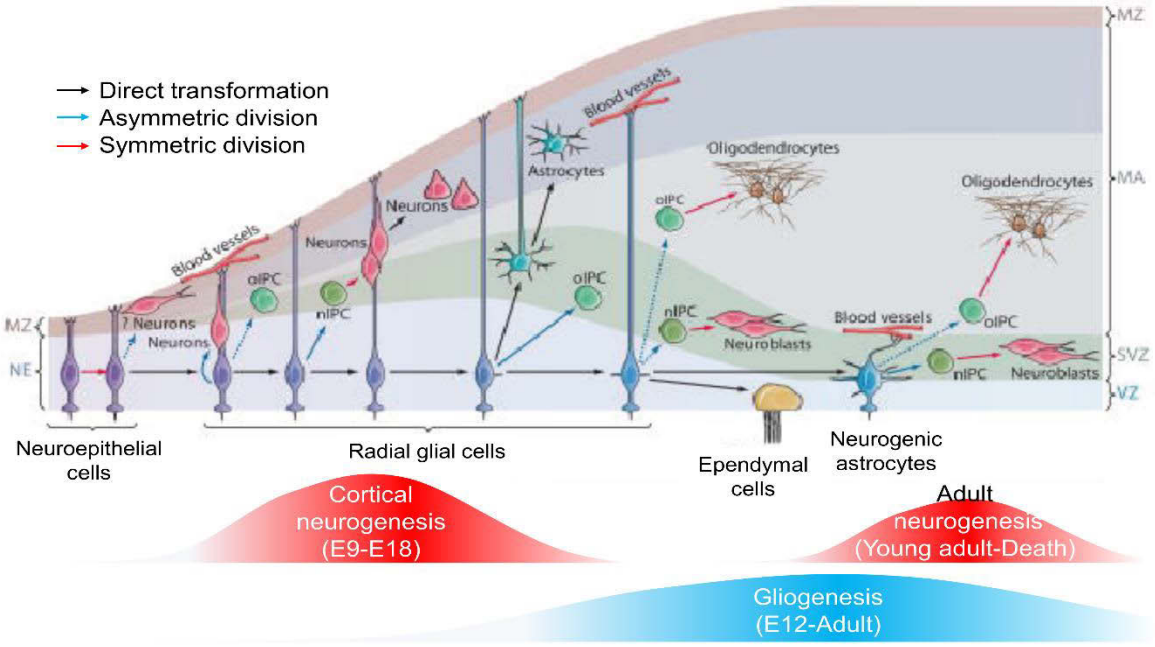

Figure 5. Timeline of neurogenesis and gliogenesis during development and adult life. Early in development, the neuroepithelium (NE) is formed by highly proliferative cells that divide symmetrically to increase the progenitor pool, the neuroepithelial cells. As the NE thickens, these cells transition into radial glial cells, which display a high degree of apico-basal polarity. The cell body remains in the ventricular zone (VZ) where it divides, at the same time as it projects a long process to the mantle zone (MZ), the outer-most layer of the developing CNS. At the onset of neurogenesis these cells divide asymmetrically to self-renew and to generate neuroblasts, which migrate into the mantle zone (MA) along the RGC processes, or a neuron-committed intermediate progenitor cell (nIPC) or a basal radial glia cell, both of which can generate more neurons though asymmetric divisions or symmetric consumptive divisions. As early as E12 for oligodendrocyte progenitor cells (oIPC), E14-15 for ependymal progenitors and E18 for astrocytes, the RGCs start switching from neurogenesis to gliogenesis. Astrocytes and oIPCs continue dividing in adult life. A particular type of astrocytes in the adult can re-enter the cell cyle and generate neuroblasts that migrate to the olfactory bulb in a process known as adult neurogenesis. Note the continuity of RGCs between the neurogenic and gliogenic periods. This means that early in development, neuron-restricted or bipotential progenitors are found, but not glia-restricted stem cells. On the contrary, towards the end of embryogenesis, neuron-restricted progenitors have withered and some glial-restricted progenitors are present. The latter proceed, nonetheless, from earlier bipotential progenitors. Adapted from Kriegstein and Alvarez-Buylla, 2009.

The existence of an ependymal precursor cell with a defined molecular signature or identifiable markers has not been described. This complicates their study and opens the great question of what happens in these cells between the last division of their progenitors and the onset of their differentiation at early postnatal stages. Nonetheless, they are known to derive from RGCs and be postmitotic (Spassky et al., 2005).

1.3.3.2. The cellular and molecular mechanisms of the gliogenic switch

As it was stated before, the bulk of gliogenesis occurs when most of the neurogenesis has been completed. RGCs change in terms of their competence with time, this is, they are more prone to produce neurons earlier and more glia later, in a phenomenon called progressive competence restriction. Cortical neurogenesis in rodents lasts from E12 to E18 approximately. The switch to gliogenesis in the brain happens around E16-E18 (Akdemir et al., 2020; Molofsky and Deneen, 2015). Roughly, the timeline of the different neuroglia types is:

- Astrocytes are mostly first seen at around E18, although some S100β^{+} cells are seen in the LGE (but not in the pallium) as early as E16 (Rowitch and Kriegstein, 2010).
- Oligodendrocyte progenitors are generated in three consecutive waves from ventral to dorsal territories at E12 (the exception to gliogenesis following neurogenesis), E15 and P0 (Kessaris et al., 2006). Their differentiation, though, arrives postnatally (Miller and Gauthier, 2007).
- Ependymal progenitor birth peaks at E15, but do not differentiate until the first postnatal days (Spassky et al., 2005).

The gliogenic switch is both temporally and spatially regulated. It does not happen in all regions of the brain at the same time. This is partly because the extrinsic environment of the precursor cells is determinant for its differentiation. However, this does not discard the presence of cell-autonomous mechanisms, but rather accentuate the synergy of both, to ensure the right type and number of cells are produced at the correct time (Miller and Gauthier, 2007).

At the onset of gliogenesis, the collaboration of several mechanisms ensures that RGCs shift their differentiation from neurons to glia. Several members of the interleukin 6 (IL-6) family have a role in astrogenesis: the ciliary neurotrophic factor (CNTF), the leukemia inhibitory factor (LIF) and cardiotrophin 1 (CT-1) are among the molecules that promote it (MuhChyi et al., 2013).

CT-1 is the key gliogenic ligand expressed in newly born neurons. Hence, neurons themselves are one of the essential elements that, in a feedback loop, instruct the RGCs in the germinal areas from whence they come to start producing glia. This puts forward the idea of

a cellular timer mechanism in which one daughter cell, newborn neurons, alters the environment to instruct their progenitors to start producing a second type of cells: astrocytes (Barnabé-Heider et al., 2005). CT-1 binds the coreceptors LIFRβ and gp130 and causes them to heterodimerize. This in turn results in the activation of the JAK-STAT pathway. The STATS are transcription factors that, in collaboration with the coactivators p300/CBP, are able to directly transactivate the transcription of the *gfap* and *s-100β* genes, both essential for astrocyte specification (Figure 6, Nakashima *et al.*, 1999; Miller and Gauthier, 2007).

Besides CT-1-dependent activation of the JAK-STAT pathway, the latter can be triggered by BMP and Notch signaling. BMP-2 can both promote neurogenesis or gliogenesis depending on the cellular context. During gliogenesis, when pro-neural genes like neurogenin-1 (ngn1) are at low levels, BMP-2 can: (i) enhance the expression of pro-neural gene inhibitors like Id1 (Viñals et al., 2004) and (ii) promote transactivation of gliogenic genes through the formation of a complex between its downstream effector Smad1 and STAT:p300/CBP (Yanagisawa *et al.*, 2001, Figure 6). However, during neurogenesis, the accumulation of ngn1 in the presence of BMP-2 leads to the sequestration of the STAT:p300/CBP complex, which is no longer available to transactivate gliogenic genes (Miller and Gauthier, 2007).

Notch signaling also has an inhibitory effect on neurogenesis to prevent RGCs to perform terminal symmetric consumptive divisions (Gaiano et al., 2000), but it also promotes gliogenesis. Hence, Notch signaling presents two temporally dissociative effects. During gliogenesis, binding of Notch ligands results into Notch cleavage and activation and, in turn, the formation of a transcriptionally active complex RBP-Jκ. This complex can both (i) promote the expression of Hes proteins, which inhibit neurogenic genes (Sakamoto et al., 2003), and (ii) bind to the *gfap* promoter in the presence of an active JAK-STAT pathway (Liu et al., 2016) (Figure 6).

Some other mechanisms that contribute to the gliogenic switch would be the expression of the proastrocytic transcription factor nuclear factor 1 (NFI), which probably acts in collaboration with the JAK-STAT pathway (Miller and Gauthier, 2007). Also the CNTF-dependent cytoplasmic translocation of the nuclear receptor co-repressor (N-CoR), a repressor of multiple transcription factors, prevents the inhibition of RBP-Jκ by said repressor. This enables the binding and activation of *gfap* at its promoter by RBP-Jκ (Hermanson et al., 2002) (Figure 6).

Figure 6. A simplified view of the mechanisms of gliogenesis switch. Several molecules and pathways synergistically participate in the down-regulation of neurogenesis and up-regulation of gliogenesis. CT-1 causes the dimerization of the gp130 and LIFRβ receptors, which activates the JAK-STAT pathway. Its downstream effector transcription factor STAT3 forms a complex with co-activators such as p300 to promote the expression of the *gfap* gliogenic gene. BMP-2 signaling promotes the formation of a complex of its downstream activator Smad with STAT:p300, further promoting the expression of gliogenic genes. Notch signaling also participates in this process by activating the pro-gliogenic RBP-Jκ transcriptionally active complex and expressing anti-neurogenic genes such as Id1. Other gliogenesis mechanisms is the collaboration of the pro-astrocytic transcription factor NF-I with the role of Smad:STAT:p300. From Miller and Gauthier, 2007.

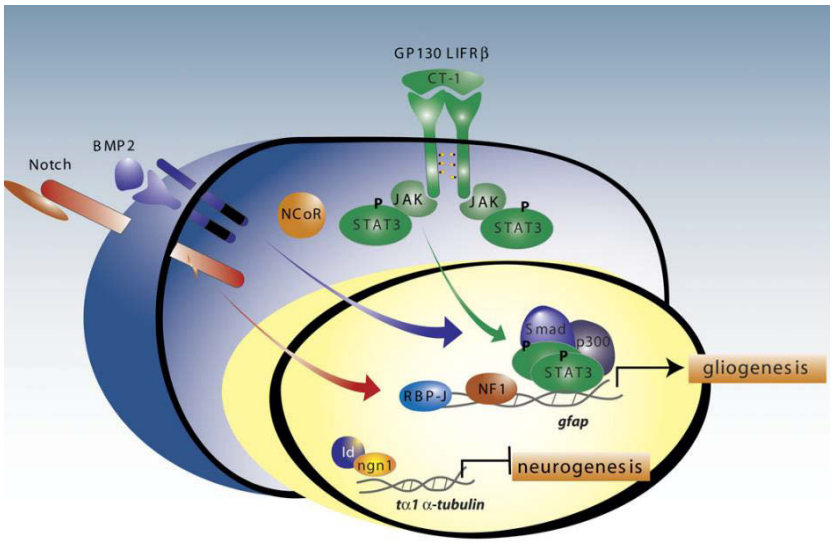

Concerning oligodendrocyte gliogenic switch, the migratory precursors of these cells have been proven to be specified initially in Shh-producing areas, on the ventral part of the telencephalon and spinal cord (Tekki-Kessaris et al., 2001). Indeed, the inhibition of this signaling pathway leads to a reduction in the output of oligodendrocytes (Spassky et al., 2001) and its ectopic expression leads to the increase of cells displaying oligodendrocyte progenitor markers (Nery et al., 2001). In areas away from the ventral Shh-producing centers, the induction of FGF signaling, as well as the inhibition of the Wnt and BMP pathways have been proposed as alternative mechanisms for oligodendrocyte lineage specification (Foerster et al., 2019).

1.4. Tools for the study of the origin and relationship of CNS populations.

1.4.1. Cell fate-mapping

One of the most important goals in developmental biology is to understand the origin of adult cell populations from their embryonic precursor cells, since the site of generation of a determined cell type can define its function in the adult organism. For instance, the ganglionic eminences (LGE and MGE) of the subpallium are the site of origin of GABAergic inhibitory neurons that populate the neocortex, whereas the glutamatergic excitatory neurons are born in the pallium, to later migrate to the incipient cortical plate (Marín and Müller, 2014). Another prominent example is the oligodendrocyte genesis in the spinal cord.

They were initially described to arise in the ventral neuroepithelium of the spinal cord, but subsequent studies proved that more dorsal domains, with a different regional identity, could also be a center for oligodendrocyte generation (Fogarty et al., 2005).

Fate mapping has emerged as one of the most widespread tools to investigate the embryonic origin of cell populations. It consists of labeling a group of cells with a distinctive and stable marker that is transmitted to their descendants so that the entire lineage is labeled. Before the advent of the era of genetic engineering, fate mapping relied on laborious and less thorough systems. These included dye injections in precursor cells of the embryo to follow the dye-labeled cell progeny, tissue ablations to assess the location of morphological defects in adult structures derived from the damaged structures, or chimera tissue grafting, which allowed to trace the chimeric cell population in a wild type background (Gross and Hanken, 2008; Selleck and Stern, 1991; Weisblat et al., 1978).

In the last three decades though, genetic engineering has been key to develop a new type of cell population origin tracing methodology: genetic fate mapping. The most broadly used technique is the one based on the Cre/loxP system. It is based on the P1 bacteriophage Cre recombinase, an enzyme that catalyzes the recombination between two consensus DNA sequences, which act as well as recognition sites for the enzyme: the loxP sites. Since these sequences present a directionality, they can be used to insert or invert the DNA sequence between both loxP sites. When both sequences are present in *cis,* the former happens when they are in the same orientation, whereas the latter occurs when they have opposing directions. When the sequences are in *trans*, this is, on different chromosomes (like an exogenous plasmid and the endogenous chromosome), an interchromosomal recombination occurs to exchange the sequences between the two DNA molecules or the insertion of one chromosome into the other, depending on the orientation of the loxP loci. A great advantage of this system is that it does not require coactivators in eukaryotes, despite being a phage-derived machinery. Besides, the consensus loxP sequence is long enough (34 base pairs) so that its random occurrence in the mammalian genome is extremely improbable (Nagy, 2000).

For fate mapping a specific cell population, this system needs two elements. On the one hand, a transgenic line bearing a Cre expression cassette under the influence of a structure, tissue or cell type-specific promoter. On the other hand, a transgenic line that provides the sequence for a reporter gene, which is typically a fluorophore or the *lacZ* gene,

detected by the β-galactosidase activity, in the presence of the Cre recombinase. The reporter gene is typically downstream from a constitutive promoter and a *Stop* codon expression cassette, flanked by two loxP sites. When the two transgenic lines are crossed, the expression of the Cre from the specific promoter in certain cells eliminates the *Stop* codon in the descendant cells. Thus, expression of the reporter gene can proceed from its upstream constitutive promoter (Figure 7A) (Nagy, 2000). This system can be adapted to achieve a tissue/cell-specific, also known as "conditional", knock-out (KO) (an essential part of a gene is excised in the presence of the Cre, Gavériaux-Ruff and Kieffer, 2007), specific gene repair (the loxP-flanked construct disrupts a gene sequence, which recovers its full functional form upon Cre-mediated excision, Dragatsis and Zeitlin, 2001) or conditional cell ablation (expression of a toxin upon Cre-mediated retrieval of a loxP-flanked *Stop* sequence that impedes its expression otherwise, Kessaris *et al.*, 2006).

A very useful variation of this conditional gene expression by the Cre/loxP system is the inducible Cre expression. In order to modify gene expression in all the above discussed ways (induction of a reporter, conditional KO or gene repair or cell population ablation) in a specific cell population at a desired timepoint, the Cre recombinase is fused to a mutated estrogen receptor (ER) resulting in the $CreER^{T2}$ construction. In uninduced conditions, this fusion protein remains in the cytosol due to its interaction with the Heat-shock protein 90 (Hsp90) and hence unable to promote recombination in the genome. However, in the presence of the estrogen synthetic analog tamoxifen, which competes with Hsp90 in its interaction with the ER, the CreER fusion protein can be translocated to the nucleus to fulfill its function (Figure 7B) (Kim et al., 2018; Valny et al., 2016).

One of the key aspects in the success of the genetic fate mapping is the use of a reporter line that ensures strong and stable expression of the reporter. The most commonly used locus for Cre-reporter mice is the Gt(ROSA)26Sor or ROSA26 locus. Gene expression from this gene is ubiquitous (Zambrowicz et al., 1997) but poor in the case of fluorescent reporters (Madisen et al., 2010). Nonetheless, it allows the insertion of exogenous stronger promoters than the ROSA26 endogenous one to drive reporter expression. One of the most used transgenic reporter lines, which has been used in the present work (see Chapter 2 - Published work in *Neuron*) is the Ai14, which has the following modifications to ensure a strong and stable expression of the reporter: (i) the strong synthetic CAG promoter and (ii) the

woodchuck hepatitis virus postranscriptionally regulatory element, to ensure high stability of the mRNA (Madisen et al., 2010).

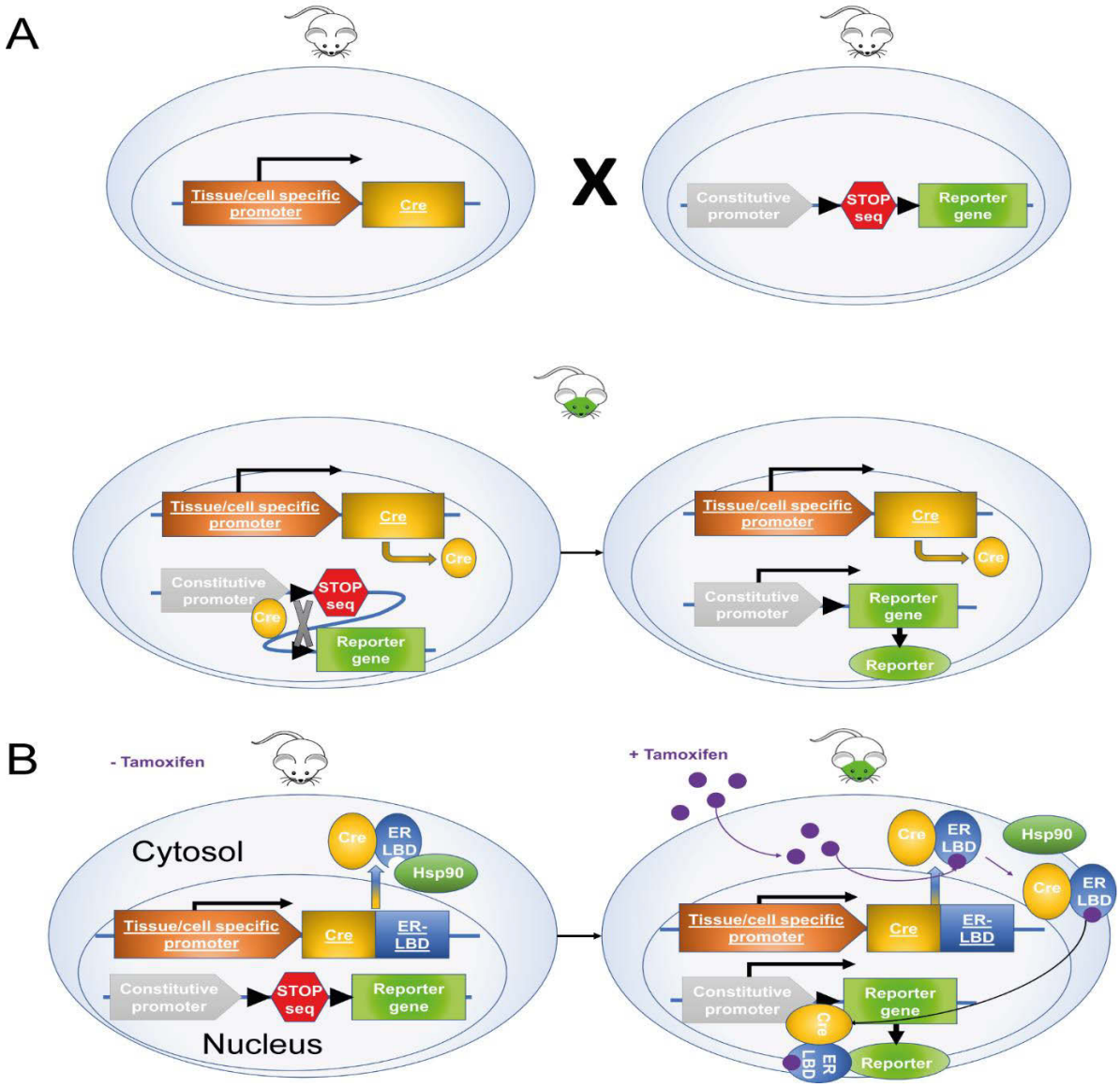

Figure 7. Conditional and inducible Cre recombinase expression. (A) Depiction of Cre-mediated tissue or cell-specific recombination. For fate mapping studies a mouse line that expresses the Cre under the control of a specific tissue or cell population of interest, is crossed with a line that synthesizes a reporter gene only in the presence of Cre. In unrecombined conditions, a loxP-flanked stop codon upstream of the reporter sequence prevents reporter expression. The descendants of such crossing express the Cre in the tissue or cells of interest, where it drives excision of the flanked stop codon sequence, via recombination between the two loxP sites, hence allowing the expression of the reporter. (B) Scheme of an inducible Cre-mediated reporter expression. This system varies with respect to the previous one in that it expresses the Cre fused to the ligand-binding domain of an estrogen receptor (ER) that locates to the cytosol and is bound to Hsp90. As a consequence, in uninduced conditions, the Cre cannot mediate reporter gene expression. In the presence of tamoxifen, this molecule binds to the ER, releasing the Cre-ER fusion protein from Hsp90. The former is now free to go into the nucleus and drive reporter expression as in A. Adapted from Kim *et al.*, 2018.

This strategy has been used to promote conditional Cre expression in many specific cell types of the CNS, such as RGCs through the Nestin-Cre line (Dubois et al., 2006), astrocytes including adult neural stem cells (NSCs) via the GFAP-Cre line (Casper et al., 2007), or oligodendrocytes, using a PLP-Cre mouse (Doerflinger et al., 2003). However, some of the mostly used Cre driver lines in the CNS are not cell type-specific, but territory-specific. As it was discussed before, the embryonic neuroepithelium is compartmentalized in terms of their transcription factor expression. Thus, the pallium expresses Emx1, the LGE, Gsh2 and the MGE, Nkx2.1 and Gsh2, among others (Rowitch and Kriegstein, 2010). This arealization has been the source of successfully used Cre-driver lines for fate mapping cells deriving from either three of these embryonic structures.

The Emx1-Cre, Gsh2-Cre and Nkx2.1-Cre lines have allowed researchers to study the spatial origin of different neuroglia. For instance, oligodendrocytes present three different sources in the embryo, from ventral (MGE) to more dorsal (LGE and pallium) that are activated in consecutive order during embryogenesis to populate both the striatum and neocortex (Kessaris et al., 2006). It has also been established that astrocytes in the spinal cord and forebrain are allocated regionally in the adult in close relation to their site of origin (this is, without tangential migration, Tsai *et al.*, 2012). Finally, it has been discovered that adult NSCs are located at their site of origin, with the Nkx2.1 domain contributing to some of these cells on the very ventral part of the adult lateral ventricle, the Gsh2 domain generating most cells on the lateral wall of the lateral ventricle, and the Emx1 territory giving rise to the dorsal stem cells of the lateral ventricle (Xu et al., 2008; Young et al., 2007). These studies have encouraged us to use the same fate mapping strategy to inquire into the spatial origin of ependymal cells from their RGCs precursors distributed all along the neuroepithelium, and whether ependymal precursors migrate away from their site of origin.

1.4.2. Clonal analysis techniques

The understanding of how a group of similar or distinct cells in the adult who share a common embryonic ancestor, this is, a clone, is established is one of the major goals in developmental biology and, particularly, in the study of the CNS. These clonal relationships provide invaluable information about the specification mechanisms, migration patterns and functional interactions among cells. As a consequence, many efforts and techniques have been focused on the construction of such lineage trees in a variety of tissues.

Retroviral injection of a single progenitor is one of the earliest used methods in clonal analysis. It consists of the infection of a single progenitor or several ones in a sparse manner. The retrovirus encodes a reporter gene, usually a fluorescent protein-coding sequence or a gene that is expressed into a protein with a specific enzymatic activity, such as the β-galactosidase activity from the *lacZ* gene. The presence of the reporter can be detected in cells descending from the infected ancestor, this is, the entire clone. In order to achieve single or very sparse progenitor labeling, a very low titer of the virus must be used. Nonetheless, even very low viral titers can lead to the most common mistakes in lineage analysis: the splitting and the lumping error. The former consists of considering one clone as two independent ones due to long-distance migration of the cells. The latter entails the inclusion of one or several cells from a clone into another one, usually because the first have migrated away from their site of origin and come closer to cells of another clone (Costa et al., 2009). Apart from the lack of resolution inherent to the use of only one reporter marker, there are several disadvantages to this method: the random integration of the retroviral-encoded reporter gene can lead to mutagenesis in essential genes or regulatory sequences or the silencing of the expression of the reporter are the main concerns (Ma et al., 2018). A variant of this method is the use of dual color tracing with two retroviruses encoding two different fluorophores. The logic behind it is that, if a specific cell presents a low probability of being infected when using a low-titer virus solution, the probability of it being infected by two different ones (each encoding a different reporter) is even scarcer. Thus, double-labeled clones are subject to lineage analysis with a lower chance to make a splitting or lumping error (Costa et al., 2009).

Another method of lineage tracing relies also on retroviral infection, but increases the resolution to practically one distinguishable tag per clone. This is the retroviral bar-coding strategy. It consists of infecting the desired tissue (like the VZ that contains all neuron and glia progenitors) with a library of many distinct retroviral vectors, each bearing a unique DNA sequence that acts as an identifier, and a reporter (like β-galactosidase activity or a fluorophore). After infection of a progenitor cell, the genetic tag is transmitted to the descendants. Hence, a clone is composed of cells that contain all the same genetic label. Said technique is applicable, for instance, in studies of clonal cell dispersion in the brain (Walsh and Cepko, 1992), and has been used to identify neuronal and glial clones (McCarthy et al., 2001). However, even if recent studies have optimized the process of tagged-cell retrieval by applying

laser microdissection (Fuentealba et al., 2015), instead of tedious manual dissection of all reporter-positive cells (McCarthy et al., 2001; Walsh and Cepko, 1992), it presents some inconveniences. Despite exquisite resolution of clonality, due to the unique genetic tags, each cell's label must be amplified via PCR and sequenced without loss (Costa et al., 2009).

1.4.2.1. The *Brainbow* technique

The need to map the highly complex circuitry of neuronal and glial cells in the brain led to the development of a new fluorophore-labeling transgene-based technique. Initially, it allowed to single-out all the different presynaptic cells that innervated a determined postsynaptic neuron, in interactions that can involve many cells in a complicated, dense meshwork of axons and dendrites. The development of the *Brainbow* strategy (an acronym of the words *brain* and *rainbow*) opened the possibility to facilitate the laborious task of circuit map elaboration, for it labels each cell with a unique color. It is based on the combinatorial expression of three or more fluorescent proteins that can generate a wide arrange of hues, this is, color identities in the RGB space (formed by the combination of the colors red, green and blue) (Livet et al., 2007). The *Brainbow* expression cassette encodes three or four fluorescent proteins in tandem. Upstream of said sequences, three mutually exclusive 5' loxP site variants are located one after the other. Each of these loxP variants has its 3' counterpart for recombination immediately downstream of each of the fluorophore-encoding transgenes. Thus, the Cre recombinase recognizes the loxP variants in defined pairs (a 5' and its associated 3'), since these are mutually exclusive (Branda and Dymecki, 2004). Upon recognition, it catalyzes recombination (and the consequent transgene excision) between any of the three pairs of loxP sites, thus, leading to the stochastic expression of one of the fluorophores from a single *Brainbow* construct (Livet *et al.*, 2007). The transgene sequences have been adapted to direct the fluorophore to different subcellular compartments. The only one that we have used for our studies is that which directs expression of the fluorophores to the nucleus, known as *Nucbow* (Figure 8A).

One transgene copy does not yield a great resolutive power, since it can only label a cell with three different fluorophores. The real power of this technique, however, relies on the combinatorial potential resulting of several copies of the transgene that coexist in a single cell. If genome integration of many copies of the *Brainbow* cassette is achieved, stochastic recombination will individually affect each copy. In consequence, the pallet of colors

generated by different dosages of each fluorophore is exponentially increased (Livet *et al.*, 2007; Loulier *et al.*, 2014, Figure 8B).

Brainbow has been used to study circuits and interactions of neurons, but also glia, since conditional expression of the Cre in different cell types can be achieved via different Cre-expressing lines. Furthermore, it can be coupled to a tamoxifen-inducible system to ensure conditional expression at a desired timepoint, in Cre-reporter *Brainbow* lines. For instance, it has been used to visualize individual oligodendrocytes and their processes and interactions with neurons during myelination, in a tamoxifen-inducible scheme (Dumas et al., 2015). Also, inducible *Brainbow* expression has been adapted in non-mammals, like zebrafish and *Drosophila*, to study neuronal circuitry (Hadjieconomou et al., 2011; Pan et al., 2011).

One of the most important applications of *Brainbow* though, is the lineage tracing of cell clones. It has been applied in clonality studies as early as the blastomere stage (Tabansky et al., 2013), but has also been adapted for the assessment of cell families in the nervous system of mice and chicks (Loulier et al., 2014). The system has been modified so that it drives fluorescent protein expression from a strong CAG constitutive promoter, but also to ensure stable expression of the transgenes throughout cell generations. For this purpose, the whole *Brainbow* cassette is bordered by sequences recognized by a transposase (piggyBac or Tol2 transposases), which translocates the flanked DNA into the genome (Loulier *et al.*, 2014, Figure 8A).

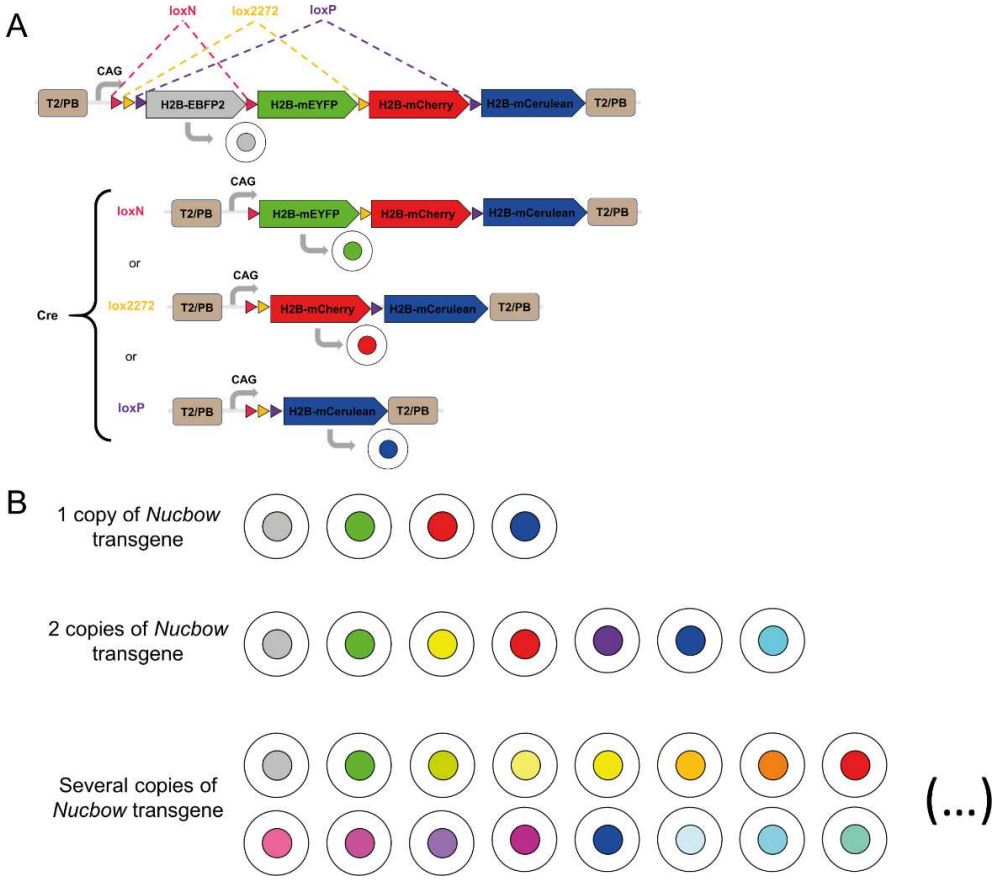

Figure 8. The *Brainbow* strategy for clonal analysis. (A) Scheme of the *Nucbow* transgene. It consists of three nuclear fluorescent protein-coding sequences encoded in tandem. Mutually exclusive variants of the loxP site flank the coding sequences as depicted so that upon stochastic Cre-mediated recombination, an excision of part of the transgene occurs and one of the three fluorescent proteins is expressed. In the unrecombined state, the UV-shifted EBFP2 protein is expressed. The tandem-encoded fluorophores are the yellow-green mEYFP, the red-orange mCherry and the blue-green mCerulean and their expression is driven from a constitutive CAG promoter. The whole expression cassette is flanked by T*ol2* or *PiggyBac* (T2/PB) target sequences. These are recognized by said transposases who catalyze the integration of the cassette in the genome for stable fluorophore expression across cell generations. (B) The combinatorial power of *Brainbow* (and with it the clonal resolution) increases with the number of copies of the transgene in a single cell. Whereas one copy of the transgene can only tag a cell with three different markers, several copies generate the possibility of a unique color label per cell, since each transgene undergoes stochastic recombination. Adapted from Loulier *et al.*, 2014.

The fact that this technique does not rely on sparse labeling of progenitors and its robustness in cell family identification based on its increased clonal resolution have been key to select it for our studies. We have used the *Brainbow* technique to label RGC progenitors and study their progeny in the neurogenic niche.

1.4.2.2. Mosaic Analysis with Double Markers (MADM)

Genetic mosaicism, this is, the presence of different genotypes in different cells within the same organism, is a powerful technique to study gene function. It allows to assess the effect of a specific mutation in a cohort of cells in an otherwise wild type background. This permits bypassing the need for such gene in other tissues or earlier in development and is thus a great tool for cell autonomous gene function studies. A new method was developed by Zong et al. which differentially labels cells within a mosaic, this is, one cell with a given genotype presents one label and another cell with a different genotype displays a different one. It consists of two reciprocally chimeric alleles based on the green and red fluorescent proteins (GFP and the improved red fluorescent protein tandem dimer Tomato, hereafter called tdT) located on the same locus of homologous chromosomes. One allele contains the N-terminal sequence of the GFP and the C-terminal part of the tdT ($MADM^{GT}$). Its homologous allele presents the N-terminal sequence of the tdT and the C-terminal end of the GFP ($MADM^{TG}$). Both terminal parts in the two alleles are separated by a loxP-containing intron. In the absence of Cre, and in the allelic configuration just described, no functional fluorophore can be expressed due to the truncation of their sequence. Nonetheless, upon Cre expression in a cell, an interchromosomal recombination between loxP sites occurs, hence restoring a fully-functional GFP and tdT sequence on each allele ($MADM^{GG}$ and $MADM^{TT}$) (Zong *et al.*, 2005, for a detailed representation of this allelic configuration, see Chapter 2 – Published work in *Neuron*, Figure 4B).

After DNA replication, four reciprocally chimeric alleles are present in one cell, two $MADM^{TG}$ and two $MADM^{GT}$. If interchromosomal recombination takes place during the G2 phase, hence restoring one $MADM^{GG}$ and one $MADM^{TT}$, there are two different outcomes in the cell progeny dependent on allele segregation. If one daughter cell inherits the fully functional GFP and tdT alleles, this is $MADM^{GG}$ and $MADM^{TT}$, whereas the other receives the two non-functional reciprocally chimeric ones, this is $MADM^{TG}$ and $MADM^{GT}$, the former cell and its descendants will display both markers (yellow, from the combination of green and red), whereas the latter will present none. This is called a G2-Z event. On the contrary, if both $MADM^{GG}$ or $MADM^{TT}$ alleles are segregated into one daughter cell each, descendants will show one marker (green or red) and its sister lineage, the other. This is called a G2-X event. If recombination takes place before the replication of the DNA, a cell displaying both markers

(yellow) is generated (Zong *et al.*, 2005, see the Chapter 2 – Published work in *Neuron*, Figure 4B).

As it was briefly stated before, this technique was developed to study genetic mosaicism, discernable by the two different fluorescent markers of MADM. In this way a mutation for a gene of interest ($gene^{mut}$) is genetically linked to one MADM allele via meiotic recombination ($MADM^{TG}$;$gene^{mut}$ / +;$gene^{WT}$, linked in a chromosome "n"). Afterwards, a crossing with a wild type animal containing the other MADM allele in homozygosis ($MADM^{GT}$; $gene^{WT}$ / $MADM^{GT}$;$gene^{WT}$) will generate a progeny with the mutation linked to one MADM allele and a wild type version of the gene of interest ($gene^{WT}$) linked to the homologous MADM allele ($MADM^{TG}$;$gene^{mut}$ / $MADM^{GT}$;$gene^{WT}$). Thus, after Cre expression, interchormosomal recombination and a G2-X event, cells bearing one MADM marker (green or red) will be homozygous for the wild type allele of interest ($MADM^{GG}$;$gene^{WT}$ / $MADM^{GT}$;$gene^{WT}$) and homozygous for the mutation of interest in the cells with the other MADM label ($MADM^{TT}$;$gene^{mut}$ / $MADM^{TG}$;$gene^{mut}$). The assessment of the heterozygosity can also be done for cells displaying both MADM markers (yellow, $MADM^{GG}$;$gene^{WT}$ / $MADM^{TT}$;$gene^{mut}$) after a G2-Z event (Hippenmeyer et al., 2010).

Although mosaicism is highly interesting for functional gene studies, just like *Brainbow,* MADM has been applied for studies of brain cell clonality. Furthermore, MADM enables the lineage tree analysis at a single cell resolution and the elucidation of the cell division pattern, (symmetric versus asymmetric) as well as the replication potential of the daughter lineages (limited versus large capability of successive cell divisions, Gao *et al.*, 2014). For instance, if we observe four cells of two different kinds forming a clone marked with *Nucbow*, all we could say is that they have a common progenitor that divided twice, but the four cells could have emerged via two asymmetric or two symmetric divisions (Figure 9A). In contrast, MADM has the potential to reveal what type of cell division occurred, since the two daughter lineages are labeled distinctly (Figure 9B). However, it must be considered that in order to be useful for lineage tree analysis, labeling of MADM must be sparse, unlike *Brainbow* or retroviral bar-coding, which can be ample, but do not offer information about the mode of division in daughter lineages. These advantages and disadvantages for each method have made it necessary to combine both in our study of the lineage of adult neurogenic niche cells. On the one hand, *Brainbow* has given us the power to perform a high-throughput clonal analysis of

large numbers of ependymal and adult NSCs from the neurogenic niche. On the other hand, we have analyzed a more reduced cohort of cells using MADM, which provided us with valuable information about cell division patterns.

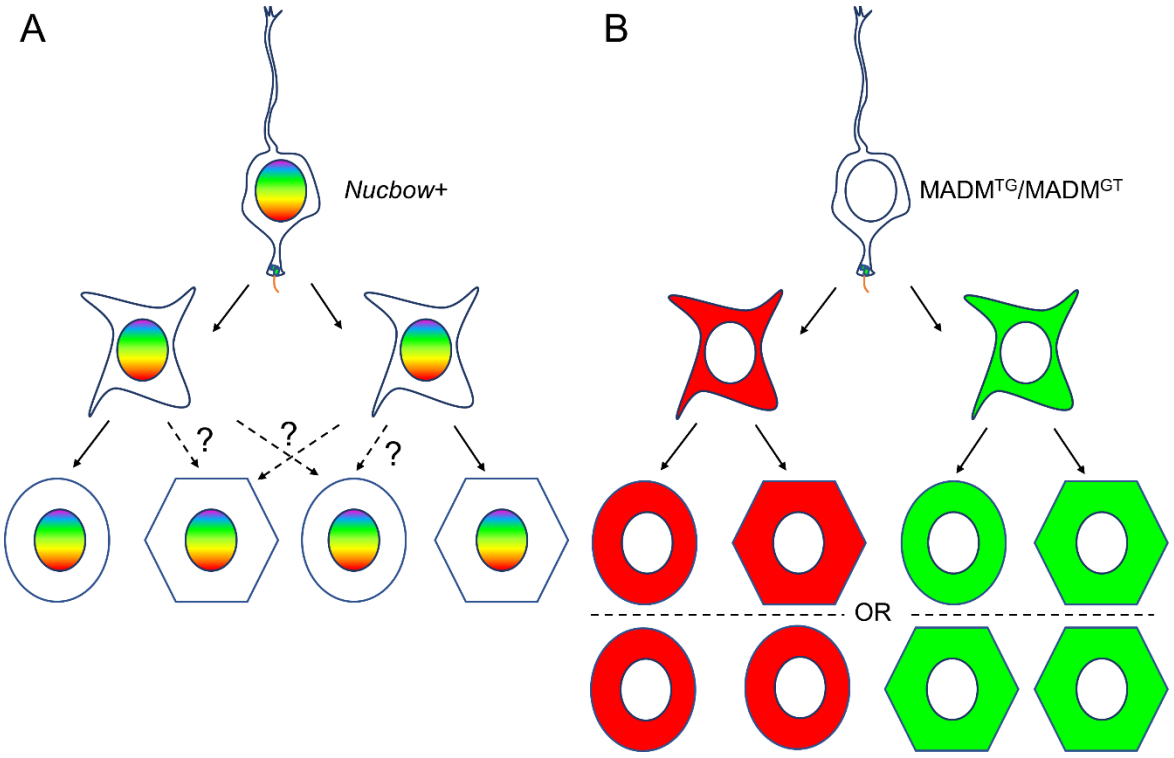

Figure 9. Comparison of *Brainbow* and MADM techniques in clonal analysis. (A) If we considered four cells of two distinct cell types (two and two, here shown by two different morphologies, the circle and the hexagon) labeled with the same *Nucbow* marker, it would be safe to say they form a clone coming from a common progenitor that divided twice. However, it could not be assessed whether these four cells were born via two symmetric divisions or two asymmetric divisions (dotted arrows with question mark). (B) If we consider the same population forming a clone of four cells, two with one MADM label (red) and two with the other (green), it could be said what type of cell division generated these cells, either two asymmetric (upper panel of daughter cells) or two symmetric (lower panel).

1.4.3. Transgene delivery to brain progenitors: the *in utero* electroporation technique

Genetic manipulation is a powerful tool to study gene function in the brain. Transgenic animals, gene KOs and knock-ins, as well as mutagenesis have served a precious purpose to elucidate the developmental schemes of the mammalian forebrain. However, conditional expression of the transgenes or KO of a particular gene in all specific cell types cannot be achieved, for it requires an extensive knowledge of the regulatory sequences that govern cell specification and function in the brain (Saito and Nakatsuji, 2001). Furthermore, the generation of transgenic lines (with or without conditional expression) or the packaging of DNA elements in retroviral particles for effective gene delivery in the brain are time-

consuming processes. These require DNA microinjection in embryonic stem cells, transplantation *in utero*, transgene-bearing selection processes, production of viral stocks using mammalian cells in culture, etc. (Tabata and Nakajima, 2001).

Delivery of nuclei acid elements using electroporation *in ovo* in chick embryos or cell culture systems preceded the use of such technique in live mice. The possibility to do it in mouse brains opened a new world of opportunities for gene function, cell behavior and cell migration studies in the forebrain. The *in utero* electroporation (IUE) technique, as it was known upon development, proved a highly efficient manner to introduce exogenous genetic material, such as plasmids, into brain cell progenitors, the RGCs. It thus allowed over-expression or knock-down (KD) of genes of interest via plasmids expressing a protein under a strong promoter, or the use of shRNAs and miRNAs, respectively (Wang and Mei, 2013). It was also helpful in tagging progenitors with fluorescent reporters, which made it possible to film cells *ex vivo* in cortical slices using time lapse microscopy and analyze their behavior, i.e. cell division, delamination from apical surface, migration, etc. (Nishimura et al., 2012; Pilz et al., 2013).

IUE starts by anesthetizing a timed-pregnant female and exposing the utero by retrieving it from the abdominal cavity through a surgically practiced incision in the abdominal wall. Then the DNA molecules are injected into the developing ventricles of the embryo (lateral or third ventricles) in a stained solution, in order to observe the filling of the ventricular cavity, an indicative of successful injection. Afterwards, two electrodes are placed surrounding the developing telencephalon and electrical pulses are applied. This fulfils a double function. First it permeabilizes the membranes of cells on the ventricular surface for the incorporation of exogenous DNA molecules, such as plasmids. Second, since the DNA is negatively charged in physiological conditions, the injected molecules in the ventricle migrate towards the anode (positively charged electrode) in the electrical field, and thus move towards the RGCs on the ventricular walls (Saito and Nakatsuji, 2001; Tabata and Nakajima, 2001; Wang and Mei, 2013, Figure 10).

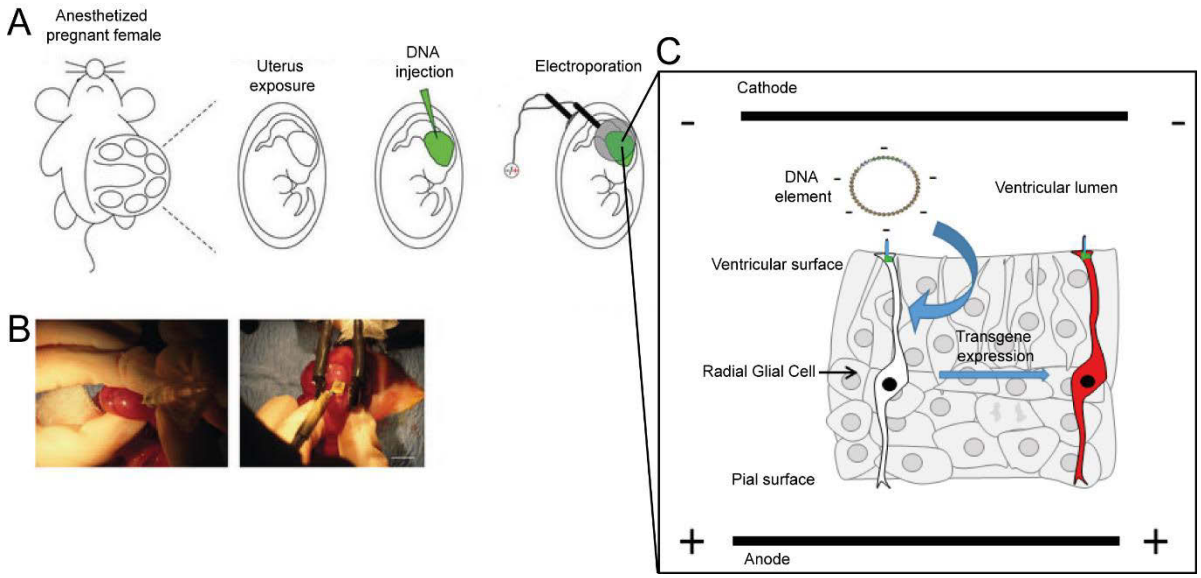

Figure 10. *In utero electroporation* procedure. IUE serves to deliver transgenes into the RGC progenitor pool. (A) Scheme of the general procedure of the IUE. A timed-pregnant mouse is anesthetized and the uterus is carefully retrieved from the abdomen. Then a stained DNA solution is injected into the lateral ventricles and an electrical pulse is applied. (B) Photographs of an exposed uterus being injected and electroporated. (C) Scheme of the principle of IUE. The DNA element introduced via microinjection into the ventricular lumen is negatively charged in physiological conditions. The application of an electrical current produces its migration towards the anode, placed extrauterine, adjacent to the ventricular surface. There it is incorporated through electrically-permeabilized cell membranes into the RGCs, who express the transgene borne by the plasmid. Adapted from Dal Maschio *et al.*, 2012.

1.5. Objectives and hypotheses

In the first part of my thesis work, which was published in the journal *Neuron* in March 2019, we undertook the task to unveil the glial cell lineage that generates the adult mammalian neurogenic niche, whose main components are multiciliated ependymal cells and adult neural stem cells (see below, Chapter 2).

In order to perform a clonal analysis we first determined, via Cre-lox fate mapping the spatial origin of ependymal cells, since it was important to consider or rule out a potential migration bias in our clonal analysis. We hypothesized that multiciliated ependymal cell progenitors do not migrate, since there are no known functional specificities in differently allocated ependymal cells along the ventricular walls. Besides, RGCs are localized along the entire embryonic VZ, thus making it unnecessary for a focal generation of ependymal cells. Initially we were set to determine the cell division types that generated ependymal cells during late gestation (E14.5-E15.5) upon the last division of their progenitors. We theorized that

ependymal-generating symmetric divisions existed, since ependymal doublets were observed during the development of the neurogenic niche, this is, two cells in close proximity (sometimes in physical contact) in a similar state of ependymal differentiation. We have used the *Brainbow* and MADM techniques to establish the ontogeny of the neurogenic niche cells and validate our hypotheses.

CHAPTER 2. ON THE COMPOSITION OF THE NEUROGENIC NICHE AND ITS REGULATORS

2.1. Ependymal cells and centriole amplification. Birth, development, characteristics, function and implication in disease.

2.1.1. Multiciliated epithelia in mammals

As it was briefly introduced before, neuroglia comprises a wide arrange of non-neuronal cells, highly heterogeneous in morphology and function, who have the primary role to keep homeostasis in the nervous system and defend it against external insults, such as pathogens. Thus they play a major role from the development to the survival and death of its cells (Verkhratsky et al., 2014).

Among these cells, the least studied group of glial cells is the ependymal cell group. Ependymal cells or ependymocytes belong to a highly specialized kind of cell called multiciliated cell (MCC). MCCs line the lumen of body cavities, such as the ventricular system of the CNS (lateral ventricles, third and fourth ventricles and aqueduct in the brain and central canal, within the spinal cord), forming a continuous epithelium. The most prominent characteristic of MCCs is the presence of bundles of motile cilia at its apical surface, each of which is nucleated by a modified centriole at its base, or basal body, docked to the apical plasma membrane. The motile cilia are membrane protrusions containing a microtubule-based axoneme whose bending causes the motility of the whole structure. They project into the ventricular cavity to ensure the circulation of body fluids containing particles and/or cells along the epithelial surface (Delgehyr et al., 2015; Spassky and Meunier, 2017).

There are other MCCs in the body outside of the CNS. They exist in the respiratory tract and auditory canal (ear, nose, throat and lungs). Mucus is produced *in situ* and moved along the surface of the ciliary layer, in a “gel-on-a-brush” movement. The pathogens and toxic particles inhaled adhere to the mucus layer and are displaced to the pharynx, where they are

swallowed. As a consequence, ciliary defects cause chronic infections of the respiratory and auditive systems (Spassky and Meunier, 2017).

MCCs line the epithelium of the female reproductive system, from the ovary fimbria to the Fallopian tubes and uterus. This multiciliated epithelium transports the ova into the uterus during each menstrual cycle. In the male, MCCs are present in the efferent duct, which concentrates the sperm by resorbing testis fluid. The beating of the cilia is actually opposite to the direction of the epididymis, where the sperm is headed. According to mathematical modelling, the reflux created by MCCs serves to let through the sperm that is only appropriately concentrated thanks to its higher viscosity. Motile cilia disfunctions in both males and females are thus linked to infertility (Spassky and Meunier, 2017).

2.1.2. Ependymal cell functions and derived pathologies

2.1.2.1. Cerebrospinal fluid flow-derived functions and planar cell polarity

The ependymal epithelium covers the ventricular system of the CNS in all its length. It is formed by four communicating cavities: the two lateral ventricles deep within the forebrain, which communicate via the interventricular foramen with the third ventricle, surrounded by the diencephalon. The third ventricle and the fourth ventricle, which lies within the hindbrain, are connected via the aqueduct that runs along the midbrain. Finally, the fourth ventricle communicates with the central canal, located inside the spinal cord, to complete the enclosed ventricular system. This system is a liquid-filled cavity in which the Cerebrospinal Fluid (CSF) is produced and flows. The CSF in the embryo contains numerous growth factors that are essential for the development of the CNS. These are sensed via the primary cilium that apical RGCs extend into the lumen of the ventricular cavity. In postnatal stages, the coordinated beating of the ependymal cell motile cilia is key for the propulsion of the CSF, the most studied function of ependymal cells (Jiménez et al., 2014).

Figure 11. Ventricular system in the human brain. The ventricular system is formed by a group of communicating cavities where the CSF flows. The lateral ventricles are located deep within the brain hemispheres and they connect with the third ventricle through the intraventricular foramen. The third ventricle, which is adjacent to the diencephalon, is joined to the fourth ventricle in the hindbrain via the aqueduct, which passes through the midbrain. Finally, the ventricular system of the brain forms a continuum with that of the spinal cord, since the fourth ventricle communicates with the central canal, the CSF-filled cavity that runs from the brain to the ventriculus finalis or fifth ventricle, at the base of the spinal cord. A: anterior, P: posterior, D: dorsal, V: ventral. From Nieuwenhuys, Voogd and Huijzen, 2008.

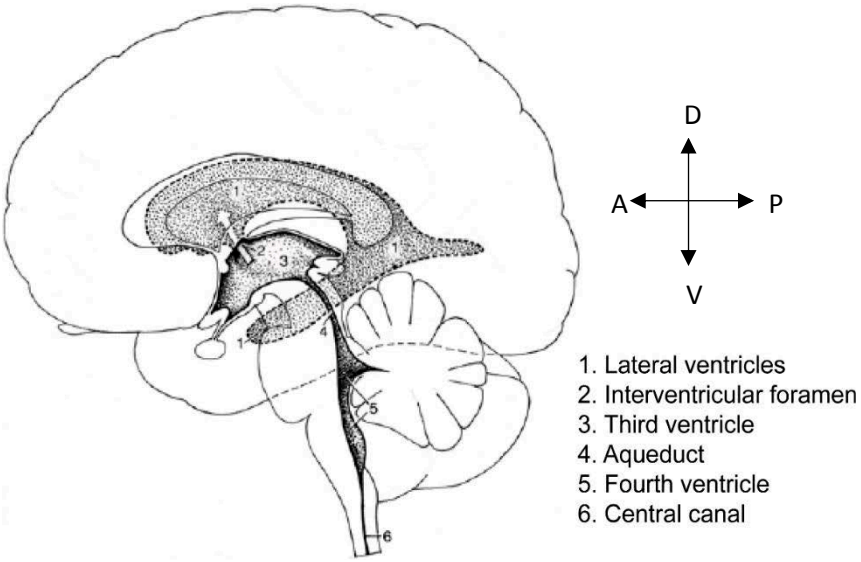

The CSF is a clear, slightly viscous liquid produced by the choroid plexus. This is a highly vascularized membranous organ located in all ventricles of the brain (lateral, third and fourth ventricles) consistent of cells of epithelial nature resting on a basal lamina. These epithelial cells transport ions such as Na^+, Cl^- and HCO_3^- from the blood to the ventricles to create an osmotic gradient. Such differential ion concentrations causes water to leave the circulatory system and enter the ventricles, hence replenishing the CSF (Emerich et al., 2005). The flow of this medium is necessary for the delivery of nutrients, signaling factors and the clearance of waste and neurotoxic substances (Siyahhan et al., 2014). It has also been implicated in static mechanical brain protection and the development and organization of the CNS, not only in the embryo thanks to the distribution of growth factors, but also in the adult through the support of neuronal migration guidance (Sawamoto et al., 2006).

Different forces contribute to establish a CSF flow. Some of these are the heartbeat, body movements in lower vertebrates like zebrafish, the balance between CSF production by the choroid plexus and its reabsorption in the subarachnoid space (at the pial surface) and, of course, ciliary beating of ependymal cells (Butler et al., 2017; Olstad et al., 2019; Siyahhan et al., 2014). Although the role of ependymal cilia beating in diffusion of molecules of the CSF by creating constant motion and currents has been postulated for many years now (Del Bigio, 2010; Worthington and Cathcart, 1963), a more complicated relationship between ciliary

beating and CSF flow has been elucidated. The use of fluorescent particle tracking in higher vertebrate brain explants or by injection of said particles into the ventricular system of transparent organisms (zebrafish larvae) has helped to clarify that CSF flows are not random along the ventricular system. Rather than that, different populations of motile ciliated cells are spatially organized in modules that create complex spatiotemporally regulated flow networks from zebrafish (Olstad et al., 2019) to mammals, like rodents and pigs (Faubel et al., 2016), which correlate with ciliary beating. This means that the general CSF flow is subdivided in flow domains that create intraventricular (Faubel et al., 2016) or interventricular (Olstad et al., 2019) boundaries with little exchange, possibly to establish local concentration of substances, according to the needs of different anatomical sections of the ventricular system. This, in combination with spatial divergences in the transcriptomics of the choroid plexi of different ventricles that notably affect the secretome in each brain region, help establish a regionalized CSF (Lun et al., 2015).

The coordinated beating of the cilia to create directional near-wall CSF flow is possible by the existence of a planar cell polarity (PCP) in the multiciliated epithelium. It consists of the polarization or differential distribution of cellular structures along the epithelium plane (this is, perpendicularly to the apico-basal axis). Thus, another major characteristic of ependymal cells is that they display epithelial PCP, which is composed of rotational, translational and tissue-level polarity (Wallingford, 2010).

Rotational polarity refers to the orientation of basal bodies at an individual level, which can be determined by the presence of the basal foot, an electron-dense conical appendix attached laterally to the basal body microtubule barrel (Wallingford, 2010). This is perfectly discernible via Transmission Electron Microscopy or TEM (Guirao et al., 2010; Hirota et al., 2010) and it is an indicative of basal body rotational orientation, the direction of the ciliary stroke and, as a consequence, the direction of the fluid flow. In properly functioning ependymal cells, all basal bodies at the apical surface display the same rotational polarity, so that cilia beat in a coordinated manner, all in the same direction, and directional fluid flow can be established (Wallingford, 2010) (Figure 12A).

It is set in ependymal cells during ciliogenesis, this is, the first two postnatal weeks. It is the result of the coupling of hydrodynamic forces acting on motile cilia with PCP signaling in ependymal cells. The initial bulk of CSF flow existent in the ventricles during ependymal

differentiation has been shown to be sufficient to rotate the initial random orientation of the motile cilium, in order to settle beating plane parallel to the direction of the flow. This external cue requires PCP signaling to establish such orientation. Namely, the PCP proteins Van Gogh-like 2 (Vangl2) (Guirao et al., 2010) and Dishevelled (Dvl) (Park et al., 2008) have been found to be necessary for rotational polarity (Figure 12A).

Translational polarity in ependymal cells denotes the asymmetric distribution of basal body patches on the cellular cortex. Basal bodies migrate to the anterior pole of the apical surface in ependymal cells at roughly the same time as the establishment of rotational polarity. It does not seem to be regulated by PCP signaling, but motor proteins of the cytoskeleton, such as non-muscle myosin II, a protein that is expressed in ependymal cells but not in their neighbor, surrounding adult NSCs (Hirota et al., 2010). The primary cilium of ependymal monociliated progenitors is also key for translational polarity. This structure is polarized before the onset of ependymal differentiation, this is, it locates itself at one pole of the cell around birth. It is possible that primary cilia act as sensory antennae that detect the bulk of CSF flow resulting from its production by choroid plexus and reabsorption (Mirzadeh et al., 2010) (Figure 12B).

Finally, tissue level polarity consists of the presence of the same ciliary tuff asymmetric disposition in the cell (translational polarity) and ciliary stroke direction (rotational polarity) across a group of cells. It has been shown to be instructed by Vangl2 and Frizzled in a non-cell autonomous manner (Wallingford, 2010) (Figure 12C).

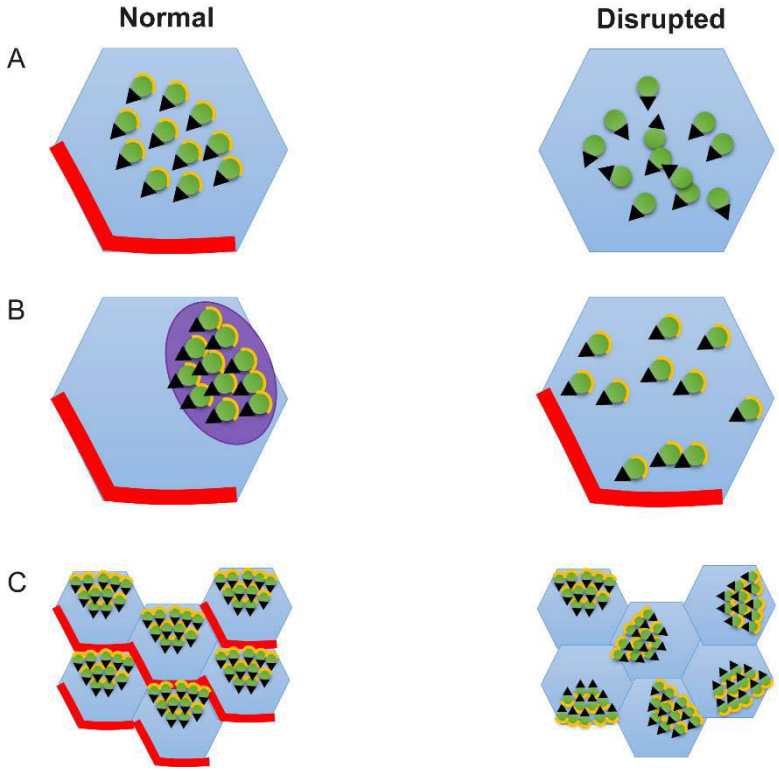

Figure 12. Planar Cell Polarity in ependymal cells. (A) Rotational polarity consists of the same individual orientation of the basal body (green circle), determined by the presence of the basal foot on the wall of the centriole (black triangle). This orientation is a read-out of the ciliary stroke direction upon beating and can therefore predict the CSF flow orientation. It is controlled by members of the PCP pathway, such as Vangl2 (shown in red, located on the pole opposite to where the basal body patch is located) and Dvl (shown in yellow), localized to the centrioles. (B) Translational polarity is the asymmetric distribution of subcellular structures, such as the basal bodies of ependymal cells, within the cell. In ependymal cells it is not controlled by PCP signaling, but motor proteins, such as non-muscle myosin II, located close to the basal body patch (shown in purple). It has been shown to be established early, by the primary cilium, even before centriole amplification. (C) Tissue level polarity is the organization of cells within a tissue with a similar translational and rotational polarity. It has been proposed to be organized in a non-autonomous cell manner and be dependent on PCP signaling actors, such as Vangl2.

2.1.2.2. Other functions of ependymal cells

Ependymal-maintained CSF flow is essential for adult NSC proliferation in the SVZ and neuroblast migration to the olfactory bulb (see Chapter 2 - The neurogenic niche, adult neural stem cells and adult neurogenesis). It has been shown that the increase of CSF fluid flow can increase the proliferation of these cells by opening of epithelium sodium channels expressed on their apical surface (Petrik et al., 2018). Furthermore, the secretome of the choroid plexus contains factors that enhance stem proliferation in the adult neurogenic niche, molecules that are diffuse thanks to the coordinated beating of the ependymal cilia (Silva-Vargas et al., 2016). Ependymal beating not only contributes to new neuron birth upon generation of near-wall CSF flow, it also guides neuroblast migration from their site of origin, the SVZ, to their destination in the olfactory bulb. Ependymal-created CSF directional flow is parallel to this stream of neuroblasts and ciliary mutants present an impaired migration of these prospective neurons (Sawamoto et al., 2006).

Finally, microarray analyses upon brain infection have revealed a less studied function of ependymal cells: their potential implication during disease. These cells can upregulate immune system mediators, like genes from the antigen-presenting pathway, as well as diffusible molecules like cytokines or chemokines, in order to mediate inflammation and ensure leukocyte recruitment from the CSF, cells that previously exited from the choroid plexus vascularized network, into the brain parenchyma (Mishra and Teale, 2012).

2.1.2.3. Ependymal cells as neural stem cells: reality or myth.

Ependymal cells have an essential role in promoting neurogenesis and guiding neuroblast migration thanks to the directional CSF flow they generate (Petrik et al., 2018; Sawamoto et al., 2006). However, for many years, whether they themselves could be proliferative and give rise to new neurons in physiological conditions or upon injury, remained an open question. Some early studies used autoradiography to detect proliferation in the ventricular walls by using thymidine nucleotides labeled with radioactive isotopes, like tritrium (^{3}H), which are only incorporated by cycling cells (Bruni, 1998). While some of them claim the presence of cells that have incorporated the radioactive label on the ependymal layer (Altman, 1963), but without clear anatomical points of reference, others show clear incorporation of [^{3}H] thymidine or bromodeoxyuridine (BrdU), a thymidine analog, only in the subependymal layer (Hauke et al., 1995).

Later studies claim that ependymal cells enter the cell cycle and generate rapidly dividing amplifying progenitors in physiological conditions to contribute new neurons to the olfactory bulb (Johansson et al., 1999). However, they fail to couple BrdU staining with ependymal markers and they base their conclusion on BrdU$^+$ cell proximity to the ventricular surface, as well as the use of ventricle-injected dyes that could very well diffuse to the neighbor proliferative non-ependymal cells. In an area of the brain where VZ ependymal cells and SVZ proliferative cells are densely packed, the use of markers that allows setting them apart is crucial.

In 2005, Spassky *et al.* managed to replicate previous experiments of [^{3}H] thymidine and BrdU incorporation with clear markers of mature ependymal cells, like the presence of cilia in TEM images or immunolabels, respectively. Hence, this study settled the current consensus about ependymal cells, which is that they are postmitotic in physiological

conditions (Spassky et al., 2005). A single-cell RNA-seq study later corroborated this by establishing that ependymal cells were transcriptionally different from adult NSCs and that they did not proliferate *in vivo* (Shah et al., 2018). Besides, this work suggests that ependymal cells do not replicate either upon injury, like stroke. Nevertheless, a previous one convincingly proves that stroke induction leads to the proliferation of ependymal cells. According to its authors, constitutive Notch signaling, which is active in ependymal cells, maintains ependymal cells in a quiescence state in normal conditions. However, its inhibition or the presence of a stroke can reactivate these cells to generate new neurons that will colonize the olfactory bulb (Carlén et al., 2009). The difference with the previous report is the mode of stroke induction. The latter achieves it through middle cerebral artery occlusion, whereas the former does it by collagenase injection in the ventricles. It is possible that Carlén et al. are closer to the reality of a stroke and that hence, ependymal cells indeed can be reactivated upon said trigger.

To sum up, adult forebrain ependymal cells are postmitotic *in vivo* under normal circumstances, but they could act as a reservoir of potential neuroblasts in case the brain suffers damage and needs repair.

2.1.2.4. Hydrocephalus, a condition linked to ependymal cell function

Defects in CSF homeostasis can lead to a pathological condition known as hydrocephalus. It is caused by the accumulation of CSF in the ventricles, which in turn, causes their enlargement and constriction of the brain parenchyma (Figure 13). It is a highly complex disease due to the existence of several subtypes with different etiologies and pathophysiological mechanisms. Among the most common and severe symptoms are a reduced mobility, an impaired cognition, sensory deficits, epilepsy, endocrine dysfunction, which can affect growth in children or fertility, vomiting, depression and chronic headaches (Vinchon et al., 2012). It can be fatal if left untreated in up to 50% of the cases. Currently, the primary treatment is the surgical insertion of a shunt catheter to extract the accumulating CSF from the ventricles and conduct it into the peritoneal cavity or an alternate absorption site, which is not risk-free (infection, hemorrhage, etc.) (Lee, 2013).

The knowledge about the genetic and molecular causes of hydrocephalus is essential, like in all diseases, to the development of new therapeutic strategies. According to the age of

onset, it can be congenital, pediatric or adult hydrocephalus (Hamilton et al., 2016; Shaheen et al., 2017), with a defined genetic cause or environmental, such as an infection, subarachnoid hemorrhage or brain trauma. Among the genes mutated found in congenital hydrocephalus, we can find EML1, a gene that encodes a microtubule-binding protein that regulates PCP and whose ablation causes abnormal migration pattern of CNS cells during development (Shaheen et al., 2017), MPDZ, which encodes for a tight junction protein essential for epithelial polarity (Al-Dosari et al., 2013) or CCDC88C, which also seems to be involved in the Wnt-PCP pathway (Drielsma et al., 2012).

Congenital hydrocephalus is also linked to ciliary motility defects. Primary ciliary dyskinesia (PCD) is a pediatric syndrome caused by disfunction of motile cilia and flagella. Consequently, all body organs whose function depends on it are affected. Therefore, PCD causes chronic respiratory infection, otitis, male infertility, and situs inversus as the most common symptoms (see above, Chapter 2- 2.1.1 *Multiciliated epithelia in mammals*). Nonetheless, it has also been linked to female infertility and hydrocephalus. Several reports of families affected by hydrocephalus have linked it to PCD, but the incidence of such malformation in PCD patients is very low (Lee, 2013; Spassky and Meunier, 2017).

Many models of PCD have been developed in rodents, since the prevalence of hydrocephalus in such animals with disrupted ependymal development or function is high, although the disease mechanisms are diverse. Some of them are based on mutations on intraflagellar transport motor proteins, such as Kif3A and Ift88 mutants. These proteins are essential for the formation, maintenance and function of cilia and their loss before birth leads to the absence of motile cilia on ependymal cells and the development of hydrocephalus in mice (Liu et al., 2014; Mahuzier et al., 2018). Other PCD models are based on animals able to produce motile cilia but, due to the absence of ultrastructure axoneme components in the cilium, usually visible by TEM analysis, they lack the ability to beat and produce a functional CSF flow. This is the case, for instance, of the Mdnah5 and Hydin mutants (Lechtreck et al., 2008). Deficits in PCP can also entail an improper motile cilia function, despite the presence of a normal number of cilia with usual length. Thus, ablation of the already mentioned PCP gene Dvl has also been implicated in the onset of hydrocephalus (Ohata et al., 2014). Finally, mouse models that include a PCD phenotype, this is, infertility, aberrant respiratory tract epithelial function and hydrocephalus, due to a complete absence of motile cilia in all

multiciliated tissues, turn to deletion of upstream genes that control MCC differentiation. Such is the case of Geminin coiled-coil domain-containing protein 1 (GemC1) (Terré et al., 2016), a gene that will be extensively reviewed and studied in this work (see Published work in *Neuron* and work ready for submission), and its downstream effector, FoxJ1 (Chen et al., 1998) (Figure 13).

Since hydrocephalus is due not only to problems in the production or function of motile cilia, but also the balance of CSF production and absorption, other hydrocephalus rodent models have been established. Notably, KO or mutation of genes that control choroid plexus proper development and function, like Rfx-3 (Baas et al., 2006) and Tg737 (Banizs et al., 2005). The latter is a curious case, since the onset of hydrocephalus precedes normal motile cilia development (first postnatal week), accompanied by an increase of CSF production due to ion transport defects. However, cilia that develop after the hydrocephalus are short and disorganized. This leads to the hypothesis that this gene's mutation causes hydrocephalus via cilia-independent mechanisms, but these structures are subsequently aberrant, probably due to a built-up intracranial pressure, which can feedback the worsening of the pathology (Banizs et al., 2005; Taulman et al., 2001).

The differences in hydrocephalus penetrance in cilia-related mutations across species can be explained due to divergences in size of ventricular system and genetic disparity between animals. Thus, as mentioned, motile cilia defects lead to hydrocephalus in almost all individuals in rodents, whereas in humans the incidence of hydrocephalus in patients with PCD is low. To make things even more complex, zebrafish can develop hydrocephalus, but not because of motile cilia ablation, but primary cilium defects (Olstad et al., 2019). In humans, ciliary beating is thought to be more determinant for near-wall CSF flow, whereas macroscopic CSF dynamics is controlled by pulsatile CSF production from the choroid plexus, ventricular wall expansion and contraction and arterial pressure (Spassky and Meunier, 2017).

Figure 13. Hydrocephalus in humans and mouse models. (A) Sagittal brain magnetic resonance image of a patient with non-communicating hydrocephalus due to aqueduct stenosis (green arrow). The obstruction to CSF flow between the third and fourth ventricles lead to the enlargement of the ventricular cavities and constriction of the brain parenchyma. The image to the right shows the same patient after practicing an endoscopic third ventriculostomy, which consists of making an opening on the floor of the third ventricle, so that the excess of CSF is evacuated. Adapted from Kahle *et al.*, 2016 . (B) A mouse model of hydrocephalus, in this case due to a homozygous mutation of the axonemal dynein Mdnah5. Mice display a head bulge due to the enlargement of the ventricles, growth retardation and early postnatal death. These phenotypes are common in other hydrocephalus models, like GemC1 KO models. Adapted from Ibañez-Tallon, Gorokhova and Heintz, 2002.

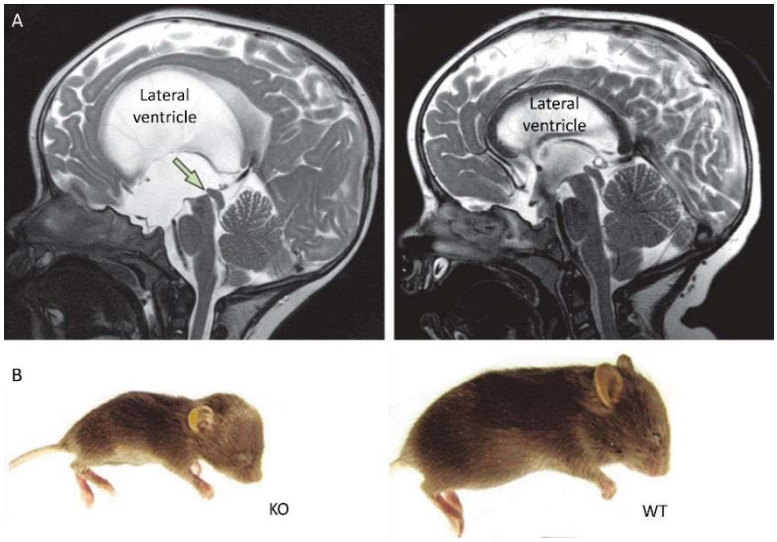

2.1.3. Ependymal birth and specification mechanisms

Multiciliated ependymal cells are born during late-gestation from RGCs. Birth dating experiments with BrdU showed that the bulk of these cells is born between E14 and E16. Besides, they are born in a caudo-rostral gradient, with the first ependymal cells becoming postmitotic in the caudal regions of the ventricle lateral walls, and then progressing rostrally as more and more ependymal cells are produced. The same authors of the study proved a continuity between RGCs and ependymal cells by carrying out striatal injections of AdenoCre viruses in GFP reporter mice (Spassky et al., 2005). At P0, the only bridge between the VZ and the striatum consists of the RGC processes that expand between the two (Tramontin et al., 2003). Thus, viral injections in the striatum would only label cells *in situ* or VZ cells that extended a long process into such area. Indeed, after P0 infection with AdenoCre viral particles in the striatum, the soma of RGCs appeared labeled two hours later in the VZ. Furthermore, some of these cells generated ependymal cells in the adult brain that retained such marker, hence proving the continuity between RGCs and ependymal cells (Spassky et al., 2005).

The most upstream specificators of the MCC fate that have been identified are a family of micro-RNAs (miRNAs). These encode a class of small (21-25 nucleotide-long), non-coding RNAs that regulate gene expression through post-transcriptional repression. Most of them bind to mRNAs on their 3'UTR, which then targets the mRNA for degradation or translation repression (Wahid et al., 2010). The family of miR-34/449 are an evolutionary conserved group of miRNAs that are expressed in MCC epithelia, like the multiciliated epidermis of *Xenopus laevis* embryos and primary cultures of human airway mucociliary epithelial cells (Marcet et al., 2011), as well as mouse respiratory epithelium (Song et al., 2014). The brain also expresses some of these miRNAs, although it has not been described specifically in MCC organs, but whole-brain lysates. They are encoded in three different loci that produce six components of the family (miR-34a, miR-34b/c and miR-449a/b/c). Although they are necessary for multiciliation, they show functional redundancy, since combined double knock-out (DKO) of some of the three loci does not display any particular phenotype. Only a DKO of miR-34b/c and miR-449a/b/c presents perinatal increased mortality (Wu et al., 2014). Other studies have used triple knock-out (TKO) of the three loci that shows a PCD-like phenotype in mice. The physiological consequences range from infertility, due to a defective gamete transport in the female reproductive organs and absent spermatogenesis, to growth impairment and high lethality, rooted in mucociliary airway clearance deficits, which cause respiratory infections. Curiously, surviving animals do not develop hydrocephalus (Otto et al., 2017; Song et al., 2014) (Figure 14).

The expression of miR34/449 family members target cell cycle proteins, such as cyclins and their dependent kinases, and checkpoint activation genes and trigger cell cycle exit. Hence, in the absence of these regulatory molecules, cell cycle progression genes are upregulated and an increase of proliferative markers, such as Ki67, PCNA and BrdU incorporation is observed in multiciliated epithelia, such as the respiratory one (Otto et al., 2017). Notch 1 and Delta-like 1 (Dll1) have also been identified as targets, since they present miR-449 binding sites on their 3'UTR (Marcet et al., 2011). The Delta/Notch signaling pathway is part of a two-component system in which a signal-sending cell expresses membrane-bound ligands (like Delta) on the surface and a signal-receiving cell that expresses a receptor (Notch) as a transmembrane protein. The interaction of both cell types causes the proteolytic cleavage of the Notch intracellular domain (NICD) off the receptor, which is then free to travel to the

nucleus and promote gene expression (Guruharsha et al., 2012). This binary system has been hypothesized to be key for the acquisition of different cell fates in multiciliated epitheliums, where MCCs are in close association with other cell types to jointly maintain the proper function of the whole system (Cibois et al., 2015). Upon over-expression of miR-449 in a human airway mucociliary epithelial cell culture or *Xenopus* embryos, a down-regulation of Notch1 and Dll1 takes place and an increase in mutlticiliogenesis follows (Marcet et al., 2011). This mechanism seems to be conserved with some differences across vertebrates. Not only in amphibians, mouse and humans is Notch signaling a regulator of multiciliogenesis. In zebrafish pronephros MCCs, during essential fluid propulsion in the developing kidney, the alternate Jagged2 (ligand)/Notch3 (receptor) signaling pathway negatively regulates ciliogenesis. Thus KD of any of these two components or over-expression of Notch leads to an increase or decrease of multiciliogenesis, respectively, in the zebrafish pronephros (Liu et al., 2007) (Figure 14).

BMP signaling is another regulator of MCC cell fate and their associated cells, like goblet cells, a specialized mucus-secreting cell essential in mucociliary epithelia like embryonic *Xenopus* epidermis and human airway epithelial cell cultures. Fine tuning of BMP signaling is essential for correct organogenesis in MCC systems. BMP signaling blocking leads to higher MCC differentiation in mucociliary epithelia, whereas its chronic activation has the opposite effect. Furthermore, BMP does not regulate MCC differentiation independently of Notch, but there is crosstalk between both pathways. BMP activity triggers Notch ligand (Dll1) upregulation, thereby preventing MCC specification, only when both are activated at the same stage (Cibois et al., 2015) (Figure 14).

Considering the mammalian brain, there are less studies targeting the MCC fate acquisition of the brain ependyma. A TKO of the miR-34/449 family entails perinatal increased mortality probably due to brain defects, namely, smaller forebrain structures implicated in many functions, including reward pathways, feeding, and social behaviors (Wu et al., 2014). However, these deficits are present at least since E18.5, before the differentiation of ependymal cells (Spassky et al., 2005) and consequently cannot be linked to an aberrant MCC function or presence. Even though a direct link between miRNAs and MCC differentiation has not been proven yet, Notch signaling seems to play a role in such process. An over-expression of NICD (Notch signaling activation) inhibits both neuronal and MCC differentiation in the

neuroepithelium, this is, cells retain their radial glia characteristics (Kyrousi et al., 2015). Interestingly, Notch signaling is present in mature ependymal cells of the adult brain and seems to be necessary to keep their postmitotic stage and repress them from generating neuroblasts that migrate to the olfactory bulb (Carlén et al., 2009; Zhao et al., 2009). However, a study proving whether Notch is necessary for ependymal specification is lacking.

The mechanism by which Notch is able to favor an MCC fate has also started to be elucidated. This signaling pathway activates the expression of Multicilin, a protein encoded by the gene *mcidas*, which is necessary for multiciliation in *Xenopus* epidermis, mouse tracheal epithelial cells and neuroepithelium. This protein is directly downstream of GemC1, whose function in promoting ependymal fate can also be tuned by Notch activity (Kyrousi et al., 2015; Stubbs et al., 2012) (Figure 14).

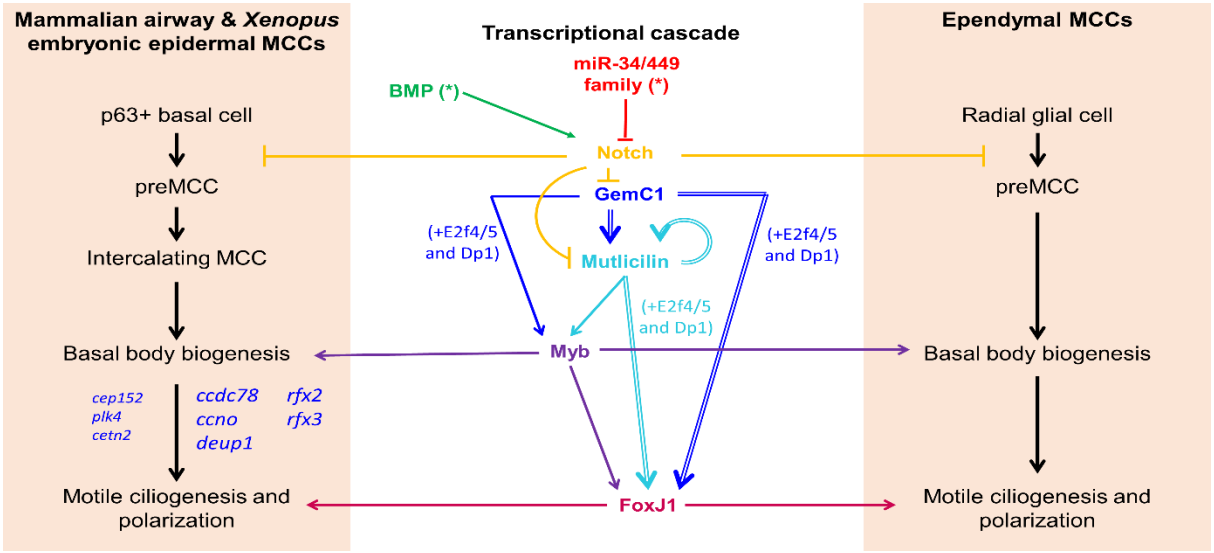

Figure 14. Multiciliated cell specification. The most upstream regulator of MCC fate is a family of micro-RNAs, the miR-34/449 family. They down-regulate Notch activation in the mammalian airways and *Xenupus* embryonic epidermis. Although these mi-RNAs have not been shown to have a role in ependymal specification, Notch is known to maintain RGCs and prevent their differentiation in ependymal or neuronal cells. It does so by inhibiting GemC1 or Multicilin, the former being upstream of the latter and being able to induce its expression by directly binding to its regulatory sequences. These proteins form complexes with the E2F transcription factors E2F4 or E2F5 and their co-activator Dp1 (see Chapter 2 – The Geminin family: regulators of DNA replication with a role in multiciliogenesis). Thus, they activate gene expression of transcription factors directly involved in multiciliogenesis (Myb, FoxJ1, Rfx2, Rfx3). GemC1 and Multicilin are also responsible for the activation of genes directly present in centriole amplification, like *ccdc78*, *ccno* and *deup1* and, in a lesser extent and not in all tissues, *cep152*, *plk4* and *cetn2*, to cite a few. Arrows formed by double lines indicate a direct binding to the regulatory sequences of the genes at the end of said arrows. Asterisks indicate that this pathway has not been shown to act in ependymal cell specification. Modified and updated from (Brooks and Wallingford, 2014).

2.1.4. Ependymal differentiation

2.1.4.1. Basal bodies and motile cilia

As previously stated, ependymal cells' primary characteristic is the presence of an apical ciliary tuff and basal bodies that nucleate all cilia. The process of differentiation thus entails that a monociliated RGC, which presents one primary cilium that protrudes into the ventricular lumen and the centrosome at its base, must amplify its centrioles from two to several dozens (Spassky and Meunier, 2017).

The centriole is a barrel-like cylindrical structure consisting of nine microtubule triplets that display radial symmetry. The triplets are formed of three complete microtubule, A, B, and C, from inner to outer-most one, composed of heterodimers of α- and β-tubulin. This microtubule scaffold encircles a centriole lumen, where a well-defined structure known as the cartwheel is found. It is located on the proximal end of the centriole, this is, the pole of the centriole that is associated with another orthogonally-arranged centriole to form the centrosome and the site of new centriole formation via the centriolar pathway. The cartwheel resembles the hub and spokes of a wheel, where the wheel is formed by the microtubule triplets and the spokes contact it on each of the outer-most A microtubule (Winey and O'Toole, 2014; Zhang and Mitchell, 2015). The cartwheel, whose major protein component is Sas6, plays a key role in the assembly of new centrioles and maintenance of the ninefold symmetry (Nakazawa et al., 2007). Therefore, once these new centrioles are synthesized, it disappears as they proceed through the cell cycle in vertebrate cells. Basal bodies at the base of motile cilia in MCCs, on the other hand, appear to maintain their cartwheels after assembly, probably to ensure centriolar stability, due to the mechanical stress that ciliary beating puts on the basal body (Winey and O'Toole, 2014; Zhang and Mitchell, 2015) (Figure 15A).

On the exterior walls of the centrioles, upon completion of the cell cycle or upon basal body maturation in MCCs, structures called the distal and subdistal appendages are formed, a marker of centriole maturation. In non-MCCs, these structures are found on the older or "mother" centriole. In basal bodies, they are called the basal foot and transitional fibers, respectively. They are essential for their function as microtubule-organizing centers of the cell, as signaling platforms, primary cilium formation and anchoring of the centriole or basal body to the plasma membrane (Winey and O'Toole, 2014). Basal bodies and some immotile cilia (like in photoreceptors) also present a structure known as the rootlet. This is a thick striated

bundle of filaments that projects from the proximal end of the basal body and extends close to the nucleus. It has been suggested to confer mechanical support, which is essential for the long-term maintenance of ciliary function (Garcia and Reiter, 2016) (Figure 15B).

Surrounding the two centrioles a matrix of proteins known as the pericentriolar material is assembled. It plays a role in centriole duplication, microtubule stability in the mitotic spindle, centrosome integrity and basal body multiplication (Mercey et al., 2019a; Woodruff et al., 2014).

Basal bodies act as anchors for all primary and motile cilia. The primary cilium is immotile and is extended from a single basal body corresponding to the mother centriole of the centrosome, while the younger or "daughter" centrioles lies orthogonally to it. In MCCs, after multiplication of the two centrioles to several dozens, apical-wards migration to the plasma membrane and docking, each basal body nucleates a motile cilium. Cilia, either primary or motile, are virtually present in all body cells and are formed by a structure called the axoneme, based on microtubule filaments. Motile cilia axonemes are made of nine outer doublet microtubules (formed of tubules A and B) and two single central pair of microtubules, a structure known as 9+2. Primary cilia lack the central pair of microtubules and are hence known as 9+0. The microtubule doublets are held together by a proteinous linkage called nexin. Apart from the inner pair of central microtubules, motile cilia possess radial spokes and dynein arms. As mentioned earlier, dynein is a microtubule-associated motor protein. The dynein arms are hence the motors that permit the sliding of microtubules and consequent ciliary beating. They are attached to the A tubule in each doublet and their head projects towards the B tubule of the neighboring doublet. Ciliary bending requires the coordinated action of the central microtubule pair, the radial spokes and the dynein arms (Dawe et al., 2007) (Figure 15C).

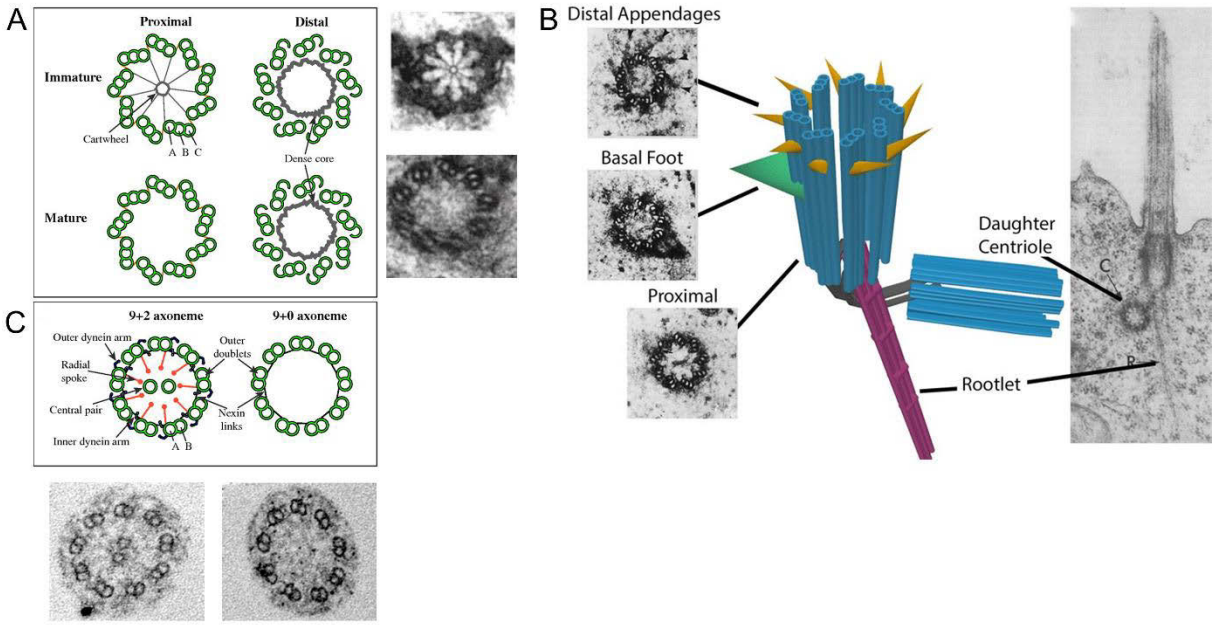

Figure 15. Ultrastructure of centrioles and ciliary axonemes. (A) Centrioles are formed by triplets of microtubules (A, B and C) that display nine-fold symmetry. In immature centrioles and basal bodies, they present in their proximal lumen a structure known as the cartwheel, formed by a central hub and spokes that connect with the inner A microtubule. Cross-sections of centrioles with and without cartwheel are displayed on the right, as seen via electron microscopy. (B) On the external walls of their barrel-like structure, centrioles display a series of structures, like distal and subdistal (not shown) appendages, a basal foot and a filamentous rootlet, essential for membrane anchoring, cilia nucleation and, consequently, its function. (C) Cilia are membrane protrusions that contain a microtubule-based structure known as the axoneme. Like centrioles, it presents nine-fold symmetry, but it is composed of doublets, and not triplets, of microtubules. These are linked together by nexin connections and, in motile cilia, present outer and inner dynein arms, motor complexes essential for ciliary bending. Motile cilia also have a pair of central microtubules and radial spokes, which is the reason why they are said to contain a 9+2 axoneme, whereas immotile cilia do not present central microtubules or spokes. They present a 9+0 axoneme. Cross-sections of 9+2 and 9+0 cilia with and without a central pair of microtubules, respectively, are shown below, as seen via electron microscopy. Images adapted and modified from Dawe, Farr and Gull, 2007, Nakazawa *et al.*, 2007, Voronina *et al.*, 2009, Garcia and Reiter, 2016 and Zhu *et al.*, 2019.

2.1.4.2. Centriole amplification in MCCs

In order to achieve the high centriole numbers characteristic of MCCs, vertebrates have evolved specific mechanisms that differ from normal centriole duplication in cycling cells (Zhao et al., 2013). Two distinct modes of centriolar amplification co-exist in them: the centriolar pathway, highly similar to centriole duplication in cycling cells, and the *de novo* or deuterosomal pathway. Both act simultaneously and in a synchronous manner in MCCs during a centriole amplification pathway that comprises several stages (Al Jord et al., 2014; Mercey et al., 2019b).

In postmitotic monociliated ependymal progenitors, the Deup1 and Ccdc78 proteins are recruited to the daughter centriole. These form part of the deuterosomes, electron-dense platforms that can nucleate procentrioles during their maturation (Sorokin, 1968). The aforementioned deuterosomal proteins are in turn responsible for the recruitment of Cep152 and Plk4, essential in centriole biogenesis (Sonnen et al., 2013). This happens, though, differently from centriole duplication. Whereas in cycling cells, these two proteins are symmetrically located in mother and daughter centrioles in order to perform semiconservative centriole duplication (each new centrosome is formed by a mother and a newly formed daughter centriole), in ependymal progenitors, they are asymmetrically recruited with higher presence on the daughter centriole (Al Jord et al., 2014). As new deuterosomes are formed on the proximal wall of the daughter centriole, spherical assemblies of these platforms and new procentrioles are formed. One or two deuterosomes are formed at the same time on the daughter centriole and later released into the cytoplasm with the procentrioles attached to them. Several rounds of this process follow so that, when observed via structured illumination microscopy, these appear as rings or *halos* in the cytoplasm that are positive for Sas6. Thus this is called the *halo* or amplification phase of centriole multiplication (Al Jord et al., 2014) (Figure 16A). Once all spherical assemblies are formed and released into the cytoplasm, a synchronous growth of the procentrioles and the acquisition of some mature centriolar markers (like GT335 antibody labeling, which corresponds to glutamylated tubulin) occurs. When using time-lapse fluorescence microscopy methods, this process is observed as an intensification of the halo signals, disposed in a ring like the “petals” of a flower, around the deuterosomes and is hence known as the *flower* or growth phase of centriole amplification (Figure 16B). The process concludes with a simultaneous detachment of the procentrioles from the deuterosomes in the so-called disengagement phase, and their apical migration and docking to the plasma membrane. After that, each now mature centriole or basal body nucleates a single motile cilium (Figure 16C). This deuterosomal pathway contributes to the formation of 90% of the basal bodies (Al Jord et al., 2014).

Synchronously to this process, the centriolar pathway is responsible for the formation of about 10% of the new basal bodies. As deuterosomes are formed on the wall of the daughter centriole during the halo stage, procentrioles also start to grow on the proximal segment of the mother and daughter centrioles, displaying an orthogonal configuration, just like during centriole duplication in cyclinc cells. At the same time as procentrioles start growing from deuterosomes in the flower stage, procentrioles budding from the mother and daughter centrioles do so as well. And finally, the disengagement from these is also coordinated with the detachment of procentrioles from deuterosomes (Figure 16C) (Al Jord et al., 2014).

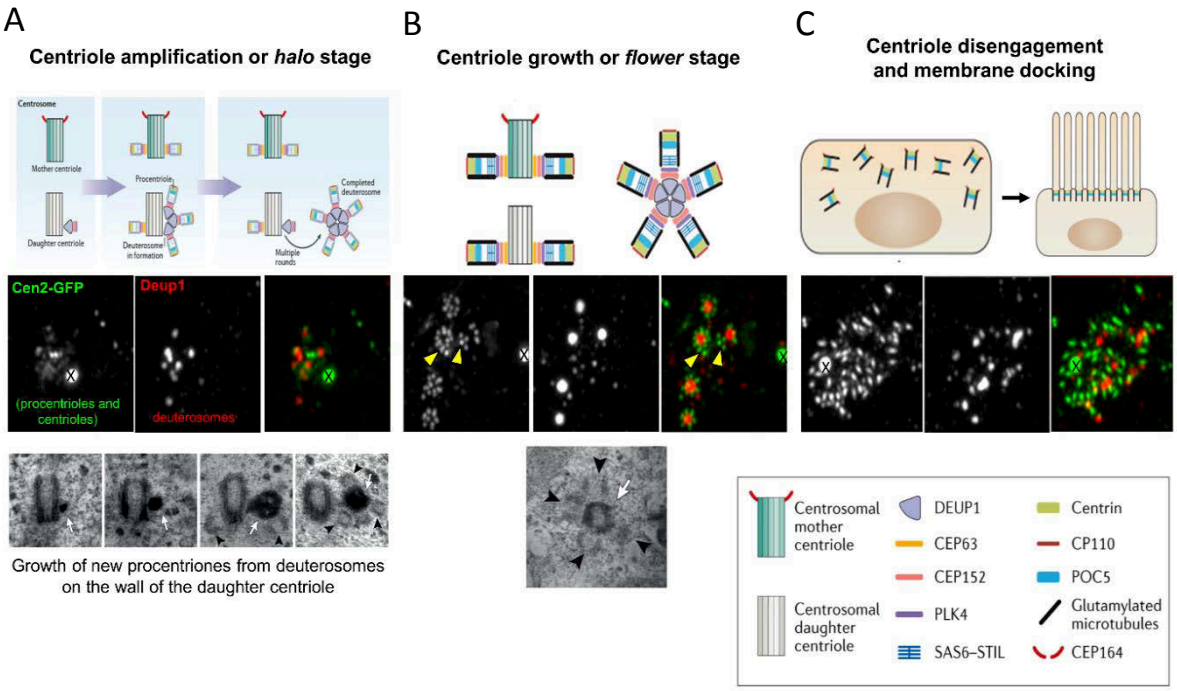

Figure 16. Process of centriole amplification in multiciliated cells. Centriole amplification in MCCs is a stepwise, highly synchronous process that entails several stages. (A) During the *halo* or amplification phase, procentrioles start to form mainly from electron-dense platforms called deuterosomes, made of the protein Deup1. Simultaneously to the deuterosomal pathway, a minority of procentrioles arise on the proximal wall of the mother and daughter centrioles, in the centriolar pathway. Several rounds of this process occur in which deuterosome-attached procentrioles are released into the cytoplasm. This process has been studied via immunofluorescence, in which small rings or halos are visible in a transgenic mouse line that expresses the centriolar protein Centrin-2 fused to the GFP (in green) (Higginbotham et al., 2004). The mother and daughter centrioles are seen as two close bright spots and a centrin-2-GFP big aggregate (with an "X" on top) is formed inevitably in this line during centriole amplification. The halos are associated to spherical structures labeled with an antibody that recognizes Deup1 (red) (unpublished, Spassky group images). TEM analysis reveals that the deuterosomes (white arrows) nucleate nascent procentrioles (black arrows) and form on the wall of the daughter centriole during the *halo* phase. (B) Procentrioles start growing attached on the deuterosomes or on the walls of the mother and daughter centrioles during the growth or *flower* phase. The two paralogs Deup1 and Cep63 control one process or the other, respectively. Proteins essential for centriole duplication in cycling cells, such as Cep152 and Plk4 are also present in centriole amplifications in MCCs, as well as the cartwheel protein Sas6.

During this phase procentrioles grow in size and acquire mature centriole traits, like glutamylated tubulin or protein of centriole 5 (POC5). Distal proteins like Cp110, which regulates axonemal length, are also recruited to the procentrioles on this stage. When observed via immunostaining, growing procentrioles arrange themselves like the petals of flower, around the now bigger deuterosome spheres or around the mother and daughter centrioles (yellow arrowheads, unpublished, Spassky group images). This can also be seen in TEM images, where procentrioles (black arrowheads) are seen budding from a black, electron-dense deuterosome (white arrow). (C) Mature centrioles disengage simultaneously from the deuterosomes and mother and daughter centrioles and migrate to the apical membrane, where they dock and nucleate the motile cilia that can now grow. Adapted from Spassky and Meunier, 2017 and unpublished images of the Spassky team.

2.2. The neurogenic niche, adult neural stem cells and adult neurogenesis

Multiciliated ependymal cells line the ventricular cavities forming a continuous barrier of epithelial cells that separate the CSF from the SVZ and the rest of the brain parenchyma in the adult. Apart from their multiple basal bodies, characterized by EM, they possess lateral processes interdigitated with those of other ependymal cells, microvilli and an electron-luscent cytoplasm where numerous mitochondria and a large spherical nucleus can be found (Doetsch et al., 1997). Most ependymal cells are discernable by the presence of multiple long motile cilia and a large apical contact with the ventrcicular lumen. However, a subclass of ependymal cells, called E2, are biciliated with a somewhat less extense apical contact, longer cilia and a 9+2 axoneme. They also differ from the classic ependymal cells because their mitochondria are located around the nucleus, and not near the basal bodies. They were discovered only slightly over ten years ago because their frequency on the wall is more than ten times smaller than regular ependymal cells (Mirzadeh et al., 2008). In contrast, these biciliated cells have been shown to be the most prevalent cell type on the spinal cord VZ, lining the central canal. Furthermore, unlike MCCs on the lateral ventricle, E2 cells of the spinal cord have been shown to proliferate in the spinal cord under physiological conditions, but they have not been described to migrate away from the VZ and differentiate into neurons or glia (Alfaro-Cervello et al., 2012).

Back to the ventricular-subventricular zone (V-SVZ), other important cell types have been identified. One of the most important is SVZ astrocytes. These are called B1 cells and present irregular contours, an invaginated nucleus, an electron-luscent cytoplasm and abundant intermediate filaments, cytoskeletal components heavily composed of GFAP, a marker of astrocytes. They are located in close contact with ependymal cells. They extend

many processes to the ependymal layer and their cell body is located immediately beneath the ependyma. They present a short apical process, squeezed in between the ependymal cell bodies, that ends in the ventricular surface forming a small apical contact, more than ten times smaller in average than the one of ependymal cells. These B1 cells also present a primary cilium on their ventricular contact, protruding into the ventricular lumen, with a 9+0 axoneme. (Doetsch et al., 1997; Mirzadeh et al., 2008). They are generated from RGCs, as it was shown by the same experiment performed by Spassky et al. in 2005 to prove RGCs were precursors of ependymal cells. RGCs persist until the next postnatal week and extend a long process from their cell body in the VZ until the pial surface. The injection of a Cre-expressing adenovirus in a Cre reporter mouse at P0 away from the ventricle, in the brain parenchyma, led to labeling of RGCs away from the site of infection, since the viruses entered RGCs through their long extending processes. These reporter-positive RGCs differentiated a few days later into $GFAP^+$ astrocytes of the V-SVZ, along with other cell types (Merkle et al., 2004). However, it was seen via retroviral barcoding (see Chapter 1 – 1.4.2. Clonal analysis techniques) that B1 cell-precursors diverge from the other forebrain cell lineages during mid-fetal gestation (E13-E15) and then remain largely quiescent until their reactivation at different times during the adult life (Fuentealba et al., 2015). It was suggested that B1 progenitor cells slow down their cell cycle via upregulation of p57 in the embryo to become this quiescent-like cells described before (Furutachi et al., 2015).

B1 cells in the V-SVZ are found single or forming clusters of cells that display small ventricular contacts, surrounded by ependymal cells with large apical contacts, arranged in a rosette-like or pinwheel structure (Figure 17A), as it is seen on ventricular wholemounts immunostained with cell-cell adhesion markers, like β-catenin or Zonula occludens protein 1 (ZO-1) (Figure 17B).

The other two major types of the V-SVZ are B2, C and A cells, which do not display apical contacts and hence do not form part of the superficial pinwheel structure. B2 cells are rather multipolar astrocytes with a stellate morphology like parenchymal astrocytes and are localized basally to ependymal and E cells, in the interface between the V-SVZ and the striatal parenchyma (Platel and Bordey, 2016). C cells are immature neuronal-committed progenitors with fewer processes than B1 cells, a more spherical shape and a cytoplasm that is more electron-dense than that of B1 astrocytes. Its nucleus is also highly invaginated and it does not

present the intermediary filaments characteristics of B1 cells. Finally, A cells are neuroblasts with electron-dense cytoplasms and an occasionally invaginated nucleus. They possess a thin leading process and a thick trailing one, a morphology typical of migrating immature neurons. They form tangential migrating chains that split and separate along the antero-posterior axis of the V-SVZ. They are separated from the striatum and the ependyma by extensions of B2 and B1 cells that form sheaths around such cell chains (Doetsch et al., 1997, 1999a) (Figure 17A).

Other minority cell types identified in the V-SVZ are tanycytes, which are defined as specialized ependymal cells that extend long processes into the brain parenchyma (Furube et al., 2020), and microglia, which fulfil immunological functions in the CNS (Doetsch et al., 1997).

B1, C and A cells form a lineage continuum that is the base of adult neurogenesis. This is the formation of neurons *de novo*. The brain had long been considered a non-renewable structure, with virtually no generation of new neurons. Until, in the 1960s, Altman proved, upon [^{3}H] thymidine treatment in rats and autoradiographic detection, the presence of a migratory stream of cells from the subependymal layer to the olfactory bulb (Altman, 1969). Later, with the coming of genetic engineering and the use of transgenic animals, adult neurogenesis could be further demonstrated with tissue grafts. Thus, when neuroblasts labeled with a reporter (β-galactosidase) were implanted in the adult SVZ of a wild type (blank background tissue) mouse via stereotaxic injections, the former were seen migrating to the olfactory bulb. Besides, injections in other areas yielded no migration of the donor's transgenic neuroblasts (Lois and Alvarez-Buylla, 1994). Shortly afterwards, the identity of the adult NSC precursor was revealed. Treatment with the anti-mitotic agent cytosine-β-D-arabinofuranoside led to the depletion of neuron progenitors (C cells) and neuroblast (A cells) migrating chains in mice SVZ, due to consumptive divisions and migration, respectively, but left ependymal and what are now known to be B1 cells intact in the V-SVZ. Of these two, only the astrocytes, but not the ependymal cells, showed proliferative capacity and were from then on appointed as the primary adult NSCs of the V-SVZ neurogenic niche (Doetsch et al., 1999a, 1999b).

In the adult rodent, four in five B1 cells undergo symmetric consumptive divisions to generate two transit-amplifying C cells, whereas the other 20% perform symmetric proliferative divisions to maintain the pool of adult NSCs. Asymmetric self-renewing divisions

are thought to be absent. A direct consequence of this cell division dynamics is that B1 cell density and adult neurogenesis decrease significantly with age (Obernier et al., 2018). C cells are rapidly-dividing progenitors organized in clusters juxtaposed in between the chains of migrating neuroblasts that have been proposed to divide symmetrically around three times before being consumed in a symmetric division that generates two A cells. Lastly, these neuroblasts have also been found to divide once or twice before reaching their final destination in the olfactory bulb (Doetsch et al., 1999b; Ponti et al., 2013). Once they are generated in the SVZ, they migrate tangentially to join the rostral migratory stream (RMS), a network of interconnecting paths that leads neuroblasts rostrally, away from the SVZ, into the olfactory bulb. There, they migrate radially and differentiate into granule cells or periglomerular neurons (Doetsch et al., 1999b; Lim and Alvarez-Buylla, 2016).

Adult neurogenesis is a well-established phenomenon in rodents who, although with a significant decline over the years, produce thousands of new neurons every day (Kriegstein and Alvarez-Buylla, 2009) (Figure 17C). New neurons have also been found to generate *de novo* in invertebrates (Brenneis and Beltz, 2019), birds (Alvarez-Buylla and Kirn, 1997), or fish, a group where zebrafish has emerged as a potent model of constitutive neurogenesis throughout life and neural regeneration upon injury (Kizil et al., 2012; Ogino et al., 2016). However, adult neurogenesis in humans remains a matter of controversy.

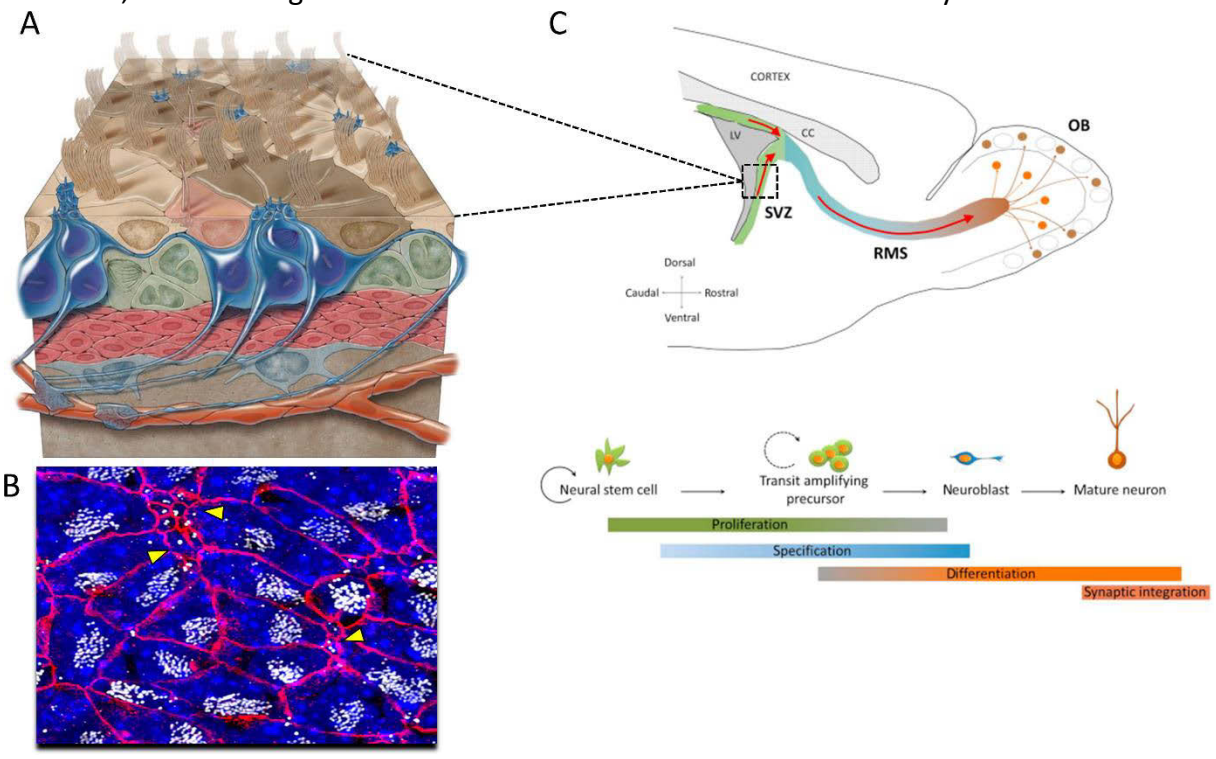

Figure 17. Pinwheel architecture in the Ventricular-Subventricular zone and adult neurogenesis. (A) Schematic representation of the V-SVZ neurogenic niche. Multiciliated ependymal cells (brown cells) present large apical contacts, from which the motile cilia protrude into the ventricular lumen. They arrange themselves around the small apical contacts of adult neural stem cells or B1 cells (blue cells), from which a primary cilium protrudes into the lumen, forming a pinwheel structure as seen on V-SVZ wholemounts. B1 cells extend a basal process that contacts blood vessels. Rapid transient-amplifying progenitors or C cells (green cells) divide in the SVZ and generate neuroblasts or A cells unsheathed by the processes of B1 cells. Other minority cells in the neurogenic niche are biciliated ependymal cells or E2 cells (pink cells) and B2 astrocytes (light blue cells). Adapted from (Mirzadeh et al., 2008). (B) Labeling of V-SVZ wholemounts with cell-cell adhesion markers like β-catenin (in red) reveals the pinwheel structure in the neurogenic niche, with ependymal cells characterized by the presence of multiple basal bodies (in white) around small apical contacts with two centrioles on the surface (yellow arrowheads). (C) The SVZ neurogenic niche is one of the two sites of adult neurogenesis. B1 cells divide symmetrically to generate C cells, which are committed to the neuronal lineage and divide rapidly to give rise to A cells. These migrate in chains out of the SVZ to form the Rostral Migratory Stream (RMS) to the olfactory bulb (OB), where they differentiate into interneurons and integrate the local circuitry. Adapted from De Chevigny, Cremer and Coré, 2017.

We have used the *Brainbow* and MADM techniques reviewed earlier (see Chapter 1 – 1.4.2.1. The *Brainbow* technique and 1.4.2.2. Mosaic Analysis with Double Markers) to establish the clonal relationships between multiciliated ependymal cells and B1 cells in the formation of the neurogenic niche. These have also helped us elucidate the mode of cell division of their progenitors, as well as the temporality of generation of both cell types.

2.2.1. Adult neurogenesis in humans

In 1998, the first clear evidence pointing towards the existence of adult neurogenesis in humans was published. A limited number of cancer patients, who were given BrdU for diagnostical purposes, were examined post-mortem in the look for $BrdU^+$ cells displaying mature neuronal markers like NeuN. Some of these cells were identified in the second neurogenic niche that has been identified in vertebrates: the subgranular zone (SGZ) of the dentate gyrus of the hippocampus. Some cells with proliferative markers were also found in the SVZ, but failed to correlate with NeuN or GFAP (Eriksson et al., 1998). The presence of an RMS and immature neurons with cell markers like doublecortin (DCX) and the proliferation marker Ki67 were observed in the SVZ of infants. However, these cells were later undetectable in older children (Sanai et al., 2011). Other studies have reached similar conclusions, claiming that proliferating $Ki67^+$ cells in the SVZ and SGZ of the hippocampus immunoreactive for DCX can be found in young children, but not in older ones or adults (Dennis et al., 2016; Sorrells et al., 2018). However, as it was previously stated, this remains an area of controversy, since

other groups have reported the presence of unchanged adult neurogenesis in the SGZ until the tenth decade of human life, with a noticeable decrease in this activity in patients of Alzheimer's disease, using the same immature neuronal marker DCX, among others (Boldrini et al., 2018; Moreno-Jiménez et al., 2019).

These studies make clear the difficulty of performing studies in human adult tissues, due to the rare optimum brain tissue availability, the handling of post-mortem samples and the lack of noninvasive research methods (Kumar et al., 2019). A thorough study that evaluates the impact of fixation and pre-immunostaining treatments has been published (Flor-García et al., 2020). The authors insist on the importance of assessing differences in antibody sensitivity used on immunohistochemistry studies, tissue handling or post-mortem delay to produce robust data in the research of human adult neurogenesis.

2.3. The Geminin family: regulators of DNA replication with a role in multiciliogenesis

The Geminin family is formed by three evolutionary conserved and homologous interacting proteins. These are Geminin, Mcidas and GemC1. They all present a central domain called coiled-coil, homologous among one another (Balestrini et al., 2010; Pefani et al., 2011; Quinn et al., 2001). Based on this domain, Geminin is conserved throughout vertebrates, from humans and mice to amphibians (*Xenopus*) and fish (zebrafish), but also invertebrates (*Caenorhabditis elegans* and *Drosophila*), where it carries out some of the best described functions of vertebrate Geminin (Kroll, 2007; Pefani et al., 2011; Quinn et al., 2001). On the contrary, the coiled-coil domain of Mcidas and GemC1 is conserved throughout vertebrates, including human, mouse, amphibians and fish, but they are absent in invertebrates (Balestrini et al., 2010; Pefani et al., 2011; Zhou et al., 2015). Besides this domain, Mcidas and GemC1 are homologous in another C-terminal domain, named TIRT, conserved at least in humans, mice and *Xenopus*. Thus, Mcidas and GemC1 would be paralogs that arose from a primordial Geminin gene, probably at the double round of genome duplication that originated the vertebrate genome (Terré et al., 2016).

Geminin was the first member of the family to be discovered. It was identified in two independent cDNA screens of genes that would have an impact on *Xenopus* development.

One of them identified it as a nuclear protein degraded during mitosis, during the metaphase to anaphase transition, due to the presence of a destruction box on its N-terminal domain. Such motif is the target of the anaphase-promoting complex, a multiprotein complex that promotes ubiquitination of its substrates and hence promotes its degradation. Geminin that lacked such motif or its over-expression inhibited DNA replication, but only at the moment of replication firing. The coiled-coil domain was necessary for this function (McGarry and Kirschner, 1998). The mechanism for this role in DNA replication control was later elucidated. Wohlschlegel et al. proved that Geminin could bind to the Cdt1 protein (Wohlschlegel et al., 2000), a licensing factor that is recruited to the origins of replication during G1 to assemble the pre-replication complex (pre-RC). Cdt1 is necessary, along with Cdc6, for the recruitment of the mini-chromosome maintenance complex, formed by six proteins (MCM2-7) (Figure 18). This is the core component of the replicative DNA helicase, which unwinds the DNA double helix to ensure DNA synthesis by the DNA polymerase. Its successful loading onto replication origin DNA entails origin licensing (Pozo and Cook, 2016). Geminin expression is upregulated during S phase and persist through G2 and, by sequestering Cdt1, it ensures there is no re-replication of the genome. Geminin would thus be an additional mechanism emerged in evolution to ensure DNA is replicated only once per cell cycle (Wohlschlegel et al., 2000).

Because of its function in DNA replication regulation, Geminin ablation in embryonic stem cells causes re-replication and polyploidy, the generation of abnormal nuclei, activation of the DNA damage response, checkpoint activation and finally, apoptosis, unless Cdt1 is also depleted. Thus, Geminin KO homozygous mice die at pre-implantation stages and do not progress from the morula eight-cell stage (Gonzalez et al., 2006; Hosogane et al., 2017). Loss of Geminin in cycling cells lead to polyploidy, thus ascertaining its role to prevent endoreplication (Tachibana et al., 2005).

The other screen performed by the Kirschner group in 1998 put forth the idea that Geminin as a binary agent, not only involved in DNA replication regulation, but also in development. The injection of geminin RNA could induce the acquisition of a neuroectoderm fate in detriment of the superficial ectoderm, which becomes the epidermis. The mechanisms described herein implied the inhibition of epidermal keratin and BMP4 signaling, which is complementary and non-overlapping with Geminin in *Xenopus* embryos, as well as the induction of early pro-neural genes and the expression of Geminin in a positive-feedback loop

(Kroll et al., 1998). Furthermore, its conditional deletion in the neural tube has been shown to cause patterning defects in said structure, independently of cell cycle progression and without apoptosis, with ventral neuron generation and dorsal progenitor specification highly impaired (Patterson et al., 2014).

The expression of Geminin is high in embryonic stem cells and the epiblast, precursor of the three germ layers, and it helps maintain the expression of the pluripotency factors Oct4, Sox2 and Nanog. It also inhibits trophoblast fate and promotes the generation of a neural precursor lineage in detriment of the mesodermal one *in vitro*. Its conditional ablation in the developing cortex is responsible for an enrichment of the progenitor pool, whereas its over-expression favors the generation of terminally-differentiated neurons (Patmanidi et al., 2017).

In all, Geminin is a binary actor that can influence the transcription of many genes to establish fate commitment at different stages during development and regulate cell cycle progression due to its role in DNA replication regulation.

Mcidas, like Geminin, has been proposed to participate in cell cycle control and cell fate decisions. It forms heterodimers with Geminin via their homologous coiled-coil domains and tampers with Geminin function in DNA replication licensing, probably by sequestration (Caillat et al., 2013; Pefani et al., 2011). It has nonetheless not been described to be an active part of the pre-RC, like GemC1 (Figure 18).

Mcidas encodes a nuclear protein called Multicilin that has been involved in cell fate acquisition. Namely, in this respect, it was firstly described to be necessary and sufficient for MCC generation in the *Xenopus* embryo epidermis. In this report, Multicilin was shown to be downstream of Notch, which is able to inhibit the former's influence on multiciliation (Stubbs et al., 2012). This protein does not act alone, but it associates with transcription factors E2F4 or E2F5 and their co-activor Dp1 to form a ternary complex called EDM via their C-terminal TIRT domain. The transcriptional activity of this complex transactivates a series of genes related to MCC fate specification, such as *foxj1*, *c-myb* and *rfx2*. Centriole biogenesis gene transcription is also regulated by the EDM. Among these they were found structural components of the centriole, regulators of new centriole biogenesis at the proximal pole of the mother centriole (*plk4*, *cep152*, *sas6*), essential agents of the deuterosomal pathway, such as *deup1*, or cyclin O (*ccno*) (Ma et al., 2014). The latter is a gene necessary for the assembly

of deuterosomes whose ablation causes hydrocephaly, mucociliary clearance defects and reduced ciliary numbers in MCCs (Funk et al., 2015). Much like Multicilin inhibits Geminin function in DNA replication licensing inhibition, Geminin can bind the EDM complex and hinder its function in MCC specification (Ma et al., 2014).

Mcidas is located in a conserved locus that also contains *ccno* and *cdc20b*. The latter bears the sequence of the miR-449 non-coding molecule that were discussed before and who have been suggested to be upstream of the MCC specification cascade. Mutations in *mcidas* or *ccno* are present in a human syndrome called congenital mucociliary clearance disorder, characterized by the presence of lesser numbers of cilia and basal bodies (Boon et al., 2014).

Much like Geminin, Mcidas or Multicilin seems to have a binary role. On the one hand, it can hinder Geminin's action in DNA replication inhibition. On the other, it is directly responsible for the expression of genes essential for the MCC stage.

The third member of the Geminin family, GemC1 (Geminin coiled-coil domain-containing protein 1) was discovered in 2010 in an open reading frame sequence homology search with already known DNA replication factors. That is how it was found that the *Xenopus* sequence of GemC1 is homologous in its coiled-coil domain to that of Geminin, and that it is conserved in vertebrates. Blocking the action of GemC1 by neutralizing antibodies resulted in the inhibition of DNA replication in *Xenopus* egg extract. When using morpholinos to knock-down its expression in the fertilized egg, a delay in embryo development, a decrease in cell density and total DNA content reduction was reported (Balestrini et al., 2010).

GemC1 interacts with various components of the pre-RC. Namely, CDK2-Cyclin E, TopBP1 and Cdc45. The first two are needed for GemC1 loading onto the chromatin, being GemC1 a phosphorylation substrate of CDK2. Constitutive phosphorylation of GemC1 leads to an increase in DNA replication due to enhanced origin firing. GemC1 is needed for Cdc45 recruitment to replication origins (Balestrini et al., 2010), a proliferation-associated marker that is part of the replicative helicase, along with MCM2-7 and the GINS complex for unwinding of the DNA. It is this denaturation activity that permits the DNA polymerase to load onto the exposed DNA and initiate synthesis of the new strands (Köhler et al., 2016). The same role as promoter of DNA replication firing was found to be essential as well in mammalian cells *in vitro*, namely mouse NIH 3T3 fibroblasts (Balestrini et al., 2010).

GemC1 is upstream of Mcidas and induces its expression in MCC progenitors. Both are sufficient and necessary for the transformation of RGCs into ependymal MCCs in the neurogenic niche, since their over-expression leads to supernumerary MCCs and their knock-down diminishes their differentiation, in RGCs both *in vivo* and *in vitro*. In turn, GemC1 in the telencephalon has been shown to be downstream of Notch activity, which inhibits both neurogenesis and ependymal generation, and promotes RGCs to stay undifferentiated (Kyrousi et al., 2015). This functional hierarchy has also been shown in lower vertebrates, like zebrafish, where Notch signaling blockage causes the differentiation of MCCs in the kidney tubules at the expense of monociliated cells. In these animals GemC1 also acts upstream of Mcidas and their KD leads to the absence of the mammal *foxj1* ortholog *foxj1b* (Zhou et al., 2015).

For these reasons, GemC1 has been defined as a master gene of multiciliogenesis. It directly transactivates *mcidas* and *foxj1* expression by binding to their promoter sequences in mouse cells. Mcidas is also able to bind its own promoter and that of *foxj1* to enhance gene expression. In the same way that Mcidas forms a ternary complex with E2F transcriptions factors and Dp1, GemC1 co-operates with E2F4 or E2F5 and Dp1, forming a complex called EDG, for which its TIRT domain in necessary. This protein formation regulates gene expression *in vivo*, in mouse trachea and oviduct, of genes that are essential for centriole amplification, much like Multicilin. Apart from MCC specification genes like *foxJ1* and *mcidas*, it triggers the expression of *deup1, ccno* and, in a milder fashion, *plk4* and *cep152* (Arbi et al., 2016; Terré et al., 2016).

In the same way as Mcidas, GemC1 interacts through its coiled-coil domain with Geminin (Caillat et al., 2015). On the one hand, although it has not been shown directly like with Mcidas (Pefani et al., 2011), it is likely that GemC1 modulates the function of Geminin when co-expressed in cells by hindering its activity in DNA replication inhibition (Caillat et al., 2015). On the other hand, Geminin expression has been proved to impede GemC1-dependent transactivation of genes like *foxj1* (Arbi et al., 2016; Terré et al., 2016).

Two KO models of GemC1 have been generated. They both display the same phenotypes, with litters born at normal ratios, hence suggesting its function is not crucial during development, but poor postnatal growth. They are devoid of MCC in the airways and present testes hypocellularity and low sperm count in males, as well as a loss of primordial

and secondary follicles and absence of MCCs in the oviduct, in females. These histological traits lead to infertility of GemC1 KO homozygous mice, and the premature death likely caused by defects in airway mucus clearance. These mice also display hydrocephalus with high penetrance, due to the acquisition of NSC traits on the ventricular wall, in detriment of MCCs (Arbi et al., 2016; Lalioti et al., 2019a; Terré et al., 2016).

Figure 18. Role of DNA pre-replication complex. The Geminin family plays a role in DNA replication initiation.

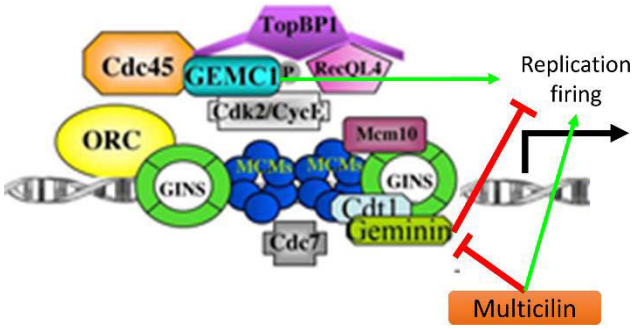

Geminin interacts with Cdt1, a licensing factor that is necessary for the recruitment of MCM2-7 to the chromatin and open it for replication. Hence, Geminin inhibits replication firing. Multicilin does not have a direct role on replication firing, but its interaction with Geminin through their homologous coiled-coil domains can prevent Geminin from fulfilling the role just described. Finally, GemC1, the third member of the family is recruited to chromatin by TopBP1 and is the substrate of CDK2-CyclinE. Upon phosphorylation, it recruits Cdcd45 to the chromatin, where it contributes as part of the replicative helicase to open the double strand of DNA for it to be accessible for the DNA polymerase. Adapted from Balestrini *et al.*, 2010.

2.4. Objectives and hypotheses

Even though Geminin has not been implicated in multiciliated epithelia cell fate acquisition, its antagonist GemC1 has been established as a master gene of multiciliogenesis in all multiciliated cell-bearing mammal epithelia. This has prompted us to investigate the molecular mechanisms that govern the establishment of the neurogenic niche, notably if Geminin family members can alter the modes of divisions and modify the final output of neurogenic niche cells. We hypothesized that both Geminin family members, since they have antagonistic functions in DNA replication, they could also have them in cell fate specification. This has made part of the article published in *Neuron* in March, 2019, to complement the lineage analysis study performed with *Brainbow* and MADM.

Article 1.

Adult Neural Stem Cells and Multiciliated Ependymal Cells Share a Common Lineage Regulated by the Geminin Family Members. Published in *Neuron* (2019)

Article

Neuron

Adult Neural Stem Cells and Multiciliated Ependymal Cells Share a Common Lineage Regulated by the Geminin Family Members

Highlights

- High-throughput clonal analysis shows a common origin of ependymal and B1 stem cells
- Ependymal cells are mostly produced through symmetric divisions
- B1 cells are generated through asymmetric divisions with ependymal cells
- Geminin family members tune the proportion of ependymal and B1 stem cells in clones

Authors

Gonzalo Ortiz-Álvarez, Marie Daclin, Asm Shihavuddin, ..., Alice Meunier, Auguste Genovesio, Nathalie Spassky

Correspondence

nathalie.spassky@ens.fr

In Brief

Adult neurogenesis persists in mammals. Ortiz-Álvarez et al. analyze the clonal relationship among ependymal cells and B1 astrocytes, which together compose the adult neurogenic niche. They show that their proportion is tuned by the DNA replication regulators Geminin and GemC1.

Ortiz-Álvarez et al., 2019, Neuron *102*, 159–172
April 3, 2019 2019 The Author(s). Published by Elsevier Inc.
https://doi.org/10.1016/j.neuron.2019.01.051

CellPress

Neuron
Article

Adult Neural Stem Cells and Multiciliated Ependymal Cells Share a Common Lineage Regulated by the Geminin Family Members

Gonzalo Ortiz-Álvarez,[1,6] Marie Daclin,[1,6] Asm Shihavuddin,[1,5] Pauline Lansade,[1] Aurélien Fortoul,[1] Marion Faucourt,[1] Solène Clavreul,[2] Maria-Eleni Lalioti,[3] Stavros Taraviras,[3] Simon Hippenmeyer,[4] Jean Livet,[2] Alice Meunier,[1] Auguste Genovesio,[1] and Nathalie Spassky[1,7,*]

[1]Institut de Biologie de l'Ecole Normale Supérieure (IBENS), Ecole Normale Supérieure, CNRS, INSERM, PSL Université Paris, 75005 Paris, France
[2]Sorbonne Université, INSERM, CNRS, Institut de la Vision, 75012 Paris, France
[3]Department of Physiology, Medical School, University of Patras, 26504 Rio, Patras, Greece
[4]Institute of Science and Technology Austria, Am Campus 1, 3400 Klosterneuburg, Austria
[5]Present address: Department of Applied Mathematics and Computer Science, Technical University of Denmark (DTU), 2800 Kgs. Lyngby, Denmark
[6]These authors contributed equally
[7]Lead Contact
*Correspondence: nathalie.spassky@ens.fr
https://doi.org/10.1016/j.neuron.2019.01.051

SUMMARY

Adult neural stem cells and multiciliated ependymal cells are glial cells essential for neurological functions. Together, they make up the adult neurogenic niche. Using both high-throughput clonal analysis and single-cell resolution of progenitor division patterns and fate, we show that these two components of the neurogenic niche are lineally related: adult neural stem cells are sister cells to ependymal cells, whereas most ependymal cells arise from the terminal symmetric divisions of the lineage. Unexpectedly, we found that the antagonist regulators of DNA replication, GemC1 and Geminin, can tune the proportion of neural stem cells and ependymal cells. Our findings reveal the controlled dynamic of the neurogenic niche ontogeny and identify the Geminin family members as key regulators of the initial pool of adult neural stem cells.

INTRODUCTION

Neurons and glial cells are continuously produced throughout life. In the adult, a subpopulation of astrocytes (type B1) located in the ventricular-subventricular zone (V-SVZ) region of the lateral ventricles (LVs) retain stem cell properties; i.e., self-renewal and multilineage differentiation (Doetsch et al., 1999). These cells have a multipolar shape, contact both the LV and the blood vessels, and are surrounded by multiciliated ependymal cells (Shen et al., 2008; Tavazoie et al., 2008; Mirzadeh et al., 2008). The coordinated beating of ependymal cilia contributes to cerebrospinal fluid (CSF) dynamics, which is crucial for the exposure of type B1 cells to trophic and metabolic signals and to clear toxins and waste from the brain (Spassky and Meunier, 2017). Proper functioning of adult neurogenesis thus depends on the production and positioning of the controlled number of ependymal cells and type B1 astrocytes composing the neurogenic niche.

Type B1 astrocytes and ependymal cells are both derived from radial glial cells (RGCs) between embryonic day 13.5 (E13.5) and E15.5 and progressively acquire identical phenotypic markers (Sox2, Sox9, Nestin, and CD133) (Ferri et al., 2004; Mirzadeh et al., 2008; Sun et al., 2017). However, in the adult, these cells have very different morphologies and fulfill different functions: e.g., although B1 astrocytes are reactivable quiescent neuronal progenitors, multiciliated ependymal cells are postmitotic throughout life (Fuentealba et al., 2015; Furutachi et al., 2015; Shah et al., 2018; Spassky et al., 2005). It is totally unknown how these cells are allocated to the neurogenic niche and how they acquire their common characteristics and distinct identities and functions.

Recent studies have demonstrated that GemC1 and Mcidas are early regulators of multiciliogenesis in different organs (Arbi et al., 2016; Boon et al., 2014; Kyrousi et al., 2015; Ma et al., 2014; Stubbs et al., 2012; Terré et al., 2016; Zhou et al., 2015). Interestingly, these coiled-coil proteins, together with their antagonist Geminin, are part of the Geminin superfamily, which was initially characterized for its role in DNA replication control (Balestrini et al., 2010; McGarry and Kirschner, 1998; Pefani et al., 2011). More recently, Geminin was found to regulate neural cell fate and to be highly expressed in cycling type B1 cells in the adult SVZ (Khatri et al., 2014; Sankar et al., 2016).

Here we exploited high-resolution lineage-tracing techniques—multi-addressable genome-integrative color (MAGIC) markers (Loulier et al., 2014) and mosaic analysis with double markers (MADM) strategies (Gao et al., 2014)—in the mouse brain to show that type B1 astrocytes and ependymal cells share a common RGC progenitor. These RGCs first produce type B1 astrocytes through both symmetric and asymmetric divisions. Ultimately, ependymal cells are produced through terminal

This is an open access article under the CC BY-NC-ND license (http://creativecommons.org/licenses/by-nc-nd/4.0/).

symmetric division. We also examined the role of antagonist regulators of DNA replication (GemC1 and Geminin) in lineage progression. We show that GemC1 promotes premature symmetric division of RGCs producing ependymal cells at the expense of astrocytes, whereas Geminin favors symmetric divisions producing type B1 astrocytes. Altogether, we show that ependymal cells and type B1 astrocytes share a common lineage in which type B1 cells are produced first, followed by a majority of ependymal cells. This dynamic can be modulated by the Geminin family members.

RESULTS

Ependymal Cells Originate from Locally Differentiated RGCs

Multiciliated ependymal cells are generated from RGCs around E15 (Spassky et al., 2005). To determine how these cells develop, we performed a single injection of 5-ethynyl-2'-deoxyuridine (EdU) at E15.5 and studied the relative positions of EdU^+ ependymal cells on the ventricular walls at post-natal day 15 (P15). EdU^+ ependymal cells were often juxtaposed or close to each other (Figures S1A–S1C). To quantitatively assess their spatial distribution, we performed a nearest neighbor distance (NND) analysis on the datasets. The NNDs among EdU^+ ependymal cells were significantly shorter than in simulated random datasets, suggesting that ependymal cells born at the same time remain in the same area (Figure S1D). To further test this possibility, we employed a genetic fate-tracing strategy. We crossed the Ai14 transgenic mouse line, which expresses tdTomato after Cre-dependent excision of a "floxed stop" cassette (Madisen et al., 2010), with Emx1-Cre, Gsh2-Cre, or Nkx2.1-Cre transgenic mice, which express Cre recombinase in the dorsal-medial, lateral, and ventral regions of the LVs, respectively (Figures 1A–1C). At P10, almost all ependymal cells were tdT^+ in Cre-expressing ventricular walls (Figures 1D–1F), whereas they were tdT^- in Cre-negative regions (Figures 1G–1I), showing that ependymal cells do not migrate out of their site of origin during maturation (Figures 1J–1M). We observed similar results in all caudo-rostral regions examined. Together, these results show that ependymal cells are produced locally and do not migrate long distances from their site of origin.

IUE Labels Ependymal Cells and Type B1 Astrocytes in the V-SVZ

Given that ependymal cells develop locally from RGCs, we labeled their progenitors at E14.5 in the lateral ganglionic eminence (LGE) by *in utero* electroporation and traced their lineage at later stages. We first verified that cells targeted by *in utero* electroporation (IUE) are cycling by injecting EdU at E13.5 or E14.5. The next day, 78% ± 2% of electroporated cells were indeed EdU^+ (Figure S2), confirming that cycling cells are preferentially transfected by IUE and that progenitor fate can be traced by this technique, as shown previously (Loulier et al., 2014; Stancik et al., 2010).

We then characterized the progeny of cells electroporated at E14.5 with the H2B-GFP plasmid by immunostaining the V-SVZ at P10–P15 with FoxJ1 and Sox9 antibodies to distinguish ependymal cells ($FoxJ1^+Sox9^+$) from other glial cells ($FoxJ1^-Sox9^+$) (Sun et al., 2017; Figures 2A and 2B). We observed that around two-thirds of GFP^+ cells were ependymal cells, whereas most of the remaining $FoxJ1^-$ cells were $Sox9^+$ astrocytes (Figure 2C). We also performed FGFR1OP (FOP) and glial fibrillary acidic protein (GFAP) staining to distinguish ependymal cells (multiple FOP^+ basal bodies and $GFAP^-$) from astrocytes (FOP^+ centrosome and $GFAP^+$). Most electroporated cells close to the ventricular surface were either $GFAP^-$ ependymal cells containing multiple FOP^+ basal bodies or $GFAP^+$ astrocytes with one FOP^+ centrosome (Figure 2D). A ventricular contact emitting a primary cilium was also observed on GFP^+ astrocytes (Doetsch et al., 1999). The GFP^+ astrocytes often had an unusual nuclear morphology with envelope invaginations, as reported recently (Cebrián-Silla et al., 2017). Noteworthy, neuroblasts with their typical migratory morphology were observed deeper in the tissue and at a distance from the electroporated area in the direction of the olfactory bulb (data not shown).

To further test whether some of the astrocytes originating from the electroporated RGCs could act as adult neural stem cells (type B1 astrocytes), we permanently labeled RGCs and their progeny by IUE of a transposable *Nucbow* vector at E14.5 (nuclear MAGIC markers; Loulier et al., 2014) and administered EdU through the animals' drinking water for 14 days starting at P21 (Figure 2E). One week after the end of EdU administration, $EdU^+Nucbow^+$ neurons were observed on each olfactory bulb section, showing that cells derived from electroporated RGCs at E14.5 are adult neural stem cells that give rise to olfactory bulb neurons (Figure 2F and 2G).

These results show that electroporation of RGCs at E14.5 labels multiciliated ependymal cells and adult neural stem cells (type B1 astrocytes) that are retained in the V-SVZ at adult stages.

Lineage Tracing Using MAGIC Markers Shows that Ependymal Cells Derive from Symmetric and Asymmetric Divisions of RGCs

We then took advantage of the large panel of distinct colors produced by the MAGIC markers approach to trace and analyze the lineage of ependymal cells. The V-SVZ of P15–P20 brains electroporated with the Nucbow vector at E14.5 were immunostained with the ependymal marker FoxJ1 in far red, and colors were automatically analyzed to avoid any eye bias (Figures 3A–3C). Briefly, FoxJ1 staining was first used as a reference for the ventricular surface, and 25-μm-thick 3D image stacks of the ventricular whole-mounts were segmented as described previously (Shihavuddin et al., 2017). $Nucbow^+$ cells were then sorted as $FoxJ1^+$ or $FoxJ1^-$ (Figure S3; Figure 3D). To define the criteria that identify two cells as sister cells, 2 independent researchers manually picked 49 pairs of cells with similar Nucbow colors (Figure S4A). Both their color content (saturation, value, and hue in the RGB tridimensional space) and their 3D spatial distances were computed (Figure 3E; Figures S4B and S4C). The maximum difference found for each of these parameters was chosen as a threshold for automatic analysis of all $Nucbow^+$ cells in each brain (Figures S4D–S4G). This automatic analysis of all cells from 6 electroporated brains (corresponding to a total of 7,668 $Nucbow^+$ cells and

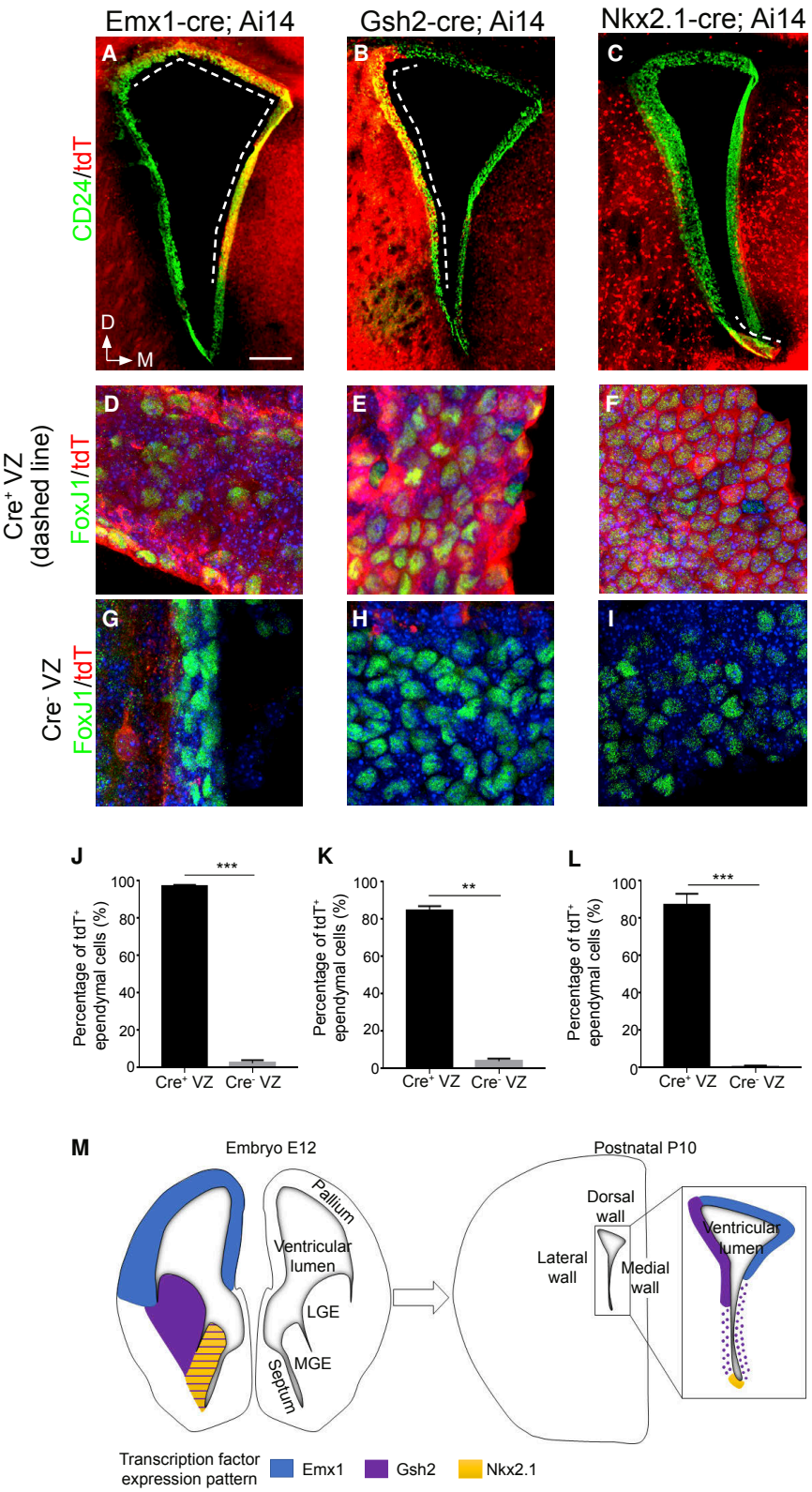

Figure 1. Ependymal Cell Progenitors Are Produced Locally along the Brain Ventricles

(A–C) Representative images of coronal sections of Emx1-Cre; Ai14 (A), Gsh2-Cre; Ai14 (B), and Nkx2.1-Cre; Ai14 (C) forebrain at P10, immunostained with CD24 (green) and DsRed (tdT, red) antibodies. $CD24^{+}tdT^{+}$ ependymal cells are only observed in the Cre-expressing domains in each mouse line (indicated by a dashed line).

(D–I) Representative high-magnification images of the Emx1-Cre; Ai14 (D and G), Gsh2-Cre; Ai14 (E and H), and Nkx2.1-Cre; Ai14 (F and I) coronal sections immunostained with FoxJ1 (green) and DsRed (tdT, red) antibodies in the Cre^{+} domains (D–F) or Cre^{-} domains (G–I), respectively. In the Cre^{+} domains, almost all ependymal cells are tdT^{+}, whereas very few cells are double-labeled in the Cre^{-} domains in each mouse line.

(J–L) Quantification of the mean percentage of tdT^{+} ependymal cells in different areas of the ventricular zone from n = 6, n = 4, and n = 5 mice from each of the three transgenic mouse lines: Emx1-Cre; Ai14 (J), Gsh2-Cre; Ai14 (K), and Nkx2.1-Cre; Ai14 (L), respectively. Error bars indicate the SEM. The p values were determined with a Mann-Whitney test; $^{**}p \leq 0.01$ and $^{***}p \leq 0.001$.

(M) Schematic of the expression patterns of each transcription factor in the mouse forebrain at E12 and model of the spatial origin of ependymal cells at P10. D, dorsal; M, medial.

The scale bars represent 200 mm (A–C) and 10 mm (D–I).

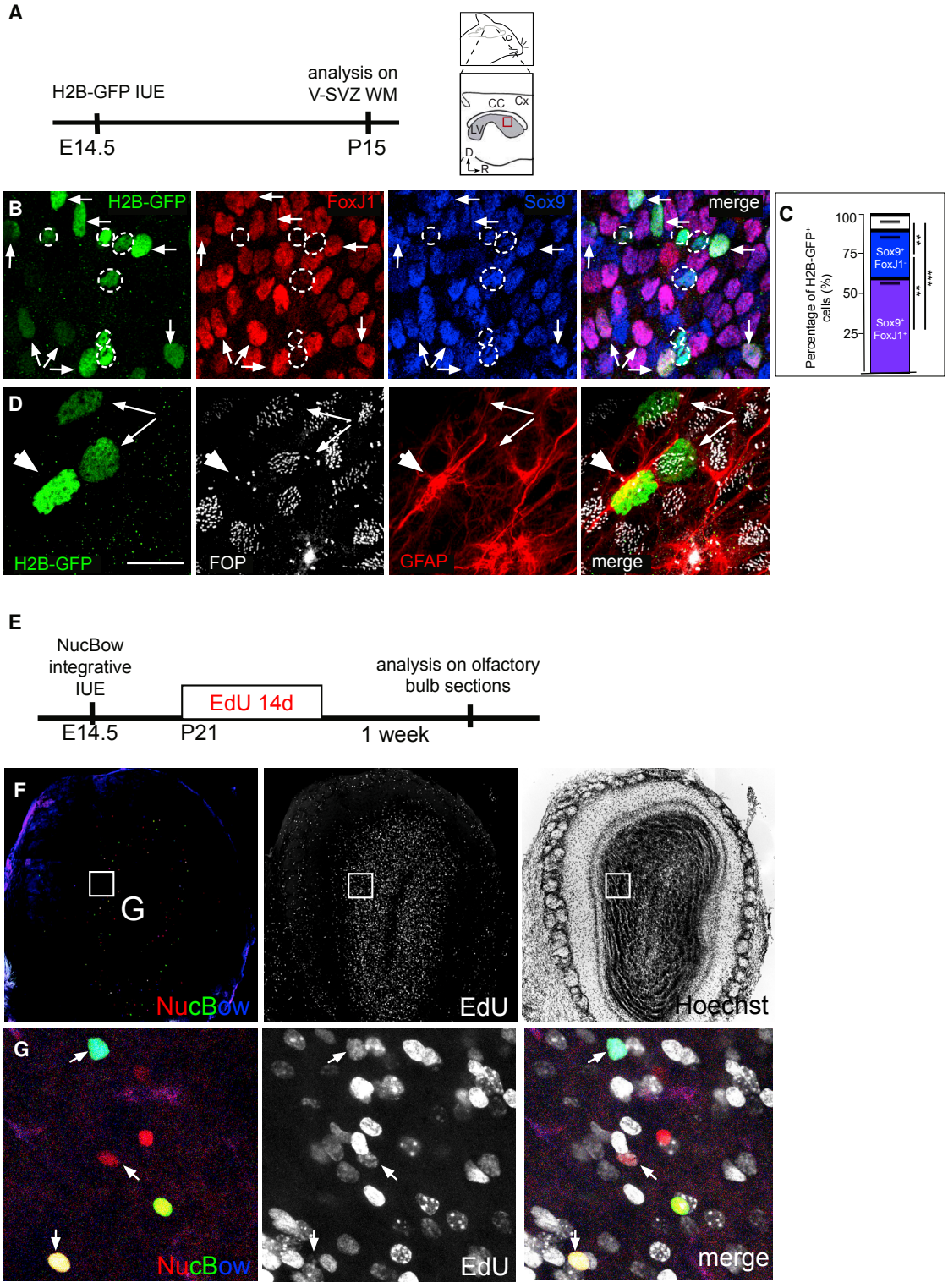

Figure 2. Radial Glial Cells Generate Ependymal Cells and Adult Neural Stem Cells (Type B1 Astrocytes)

(A) Experimental schematic for (B)–(D). The H2B-GFP-expressing plasmid was electroporated *in utero* at E14.5 and analyzed on V-SVZ whole-mount (WM) at P15. CC, corpus callosum; Cx, cortex; LV, lateral ventricle; R, rostral; D, dorsal.

(B and D) P15 V-SVZ whole-mounts were double-immunostained with FoxJ1 (red) and Sox9 (blue) antibodies (B) or FOP (white) and GFAP (red) antibodies (D). $GFP^+FoxJ1^+Sox9^+$ ependymal cells are indicated by arrows, and $GFP^+FoxJ1^-Sox9^+$ astrocytes are outlined in white (B). GFP^+GFAP^- ependymal cells with multiple FOP^+ dots are indicated by arrows, and a GFP^+GFAP^+ astrocyte with a FOP^+ centrosome is indicated by an arrowhead (D).

(legend continued on next page)

418 clones of 2 cells or more) showed that more than 80% of clones (with at least one Nucbow$^+$FoxJ1$^+$ cell) contained 8 or less cells, suggesting that most ependymal cells were derived from 3 or less cell divisions (Figures 3F and 3G; Figures S5A–S5F). We excluded the largest clones (9 to 32 cells) because we noted that they were often labeled with the most frequent labels in the dataset (corresponding to the primary colors red, green, and blue), suggesting that merging of juxtaposed clones expressing the same label had occurred (Figure S5G).

Among the 349 clones with 8 or less cells, around half contained only 2 cells, suggesting that, at E14.5, most clones were generated from one terminal cell division of RGCs (n = 6 mice; Figure 3H). These 2-cell clones were composed of 1 or 2 FoxJ1$^+$ cells in a 1:1 ratio, showing that the terminal division could be either symmetric or asymmetric (Figure 3I). Interestingly, the 3D distance between cells was higher in mixed clones (clones composed of ependymal and non-ependymal cells) compared with pure ependymal clones (Figure 3J), showing that FoxJ1$^-$ cells were deeper in the SVZ compared with FoxJ1$^+$ cells in the VZ.

Clones containing 3 to 8 cells were generated through 2 or 3 cell divisions, the last of which was either only symmetric (clones containing FoxJ1$^+$ cells only) or both symmetric and asymmetric (clones containing FoxJ1$^+$ and FoxJ1$^-$ cells). Interestingly, a majority of these clones contained more FoxJ1$^-$ cells than FoxJ1$^+$ cells, suggesting that symmetric divisions giving rise to 2 FoxJ1$^-$ cells might have occurred in these clones (Figure 3K).

Lineage tracing experiments of RGCs using the MAGIC markers strategy thus show that ependymal cells originate from either one terminal symmetric division giving rise to 2 ependymal cells or 1 asymmetric division giving rise to 1 ependymal and 1 FoxJ1$^-$ cell. Most importantly, this analysis of a large number of clones distributed along the caudo-rostral and ventro-dorsal axis of the lateral wall of the LV of 6 different electroporated brains did not reveal any regional differences. This observation suggests that the ontogeny of the neurogenic niche can be determined by analyzing individual cells along the LV.

MADM of V-SVZ Gliogenesis Reveals that Ependymal and B1 Cells Share a Common Lineage

To obtain more insight into the cellular mechanisms and the sequence of symmetric versus asymmetric divisions producing each clone, we used the MADM system coupled with IUE of Cre recombinase at E13.5 or E14.5 (Figure 4A; Gao et al., 2014). In electroporated cells, Cre recombinase mediates interchromosomal recombination, which reconstitutes cytoplasmic enhanced GFP (EGFP, green) or tandem dimer Tomato (tdTomato, red). If recombination occurs in G2 phase of the cell cycle, and each red or green chromosome segregates in separate daughter cells (X segregation), then the two descendent lineages will be permanently labeled green or red by MADM events (Figure 4B). Analysis of cell number and identity will thus allow direct assessment of the division pattern (symmetric versus asymmetric) and cell fate decision of the original dividing progenitors. Otherwise, if recombination occurs in G0/G1, or if both red and green chromosomes segregate in the same cell (Z segregation), then recombined cells appear yellow and will be excluded from the analysis (Figure 4B). We thus induced Cre activity through IUE in MADM pregnant mothers at E13.5 or E14.5 and analyzed the V-SVZ at P15–P20 after immunolabeling of centrioles combined with MADM cytoplasmic staining to identify the cell types composing each clone (Figure 4C). This approach allowed a clonal study of green-red clones because the efficiency of recombination leading to green-red clones was low in these mice (mean number of clones per animal, 5), and most recombined cells were double-labeled (yellow) (Figure 4C). Cells were considered a clone when their spatial distance was less than 100 μm, as defined previously by the Nucbow lineage-tracing experiments. Red or green cells located in the electroporated region of the V-SVZ were either multiciliated ependymal (E) cells, characterized by a few short processes and multiple FOP$^+$ basal bodies in their cytoplasm associated with long cilia, or astrocytes (type B1), whose cell body and multiple long processes were deeper in the SVZ. These astrocytes contained 2 centrosomal centrioles that occasionally contacted the ventricular surface and extended a primary cilium. These cells were thus easily discriminated from multiciliated ependymal cells (identified by multiple centrioles and long cilia) or even neuroblasts, which displayed typical migrating morphologies in the direction of the olfactory bulb and were located deeper in the tissue at larger distances from the clone. When the cells of a clone were in close proximity, their cell body or processes often contacted each other, suggesting that they might maintain communication at the adult stage (Figures 4C–4G; Videos S1 and S2). We observed very few red or green cells alone (clone of 1 cell in Figure 4H) or larger monochrome clones, if any, in the V-SVZ, suggesting that asymmetric divisions giving rise to one ventricular and one non-ventricular cell were rare in these experiments. In contrast, we found that, among the 44 clones of 2–6 cells, 48% of them contained 2 cells (21 clones), and 52% of them contained 3–6 cells (23 clones), which is in line with our findings above showing that half of the RGCs at E14.5 divided once to produce glial cells in the V-SVZ. At E13.5, RGCs also produced V-SVZ cells, but the majority divided twice or more because 90% of clones contained 3 or more cells (Figure 4H). The distance between cells in a clone was higher at E13.5 compared with E14.5, showing that cells disperse as cell divisions proceed (Figure 4I). Both the proportion of mixed clones (containing both ependymal and B1 cells;

(C) Mean percentage of astrocytes (Sox9$^+$FoxJ1$^-$), ependymal cells (Sox9$^+$FoxJ1$^+$), and others (Sox9$^-$FoxJ1$^-$) among H2B-GFP$^+$ electroporated cells. Analyses were done on n = 3 animals; a total of 441 cells were counted. Error bars represent the SEM. The p values were determined with a two-proportion Z test; ***$p \leq 0.001$, **$p \leq 0.01$.

(E) Experimental schematic for (F) and (G). Nucbow plasmids (^{PB}*CAG-Nucbow* along with the PiggyBac transposase and the self-excising Cre recombinase) were electroporated *in utero* at E14.5 and received EdU (through drinking water) for 14 days starting at P21.

(F and G) Coronal sections of the olfactory bulb (OB) were prepared 1 week after the last day of EdU administration. (G) is a high-magnification image of (F) to show that some Nucbow$^+$ interneurons in the OB are EdU$^+$.

The scale bars represent 40 μm (B), 15 μm (C), 520 μm (F), and 180 μm (G).

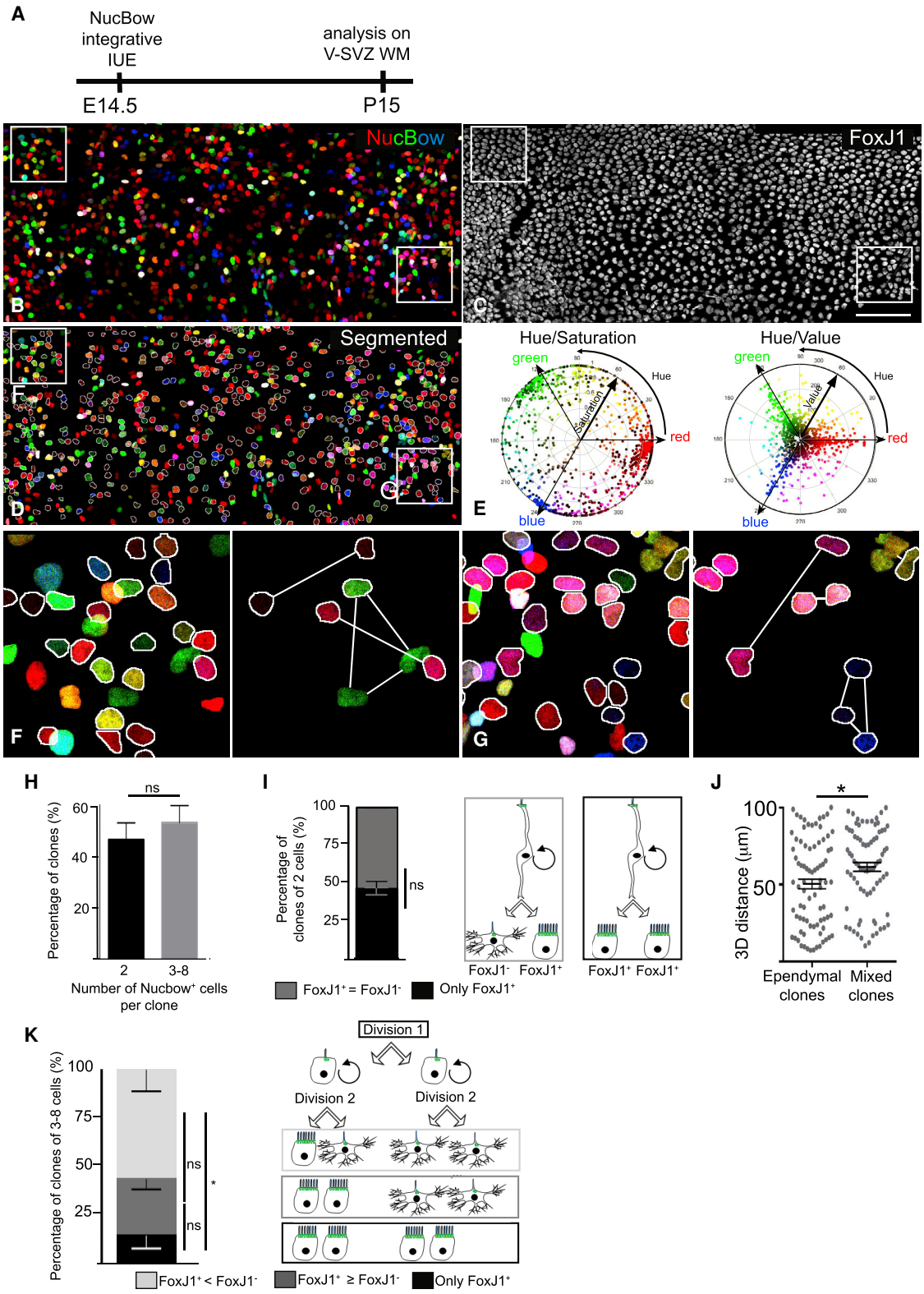

Figure 3. Clonal Analysis of Ependymal Cells with MAGIC Markers Reveals Both Symmetric and Asymmetric Divisions of RGCs

(A) Experimental schematic. Nucbow plasmids were electroporated *in utero* at E14.5 and analyzed at P15–P20.

(B–D) Representative Z-projected image of an *en face* view of the V-SVZ (B) immunostained at P15 with anti-FoxJ1 antibody (C). (D) shows a segmented image of (B) and (C), obtained using FoxJ1 staining, as a reference (STAR Methods; Figures S3–S5). FoxJ1^{+}Nucbow^{+} cells are outlined in white.

(legend continued on next page)

Figure 4J) and the number of type B1 astrocytes (Figure 4K) in the clones decreased at E14.5 compared with E13.5, suggesting that fewer type B1 astrocytes are produced compared with ependymal cells. Alternatively, type B1 astrocytes might be produced at earlier stages compared with ependymal cells. Noteworthy is that the distribution of astrocytes (B1) and ependymal cells in each clone revealed that astrocytes were produced at a lower rate than ependymal cells and that symmetric divisions producing 2 astrocytes (B1-B1) occurred more frequently at E13.5 than at E14.5 (Figure 4L; Table S1).

Together, these results show that ependymal cells and astrocytes are sister cells produced through symmetric (B1-B1 or E-E) and asymmetric (E-B1) divisions of RGCs at mid-gestation in the mouse forebrain.

To gain more insight into the molecular regulation of RGC differentiation into type B1 astrocytes or ependymal cells, we perturbed these divisions with members of the Geminin superfamily, initially described as regulators of DNA replication (Balestrini et al., 2010; Pefani et al., 2011). Two members of this family (Mcidas and GemC1) were recently identified as master regulators of multiciliated ependymal cell fate (Kyrousi et al., 2015), whereas the other member, Geminin, was found to regulate neural cell fate and to be highly expressed in cycling type B1 cells in the adult SVZ (Khatri et al., 2014; Sankar et al., 2016). We also confirmed that GemC1 and Geminin genes are expressed along the LV at E14.5, in the choroid plexus and the ventricular zone, respectively (Figure S6). Moreover, ependymal cell differentiation was totally absent in cultured cells from the GemC1 full mutant, whereas it was slightly (although not significantly) increased in cultured cells from the Geminin conditional mutant (Figures S7B–S7E).

GemC1 Expression Induces Premature Ependymal Cell Differentiation at the Expense of Type B1 Cells

Overexpression of GemC1 through IUE at E13.5 or E14.5 dramatically increased ependymal cell differentiation at the expense of SVZ cells, as shown previously (Figures S7G–S7I; Kyrousi et al., 2015). Interestingly, because B1 cells were absent, pinwheels were not observed in densely GemC1-electroporated regions (Figures S7J and S7K) compared with neighboring areas in which GemC1 electroporation was sparse (Figure S7L). Overexpression of GemC1 together with induction of Cre activity through IUE in MADM embryos at E14.5 did not change the size of the clones compared with controls, suggesting that most RGCs were already undergoing their last division at that stage (Figure 5C). In contrast, when IUE was performed at E13.5, the clones were smaller compared with controls, suggesting that GemC1 induced premature exit from the cell cycle at that stage (Figure 5C). Consistently, the average distance between cells in the GemC1 clones at E13.5 was smaller than in controls (compare Figures 4I and 5D; Mann-Whitney test, $^{**}p \leq 0.01$) and similar to E14.5 GemC1 (Figure 5D). Furthermore, overexpression of GemC1 at E13.5 or E14.5 promoted the ependymal fate because the numbers of both pure ependymal clones and ependymal cells in the clones were dramatically increased compared with controls (two-proportion Z test between controls and GemC1: $^{***}p \leq 0.001$; compare Figures 4J and 4K and 5E and 5F). Notably, although astrocytes were occasionally produced through symmetric divisions in controls, they were exclusively generated through asymmetric divisions with ependymal cells after GemC1 overexpression at E13.5 or E14.5. Indeed, no pairs of astrocytes were detected after GemC1 overexpression (Figure 6F; Table S2).

Geminin Expression Favors the Generation of Type B1 Cells

Geminin physically interacts with GemC1 and Mcidas (Caillat et al., 2013, 2015), but its role during ependymal cell generation is still unknown. We thus tested the influence of Geminin overexpression on the fate of RGCs through IUE with Cre in MADM pregnant mothers at E13.5 or E14.5 (Figures 6A and 6B). Notably, a majority of the clones contained type B1 astrocytes, characterized by an apical contact with a primary cilium and cytoplasmic extensions contacting blood vessels (Figure 6B; Video S3; Table S3). The size of the clones was slightly increased both in E13.5 and E14.5 Geminin-overexpressing clones but similar to that of controls, suggesting that Geminin does not act on the rate of cell division in RGCs (Figure 6C). Interestingly, the proportion of mixed clones and the number of type B1 astrocytes were not significantly increased after Geminin overexpression (two-proportion Z test between controls and Geminin: not significant, $p > 0.05$; compare Figures 4J and 4K and 6D and 6E; Figure 6F). However, Geminin overexpression led to significant formation of clones containing only B1 cells, which was never observed in controls (two-proportion Z test between E14.5 control and E14.5 Geminin for the B1-only population: $^{*}p \leq 0.05$; compare Figures 4 and 6D). Consistently, the number of symmetric divisions producing 2 astrocytes (B1-B1) increased significantly after Geminin overexpression at E14.5 compared with controls (Figure 6F; Table S3).

(E) Circular hue-saturation and hue-value plots of all Nucbow$^+$ cells from (D).

(F and G) High-magnification images of the insets in (D), showing examples of clones: 2 ependymal doublets and 1 triplet containing 1 ependymal cell and 2 FoxJ1$^-$ cells (F) and 3 ependymal doublets, 1 ependymal triplet, and 1 triplet containing 1 ependymal cell and 2 FoxJ1$^-$ cells (G).

(H) Mean percentages of clones containing 2 or 3–8 Nucbow$^+$ cells. Error bars represent the SEM of n = 163 clones of 2 cells and n = 186 clones of 3–8 cells; p values were determined by Mann-Whitney test; ns, $p > 0.05$.

(I) Mean percentages of clones of 2 Nucbow$^+$ cells containing 1 (mixed clones, gray) or 2 (ependymal clones, black) FoxJ1$^+$ cells. Error bars represent the SEM of n = 82 ependymal clones and n = 81 mixed clones from 6 independent experiments; p values were determined by Mann-Whitney test; ns, $p > 0.05$.

(J) Average 3D distances between the cells composing ependymal or mixed clones of 2 cells. Error bars represent the SEM of n = 82 ependymal clones and n = 81 mixed clones from 6 independent experiments; p values were determined by Mann-Whitney test; $^{*}p \leq 0.05$.

(K) Mean percentages of clones of 3–8 Nucbow$^+$ cells containing only FoxJ1$^+$ cells (black), more or an equal number of FoxJ1$^+$ compared with FoxJ1$^-$ cells (dark gray), or more FoxJ1$^-$ cells (light gray) per clone. Error bars represent the SEM of n = 186 clones of 3–8 cells; p values were determined by Mann-Whitney test; $^{**}p \leq 0.01$; $^{*}p \leq 0.05$; ns, $p > 0.05$.

The scale bars represent 100 μm (B)–(D) and 22 μm (F) and (G).

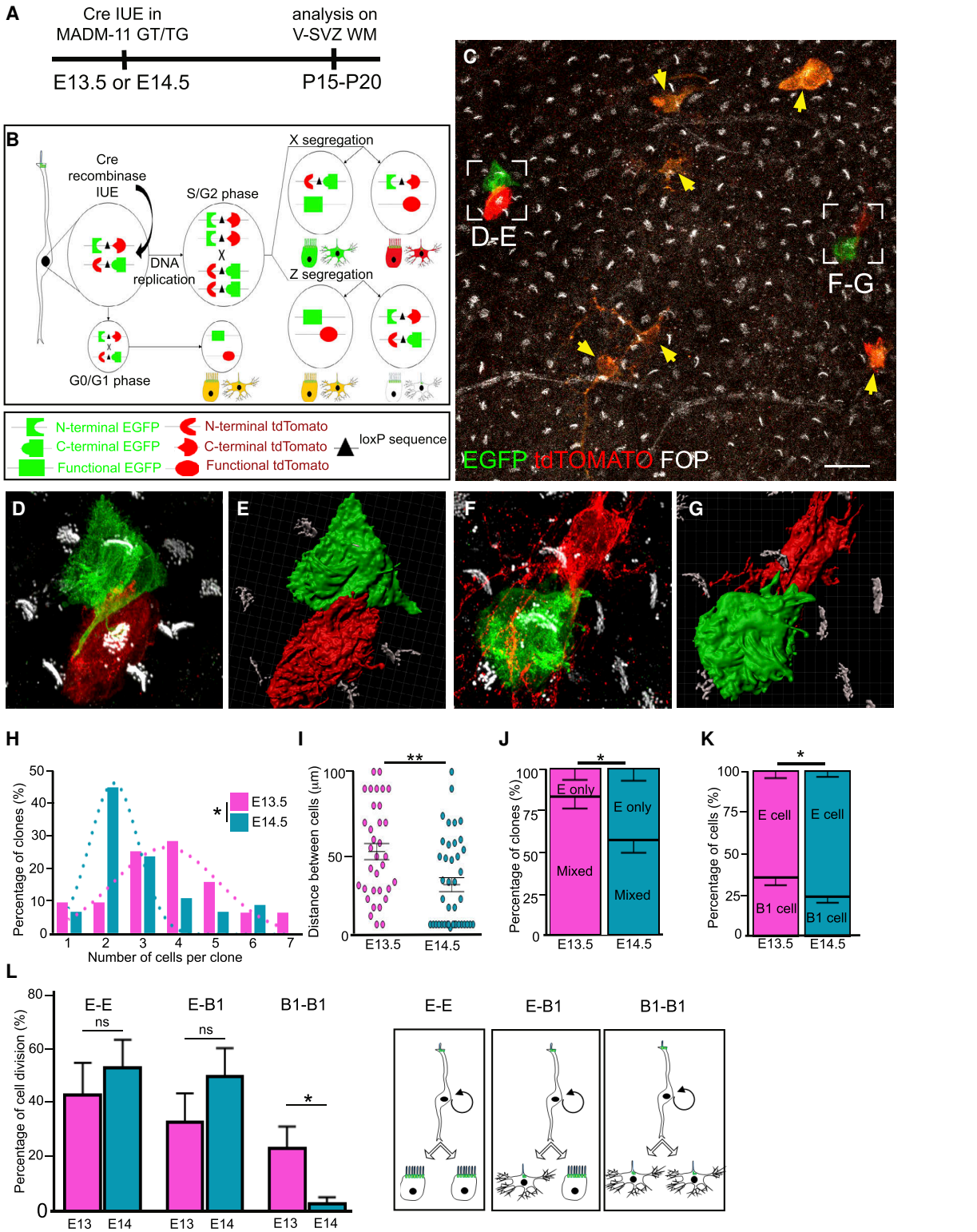

Figure 4. MADM Reveals the Presence of Ependymal-Ependymal and Ependymal-Astrocyte Divisions at E13.5 and E14.5

(A) Experimental schematic. The Cre plasmid was electroporated *in utero* in *MADM-11*$^{TG/GT}$ at E13.5 or E14.5, and V-SVZ WMs were analyzed at P15–P20.

(B) Schematic representation of Cre-mediated MADM clone induction in dividing RGCs. A G2-X event results in clones of red- and green-labeled cells, and a G2-Z event generates double-labeled (yellow) and unlabeled clones of cells. Recombination occurring in G0/G1 phases of the cell cycle leads to double-labeled (yellow) cells.

(legend continued on next page)

Altogether, these results show that ependymal cells and astrocytes are sister cells produced through symmetric or asymmetric divisions, the balance of which is modulated by the level of expression of Geminin family genes.

DISCUSSION

Using a Cre-lox fate mapping technique and complementary MAGIC markers- and MADM-based clonal analysis, our study revealed how glial cells are produced in the V-SVZ during development. First, our results proved that ependymal cells are derived from RGCs all along the embryonic neuroepithelium (pallium and lateral and medial ganglionic eminences) and differentiate locally; ependymal progenitors born in a specific area of the VZ do not migrate long distances to colonize other areas of the neuroepithelium (Figure 1). We then showed that ependymal cells and B1-type astrocytes appear at the end of neurogenesis, mainly through E-B1 asymmetric or E-E symmetric divisions of RGCs. B1-B1 symmetric divisions were less frequent and always combined with E-E or E-B1 divisions (Figure 7). These glial cells have a low migratory capacity and often contact each other, even at the adult stage. Our study thus demonstrates that multiciliated ependymal cells and adult neural stem cells, ultimately forming the adult neurogenic niche, are sister cells that share a common origin. We also provide evidence that these cells are sequentially produced, with the bulk of B1 astrocytes being produced just before the bulk of ependymal cells. Interestingly, their respective numbers are precisely regulated by the Geminin family members. Overexpression of Geminin, a gene expressed more in cycling compared with quiescent neural stem cells (Khatri et al., 2014) and in the ventricular zone at E14.5 (Figure S6), favors B1-B1 symmetric divisions (Figure 6F). On the contrary, overexpression of its antagonist, GemC1, at E14.5 induces premature terminal E-E divisions and leads to a sharp decrease in the final number of B1 cells (Figures 5E and 5F). Given that GemC1 expression is only detected in the choroid plexus at that stage (Figure S6; Arbi et al., 2016), one can hypothesize that it is expressed at very low and/or undetectable levels in these progenitors. Alternatively, GemC1 might be expressed at later stages of development because ependymal differentiation starts postnatally in controls (Spassky et al., 2005). Both possibilities should be tested further, but they might already explain why GemC1 expression at high levels and/or before its normal expression in progenitors leads to premature ependymal differentiation. The sequential expression of Geminin family members could thus be responsible for the temporal differences in glia production. The 2-fold presence of ependymal cells with respect to B1 cells (Mirzadeh et al., 2008) could result from the balance between the levels of expression of these genes. These findings raise the question of the fate decision mechanisms driving RGCs toward symmetric or asymmetric cell division. An analogous question was addressed by others concerning neuronal versus glial cell generation. Interestingly, it has been shown that the number of neurons produced by RG is predictable and that around one in 6 RGCs perform a gliogenic division only when they have exhausted their capacity to proliferate (Gao et al., 2014). At early stages of corticogenesis, RGCs would thus divide asymmetrically to produce neurons and glial progenitors, which would then generate type B1 astrocytes and ependymal cells. Similarly, we found that RGCs generate more mixed clones and more astrocytes when they are electroporated at E13.5 than at E14.5 (Figures 4J and 4K). This suggests that astrocytes are produced earlier than ependymal cells. One might hypothesize that RGCs first give rise to astrocytes until they exhaust their proliferative capacity and yield two ependymal cells through symmetric cell division at later developmental stages. Further lineage studies would be required to identify whether/which neuronal subtypes are lineally related to V-SVZ glial cells (type B1 astrocytes and ependymal cells). Importantly, although ependymal cells become post-mitotic (Spassky et al., 2005), most V-SVZ astrocytes can be reactivated in the adult (Obernier et al., 2018). Altogether, this suggests that RGCs first produce quiescent daughter cells with the potential to enter the cell cycle again (type B1 astrocytes) and then post-mitotic ependymal cells. Interestingly, the description of distinct pathways of glial production via symmetric or asymmetric division unveils the existence of two separate fate decision mechanisms that occur subsequent to the last division of RGCs. This indicates that ependymal versus astrocyte specification might be dependent on the correct segregation of organelles (i.e., centrioles or mitochondria), which have been shown to influence neural stem cell self-renewal and fate decisions (Khacho et al., 2016; Wang et al., 2009). Noteworthy is that Geminin

(C–G) Airyscan confocal image of a P15 MADM-labeled V-SVZ whole-mount electroporated with a CRE-expressing plasmid at E14.5. The ventricular wall was stained with EGFP (green), tdTomato (red), and FOP (white) antibodies. (C) Double-labeled yellow cells issued from a G2-Z recombination event are indicated by yellow arrows. Ependymal-ependymal (D and E) and ependymal-astrocyte (F and G) clones of two sister cells are shown at high magnification (D and F) and in a 3D view (E and G). See also Videos S1 and S2.

(H) Mean percentages of all clones generated from *in utero* electroporation with Cre at E13.5 or E14.5 according to the number of cells per clone (n = 6 and 16 animals at E13.5 and E14.5, respectively) are represented in a histogram. Also shown are dotted curves fitting both the E13.5 and E14.5 distributions; p values were determined with the χ^2 test for trend; *p $\leq$ 0.05.

(I) Average distance between cells composing the clones. Error bars represent the SEM of 29 and 44 clones at E13.5 and E14.5, respectively; p values were determined with a Mann-Whitney test; **p $\leq$ 0.01.

(J) Mean percentage of all clones generated from E13.5 or E14.5 containing ependymal cells only or a mixed population of ependymal cells and astrocytes (B1). Error bars represent the SEM of 29 and 44 clones at E13.5 and E14.5, respectively; p values were determined with a two-proportion Z test; *p $\leq$ 0.05.

(K) Mean percentage of ependymal and B1 cells in all clones generated from E13.5 or E14.5. Error bars represent the SEM of 117 and 134 cells at E13.5 and E14.5, respectively; p values were determined with a two-proportion Z test; *p $\leq$ 0.05.

(L) Mean percentage of E-E, E-B1, and B1-B1 cell divisions in all clones generated from E13.5 or E14.5. Error bars represent the SEM of 24 and 54 cell divisions at E13.5 and E14.5, respectively; p values were determined with a Mann-Whitney test; *p $\leq$ 0.05.

The scale bars represent 30 μm (C) and 8 μm (D–G).

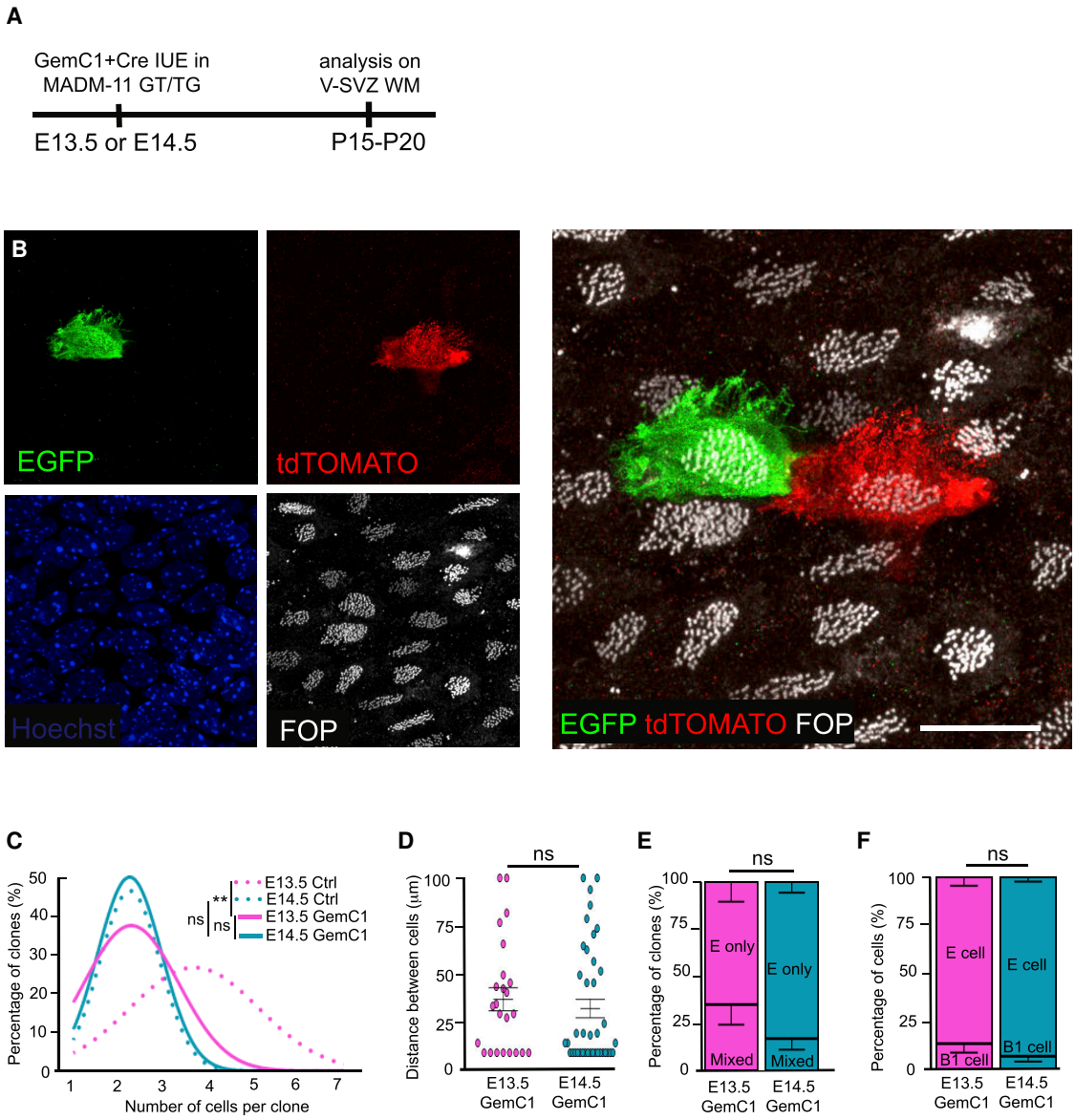

Figure 5. GemC1 Favors the Formation of Pure Ependymal Clones at Both E13.5 and E14.5

(A) Experimental schematic. GemC1 and Cre plasmids were co-electroporated *in utero* in *MADM-11*$^{TG/GT}$ at E13.5 or E14.5, and V-SVZ WMs were analyzed at P15–P20.

(B) Airyscan confocal image of a P15 MADM-labeled V-SVZ whole-mount immunostained with EGFP (green), tdTomato (red), and FOP (white) antibodies showing a clone of 2 ependymal cells.

(C) Fitting curves of the distribution of clone size according to the number of cells per clone, issued from electroporation of Cre at E13.5 or E14.5 (dotted curves; n = 6 and 16 animals at E13.5 and E14.5, respectively) or co-electroporation of Cre with GemC1 at E13.5 or E14.5 (solid curves; n = 4 and 9 animals at E13.5GemC1 and E14.5GemC1, respectively); p values were determined with a c^2 test for trend; ns, $p > 0.05$, $^{**}p \leq 0.01$.

(D) Average distance between cells composing the clones generated from co-electroporation of Cre and GemC1 at E13.5 or E14.5. Error bars represent the SEM of 20 and 41 clones at E13.5 and E14.5, respectively; p values were determined with a Mann-Whitney test; ns, $p > 0.05$.

(E) Mean percentage of all clones generated from co-electroporation of Cre and GemC1 at E13.5 or E14.5 containing ependymal cells only or a mixed population of ependymal cells and B1 cells. Error bars represent the SEM of 20 and 41 clones, respectively; p values were determined with a two-proportion Z test; ns, $p > 0.05$.

(F) Mean percentage of ependymal and B1 cells in all clones generated from co-electroporation of Cre and GemC1 at E13.5 or E14.5. Error bars represent the SEM of 57 and 110 cells at E13.5 and E14.5, respectively; p values were determined with a two-proportion Z test; ns, $p > 0.05$.

The scale bar represents 50 µm.

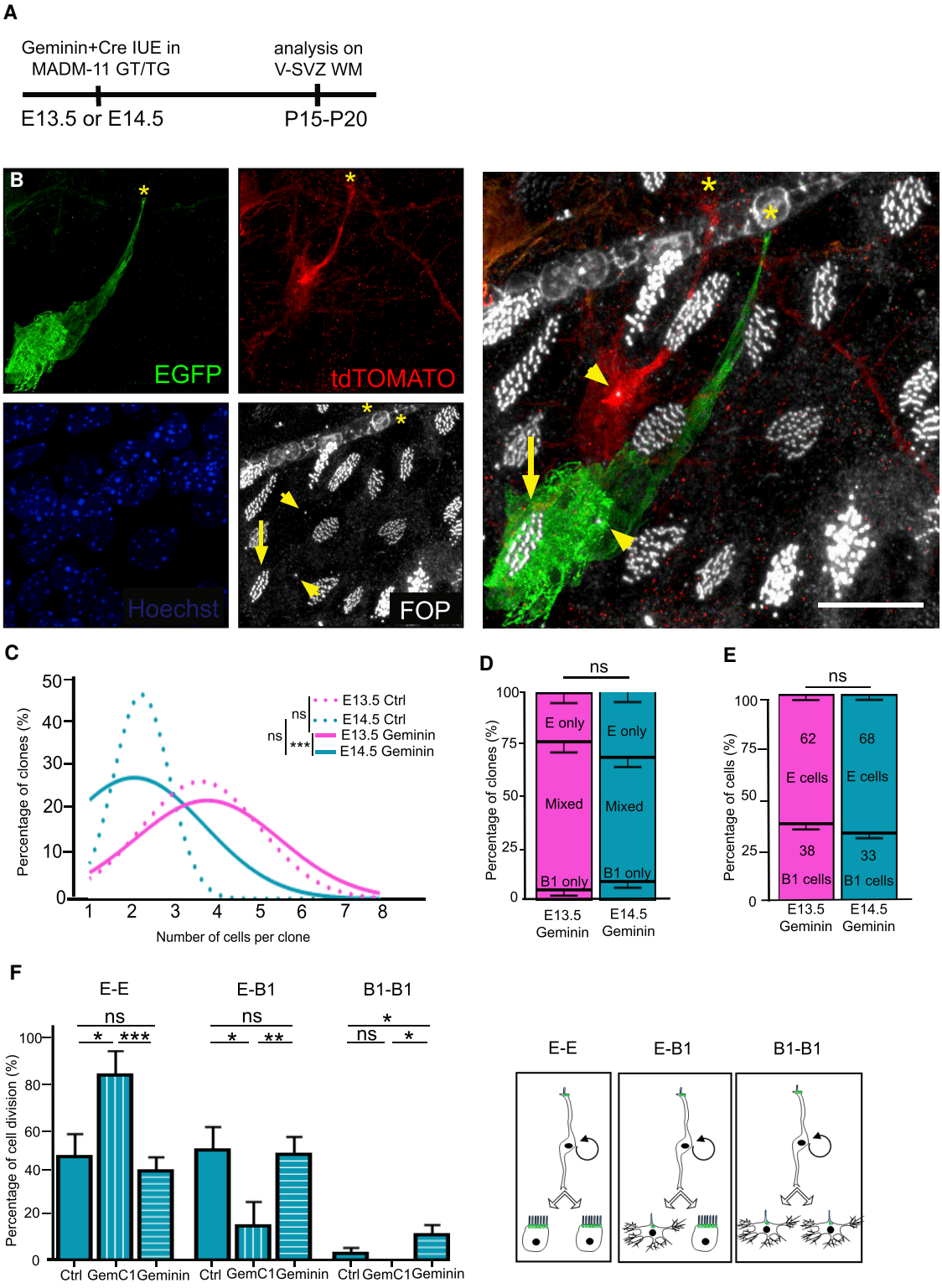

Figure 6. Geminin Favors the Formation of B1 Cell-Containing Clones at E14.5

(A) Experimental schematic. The Geminin and Cre plasmids were co-electroporated *in utero* in *MADM-11*$^{TG/GT}$ at E13.5 and E14.5, and V-SVZ WMs were analyzed at P15–P20.

(legend continued on next page)

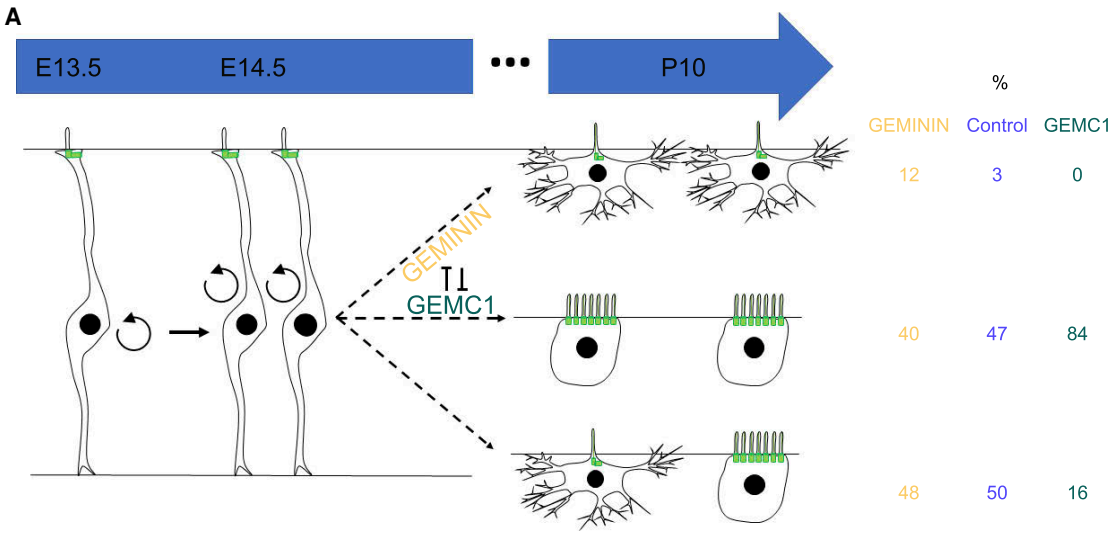

Figure 7. Ependymal Cells and B1 Astrocytes Form One Common Lineage Regulated by Geminin Family Members

(A) Model of adult neural stem cells (NSCs) and multiciliated ependymal cell generation. RGCs give rise to type B1 cells through symmetric divisions (rare event, 3%) or asymmetric divisions (frequent event, 50%) and to multiciliated ependymal cells through symmetric divisions (frequent event, 47%). The antagonistic Geminin family members Geminin and GemC1 can modulate the cell fate decision. Geminin overexpression favors symmetric divisions giving rise to type B1 astrocytes. On the contrary, GemC1 overexpression triggers symmetric divisions giving rise to ependymal cells. The percentages of E-E, E-B1, and B1-B1 divisions are indicated for IUE at E14.5 in a control situation and upon GemC1 or Geminin overexpression, respectively.

superfamily members were initially described as regulators of DNA replication. It would thus be of interest to determine whether fate decisions in RGCs are driven by DNA replication events following re-entry into the cell cycle.

STAR+ METHODS

Detailed methods are provided in the online version of this paper and include the following:

- KEY RESOURCES TABLE
- CONTACT FOR REAGENT AND RESOURCES SHARING
- EXPERIMENTAL MODEL AND SUBJECT DETAILS
- METHOD DETAILS
  - In utero electroporation
  - EdU administration and detection
  - Primary Ependymal Cell culture
  - Tissue and cell culture preparation
  - Immunostaining
  - *In situ* hybridization
  - Imaging
  - Automatic image analysis of MAGIC Markers
- QUANTIFICATION AND STATISTICAL ANALYSES
  - Fate mapping of the spatial origin of ependymal cells
  - Characterization of the cell types in the electroporated V-SVZ
  - Automatic image analysis of MAGIC markers
  - MADM transgenic image analysis
  - EdU incorporation in the V-SVZ analysis
  - Characterization of the differentiation status in the V-SVZ with or without GemC1
  - Assessment of the differentiation status of GemC1 KO and Geminin cKO primary cultures
- DATA AND SOFTWARE AVAILABILITY

(B) Airyscan confocal image of a P15 MADM-labeled V-SVZ whole-mount immunostained with EGFP (green), tdTomato (red), and FOP (white) antibodies showing a clone containing 1 GFP^+ ependymal cell (arrow) and two B1 cells (one GFP^+ and one tdT^+, arrowheads). Note that both B1 cells contain a centrosome at the ventricular surface (arrowheads), and they extend a process toward a blood vessel (yellow asterisks). See also Video S3.

(C) Fitting curves of the distribution of clone size according to the number of cells per clone, issued from electroporation of Cre at E13.5 or E14.5 (dotted curves; n = 6 and 16 animals at E13.5 and E14.5, respectively) or co-electroporation of Cre with Geminin at E13.5 or E14.5 (solid curves; n = 8 and 13 animals at E13.5 Geminin and E14.5 Geminin, respectively); p values were determined with a c2 test for trend; ns, $p > 0.05$, $^{***}p \leq 0.001$.

(D) Mean percentage of all clones generated from co-electroporation of Cre and Geminin at E13.5 and E14.5 and containing either B1 cells only, ependymal cells only, or a mixed population of ependymal cells and B1 cells. Error bars represent the SEM of 73 or 107 clones; the p value was determined with a two-proportion Z test; ns, $p > 0.05$.

(E) Mean percentage of ependymal and B1 cells in all clones generated from co-electroporation of Cre and Geminin at E13.5 and E14.5. Error bars represent the SEM of 317 or 335 cells, respectively; the p value was determined with a two-proportion Z test; ns, $p > 0.05$.

(F) Mean percentage of E-E, E-B1, and B1-B1 cell division in clones generated from E14.5 in controls or after overexpression of GemC1 or Geminin. Error bars represent the SEM of 16, 9, and 13 independent animals electroporated with Cre, Cre+GemC1, or Cre+Geminin, respectively; p values were determined with a Mann-Whitney test; $^{***}p \leq 0.001$; $^{**}p \leq 0.01$; $^{*}p \leq 0.05$; ns, $p > 0.05$.

The scale bar represents 50 mm.

SUPPLEMENTAL INFORMATION

Supplemental Information can be found with this article online at https://doi.org/10.1016/j.neuron.2019.01.051.

ACKNOWLEDGMENTS

We thank all members of the Spassky laboratory as well as the Jean-François Brunet, Sonia Garel, and Xavier Morin laboratories for comments and discussions. We thank X. Morin for the pCAAGS-H2B-GFP and pCAGGS-Cre plasmids. We thank A.-K. Konate and R. Nagalingum for administrative support and the IBENS Animal Facility for animal care. The team received support from Agence Nationale de la Recherche (ANR) Investissements d'Avenir (ANR-10-LABX-54 MEMO LIFE and ANR-11-IDEX-0001-02 PSL* Research University). The Spassky laboratory is supported by INSERM, CNRS, École Normale Supérieure (ENS), ANR (ANR-17-CE12-0021-03), FRM (Equipe FRM grant 20140329547), European Research Council (ERC Consolidator grant 647466), and Cancéropôle Île-de-France (2014-1-PL BIO-11-INSERM 121). The Livet and Hippenmeyer laboratories are supported by the European Research Council (ERC Consolidator grants 649117 and 725780, respectively). G.O.-A. and M.D. received fellowships from Labex MEMOLIFE and the French Ministry of Higher Education and Research, respectively. S.C. received fellowships from the Région Ile-de-France and Association pour la Recherche sur le Cancer (ARC).

AUTHOR CONTRIBUTIONS

N.S. designed, funded, and supervised the research. G.O.-A., M.D., P.L., A.F., M.F., S.C., J.L., and N.S. designed the experiments and performed the research. G.O.-A., M.D., P.L., A.F., A.S., A.M., A.G., and N.S. analyzed the data. S.T. and S.H. provided resources. G.O.-A., M.D., and N.S. wrote the manuscript with input from all authors.

DECLARATION OF INTERESTS

The authors declare no competing interests.

Received: July 12, 2018
Revised: December 21, 2018
Accepted: January 24, 2019
Published: February 26, 2019

REFERENCES

Al Jord, A., Lemaître, A.-I., Delgehyr, N., Faucourt, M., Spassky, N., and Meunier, A. (2014). Centriole amplification by mother and daughter centrioles differs in multiciliated cells. Nature *516*, 104–107.

Arbi, M., Pefani, D.E., Kyrousi, C., Lalioti, M.E., Kalogeropoulou, A., Papanastasiou, A.D., Taraviras, S., and Lygerou, Z. (2016). GemC1 controls multiciliogenesis in the airway epithelium. EMBO Rep. *17*, 400–413.

Balestrini, A., Cosentino, C., Errico, A., Garner, E., and Costanzo, V. (2010). GEMC1 is a TopBP1-interacting protein required for chromosomal DNA replication. Nat. Cell Biol. *12*, 484–491.

Boon, M., Wallmeier, J., Ma, L., Loges, N.T., Jaspers, M., Olbrich, H., Dougherty, G.W., Raidt, J., Werner, C., Amirav, I., et al. (2014). MCIDAS mutations result in a mucociliary clearance disorder with reduced generation of multiple motile cilia. Nat. Commun. *5*, 4418.

Caillat, C., Pefani, D.-E., Gillespie, P.J., Taraviras, S., Blow, J.J., Lygerou, Z., and Perrakis, A. (2013). The Geminin and Idas coiled coils preferentially form a heterodimer that inhibits Geminin function in DNA replication licensing. J. Biol. Chem. *288*, 31624–31634.

Caillat, C., Fish, A., Pefani, D.-E., Taraviras, S., Lygerou, Z., and Perrakis, A. (2015). The structure of the GemC1 coiled coil and its interaction with the Geminin family of coiled-coil proteins. Acta Crystallogr. D Biol. Crystallogr. *71*, 2278–2286.

Cebrián-Silla, A., Alfaro-Cervelló, C., Herranz-Pérez, V., Kaneko, N., Park, D.H., Sawamoto, K., Alvarez-Buylla, A., Lim, D.A., and García-Verdugo, J.M. (2017). Unique Organization of the Nuclear Envelope in the Post-natal Quiescent Neural Stem Cells. Stem Cell Reports *9*, 203–216.

de Frutos, C.A., Bouvier, G., Arai, Y., Thion, M.S., Lokmane, L., Keita, M., Garcia-Dominguez, M., Charnay, P., Hirata, T., Riethmacher, D., et al. (2016). Reallocation of Olfactory Cajal-Retzius Cells Shapes Neocortex Architecture. Neuron *92*, 435–448.

Delgehyr, N., Meunier, A., Faucourt, M., Bosch Grau, M., Strehl, L., Janke, C., and Spassky, N. (2015). Ependymal cell differentiation, from monociliated to multiciliated cells. Methods Cell Biol. *127*, 19–35.

Doetsch, F., Caillé, I., Lim, D.A., García-Verdugo, J.M., and Alvarez-Buylla, A. (1999). Subventricular zone astrocytes are neural stem cells in the adult mammalian brain. Cell *97*, 703–716.

Ferri, A.L., Cavallaro, M., Braida, D., Di Cristofano, A., Canta, A., Vezzani, A., Ottolenghi, S., Pandolfi, P.P., Sala, M., DeBiasi, S., and Nicolis, S.K. (2004). Sox2 deficiency causes neurodegeneration and impaired neurogenesis in the adult mouse brain. Development *131*, 3805–3819.

Fuentealba, L.C., Rompani, S.B., Parraguez, J.I., Obernier, K., Romero, R., Cepko, C.L., and Alvarez-Buylla, A. (2015). Embryonic Origin of Postnatal Neural Stem Cells. Cell *161*, 1644–1655.

Furutachi, S., Miya, H., Watanabe, T., Kawai, H., Yamasaki, N., Harada, Y., Imayoshi, I., Nelson, M., Nakayama, K.I., Hirabayashi, Y., and Gotoh, Y. (2015). Slowly dividing neural progenitors are an embryonic origin of adult neural stem cells. Nat. Neurosci. *18*, 657–665.

Gao, P., Postiglione, M.P., Krieger, T.G., Hernandez, L., Wang, C., Han, Z., Streicher, C., Papusheva, E., Insolera, R., Chugh, K., et al. (2014). Deterministic progenitor behavior and unitary production of neurons in the neocortex. Cell *159*, 775–788.

Gorski, J.A., Talley, T., Qiu, M., Puelles, L., Rubenstein, J.L.R., and Jones, K.R. (2002). Cortical excitatory neurons and glia, but not GABAergic neurons, are produced in the Emx1-expressing lineage. J. Neurosci. *22*, 6309–6314.

Hadjantonakis, A.-K., and Papaioannou, V.E. (2004). Dynamic in vivo imaging and cell tracking using a histone fluorescent protein fusion in mice. BMC Biotechnol. *4*, 33.

Hippenmeyer, S., Youn, Y.H., Moon, H.M., Miyamichi, K., Zong, H., Wynshaw-Boris, A., and Luo, L. (2010). Genetic mosaic dissection of Lis1 and Ndel1 in neuronal migration. Neuron *68*, 695–709.

Kessaris, N., Fogarty, M., Iannarelli, P., Grist, M., Wegner, M., and Richardson, W.D. (2006). Competing waves of oligodendrocytes in the forebrain and postnatal elimination of an embryonic lineage. Nat. Neurosci. *9*, 173–179.

Khacho, M., Clark, A., Svoboda, D.S., Azzi, J., MacLaurin, J.G., Meghaizel, C., Sesaki, H., Lagace, D.C., Germain, M., Harper, M.E., et al. (2016). Mitochondrial Dynamics Impacts Stem Cell Identity and Fate Decisions by Regulating a Nuclear Transcriptional Program. Cell Stem Cell *19*, 232–247.

Khatri, P., Obernier, K., Simeonova, I.K., Hellwig, A., Hölzl-Wenig, G., Mandl, C., Scholl, C., Wölfl, S., Winkler, J., Gaspar, J.A., et al. (2014). Proliferation and cilia dynamics in neural stem cells prospectively isolated from the SEZ. Sci. Rep. *4*, 3803.

Kyrousi, C., Arbi, M., Pilz, G.-A., Pefani, D.-E., Lalioti, M.-E., Ninkovic, J., Götz, M., Lygerou, Z., and Taraviras, S. (2015). Mcidas and GemC1/Lynkeas are key regulators for the generation of multiciliated ependymal cells in the adult neurogenic niche. Development *142*, 3661–3674.

Loulier, K., Barry, R., Mahou, P., Le Franc, Y., Supatto, W., Matho, K.S., Ieng, S., Fouquet, S., Dupin, E., Benosman, R., et al. (2014). Multiplex cell and lineage tracking with combinatorial labels. Neuron *81*, 505–520.

Ma, L., Quigley, I., Omran, H., and Kintner, C. (2014). Multicilin drives centriole biogenesis via E2f proteins. Genes Dev. *28*, 1461–1471.

Madisen, L., Zwingman, T.A., Sunkin, S.M., Oh, S.W., Zariwala, H.A., Gu, H., Ng, L.L., Palmiter, R.D., Hawrylycz, M.J., Jones, A.R., et al. (2010). A robust and high-throughput Cre reporting and characterization system for the whole mouse brain. Nat. Neurosci. *13*, 133–140.

McGarry, T.J., and Kirschner, M.W. (1998). Geminin, an inhibitor of DNA replication, is degraded during mitosis. Cell *93*, 1043–1053.

Mirzadeh, Z., Merkle, F.T., Soriano-Navarro, M., Garcia-Verdugo, J.M., and Alvarez-Buylla, A. (2008). Neural stem cells confer unique pinwheel architecture to the ventricular surface in neurogenic regions of the adult brain. Cell Stem Cell *3*, 265–278.

Mirzadeh, Z., Doetsch, F., Sawamoto, K., Wichterle, H., and Alvarez-Buylla, A. (2010). The subventricular zone en-face: wholemount staining and ependymal flow. J. Vis. Exp. *39*, 1938.

Morin, X., Jaouen, F., and Durbec, P. (2007). Control of planar divisions by the G-protein regulator LGN maintains progenitors in the chick neuroepithelium. Nat. Neurosci. *10*, 1440–1448.

Obernier, K., Cebrian-Silla, A., Thomson, M., Parraguez, J.I., Anderson, R., Guinto, C., Rodas Rodriguez, J., Garcia-Verdugo, J.-M., and Alvarez-Buylla, A. (2018). Adult Neurogenesis Is Sustained by Symmetric Self-Renewal and Differentiation. Cell Stem Cell *22*, 221–234.e8.

Ollion, J., Cochennec, J., Loll, F., Escudé, C., and Boudier, T. (2013). TANGO: a generic tool for high-throughput 3D image analysis for studying nuclear organization. Bioinformatics *29*, 1840–1841.

Pefani, D.-E., Dimaki, M., Spella, M., Karantzelis, N., Mitsiki, E., Kyrousi, C., Symeonidou, I.-E., Perrakis, A., Taraviras, S., and Lygerou, Z. (2011). Idas, a novel phylogenetically conserved geminin-related protein, binds to geminin and is required for cell cycle progression. J. Biol. Chem. *286*, 23234–23246.

Sage, D., Neumann, F.R., Hediger, F., Gasser, S.M., and Unser, M. (2005). Automatic tracking of individual fluorescence particles: application to the study of chromosome dynamics. IEEE Trans. Image Process. *14*, 1372–1383.

Sankar, S., Yellajoshyula, D., Zhang, B., Teets, B., Rockweiler, N., and Kroll, K.L. (2016). Gene regulatory networks in neural cell fate acquisition from genome-wide chromatin association of Geminin and Zic1. Sci. Rep. *6*, 37412.

Schindelin, J., Arganda-Carreras, I., Frise, E., Kaynig, V., Longair, M., Pietzsch, T., Preibisch, S., Rueden, C., Saalfeld, S., Schmid, B., et al. (2012). Fiji: an open-source platform for biological-image analysis. Nat. Methods *9*, 676–682.

Shah, P.T., Stratton, J.A., Stykel, M.G., Abbasi, S., Sharma, S., Mayr, K.A., Koblinger, K., Whelan, P.J., and Biernaskie, J. (2018). Single-Cell Transcriptomics and Fate Mapping of Ependymal Cells Reveals an Absence of Neural Stem Cell Function. Cell *173*, 1045–1057.e9.

Shen, Q., Wang, Y., Kokovay, E., Lin, G., Chuang, S.-M., Goderie, S.K., Roysam, B., and Temple, S. (2008). Adult SVZ stem cells lie in a vascular niche: a quantitative analysis of niche cell-cell interactions. Cell Stem Cell *3*, 289–300.

Shihavuddin, A., Basu, S., Rexhepaj, E., Delestro, F., Menezes, N., Sigoillot, S.M., Del Nery, E., Selimi, F., Spassky, N., and Genovesio, A. (2017). Smooth 2D manifold extraction from 3D image stack. Nat. Commun. *8*, 15554.

Smith, A.R. (1978). Color gamut transform pairs. ACM SIGGRAPH Comput. Graph *12*, 12–19.

Spassky, N., and Meunier, A. (2017). The development and functions of multiciliated epithelia. Nat. Rev. Mol. Cell Biol. *18*, 423–436.

Spassky, N., Merkle, F.T., Flames, N., Tramontin, A.D., García-Verdugo, J.M., and Alvarez-Buylla, A. (2005). Adult ependymal cells are postmitotic and are derived from radial glial cells during embryogenesis. J. Neurosci. *25*, 10–18.

Spella, M., Britz, O., Kotantaki, P., Lygerou, Z., Nishitani, H., Ramsay, R.G., Flordellis, C., Guillemot, F., Mantamadiotis, T., and Taraviras, S. (2007). Licensing regulators Geminin and Cdt1 identify progenitor cells of the mouse CNS in a specific phase of the cell cycle. Neuroscience *147*, 373–387.

Spella, M., Kyrousi, C., Kritikou, E., Stathopoulou, A., Guillemot, F., Kioussis, D., Pachnis, V., Lygerou, Z., and Taraviras, S. (2011). Geminin regulates cortical progenitor proliferation and differentiation. Stem Cells *29*, 1269–1282.

Stancik, E.K., Navarro-Quiroga, I., Sellke, R., and Haydar, T.F. (2010). Heterogeneity in ventricular zone neural precursors contributes to neuronal fate diversity in the postnatal neocortex. J. Neurosci. *30*, 7028–7036.

Stubbs, J.L., Vladar, E.K., Axelrod, J.D., and Kintner, C. (2012). Multicilin promotes centriole assembly and ciliogenesis during multiciliate cell differentiation. Nat. Cell Biol. *14*, 140–147.

Sun, W., Cornwell, A., Li, J., Peng, S., Osorio, M.J., Aalling, N., Wang, S., Benraiss, A., Lou, N., Goldman, S.A., and Nedergaard, M. (2017). SOX9 Is an Astrocyte-Specific Nuclear Marker in the Adult Brain Outside the Neurogenic Regions. J. Neurosci. *37*, 4493–4507.

Tavazoie, M., Van der Veken, L., Silva-Vargas, V., Louissaint, M., Colonna, L., Zaidi, B., Garcia-Verdugo, J.M., and Doetsch, F. (2008). A specialized vascular niche for adult neural stem cells. Cell Stem Cell *3*, 279–288.

Terré, B., Piergiovanni, G., Segura-Bayona, S., Gil-Gómez, G., Youssef, S.A., Attolini, C.S., Wilsch-Bräuninger, M., Jung, C., Rojas, A.M., Marjanović, M., et al. (2016). GEMC1 is a critical regulator of multiciliated cell differentiation. EMBO J. *35*, 942–960.

Wang, X., Tsai, J.-W., Imai, J.H., Lian, W.-N., Vallee, R.B., and Shi, S.-H. (2009). Asymmetric centrosome inheritance maintains neural progenitors in the neocortex. Nature *461*, 947–955.

Xu, Q., Tam, M., and Anderson, S.A. (2008). Fate mapping Nkx2.1-lineage cells in the mouse telencephalon. J. Comp. Neurol. *506*, 16–29.

Zhou, F., Narasimhan, V., Shboul, M., Chong, Y.L., Reversade, B., and Roy, S. (2015). Gmnc Is a Master Regulator of the Multiciliated Cell Differentiation Program. Curr. Biol. *25*, 3267–3273.

Zimmerman, L., Parr, B., Lendahl, U., Cunningham, M., McKay, R., Gavin, B., Mann, J., Vassileva, G., and McMahon, A. (1994). Independent regulatory elements in the nestin gene direct transgene expression to neural stem cells or muscle precursors. Neuron *12*, 11–24.

STAR★METHODS

KEY RESOURCES TABLE

REAGENT or RESOURCE	SOURCE	IDENTIFIER
Antibodies		
Rat Monoclonal Anti-Mouse CD24	BD Biosciences	Cat#557436; Clone: M1/69; RRID: AB_396700
Mouse IgG1 Monoclonal Anti FoxJ1	Thermo Fisher Scientific	Cat#14-9965-82; Clone: 2A5; RRID: AB_1548835
Chicken Polyclonal Anti GFP	Aves Labs	Cat#GFP-1020; RRID: AB_10000240
Rabbit Polyclonal Anti DsRed	Clontech Laboratories	Cat#632496; RRID: AB_10013483
Rabbit Polyclonal Anti Sox9	Millipore	Cat#AB5535; RRID:AB_2239761
Mouse IgG2b Monoclonal Anti FOP	Abnova Corporation	Cat#H00011116-M01; Clone: 2B1 RRID: AB_463883
Mouse IgG1 Monoclonal Anti GFAP	Millipore	Cat#MAB3402; Clone: GA5 RRID: AB_94844
Rabbit Polyclonal Anti ZO1	Thermo Fischer Scientific	Cat#40-2200; RRID: AB_2533456
Mouse IgG1 Monoclonal Anti Gamma-tubulin	Sigma-Aldrich	Cat#T6557; Clone: GTU88 RRID: AB_477584
Mouse IgG2b Monoclonal Anti Acetylated Tubulin	Sigma-Aldrich	Cat#T6793; Clone: 6-11B-1 RRID: AB_477585
Donkey Polyclonal anti-Chicken IgY (IgG) (H+L) AffiniPure, Alexa Fluor 488	Jackson ImmunoResearch Labs	Cat#703-545-155; RRID:AB_2340375
Donkey Polyclonal anti-Rabbit IgG (H+L) Highly Cross-Adsorbed Secondary Antibody, Alexa Fluor 594	Thermo Fischer Scientific	Cat#A-21207; RRID: AB_141637
Donkey Polyclonal anti-Rabbit IgG (H+L) Highly Cross-Adsorbed Secondary Antibody, Alexa Fluor 647	Thermo Fischer Scientific	Cat#A-31573; RRID: AB_2536183
Goat anti-Mouse IgG1 Cross-Adsorbed Secondary Antibody, Alexa Fluor 488	Thermo Fischer Scientific	Cat#A-21121; RRID:AB_2535764
Goat anti-Mouse IgG1 Cross-Adsorbed Secondary Antibody, Alexa Fluor 594	Thermo Fischer Scientific	Cat#A-21125; RRID:AB_2535767
Goat anti-Mouse IgG1 Cross-Adsorbed Secondary Antibody, Alexa Fluor 647	Thermo Fischer Scientific	Cat#A-21240; RRID:AB_2535809
Goat anti-Mouse IgG2b Cross-Adsorbed Secondary Antibody, Alexa Fluor 647	Thermo Fischer Scientific	Cat#A-21242; RRID:AB_2535811
Anti-Digoxigenin-AP, Fab fragments	Sigma-Aldrich	Cat#11093274910; RRID: AB_2734716
Chemicals, Peptides, and Recombinant Proteins		
EdU (5-ethynyl-2-deoxyuridine)	Thermo Fisher Scientific	Cat#11590926, CAS: 61135-33-9
Hoechst (bisBenzimide H 33342 trihydrochloride)	Sigma-Aldrich	Cat# B2261 CAS: 23491-52-3
T7 RNA Polymerase	Sigma-Aldrich	Cat#RPOLT7-RO
T3 RNA Polymerase	Sigma-Aldrich	Cat#RPOLT3-RO
DIG RNA Labeling Mix	Sigma-Aldrich	Cat#11277073910
RNasin Ribonuclease Inhibitors	Promega	Cat#N2511
RQ1 RNase-Free DNase	Promega	Cat#M6101
BCIP (5-bromo-4-chloro-3-indolyl-phosphate)	Sigma-Aldrich	Cat#BCIP-RO, CAS: 6578-06-9
NBT (4-Nitro blue tetrazolium chloride)	Sigma-Aldrich	Cat#11585029001, CAS: 298-83-9

(*Continued on next page*)

Continued

REAGENT or RESOURCE	SOURCE	IDENTIFIER
Critical Commercial Assays		
Click-iT EdU Alexa Fluor 488 Imaging Kit	Thermo Fisher Scientific	Cat#C10337
Click-iT EdU Alexa Fluor 594 Imaging Kit	Thermo Fisher Scientific	Cat#C10339
Click-iT EdU Alexa Fluor 647 Imaging Kit	Thermo Fisher Scientific	Cat#C10340
Experimental Models: Organisms/Strains		
B6.129S2-Emx1$^{tm1(cre)Krj}$/J	The Jackson Laboratory (Gorski et al., 2002)	Cat#JAX:005628, RRID: IMSR_JAX:005628
B6;CBA-Tg(Gsx2-icre)1Kess/J	Gift from the laboratory of N. Kessaris (Kessaris et al., 2006)	Cat#JAX025806 RRID: IMSR_JAX:025806
C57BL/6J-Tg(Nkx2-1-cre)2Sand/J	The Jackson Laboratory (Xu et al., 2008)	Cat#JAX:008661, RRID:IMSR_JAX:008661
B6;129S6-*Gt(ROSA)26Sor*$^{tm14(CAG-tdTomato)Hze}$/J	The Jackson Laboratory (Madisen et al., 2010)	Cat#JAX:007908, RRID:IMSR_JAX:007908
MADM-11^{GT}	Hippenmeyer et al., 2010	Cat#JAX:013749 RRID:IMSR_JAX:013749
MADM-11^{TG}	Hippenmeyer et al., 2010	Cat#JAX:013751 RRID:IMSR_JAX:013751
RjORL:SWISS	Janvier Labs	N/A
GemC1$^{KO/KO}$	Arbi et al., 2016	N/A
Geminin$^{flox/flox}$	Spella et al., 2011	N/A
NestinCre $^{\pm}$	Zimmerman et al., 1994	N/A
Recombinant DNA		
^{PB}CAG-Nucbow Plasmid	Loulier et al., 2014	N/A
CAG-hypBase Plasmid	Loulier et al., 2014	N/A
CAG-seCre Plasmid	Loulier et al., 2014	N/A
CAG-H2B-GFP Plasmid	Gift from the laboratory of X. Morin (Hadjantonakis and Papaioannou, 2004)	N/A
pCAGGS-Cre Plasmid	Gift from the laboratory of X. Morin (Morin et al., 2007)	N/A
pCAGGS-GemC1 Plasmid	Kyrousi et al., 2015	N/A
pCAGGS-Geminin Plasmid	Spella et al., 2011	N/A
pBluesCriptKS-GemC1 Plasmid	This paper	N/A
pBluesCriptKS-Geminin Plasmid	Spella et al., 2007	N/A
Software and Algorithms		
Fiji	Schindelin et al., 2012	https://imagej.nih.gov/ij/download.html; RRID: SCR_003070
MATLAB	MATLAB and Statistics Toolbox Release 2012b, The MathWorks, Natick, Massachusetts, United States	https://fr.mathworks.com/products/matlab.html; RRID: SCR_001622
GraphPad Prism	GraphPad Prism version 7.00 for Windows, GraphPad Software, La Jolla California USA	https://www.graphpad.com/; RRID: SCR_002798
Other		
Glass capillaries (for IUE)	Harvard Apparatus	Cat#30-0019
CUY21EDIT Square Wave Electroporator	Nepagene	N/A
ProbeQuant G-50 Micro Columns	Sigma-Aldrich	Cat#GE28-9034-08

CONTACT FOR REAGENT AND RESOURCES SHARING

Further information and requests for resources and reagents should be directed to and will be fulfilled by the Lead Contact, Nathalie Spassky (spassky@biologie.ens.fr).

EXPERIMENTAL MODEL AND SUBJECT DETAILS

Mice were bred and the experiments were performed in conformity with French and European Union regulations and the recommendations of the local ethics committee (Comité d'éthique en experimentation animale n°005). The date of the vaginal plug was recorded as embryonic day (E) 0.5 and the date of birth as postnatal day (P) 0. Healthy, immunocompetent animals were kept in a 12 h light /12 h dark cycle at 22°C and fed *ad libitum*. All the individuals used in our study were not previously subject to any unrelated experimental procedures. Pregnant females were used for IUE (see below), but their littermates and any other mice of both sexes were randomly used for all experiments in this study. Emx1-Cre$^{+/-}$ (B6.129S2-Emx1$^{tm1(cre)Krj}$/J, JAX stock #005628, Gorski et al., 2002), Gsh2-Cre$^{+/-}$ (B6;CBA-Tg(Gsx2-icre)1Kess/J, a gift from the laboratory of N. Kessaris, Kessaris et al., 2006) and Nkx2.1-Cre$^{+/-}$ (C57BL/6J-Tg(Nkx2-1-cre)2Sand/J, JAX stock #008661, Xu et al., 2008) transgenic animals were crossed with R26:tdTomato$^{mT/mT}$ homozygous animals, also called Ai14 (B6;129S6-Gt(ROSA)26Sor$^{tm14(CAG-tdTomato)Hze}$/J, Madisen et al., 2010). The presence of the Cre transgene was assessed at birth by observing the neonatal brain (when the fluorescence is still visible through the skin with no fur) under the fluorescent stereo microscope. MADM$^{GT/+}$ and MADM$^{TG/+}$ transgenic animals were a gift from the laboratory of S. Hippenmeyer (Hippenmeyer et al., 2010). Heterozygous mice were crossed to obtain homozygous MADM$^{GT/GT}$ and MADM$^{TG/TG}$ animals. These homozygous mice were then mated to obtain MADM$^{GT/TG}$ embryos. Expression of the Cre Recombinase in MADM$^{GT/TG}$ embryos was achieved by IUE of pcX-Cre plasmid (1μg/μl, Morin et al., 2007) at E13.5 or E14.5. All transgenic mice lines were kept as B6D2F1/J or C57/Bl6 background. For all other experiments involving IUE, RjORL:SWISS pregnant females were used due to their fertility and their maternal instinct. RjORL:SWISS embryos were also used for the *in situ* hybridization experiment at E14.5 and cell culture. GemC1$^{KO/KO}$ homozygous animals were incrossed to obtain GemC1-deficient cell cultures. Geminin$^{flox/KO}$ mice and NestinCre $^{\pm}$ were crossed in order to have Geminin-deficient glial progenitors in our culture system. All animals analyzed in this study were sacrificed at P15-P20, except for the adult mice sacrificed at P42 to assess the neurogenic potential of SVZ astrocytes, the embryos (and consequently, the mother, at E14.5-E15.5) used for the *in situ* hybridization studies or EdU-mediated assessment of cell cycle stage of electroporated cells, and newborn pups (P0-P2) used for the cell culture.

METHOD DETAILS

In utero electroporation

In utero electroporation of mouse embryos was performed at E13.5 or E14.5. Pregnant females were injected subcutaneously with buprenorphine (0.1 mg/kg) 15 minutes prior to surgery. They were subsequently anaesthetized by isoflurane inhalation, the abdominal cavity opened and the uterine horns exposed. With a thin glass capillary (Harvard Apparatus), 1μl of plasmid in filtered PBS was injected together with FastGreen (0.025%, Sigma) into the LVs of the embryo. The final concentrations of plasmids were 1 μg/μl ^{PB}*CAG-Nucbow*, 0.5 μg/μl *CAG-hypBase*, 0.1 μg/μl *CAG-seCre* (Loulier et al., 2014), 1 μg/μl *CAG-H2B-GFP* (a gift from the laboratory of X. Morin, Hadjantonakis and Papaioannou, 2004), 1μg/μl pCAGGS-Cre (a gift from the laboratory of X. Morin, Morin et al., 2007), or 1μg/μl pCAGGS-GemC1 or pCAGGS-Geminin (gifts from the laboratory of S. Taraviras, Kyrousi et al., 2015).

Immediately after injection, four pulses of 50 ms and 35 V were applied to the embryos' telencephalon at 950 ms intervals with an electroporator (CUY21 EDIT, Nepagene). Finally, the embryos were carefully placed back into the abdominal cavity and left to develop before sacrifice.

EdU administration and detection

To determine the spatial disposition of newborn ependymal cells and the cell cycle stage at the time of electroporation, 50 mg/kg body weight (8 mg/ml stock, dissolved in filtered PBS) of EdU (Thermo Fisher Scientific) was administered to pregnant mice by intraperitoneal injection. In the first case, a single injection was administered at E15.5. In the second one two injections were performed; the first one 2 hours before and the second one 2 hours after IUE. To assess the neurogenic potential of SVZ astrocytes, EdU was administered for 14 days through the drinking water (1 mg/ml) of P21 electroporated litters. EdU incorporation was detected using the Click-iT EdU Alexa Fluor imaging kit (Thermo Fisher Scientific for Alexa Fluor 488, 594 or 647 staining), according to manufacturer's protocol. Briefly, V-SVZ wholemounts or fixed coronal sections of the forebrain or olfactory bulbs were permeabilized in blocking solution with 0.1% Triton X-100 and 10% fetal bovine serum in PBS for 1h. After washing with PBS, sections were incubated for 1 hour with the Click-iT reaction cocktail, protected from light. The sections were washed again and incubated overnight at 4°C with the primary antibodies. After incubation with the secondary antibody for 2 hours and Hoechst staining, slices were mounted with Fluoromount-G (Southern Biotech, 0100-01) mounting medium.

Primary Ependymal Cell culture

Primary culture of ependymal cells was done like previously described (Delgehyr et al., 2015; Al Jord et al., 2014). Briefly, newborn mice (P0–P2) were sacrificed by decapitation. Their brains were dissected in Hank's solution (10% HBSS, 5% HEPES, 5% sodium bicarbonate, 1% penicillin/streptomycin (P/S) in pure water) and the extracted ventricular walls were cut manually into small pieces, followed by enzymatic digestion (DMEM glutamax, 33% papain (Worthington 3126), 17% DNase at 10 mg/ml, 42% cysteine at 12 mg/ml, using 1 mL of the enzymatic digestion solution per brain) for 45 min at 37°C in a humidified 5% CO_2 incubator. Digestion was stopped by addition of a solution of trypsin inhibitors (Leibovitz Medium L15, 10% ovomucoid at 1 mg/ml, 2% DNase

at 10 mg/ml, using 1 mL of enzyme inhibiting solution per brain). The cells were then washed in L15 and resuspended in 1 mL per brain dissected of DMEM glutamax supplemented with 10% fetal bovine serum (FBS) and 1% P/S. Cells were then seeded in a Poly-L-lysine (PLL)-coated flask (1 mL per 75 cm^2 flask), containing 5 mL of the same medium in which cells were resuspended. Ependymal progenitors proliferated for 5 days until confluence followed by shaking (250rpm) overnight at room temperature. Pure confluent astroglial monolayers were replated at a density of 7×10^4 cells per cm^2 in DMEM glutamax, 10% FBS, 1% P/S on PLL-coated coverslides for immunocytochemistry experiments and maintained overnight. The medium was then replaced by serum-free DMEM glutamax 1% P/S, to trigger ependymal differentiation gradually *in vitro* (DIV 0).

Tissue and cell culture preparation

When the immunostaining was performed on coronal sections of postnatal animals, these were previously anesthetized with a mixture of 100 mg of ketamine and 10 mg of xylazine per kg of body weight, and then were perfused transcardially with 4% PFA. Adult animals used for EdU-retaining olfactory bulb neuron analyses were not perfused, since no immunohistochemistry procedure was performed on them. After overnight fixation of the dissected brain in 4% PFA at 4°C, of either perfused or non-perfused postnatal mice or embryos, 80 μm-thick floating sections were cut on a vibratome. Wholemounts of the lateral walls of the LVs were dissected (Mirzadeh et al., 2010) from animals sacrificed by cervical dislocation and fixed for 15 minutes in 4% PFA at room temperature. Primary cultures of ependymal cells were fixed for 10 minutes in 4% PFA at room temperature.

For *in situ* hybridization, an E14.5 pregnant female was sacrificed by cervical dislocation, the embryos were retrieved and their whole brains fixed for 3 days in 4% PFA at 4°C. The sectioning of the tissue was done like described above.

Immunostaining

Tissue samples and primary ependymal cell cultures were incubated for 1h in blocking solution (1X PBS with 0.1%–0.2% Triton X-100 and 10% fetal bovine serum) at room temperature. All these were incubated overnight at 4°C in the primary antibodies diluted in blocking solution. The primary antibodies used targeted CD24 (1:200, BD PharMingen), FoxJ1 (1:500, Thermo Fischer Scientific), GFP (1:1600, Aves Labs), Dsred (1:400, Clontech Laboratories), Sox9 (1:1200, Millipore), FOP (1:600, Abnova Corporation), GFAP (1:400, Millipore) ZO1 (1:100, Thermo Fischer Scientific), Gamma-tubulin (1:500, Sigma-Aldrich) and Acetylated-tubulin (1:400, Sigma-Aldrich). The following day, they were stained with species-specific AlexaFluor fluorophore-conjugated secondary antibodies (1:400, Thermo Fischer Scientific or Jackson ImmunoResearch Labs, see Key Resources Table). Nuclei were counterstained with a 1:1500 Hoechst solution (from a 20 mg/ml stock, Sigma-Aldrich), containing the secondary antibodies for 2h at room temperature. Finally, the wholemounts were redissected to keep only the thin lateral walls of the LV (Mirzadeh et al., 2010) which were mounted with Vectashield mounting medium (Sigma, H-1000), for Nucbow samples, or Fluoromount-G mounting medium (Southern Biotech, 0100-01), for other stainings. Fluoromount-mounted slides were stored at 4°C, whereas Vectashield-mounted wholemounts were stored at −20°C to avoid color fading. Cell culture coverslides were mounted with Fluoromount-G.

In situ hybridization

The GemC1 cDNA sequence was subcloned into a pBlueScriptKS plasmid by removing the former from the same pCAGGS-GemC1 plasmid used for GemC1 overexpression (see In Utero Electroporation, Kyrousi et al., 2015). Both plasmids were doubly digested with XbaI and XhoI. Then the DNA fragment corresponding to the GemC1 cDNA size was isolated from an agarose gel and ligated to the pBlueScriptKS backbone, upstream of the T3 promoter sequence. The pBlueScriptKS-Geminin plasmid was a gift from the laboratory of S. Taraviras (Spella et al., 2007). Briefly, in this study, the open reading frame of Geminin was cloned between the EcoRI/BamHI sites of the pBlueScriptKS plasmid, upstream of the T7 promoter sequence.

pBlueScriptKS-GemC1 and pBlueScriptKS-Geminin were linearized with XbaI and EcoRI restriction enzymes. Using the T3 and T7 RNA polymerases (Sigma-Aldrich), respectively, DIG-labeled ribonucleotide mix (Sigma-Aldrich) and a Ribonuclease inhibitor (Promega), a DIG-labeled gene-specific RNA probe was generated, according to manufacturer's instructions. RNA probes were subsequently treated with a Deoxyribonuclease (Promega) for 20 min at 37°C. Once synthesized, the RNA probes were purified in a ProbeQuant G-50 Micro Column (Sigma-Aldrich).

The *in situ* hybridization was performed as previously described (de Frutos et al., 2016). Unless stated otherwise, washing steps were performed thrice for 5 min. Floating sections of E14.5 embryos were incubated for 1 hour at room temperature (RT) in the dark in 2% H_2O_2 in PBS-0.1% Tween-20 (PBT). After washing in PBT, sections were treated with Proteinase K (10 μg/ml in PBT) for 3-4 min at RT and then the reaction was stopped in a 2mg/ml glycine solution in PBT for 5 min at RT. After washes in PBT, samples were post-fixed in 0.2% glutaraldehyde in 4% PFA for 30 min at RT. The tissue was washed again in PBT and then incubated for 1 hour at 60°C in hybridization buffer (50% formamide, 5X SSC, 1% SDS, 50 μg/ml heparin and 50 μg/ml yeast tRNA, in water). RNA probes were diluted at 5-10 μg/ml in hybridization buffer and incubated with the samples at 60°C overnight. The next day, sections were washed twice in a 50% formamide, 5X SSC, 1% SDS solution, for 30 min at 60°C. They were washed again twice in a 50% formamide, 2X SSC, 0,5% SDS solution, for 30 min at 60°C. Washing at RT in TBST (0.08% NaCl, 0.002%KCl, 2.5mM Tris, from a 1M Tris pH = 7.5 stock, 0.01% Tween-20) followed and blocking in 10% FBS in TBST for 1h 30 min at RT. An anti-DIG antibody (Sigma-Aldrich) was diluted in blocking solution (1:2000) and incubated with the samples overnight at 4°C. The next day, at least 8 washes in TBST and 3 in NTMT (100 mM NaCl, 100 mM Tris, from a 1M Tris pH = 9.5 stock, 50 mM $MgCl_2$, 0.01% Tween-20) for 10 min were done. Finally,

color developing was performed in a 0.35% vol/vol BCIP (Sigma-Aldrich) and 0.34% vol/vol NBT (Sigma-Aldrich) solution, from a 50 and 100 mg/ml stock dilution in dimethylformamide, respectivelty, in NTMT.

Imaging

Fixed slices or LV wholemounts were examined with an upright Zeiss Axio Observer.Z1 epifluorescence microscope, using an apochromat 63 × 1.4 NA objective and a Zeiss Apotome with an H/D grid.

Confocal image stacks were collected with a 40 × 1.3 NA water objective on Olympus FV1000 and FV1200 microscopes, or with a 40 × 1.4 NA oil objective or a 63 × 1.4 NA oil objective on an inverted LSM 880 Airyscan Zeiss microscope with 440, 515 and 560 laser lines to excite, independently, Cerulean, mEYFP and mCherry, or Alexa 488, 594 and 633/Cy5.

Finally, images of the *in situ* hybridization sections were taken with a Leica MZ16 F Fluorescence Stereo Microscope (Leica Microsystems), equipped with a plan-apochromatic objective 1.0x (Leica, 10447157) and a Nikon DS-Ri1 High Resolution Color Camera (Nikon), with the assistance of the NIS-Element F Ver5.502 Imaging Software (Nikon).

Automatic image analysis of MAGIC Markers

For clarity, mCherry, EYFP and Cerulean Nucbow signals are represented as red, green and blue (RGB) values. 1) Local apical layer extraction*:* to maintain consistency among datasets, only cells within 25 μm of the apical surface were considered using the SME projection tool on the FoxJ1-stained cell nuclei (Shihavuddin et al., 2017). 2) Segmentation of ependymal cells stained with FoxJ1: the 3D volume occupied by each cell nucleus was delineated using FoxJ1 far red staining. RGB information was extracted from the segmented mask using the following steps implemented as a Fiji macro: Noise was reduced in a preprocessing step using 3D Gaussian filtering, where the sigma values of the Gaussian kernel was set to 1/3rd of the estimated mean nuclear radius in 3D. This was followed by Log3D filtering (Sage et al., 2005) to select objects corresponding to nuclear size; the local 3D maximum was then detected to determine the center of each cell nucleus. 3D-seeded watershed segmentation was performed from these maxima to accurately detect the nuclear border in 3D. This 3D segmentation mask was used to compute the volume and the mean color of each nucleus. 3) Segmentation of non-ependymal cells: After elimination of FoxJ1-positive ependymal cells, only FoxJ1-negative non-ependymal cells remained in the 25μm apical layer. Since there is no specific marker for these cells, they were characterized by their color information as follows: Projection: projection of the Nucbow color channels was maximized to obtain a 2D representation of all labeled non-ependymal cells. Color gradient extraction: In order to accentuate nuclear borders, the image gradient was computed from the sum of the intensities of the three RGB channels. The gradient image was further filtered with adaptive Gaussian filtering to improve the signal to noise ratio. The adaptive filter augments smoothing where the image gradient is weak and decreases smoothing where the gradient is high, in order to preserve nuclear edges. Watershed segmentation: Local maxima were extracted from the inverted smoothed gradient response to retrieve one maximum per nucleus. The seeded watershed transform was then used (Ollion et al., 2013) to detect cells in 2D. 4) Color normalization*:* RGB channels were rescaled linearly from 0 and the 99th percentile of their intensity distribution to ensure alignment of their relative intensity (1% of the most saturated cells were therefore excluded from the analysis of each sample). 5) Determination of clonal lineage*:* To identify the cell lineage, each cell was characterized by the median R G B values and their spatial location in 3D X, Y, Z. RGB values were converted to their equivalent in the HSV (Hue, Saturation, Value) color space as described in Loulier et al. (2014). This conversion was performed in MATLAB with the HEXCONE model proposed by Smith (1978).

QUANTIFICATION AND STATISTICAL ANALYSES

Quantification, image and statistical analyses were performed with Fiji (Schindelin et al., 2012), MATLAB (Mathworks, USA), Excel, and GraphPad Prism software. Quantifications throughout the study are represented as the mean value, with the exception of the clone size representation, which indicates the clone size frequency distribution (only Figure 4H), as well as the Gaussian non-linear regression curve fitting the frequency of clones of variable sizes (from 1 to 8 cells per clone, Figure 4H, 5C, 6C). Error bars indicate the Standard Error of the Mean (SEM), except for Figure S1C, in which the Standard Deviation (SD) is depicted. P values in this manuscript present the following star code: ns: $p > 0.05$ (non-significant), *$p \leq 0.05$, **$p \leq 0.01$, ***$p \leq 0.001$.

Fate mapping of the spatial origin of ependymal cells

In order to characterize the spatial origin of ependymal cells and the presence or absence of ependymal progenitor cell migration, we considered two areas along the ventricular wall in the Cre-expressing animals; a Cre-positive area, or the anatomical part of the ventricle directly derived from the embryonic Cre-expressing area (Dorsal and Dorsal Medial Walls in the Emx1Cre mice, the Lateral Wall in the Gsh2Cre mice and the ventral-most region of the wall in the Nkx2.1Cre animals), and a Cre-negative area, or the anatomical part of the ventricle that is not derived from the embryonic Cre-expressing area, according to the literature. In the Emx1-cre; Ai14 group, 14 images from n = 6 animals were analyzed, with 1615 counted cells in the Cre-positive area and 1723 cells in the Cre-negative area. For the Gsh2-cre; Ai14 individuals, 15 images from n = 4 animals were used for quantification, with 383 and 895 cells counted on the Cre-positive and Cre-negative anatomical areas, respectively. Finally, 16 images from n = 5 Nkx2.1-cre; Ai14 animals were used, with a total of 496 and 2367 cells analyzed in the Cre-positive and negative areas, respectively.

To determine whether the differences between the Cre-positive and negative areas were significant, we performed a Mann-Whitney test.

Characterization of the cell types in the electroporated V-SVZ

19 images containing 441 V-SVZ electroporated (H2B-GFP positive) cells were analyzed in n = 3 different animals. The differences between cell types (astrocytes or FoxJ1$^-$Sox9$^+$, ependymal or FoxJ1$^+$Sox9$^+$, and unknown cell type or FoxJ1$^-$Sox9$^-$) were determined in pairs via the Mann-Whitney test.

Automatic image analysis of MAGIC markers

We assessed n = 6 V-SVZ wholemounts electroporated with the MAGIC markers (Nucbow). The automated analysis of such samples yielded 7668 Nucbow$^+$ cells, which could be regrouped in clones of cells, i.e., cells with a common progenitor, based on their color characteristics (see Method Details). 1142 Nucbow$^+$ cells that belonged to 163 clones with 2 cells (326 cells) or 186 clones with 3 to 8 cells (816 cells) and that contained at least one FoxJ1$^+$ cell were taken into account. These 349 clones represented the 83% of all 418 clones found by the automated analysis with at least one FoxJ1$^+$ cell. The 17% remaining clones had 9 to 32 cells and they were excluded from the analysis. Clones of 2 cells (163 of the 349 total clones) were categorized in clones formed by 2 ependymal cells (only FoxJ1$^+$) or 1 ependymal and 1 non-ependymal cells (FoxJ1$^+$ = FoxJ1$^-$). Clones of 3 to 8 cells (186 of the 349 total clones) were subdivided in clones formed by exclusively ependymal cells (only FoxJ1$^+$), clones with as many or more ependymal cells as non-ependymal cells (FoxJ1$^+$ $\geq$ FoxJ1$^-$), or clones with less ependymal than non-ependymal cells (FoxJ1$^+$ < FoxJ1$^-$). The difference between the frequency of clones with 2 or 3 to 8 cells, as well as the difference between the percentage of types of clones (only FoxJ1$^+$, FoxJ1$^+$ = FoxJ1$^-$, FoxJ1$^+$ $\geq$ FoxJ1$^-$, FoxJ1$^+$ < FoxJ1$^-$), were determined in two-by-two comparisons with the Mann-Whitney test.

The 3D-distance between cells in pure ependymal clones and between cells in mixed clones (with at least one FoxJ1$^-$ cell) was calculated automatically and the p value was assessed using the Mann-Whitney test, as well.

MADM transgenic image analysis

In all, 314 clones of 2 or more cells were analyzed (29 E13Ctrl, 20 E13GemC1, 73 E13Geminin, 44 E14Ctrl, 41 E14GemC1 and 107 E14 Geminin), which counted for 1069 cells (117 E13Ctrl, 56 E13GemC1, 317 E13Geminin, 134 E14Ctrl, 110 E14GemC1 and 335 E14Geminin), obtained from 52 electroporated embryos (6 E13Ctrl, 4 E13GemC1, 8 E13Geminin, 16 E14Ctrl, 9 E14GemC1 and 13 E14Geminin). To assess the percentage of types of clones (Ependymal only versus Mixed and versus B1 astrocytic only), and cells (Ependymal versus B1 astrocytes), all clones were grouped, independently of animals, since the efficiency of the IUE technique and the Cre recombination in MADM mice are highly variable. This resulted in the problem of having animals with a very small number of clones (one or two) and animals with a very large number (up to 26) and, hence, not having the same weight in the statistical analysis. In order to study the difference of clone types and cell proportion among the different categories, a two-proportion Z-test was performed in each case.

The differences in cell division type (Ependymal symmetric, E-E, B1 astrocytic symmetric, B1-B1, or asymmetric, E-B1) were assessed with the Mann-Whitney test.

Finally, the clone size distribution (number of cells per clone) for each category was represented as a Gaussian non-linear regression curve, fitting the frequency of clones with several sizes (from 1 to 8 cells per clone). The differences in the clone size distribution were determined via a Chi^2 test for trend.

The distance between cells in a clone was determined by assessing the mean distance between pairs of cells in a clone, when they possessed more than 2 cells, or the only distance between the unique pair of cells in clones with 2 cells. The significance of the difference in such distance was calculated using the Mann-Whitney test.

EdU incorporation in the V-SVZ analysis

17 and 12 coronal sections of electroporated brains with stained EdU were analyzed for the E13.5 and E14.5 brains (n = 3 for each category). In these, the percentage of EdU retaining cells was assessed. The p value was calculated using the Mann-Whitney test.

Characterization of the differentiation status in the V-SVZ with or without GemC1

41 and 15 coronal sections were analyzed for the H2B-GFP and GemC1/H2B-GFP-electroporated brains, respectively. A total of 4434 and 1953 H2B-GFP$^+$ ependymal (multi-FOP stained) and non-ependymal cells (two-dot FOP stained) were counted in the V-SVZ of 3 control and 3 GemC1 brains. Even though the number of animals was the same, the difference in analyzed sections and counted cells is due to the variability of the electroporation, which causes that some brains are electroporated over a wide area, whereas others are targeted by the electroporation in a restrained zone. The difference between the percentage of electroporated ependymal cells (over the total electroporated cells) in both categories was determined with a Mann-Whitney test.

Assessment of the differentiation status of GemC1 KO and Geminin cKO primary cultures

n = 4 cultures for WT, n = 2 for GemC1$^{KO/KO}$ and n = 4 for Geminin$^{FL/KO}$;NestinCre $^{\pm}$ were quantified. In all 1015, 637 and 1638 cells were counted for each one of the genotypes, respectively. The percentage of differentiation in each condition was normalized to the WT (control). The differences between genotypes were determined in pairs using the Mann-Whitney test.

DATA AND SOFTWARE AVAILABILITY

Several macros were created using the MATLAB software to use for the automatic analysis of MAGIC markers. They will be available upon request to the corresponding author.

Neuron, Volume *102*

Supplemental Information

Adult Neural Stem Cells and Multiciliated Ependymal Cells Share a Common Lineage Regulated by the Geminin Family Members

Gonzalo Ortiz-Álvarez, Marie Daclin, Asm Shihavuddin, Pauline Lansade, Aurélien Fortoul, Marion Faucourt, Solène Clavreul, Maria-Eleni Lalioti, Stavros Taraviras, Simon Hippenmeyer, Jean Livet, Alice Meunier, Auguste Genovesio, and Nathalie Spassky

Supplementary Figure 1

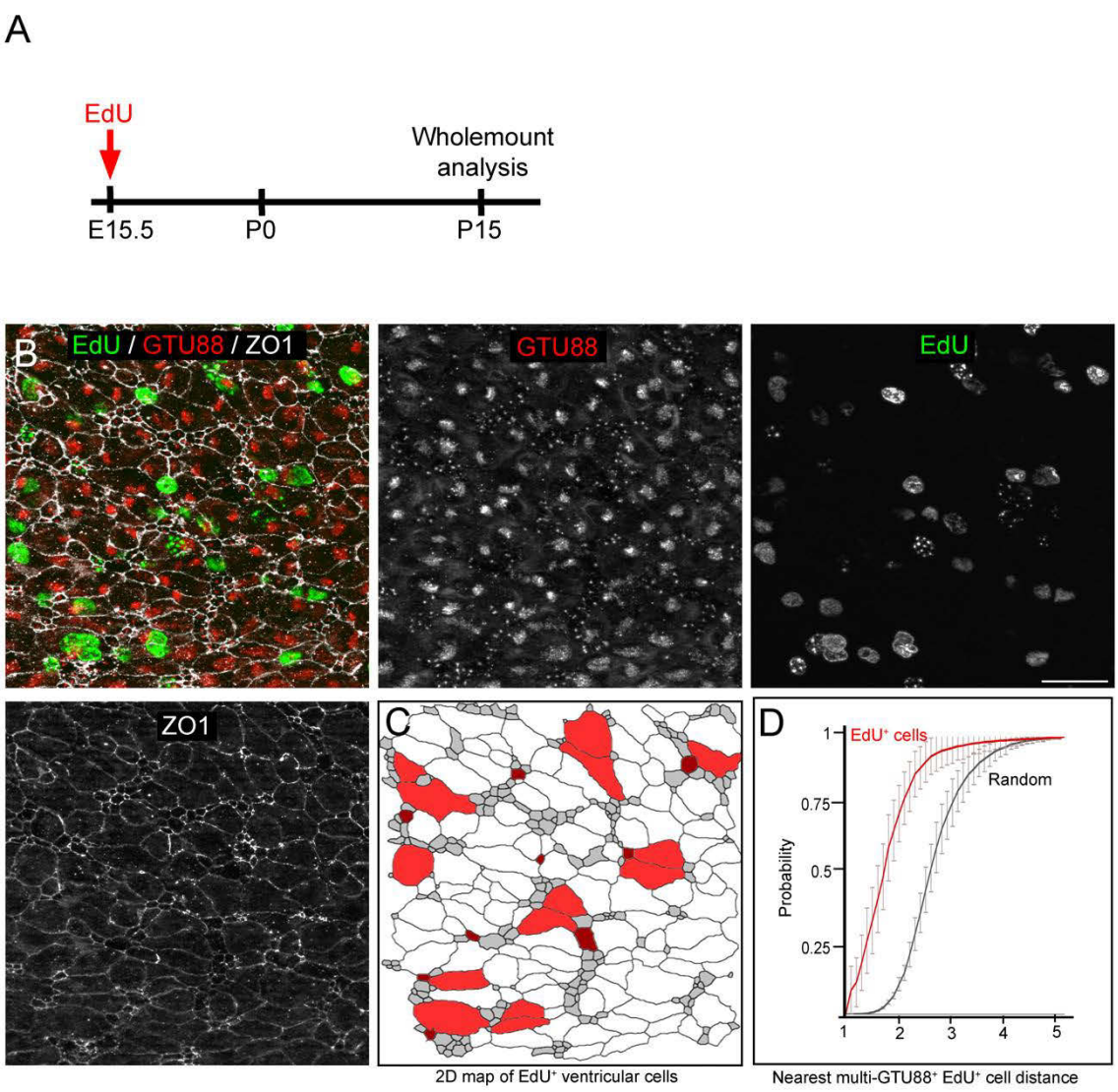

Supplementary Figure 1: Ependymal cells derived from E15.5 progenitors are closer than random at P15 (related to Figure 1)

(A) Experimental schema for (B): Timed-pregnant female mice received one injection of EdU at E15.5 and wholemounts of the V-SVZ of the offspring were analyzed at P15.

(B) Triple immunolabeling with ZO1 (white), EdU (green) and gamma tubulin (clone GTU88, basal body marker, red).

(C) 2D map of EdU^+ ependymal and B1 cells. SME projection was used to extract a 2D image of the surface in the vicinity of the apical layer of the 3D stack. Watershed segmentation was then performed on 2D image, using local maxima of the adaptive gaussian-smoothed input image as seeds. The segmented cells were then classified in ependymal multiple-dotted $GTU88^+$ EdU^+ (red), B1 double-dotted $GTU88^+$ EdU^+ (brown) or EdU^- (white) cells with a rule-based classifier applied to texture features computed from each single segmented cell.

(D) Nearest neighbor distance analysis of EdU^+ ependymal cells (with multiple $GTU88^+$ basal bodies) in the P15 V-SVZ injected with EdU at E15.5. According to the average amount and proportion of EdU^+ cells observed in 24 images obtained from 5 different mouse brains, 500 artificial images were generated, each containing a regular hexagonal grid of 345 cells with a 0.065 probability of being randomly EdU^+. From there, a distribution of the distance of the closest EdU^+ cell from each EdU^+ cell was obtained with the distance defined as the number of cells between two EdU^+ cells. A mean of the 500 cumulative distributions are represented by the black curve. The red curve represents the same computed results made on the real dataset of 25 images. Error bars represent the SD. The p-value was determined with the non-parametric Kolmogorov-Smirnov test for 2 samples; ***$p \leq 0.001$. The scale bar represents 25 µm.

Supplementary Figure 2

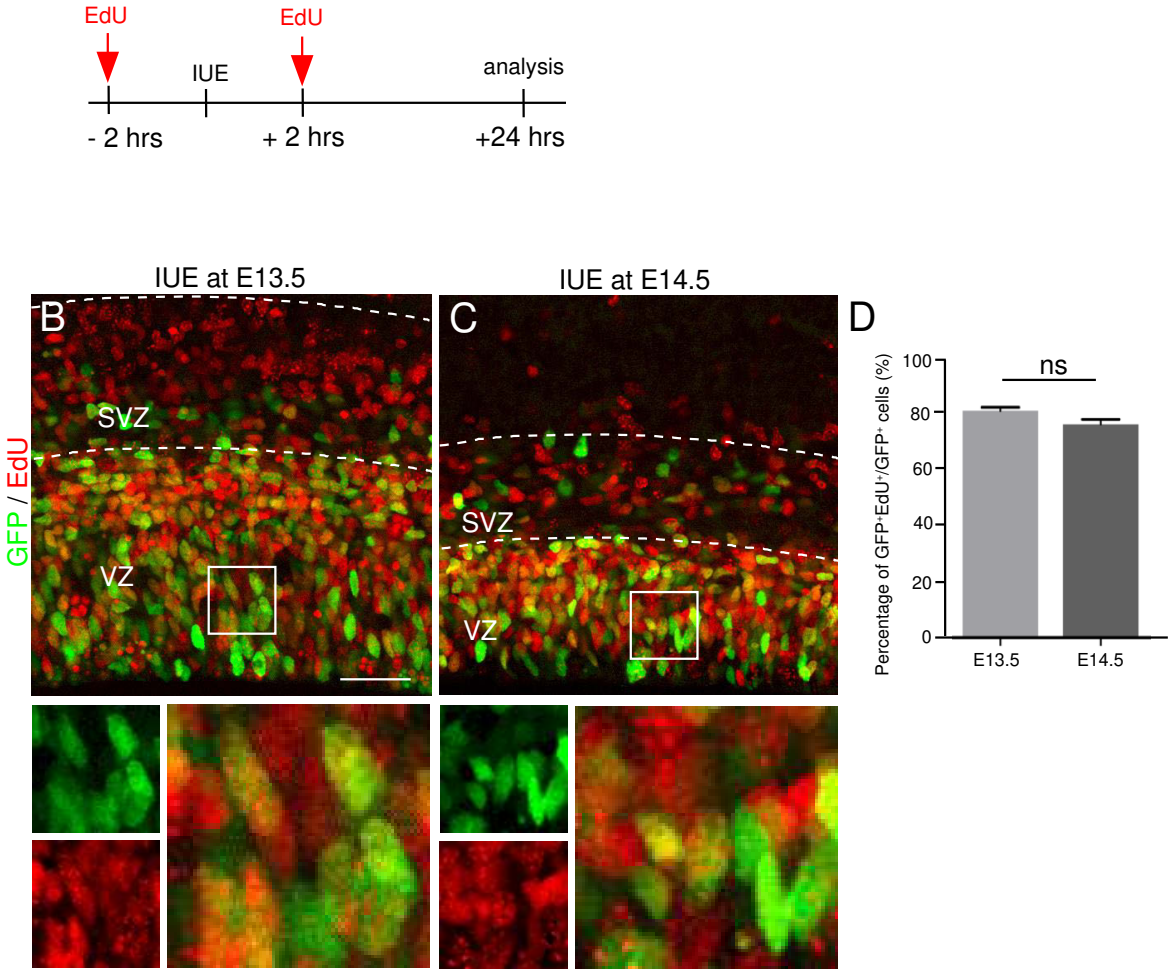

Supplementary Figure 2: *In utero* electroporation targets proliferating radial glia progenitors (related to Figure 2)

(A) Experimental schema for (B): Timed-pregnant female mice received a single injection of EdU 2 hours before and after *in utero* electroporation of H2B-GFP at E13.5 (B) or E14.5 (C) and coronal sections of the forebrain were analyzed 24 hours later.

(B-C) EdU labeling on coronal sections of the H2B-GFP$^+$ brains, 24 hours after the electroporation.

(D) Mean percentage of GFP$^+$EdU$^+$ among all GFP$^+$ cells one day after the electroporation at E13.5 or E14.5. Data are presented as the mean ± SEM. The p-value was determined by the Mann-Whitney test; ns, p>0.05, n=3 experiments. VZ, ventricular zone; SVZ, subventricular zone. The scale bar represents 75 µm.

Supplementary Figure 3

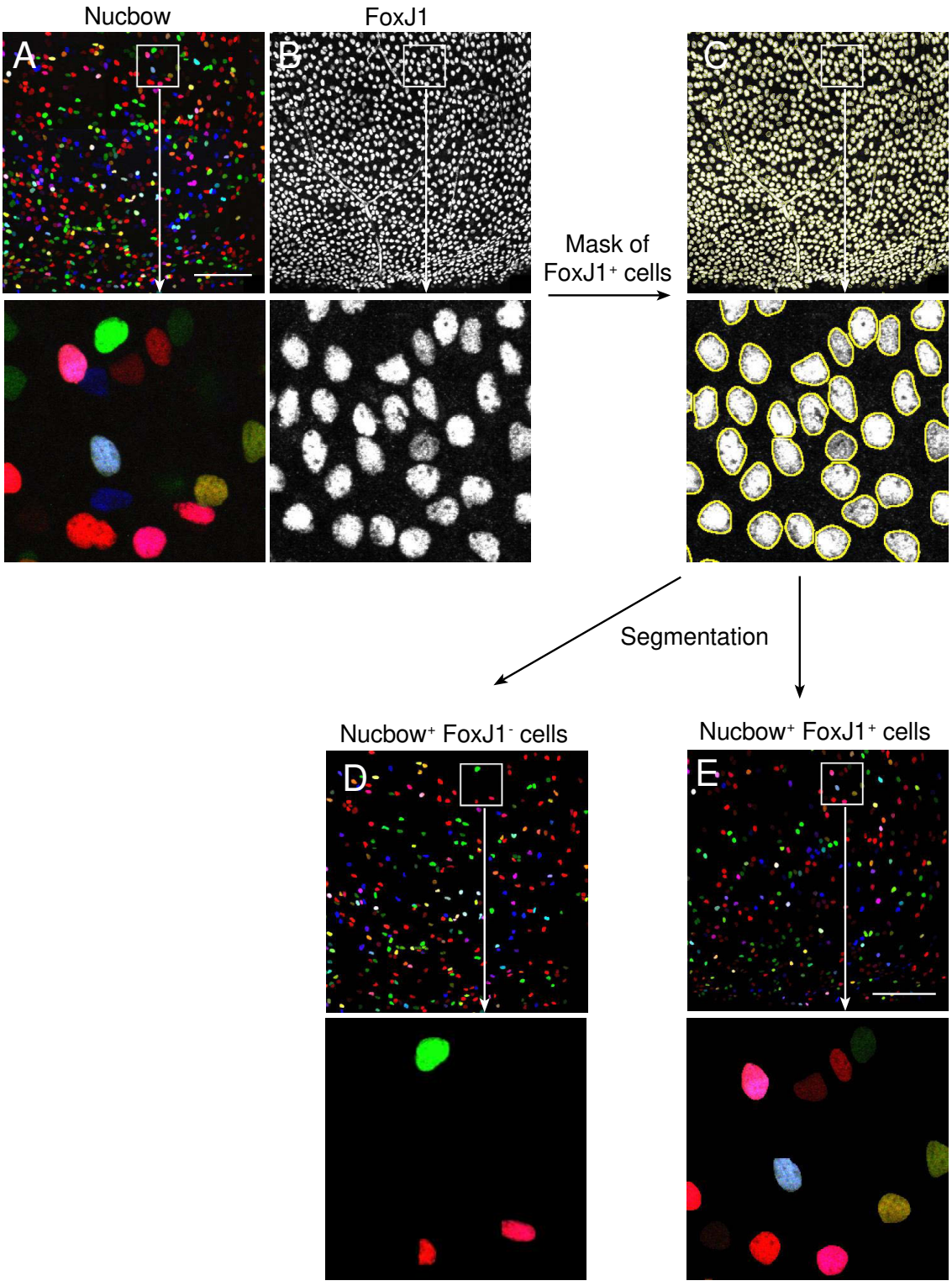

Supplementary Figure 3: Methodology for the detection of FoxJ1^{+} and FoxJ1^{-} Nucbow^{+} cells (related to Figure 3)

(A-B) Representative raw images of an *en-face* view of the V-SVZ electroporated at E14.5 with ^{PB}*CAG-Nucbow* along with the PiggyBac transposase and the self-excising Cre recombinase (A) and immunostained at P15 with FoxJ1 antibody (B).
(C) 25 µm 3D-segmentation of FoxJ1^{+} cells outlined in yellow using Gaussian smoothing, Log3D filtering and 3D watershed segmentation implemented as a Fiji macro (see methods).
(D-E) Segmented images of Nucbow^{+}FoxJ1^{-} and Nucbow^{+}FoxJ1^{+} cells, respectively. The scale bar represents 300 µm.

Supplementary Figure 4

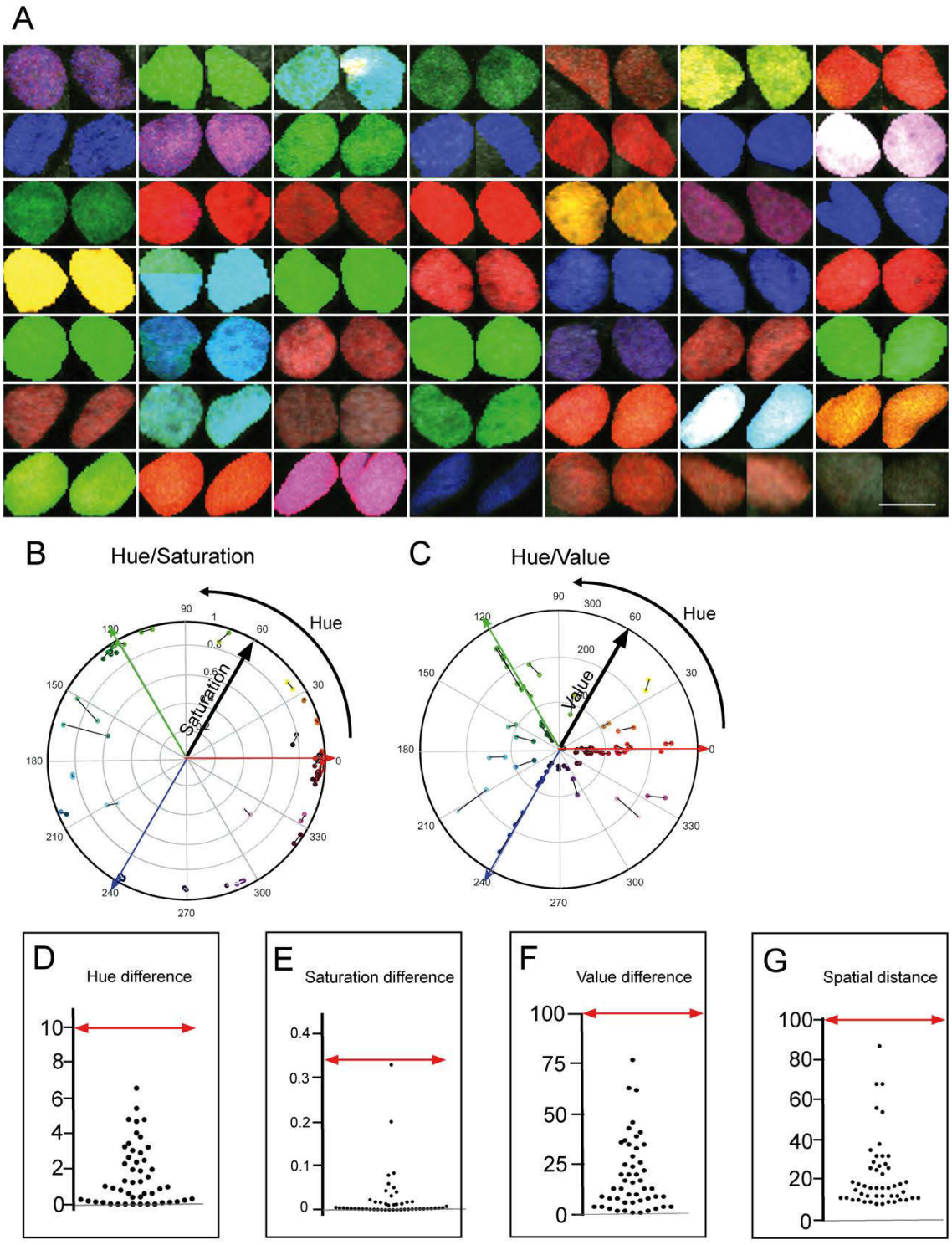

Supplementary Figure 4: Color analysis of manually selected Nucbow^{+} clones (related to Figure 3)

(A) 49 couples of cells were manually selected by 2 independent researchers from 4 different electroporated brains with ^{PB}*CAG-Nucbow* along with the PiggyBac transposase and the self-excising Cre recombinase at E14.5.

(B-C) Circular Hue-Saturation (B) and Hue-Value (C) plots of manually selected Nucbow^{+} cells shown in (A).

(D-G) Hue, Saturation, Value differences and spatial distance between each cell of the manually selected Nucbow^{+} clones shown in (A). The red arrows indicate the thresholds chosen for the automatic analysis. The scale bar represents 15 µm.

Supplementary Figure 5

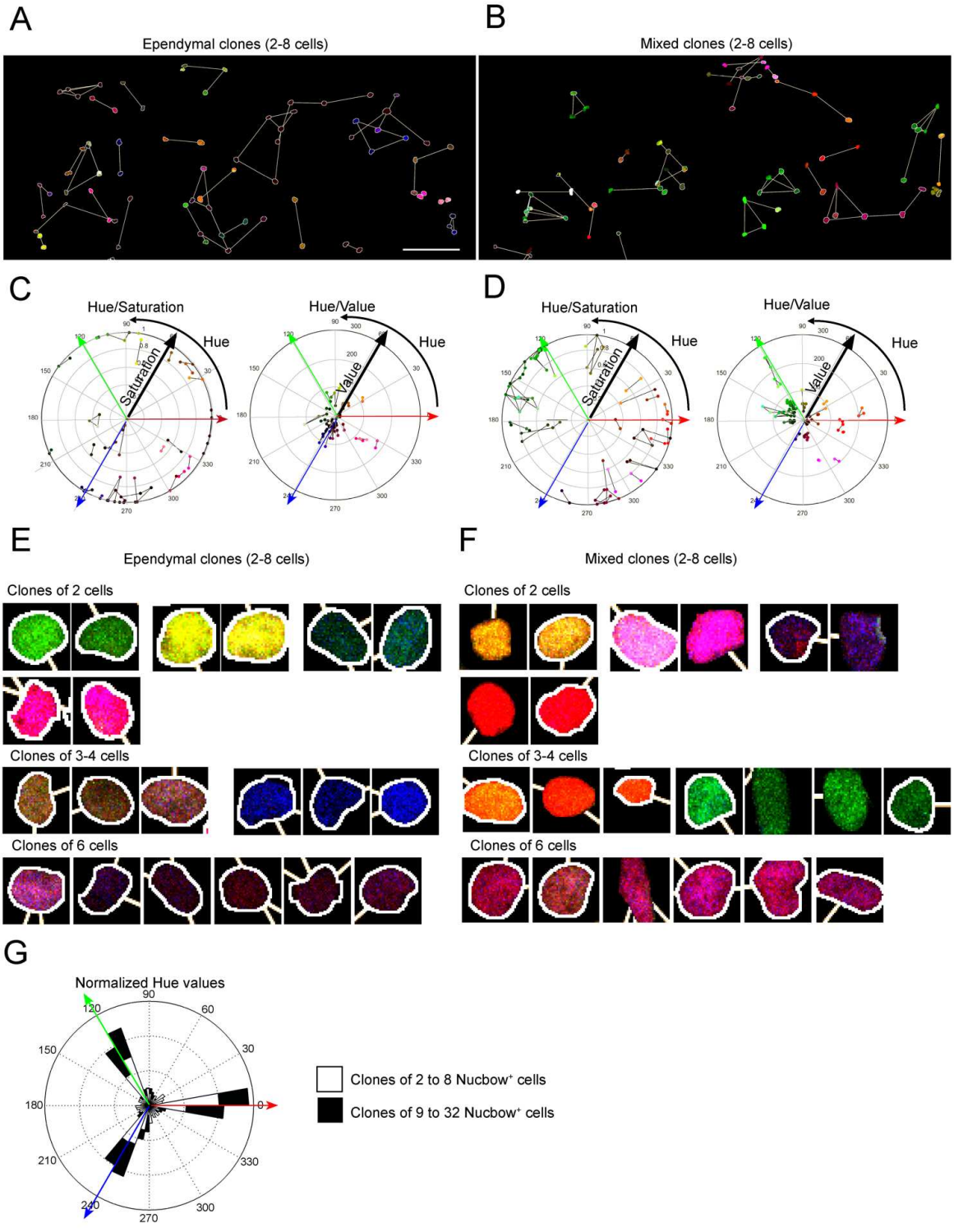

Supplementary Figure 5: Color analysis of Nucbow$^+$ clones (related to Figure 3)

(A-B) Map of Nucbow$^+$ clones containing 2 to 8 ependymal cells (A) or a mixed population of FoxJ1$^+$ and FoxJ1$^-$ cells (B).

(C-D) Circular Hue-Saturation and Hue-Value plots of all depicted Nucbow$^+$ cells from (A-B), respectively.

(E-F) Examples of ependymal cell clones formed by 2, 3 or 6 FoxJ1$^+$ cells (E) and clones containing at least one FoxJ1$^+$ cell formed by 2, 3, 4 or 6 cells. In all maps, FoxJ1$^+$Nucbow$^+$ cells are outlined in white.

(G) Normalized circular histogram of Hue values of cells contained in clones of 2 to 8 cells (small clones, white) or clones of 9 to 32 cells (big clones, black). Cells from big clones are more frequent around primary colors compared to cells from small clones (Kolmogorov-Smirnov test, p=0.001). The scale bar represents 100 µm (A-B) and 10 µm (E, F).

Supplementary Figure 6

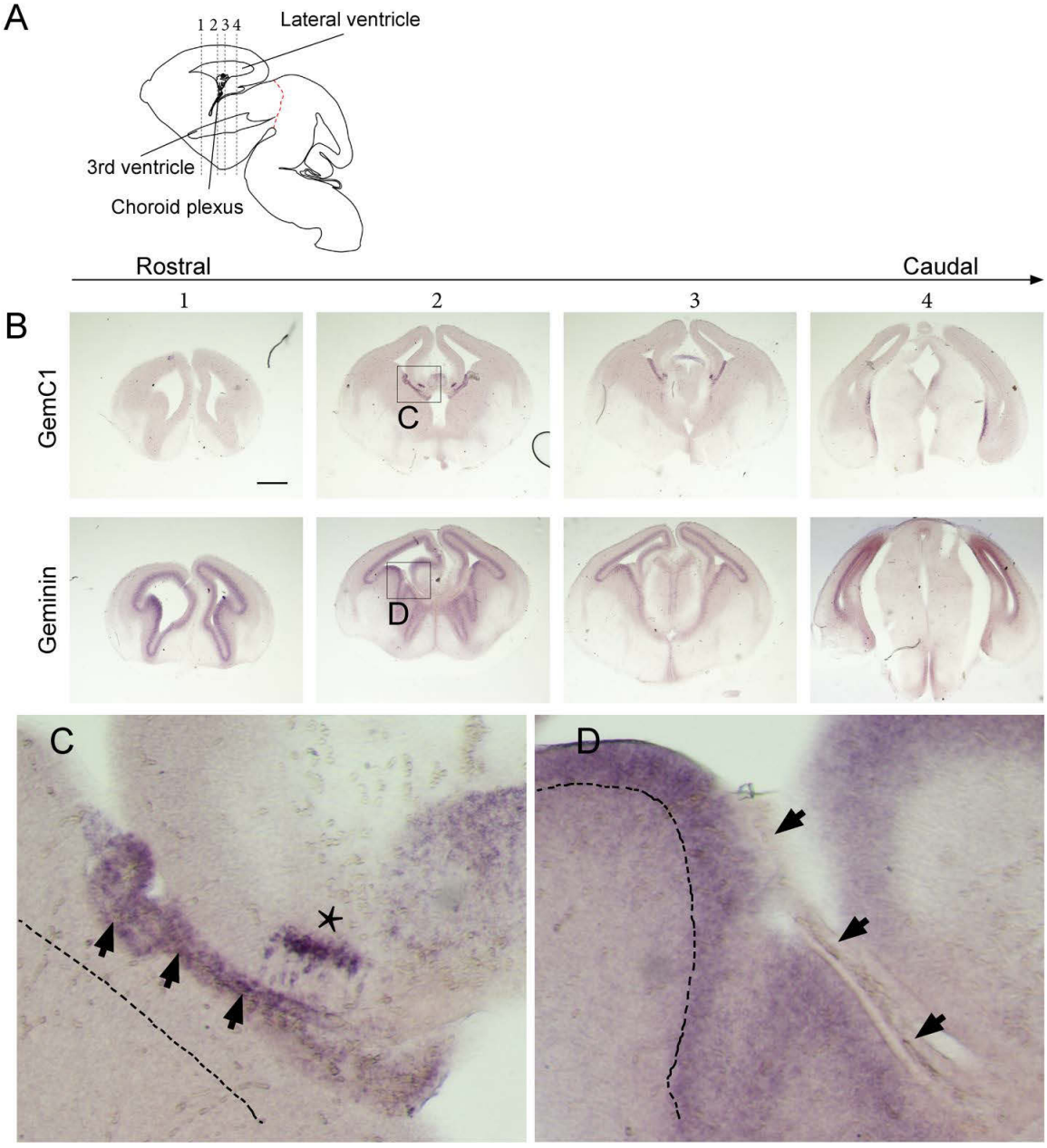

Supplementary Figure 6: Pattern of expression of GemC1 and Geminin in the E14.5 forebrain (related to Figure 5-6)

(A) Schematic representation of an E14.5 developing brain and the coronal planes (1 to 4, dashed lines) along the rostrocaudal axis of the lateral ventricles that are represented in B-C. Note that planes 2 and 3 pass along the choroid plexus. The red dashed line indicates the separation between the forebrain and the midbrain.

(B) Stereo microscope images of the i*n situ* hybridization of GemC1 and Geminin in four sections along the rostrocaudal axis.

(C-D) High magnification images of the pictures in (B) for GemC1 (C) and Geminin (D). The dashed line indicates the area of the germinal zone. Arrowheads point at the choroid plexus. The asterisk points at the fimbria.

The scale bar represents 500 µm (B) and 36 µm (C-D).

Supplementary Figure 7

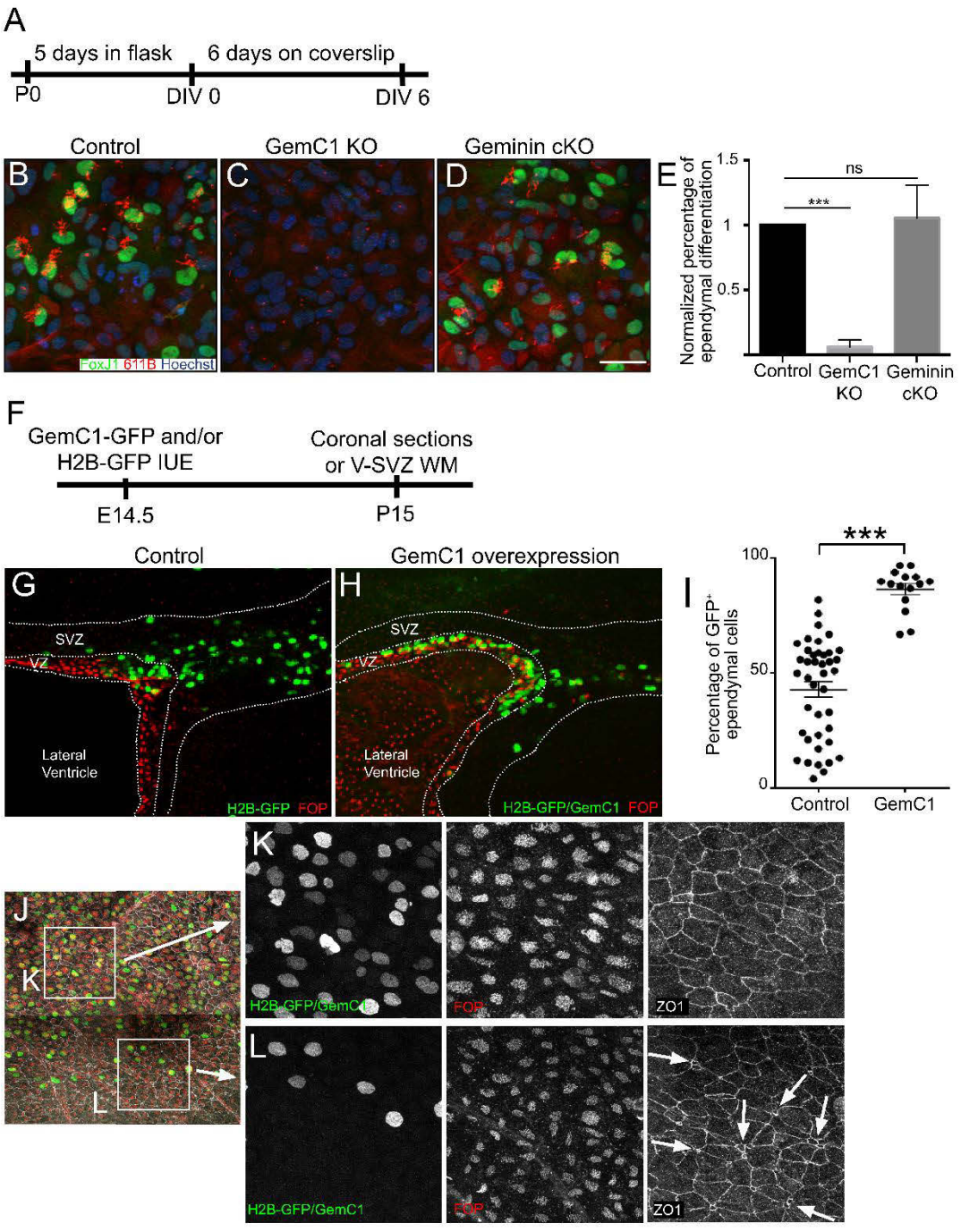

Supplementary Figure 7: GemC1 is necessary and sufficient for ependymal differentiation (related to Figure 5-6)

(A) Experimental schema for (B-E): Primary cultures of RGCs from WT, GemC1$^{KO/KO}$ or Geminin$^{flox/ko}$;NestinCre$^{\pm}$ animals were seeded in flasks containing serum-rich medium for 5 days. Ependymal progenitors were then seeded at high confluency on coverslips in serum-deprived medium and they were left for 6 days to differentiate.

(B-D) Double immunolabeling with FoxJ1 (green) and acetylated tubulin (clone 611B, cilia marker, red) for WT (B), GemC1$^{KO/KO}$ (C) or Geminin$^{flox/ko}$;NestinCre$^{\pm}$ cultures (D, Geminin cKO).

(E) Mean assessment of ependymal differentiation normalized to the percentage of differentiation of the controls (WT animal cultures). Error bars represent the SEM; p-values were calculated via the Mann-Whitney test; ns, $p>0.05$, ***$p\leq0.001$.

(F) Experimental schema: GemC1 and/or H2B-GFP plasmids were electroporated *in utero* at E14.5 and V-SVZ WM or coronal sections were analyzed at P15.

(G-H) Confocal image of coronal sections of the forebrain at P15 immunostained with GFP and FOP antibodies (red), previously electroporated with H2B-GFP (G) or GemC1 and H2B-GFP (H). Ependymal cells are identified by the co-localisation with the basal body marker FOP. VZ: ventricular zone; SVZ: Subventricular zone.

(I) Mean percentage of GFP+FOP+ ependymal cells among all GFP+ cells. Data are presented as the mean ± SEM. The p-value was determined by the Mann-Whitney test; ***$p\leq0.001$, n=3.

(J-L) Confocal images of the V-SVZ WM at P15 immunostained with GFP (green), the basal body marker FOP (red) and ZO1 (white) antibodies. (K-L) High magnification images of the insets in (J) showing that pinwheel structures are absent when most cells express GemC1 (K) whereas pinwheels (arrows in L) are present in regions weakly electroporated with GemC1 (L). The scale bar represents 20 µm (B-D), 40 µm (G-H) and 150 µm (J).

Table S1

E13.5 Cre

Clone ID	Clone Size	Composition of clones: Green cell	Composition of clones: Red cell	Clone type
1B-3	1	B		B
1C-3	1	B		B
1C-1	1	E		E
1A-5	2	E	B	M
3A-2	2	E	B	M
1C-6	2	B	E	M
1A-7	3	B	EE	M
1B-4	3	E	BB	M
1A-3	3	EE	B	M
1B-7	3	B	EE	M
1B-8	3	EB	E	M
3A-1	3	EB	E	M
1A-6	3	E	EE	E
1B-9	3	E	EE	E
5B-1	4	EE	BB	M
1A-11	4	E	EBB	M
1C-4	4	B	EEB	M
1C-5	4	EB	BB	M
3A-3	4	EBB	E	M
1B-2	4	EEB	B	M
3A-4	4	E	BBB	M
1A-8	4	EE	EE	E
1B-5	4	EEE	E	E
1A-4	5	EEEB	E	M
1A-12	5	EEEB	E	M
1C-2	5	EEB	EE	M
3B-3	5	EB	EEB	M
1B-6	5	BBB	EE	M
3B-2	6	EEBB	EE	M
1A-10	6	EEEEB	E	M
1A-9	7	EEEEB	EE	M
1B-1	7	EEB	EBBB	M

E14.5 Cre

Clone ID	Clone Size	Composition of clones: Green cell	Composition of clones: Red cell	Clone type
19B-1	1		E	E
23B-4	1		E	E
15C-1	1		E	E
6B-1	2	E	B	M
14A-2	2	B	E	M
10B-3	2	B	E	M
13A-2	2	E	B	M
13B-1	2	E	B	M
15B-1	2	E	B	M
15C-2	2	E	B	M
15C-3	2	B	E	M
15C-4	2	E	B	M
22C-1	2	B	E	M
23B-2	2	B	E	M
9B-1	2	E	E	E
9B-3	2	E	E	E
12B-1	2	E	E	E
13A-1	2	E	E	E
14A-1	2	E	E	E
14A-4	2	E	E	E
14A-5	2	E	E	E
14A-6	2	E	E	E
19A-2	2	E	E	E
23B-1	2	E	E	E
8B-4	3	B	BE	M
12A-1	3	B	BE	M
12C-1	3	EB	E	M
14A-7	3	EE	B	M
19A-1	3	B	EE	M
23B-3	3	B	EE	M
15B-2	3	BB	E	M
15B-8	3	EB	E	M
19B-2	3	EB	E	M
14A-3	3	E	EE	E
15B-4	3	E	EE	E
10B-1	4	BB	EB	M
10B-2	4	BB	EE	M
15B-5	4	EB	EE	M
12C-2	4	EE	EE	E
12C-4	4	EE	EE	E
15B-7	5	EBB	EB	M
9B-2	5	EEE	EE	E
15B-6	5	EEE	EE	E
6B-2	6	EEE	EEB	M
12C-3	6	EEEE	EE	E
15B-9	6	EEEE	EE	E
6B-3	6	EEE	EEE	E

Supplementary Table 1: MADM lineage tracing after Cre expression at E13.5 or E14.5 (related to Figure 4)

Cre activity was induced through IUE in MADM embryos at E13.5 or E14.5 and red-green clones were analyzed on V-SVZ at P15-P20. B=Type B1 astrocytes; E=Ependymal cells; M=Mixed clones; E= Ependymal clones.

Table S2

E13.5 Cre GemC1

Clone ID	Clone Size	Composition of clones		Clone type
		Green cell	Red cell	
21B-5	1		E	E
21B-6	1	E		E
21B-7	1	E		E
21B-2	2	E	B	M
21B-3	2	B	E	M
21C-5	2	B	E	M
22A-2	2	B	E	M
21A-4	2	E	E	E
22A-1	2	E	E	E
21B-4	2	E	E	E
21C-2	2	E	E	E
21C-6	2	E	E	E
22A-3	2	E	E	E
21C-1	3	E	EB	M
21A-1	3	E	EE	E
21A-5	3	EE	E	E
21C-3	3	EE	E	E
21C-4	3	E	EE	E
21A-2	4	EEB	E	M
21B-1	4	EB	EB	M
21A-6	4	EEE	E	E
21A-7	4	EE	EE	E
21A-3	5	EE	EEEE	E

E14.5 Cre GemC1

Clone ID	Clone Size	Composition of clones		Clone type
		Green cell	Red cell	
25C-1	1		E	E
25C-2	1		E	E
25A-3	1	E		E
25A-6	1	E		E
25C-3	2	B	E	M
25A-10	2	E	B	M
28A-7	2	E	B	M
25A-2	2	E	E	E
25A-5	2	E	E	E
25A-7	2	E	E	E
25A-8	2	E	E	E
25A-9	2	E	E	E
26B-2	2	E	E	E
26B-3	2	E	E	E
26B-3'	2	E	E	E
27A-1	2	E	E	E
28A-1	2	E	E	E
28A-2	2	E	E	E
28A-3	2	E	E	E
28A-4	2	E	E	E
28B-1	2	E	E	E
29A-1	2	E	E	E
29A-5	2	E	E	E
29B-1	2	E	E	E
29B-3	2	E	E	E
29B-5	2	E	E	E
25C-4	3	EB	B	M
26B-3"	3	E	EB	M
26A-3	3	B	EE	M
26B-4	5	EEEB	E	M
25A-4	3	EE	E	E
25A-6	3	EE	E	E
26A-1	3	E	EE	E
28A-6	3	E	EE	E
29A-3	3	E	EE	E
29A-4	3	EE	E	E
29A-6	3	E	EE	E
29B-4	3	EE	E	E
29A-2	3	E	EE	E
27A-2	4	EE	EE	E
28A-5	4	EEE	E	E
29A-7	4	EE	EE	E
29B-2	4	EEE	E	E
26A-2	4	EE	EE	E
26B-1	5	EE	EEE	E

Supplementary Table 2: MADM lineage tracing after Cre and GemC1 overexpression at E13.5 or E14.5 (related to Figure 5)

GemC1 overexpression together with Cre activity was induced through IUE in MADM embryos at E13.5 or E14.5 and red-green clones were analyzed on V-SVZ at P15-P20. B=Type B1 astrocytes; E=Ependymal cells; M=Mixed clones; E= Ependymal clones.

Table S3

E13.5 Cre Geminin

Clone ID	Clone Size	Composition of clones		Clone type
		Green cell	Red cell	
400-3-12c	1	B		B
404-1-3	1		B	B
404-1-5	1		B	B
394-1-2	2	B	B	A
394-1-6b	2	B	B	A
400-1-1	2	B	E	M
400-1-2	2	B	E	M
400-1-3	2	E	E	E
400-3-10	2	E	E	E
404-1-1	2	B	E	M
404-1-2	2	B	E	M
404-1-6	2	B	B	B
392-2-2	3	EB	B	M
392-2-4	3	EE	E	E
400-1-5	3	BB	E	M
400-1-9	3	E	EE	E
400-2-4	3		EBB	M
400-3-1	3	EE	B	M
400-3-3	3	B	EE	M
400-3-8	3	EB	B	M
400-3-12b	3		EEE	E
400-4-3	3	EB	E	M
400-4-3b	3	E	EE	E
404-1-7	3	EB	B	M
404-2-1	3		EEE	E
404-2-5	3	EB	B	M
394-1-4	3	EE	E	E
392-2-4b	4	BBB	B	B
392-2-5	4	EB	BB	M
394-1-1	4	EB	EB	M
394-1-5	4	EEB	B	M
394-1-5c	4	EEE	E	E
394-1-6	4	EE	EE	E
394-1-8	4	EE	EE	E
400-1-4	4	EEB	B	M
400-1-7	4		EEEE	E
400-1-8	4		EEEE	E
400-3-2	4	EE	EB	M
400-3-3b	4	EE	EB	M
400-3-4	4	EE	EB	M
400-3-5	4	EB	EB	M
400-3-6	4	EE	EE	E
400-3-9	4		EEEE	E
400-3-10b	4	EE	EB	M
400-3-12	4	EEEB		M
400-3-13	4	EBB	E	M
400-3-14	4	E	EEE	E
400-4-4	4	EB	BB	M
404-1-4	4	BB	EE	M
404-2-2	4	EBB	E	M
404-2-4	4	B	EEE	M
392-2-6	5	EBBB	B	M
392-2-9	5	B	EEBB	M
394-1-3	5	EB	EBB	M
400-4-1	5	B	EEEB	M
392-2-3	5	EEBB	B	M

E14.5 Cre Geminin

Clone ID	Clone Size	Composition of clones		Clone type
		Green cell	Red cell	
341-1-2	1		A	A
360-1-2	1	A		A
362-5-17	1	E		E
362-5-17'	1		E	E
362-5-15	2		E	E
376-4-21	1		A	A
378-4-3	1		A	A
378-4-7	1	E		E
378-4-9	1	E		E
378-5-3	1		E	E
378-3-9	1		E	E
378-3-10	1		E	E
378-3-11	1		E	E
378-3-12	1		E	E
378-3-13	1		E	E
378-3-14	1		E	E
378-3-15	1		E	E
378-3-16	1		A	A
378-3-17	1		A	A
378-3-18	1		A	A
378-3-19	1	A		A
378-3-20	1	A		A
378-3-21	1	A		A
378-3-22	1	A		A
378-3-23	1	A		A
378-3-24	1	A		A
335-1-2	2	A	A	A
376-4-19	2	A	A	A
376-4-25	2	A	A	A
376-5-8	2	A	A	A
376-5-12	2	A	A	A
376-6-4	2	A	A	A
378-3-8	2	A	A	A
378-4-2	2	A	A	A
378-4-8	2	A	A	A
378-4-26	2	A	A	A
360-1-1	2	E	E	E
376-4-4	2	E	E	E
376-4-8	2	E	E	E
376-4-9	2	E	E	E
376-4-11	2	E	E	E
376-4-12	2	E	E	E
376-5-2	2	E	E	E
376-5-10	2	E	E	E
378-3-1	2	E	E	E
378-3-7	2	E	E	E
378-4-5	2	E	E	E
378-4-11	2	E	E	E
378-4-13	2	E	E	E
341-3-2	2	A	E	M
359-2-2	2	E	A	M
359-1-1	2	A	E	M
360-1-3	2	E	A	M
362-5-1	2	A	E	M
362-5-3	2	E	A	M
362-5-10	2	A	E	M

392-2-1	6	EEEEB	B	M
392-2-8	6	EEEEBB		M
392-2-8b	6	EEBB	EB	M
400-2-1	6	EEBB	EB	M
400-2-2	6	EB	EEBB	M
400-3-7	6	EE	EEEB	M
400-4-2	6	EEB	EEB	M
394-1-4b	6	EEBB	EE	M
392-2-12	7	EEBB	EEB	M
392-2-14	7	EBB	EEBB	M
394-1-5b	7	EEBB	EEE	M
394-1-7	7	EEEB	EEA	M
400-2-3	7	EB	EEEAA	M
400-3-11	7	EBB	EEEE	M
404-2-3	7	EEE	EEBB	M
392-2-7	7	EEBBB	EE	M
392-2-11	7	EBB	EEAA	M
392-2-13	7	EEEE	EEE	E
392-2-3b	7	EEEB	EEA	M
392-2-10	8	EB	EEEEBB	M

376-4-13	2	A	E	M
376-4-23	2	A	E	M
376-4-24	2	E	A	M
376-4-28	2	E	A	M
376-5-3	2	A	E	M
376-5-4	2	E	A	M
376-5-9	2	A	E	M
376-6-2	2	E	A	M
378-3-4	2	E	A	M
378-3-6	2	E	A	M
378-4-1	2	E	A	M
378-4-12	2	E	A	M
378-4-16	2	E	A	M
378-4-21	2	E	A	M
378-4-24	2	E	A	M
378-5-2	2	E	A	M
378-5-4	2	A	E	M
359-2-1	3	E	EE	E
362-5-2	3	E	EE	E
360-1-4	3	E	EE	E
376-4-6	3	EE	E	E
376-4-16	3	EE	E	E
376-4-22	3	E	EE	E
376-5-14	3	EE	E	E
376-6-5	3	EE	E	E
378-4-6	3	EE	E	E
362-5-5	3	E	EA	M
335-1-1	3	EE	A	M
376-4-2	3	EE	A	M
376-4-15	3	A	EA	M
376-4-17	3	E	EA	M
376-4-20	3	EA	A	M
376-4-26	3	EA	A	M
376-5-13	3	AA	E	M
376-6-8	3	A	EE	M
378-3-2	3	EA	A	M
378-4-4	3	E	EA	M
378-4-15	3	EE	A	M
376-4-5	4	EE	EE	E
376-4-10	4	EE	EE	E
376-6-6	4	EE	EE	E
376-6-7	4	E	EEE	E
378-4-18	4	EE	EE	E
378-4-25	4	EE	EE	E
362-5-14	4	EE	EE	E
376-5-1	4	EA	EE	M
376-5-5	4	AEE	A	M
376-5-11	4	E	EEA	M
376-4-3	4	E	EEA	M
376-6-1	4	EA	EA	M
378-3-3	4	EA	EA	M
378-3-5	4	EE	AA	M
378-4-14	4	EE	EA	M
378-4-17	4	AA	EE	M
378-4-19	4	EA	EE	M
378-4-22	4	EEA	E	M
378-5-1	4	EE	EA	M
361-6-1	4	EE	EA	M
360-1-5	4	EEA	A	M
362-5-4	4	EE	AA	M
362-5-6	4	AA	AE	M
362-5-7	4	A	EEE	M
362-5-9	4	EAA	A	M
362-5-8	5	EE	EEE	E
362-5-18	5	EEEE	E	E
376-6-3	5	EEE	EE	E
362-5-11	5	EEE	EA	M
362-5-12	5	EEA	EA	M
376-5-6	5	AA	EEE	M
376-5-7	5	AAE	AA	M
376-4-1	5	EA	EAA	M

378-4-20	6	EEE	EEE	E
378-4-10	6	EEA	EEE	M
378-4-23	6	EEA	EAA	M
376-4-18	6	EEEAA	A	M
376-4-18bis	7	EEA	EEEE	M
376-4-14	7	EEEEA	EE	M

Supplementary Table 3: MADM lineage tracing after Cre and Geminin overexpression at E13.5 or E14.5 (related to Figure 6)

Geminin overexpression together with Cre activity was induced through IUE in MADM embryos at E13.5 or E14.5 and red-green clones were analyzed on V-SVZ at P15-P20. B=Type B1 astrocytes; E=Ependymal cells; M=Mixed clones; E=Ependymal clones.

CHAPTER 3. ON THE CELLULAR AND MOLECULAR MECHANISMS OF EPENDYMAL CELL SPECIFICATION AND DIFFERENTIATION

3.1. Cell cycle progression and its regulation

The cell cycle is the sequence of cellular events that lead to the replication of the genome, growth and cell division to generate two cells that inherit the same genotype. Oscillators regulate the ordered transition between different phases of the cycle, this is, proteins and molecules whose expression or activity oscillates during the cell cycle. These are cyclins, cyclin-dependent kinases (CDKs) and cyclin-dependent kinases inhibitors (CKIs). As it was firstly described in yeast, CDKs partner with cyclins to become catalytically active, and it is the specific combination of different types of CDKs and cyclins that leads the cell through the different phases of the cell cycle (Lim and Kaldis, 2013; Poon, 2016).

There are four phases in the cell cycle: G1, a phase of growth and synthesis of biomolecules, like proteins, S, when DNA duplication takes place, G2, another phase of growth, and M, when mitosis takes place and the duplicated genome is equally separated into two daughter cells (Poon, 2016).

Entering the cell cycle at G1 and progression through such phase depends on a balance of mitogenic and growth inhibiting signals. Mitogenic signals promote the activation of CDK4 and CDK6 via interactions with cyclin D (Massagué, 2004). The G1 is firstly dependent on these mitogenic stimuli to progress and it is during this stage that the cell decides to continue and divide or arrest. However, there is a moment in G1 when the cell becomes mitogen-independent and commits to complete division. This is called the restriction point (R) (Pardee, 1974).

Overcoming R depends on a bistable switch mechanism dependent on the Retinoblastoma protein (pRb)-E2F pathway. The nature of this switch is as follows: high levels of mitogenic signals are required to pass it, but once R is reached, low-maintenance mechanisms ensures that the cell cycle is completed (Yao et al., 2008). Before R, pRb is in an hypophosphorylated state that allows it to bind E2F1-3 transcription factors and inhibit the transcriptional activation of their target genes. A build-up CDK activity, due to the mitogenic-dependent activation of cyclin D-CDK4/6 partially phosphorylates pRb and, as a consequence,

E2F is released. Among its target genes, G1 to S transition ones are found, such as cyclins A and E, E2Fs and components of the replication machinery (polymerases and nucleotide anabolism enzymes). The expression of cyclin E causes the formation of a complex with CDK2 (cyclin E-CDK2) that further phosphorylates pRb, closing a positive feedback loop. Therefore, pRb becomes hyperphosphorylated and completely releases E2F, a phenomenon that coincides with R, to further facilitate the G1 to S transition (Henley and Dick, 2012) (Figure 19).

The pro-proliferative actions of cyclin D-CDK4/6 and cyclin E-CDK2 are counter-acted by CKIs. Of these, two distinct families exist: the CIP/KIP family, which includes p21, p27 and p57 that target CDK4, CDK6, CDK2 and CDK1 for inhibition, and the INK4 family, which includes p15, p16, p18 and p19 that only repress CDK4/6 in G1 (Lim and Kaldis, 2013; Pack et al., 2019). Of these, p27 is the one that acts in normal conditions, without senescence or growth inhibiting signals. It inhibits CDK2 during G1, but this action can be counter-balanced by an accumulation of cyclin D, which displaces p27 from cyclin E-CDK2 complexes and the built-up of cyclin E-CDK2 itself during G1, as described before, which phosphorylates p27 and targets it for degradation (Poon, 2016) (Figure 19).

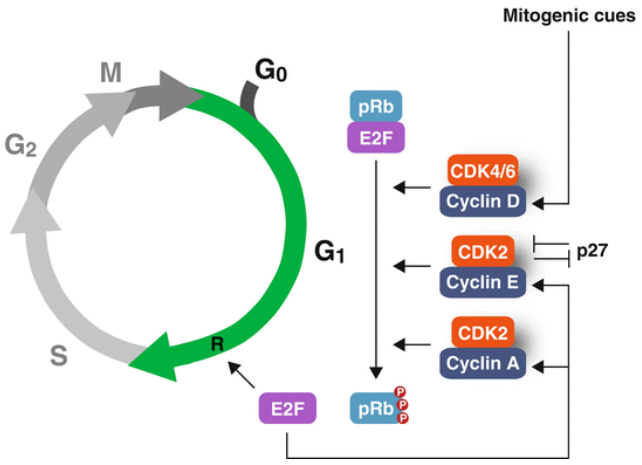

Figure 19. Regulation of G1 and restriction point. Transition through G1 phase of the cell cycle depends on the increase of CDK activity primed by mitogens. These extracellular cues promote the formation of cyclin D-CDK4/6 complexes, which start phosphorylating the retinoblastoma (pRB) protein. When unphosphorylated, this protein forms a complex with E2F transcription factors, impeding its activity as transcription activators. However, partial phosphorylation of pRb permits some E2F-dependent expression of cyclin E, which forms a complex with CDK2. This further phosphorylates pRb until it becomes hyperphosphorylated and completely releases E2F, which then further promotes the transcription of G1 to S transition cyclins in a positive feedback loop. The liberation of E2F coincides with the restriction point (R), the moment of the cell cycle from which the cell becomes mitogen-independent and is committed to divide. From Poon, 2016.

During G1 and S phases, several mechanisms exist to ensure DNA is replicated only once. As briefly introduced before (see Chapter 2 - The Geminin family: regulators of DNA replication with a role in multiciliogenesis), in G1, but even in late M, the pre-RC is formed on replication origins, via origin recognition complex (ORC), Cdc6 and Cdt1 loading to the chromatin. This in turn promotes the recruitment of MCM2-7 and its coactivators Cdc45 and

GINS, to form the replicative helicase complex whose role is to unwind the DNA double helix to proceed with DNA polymerization. CDK2 and Cdc7 promote this cascade through their phosphorylating activity. This process is called replication licensing and it is deactivated as the cell approaches S phase. Among the mechanisms that prevent re-replication of the DNA, we can find: (i) cyclin E degradation after S phase, (ii) CDK-dependent phosphorylation of MCM2-7, Cdt1, Cdc6 and ORC, which promotes their nuclear export, degradation or chromatin dissociation, (iii) cyclin A-CDK2 phosphorylation of E2F1-3 to decrease their DNA binding potential and diminish transcription of S-related genes, and (iv) the expression of E2F7/8 that are transcriptional repressors of E2F1-3. (v) Finally, Geminin, as discussed before, is a protein that accumulates during S/G2 and that binds and sequesters Cdt1 (Figure 20) (Bleichert, 2019; Blow and Hodgson, 2002; Poon, 2016).

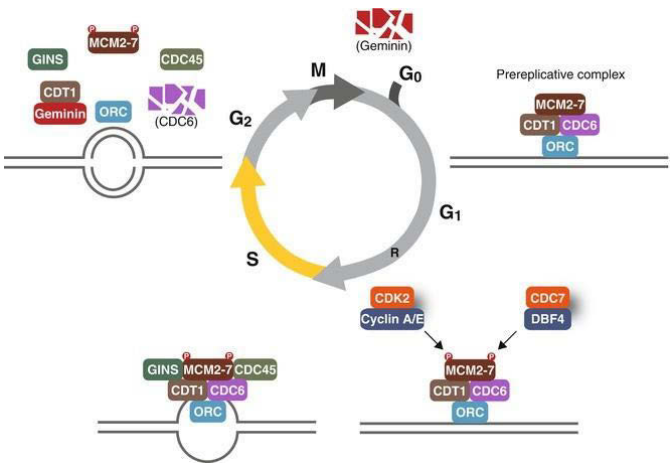

Figure 20. Regulation of S phase and inhibition of DNA re-replication. During G1, the pre-replication complex is formed by recruitment of several factors to replication origins on chromatin (ORC, Cdc6, Cdt1 and MCM2-7, in order). CDK2, in complex with cyclins A and E, and Cdc7, which partners with another cell cycle oscillator called DBF4, phosphorylate MCM2-7. This causes the recruitment of replicative helicase complex coactivators Cdc45 and GINS to open DNA and start replication. Once S phase has started, different mechanisms ensure that replication origins are licensed only once. These lead to the degradation, inactivation or nuclear export of the different factors named here. Of particular interest is Geminin, whose expression builds-up during S and G2 phases to bind and inhibit the licensing factor Cdt1. Geminin is degraded at the metaphase to anaphase transition during M so that the pre-replication complex can form again during a new cell cycle. From Poon, 2016.

After the DNA has been successfully replicated, a gap phase precedes mitosis, the G2 phase. This is a preparatory phase for mitosis during which cyclin A-CDK2, who also has a role in S phase progression and is thus activated at the beginning of it, is mots robustly activated. Cyclin A-CDK2 regulates the timing of entry into mitosis by promoting the activation of the main mitotic engine, the cyclin B-CDK1 complex, as well as controlling the time of mitotic spindle formation (De Boer et al., 2008). A possible mechanism indicates that cyclin A-CDK2 is essential for the activation of the Cdc25 family, a group of phosphatases that catalyze the retrieval of inhibitory phosphorylation from cyclin B-CDK1 during G2 (Mitra and Enders, 2004).

During the G2 to M transition a robust regulatory mechanism of cyclin B-CDK1 is established, which ensures that initial accumulation of CDK1 activity turns to abrupt activation via a feedback loop. In the G2 phase, CDK1 is inhibited by phosphorylation of the Wee1 and Myt1 kinases. However, the activation of the Cdc25 phosphatases at the end of G2 triggers the dephosphorylation of CDK1. This kinase is then free to further activate Cdc25 and impede Wee1 kinase activity, in both cases via phosphorylation. This autocatalytic event of CDK1 self-regulation is triggered by Aurora A, which activates Plk1 that in turn inhibits Wee1 and Myt1, activates Cdc25 and promotes cyclin B translocation to the nucleus (Figure 21) (Lemonnier et al., 2020; Poon, 2016; Schmidt et al., 2017).

In order to finish the cycle, cells enter mitosis for the separation of the duplicated chromosomes in two daughter cells. The key event of M is the metaphase to anaphase transition, promoted by the anaphase-promoting complex (APC/C). This must remain inactive before all chromosomes are attached to the mitotic spindle microtubules by the kinetochores. The APC/C is an ubiquitin ligase complex that promotes mitotic cyclin degradation, cyclins A and B, in combination with co-factors Cdc20 and Cdh1. The APC/C is activated by phosphorylation from cyclin B-CDK1. Hence, this mitotic engine primes its own degradation. Once activated, APC/C targets not only cyclins, but also Plk1, Cdc25 and Aurora A, this is, the same actors that previously prompted cyclin B-CDK1 activation. It also primes the degradation of Geminin, as explained earlier, and securin, whose disappearance is critical for the release of the protease separase. This one triggers the degradation of the cohesin subunit that forms the linkage that maintains sister chromatids bound together (Figure 21) (Poon, 2016; Raha and Amon, 2008).

Figure 21. Mitosis progression regulation. The main promoter of mitosis entry and progression is the complex formed by cyclin B and CDK1. It prompts its own activation in an autoregulatory feedback loop which starts by an Aurora A-mediated activation of Plk1, a kinase that phosphorylates the Wee1 kinase and Cdc25 phosphatases. The former inhibits CDK1 during G2 via phosphorylation and the latter activates it by eliminating the inhibitory phosphorylation. Plk1 inhibits and activates them, respectively, in G2. Once cyclin B-CDK1 is primed, it further triggers Cdc25 and hinders Wee1 actions, which builds up CDK activity. Once chromosomes are tethered to the mitotic spindle and ready for separation, cyclin B-CDK1 promotes its own degradation via APC/C-Cdc20, which ensures the passage from metaphase to anaphase. Moreover, APC/C-Cdc20 degrades securing, an action which releases the protease separase to then promote sister chromatid separation to different poles of the cell.

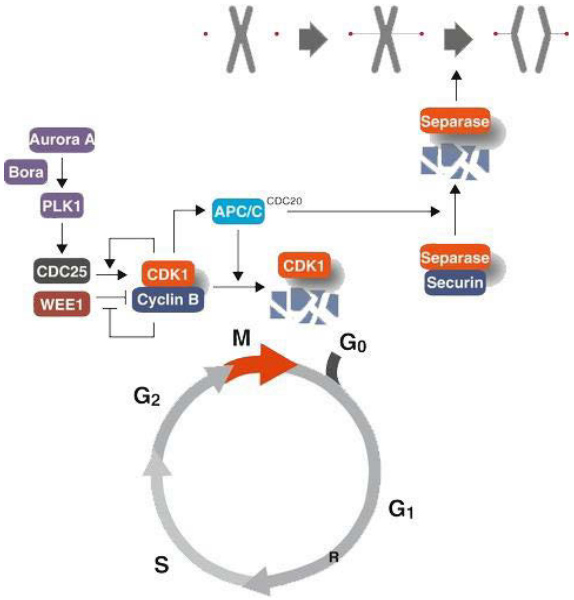

From Poon, 2016.

3.1.1. Cell cycle regulators in MCC differentiation

Cell cycle progression and terminal differentiation are intuitively thought as two independent processes necessary for tissue homeostasis. However, there is a temporal coupling between cell cycle arrest and differentiation that is usually achieved by down-regulation of the CDK activity, sometimes through an increase of the CKI-dependent CDK inactivation. Furthermore, this linkage between the halt of the cycle and initiation of differentiation is regulated by the same pathways (Myster and Duronio, 2000).

In an unexpected manner though, cell cycle progression regulators have also been implicated in differentiation mechanisms. In the CNS, cell cycle actors like cyclin D1 have been related to neuronal differentiation in neural crest-derived cells, hippocampal progenitors, motor neuron-committed stem cells of the spinal cord or in the retina (Galderisi et al., 2003; Hardwick et al., 2015).

This knowledge has prompted research on cell cycle factor-dependent mechanisms that are involved in MCC differentiation. In an elegant, very thorough study by *Al Jord* et al., the most important mitotic drivers have been proposed to govern the transition between the different phases of centriole amplification (see Chapter 2 – 2.1.4.2. Centriole amplification in MCCs). They found that a Plk1 and APC/C-dependent calibrated CDK1 activity drives ependymal progenitors through centriole amplification, but such activity is sufficiently

dampened to avoid chromosome condensation and entry into mitosis (Al Jord et al., 2017; Levine and Holland, 2017).

Another group has involved CDK2, present from late G1 to promote transition to S phase, in complex formation with cyclin A1 in motile ciliogenesis of mouse tracheal epithelial cells. CDK2 is necessary at all stages of differentiation of these cells and it acts upstream of well-known MCC differentiation program-required molecules, such as Mcidas, Myb or FoxJ1 (Vladar et al., 2018).

These studies and the indispensable role of GemC1, a master gene of ciliogenesis (Terré et al., 2016), in DNA replication in *Xenopus* and mammalian cells (Balestrini et al., 2010) have motivated us to search for a GemC1-dependent role of other cell cycle molecules in differentiation. It is likely that both the role of GemC1 in DNA replication is necessary or at least involved in MCC differentiation, rather than they being two distinct functions with no relation between them.

3.2. Checkpoint activation and cell cycle arrest

Cell cycle progression is regulated by checkpoints, mechanisms that sense and signal via defined molecular pathways the errors in the execution of cell cycle processes and, as a consequence, halt the progression to ulterior cell cycle phases until the error has been repaired (Hartwell and Weinert, 1989). They prevent the emergence of genome instability caused by a partially replicated genome or double strand breaks (DSBs), which lead to cell death or even to malignant transformations (Rhind and Russell, 2012). They act at the G1/S, G2/M and metaphase to anaphase transitions (Poon, 2016).

At the G1/S transition, DNA damage sensing causes the recruitment of the ataxia-telangiectasia mutated (ATM) and the ataxia-telangiectasia and Rad3-related (ATR) kinases. These, through phosphorylation of their effector kinases Chk1 and Chk2, stabilize p53 and avoid its nuclear export. P53 is then free to transactivate the expression of the CKI p21. Finally, this protein inhibits cyclin D-CDK4/6 and cyclin A/E-CDK2 activity, thereby arresting impeding pRb hyperphosphorylation and causing G1 arrest (Clark et al., 2000; Poon, 2016).

During G2, the onset of mitosis is hindered by the same kinases, ATM/ATR-Chk1/Chk2, which promote Wee1 activation and diminish Cdc25 phosphatase activity, thus preventing cyclin B-CDK1 activity. This DNA damage checkpoint can be activated by DSBs or by stalled

DNA replication fork progression, which in turn can be produced by DNA lesions, repetitive DNA sequences, DNA-bound protein complexes or a limited supply of deoxyribonucleoside triphosphate molecules, necessary for new DNA strand synthesis (Poon, 2016; Rhind and Russell, 2012). DSBs activate the ATM kinase, whereas the stalled replication forks expose single-stranded DNA (ssDNA) that consequently recruits the Replication protein A (RPA), which binds ssDNA in an unspecific manner, and triggers ATR activation to stop the progression of the cell cycle (Chen and Wold, 2014; Rhind and Russell, 2012).

At the main mitotic event, the metaphase to anaphase transition, a very important checkpoint is initiated in the presence of kinetochores unattached to chromosomes or microtubules, or the absence of tension on said protein complexes. Thus, it ensures a bipolar attachment of chromosomes and guarantees that cyclin B is not degraded by APC/C-Cdc20 until the proper conditions for sister chromatid separation are met (Poon, 2016; Rhind and Russell, 2012).

Although the three described checkpoints are the classical ones and have been established for years, recently a new S/G2 checkpoint was described. In it, ATR controls the S/G2 transition by preventing the accumulation of pro-mitotic gene products, such as cyclin B and Plk1, induced by CDK1. ATR hence antagonizes CDK1 activity until the genome is fully replicated (Saldivar et al., 2018).

3.2.1. DNA damage and replicative stress

Exogenous and endogenous insults, such as UV light, ionizing radiation, or genotoxic metabolites, jeopardize DNA integrity. They lead to the activation of the DNA damage checkpoint and DNA repair pathways, which integrate the DNA damage response (DDR), and whose role is to prevent genomic instability. If this genomic instability persists, cell death, senescence or tumorigenesis are the possible outcomes (Gaillard et al., 2015).

When the DDR is prompted by problems in DNA replication, a slowing down or stalling of the replication fork occurs, a phenomenon defined as replicative stress. Several sources have been identified for replicative stress, to cite a few: nicks, gaps and stretches of ssDNA that could be converted into DSBs by the replication machinery, DNA lesions from radiation or chemical mutagens, incorporation of ribonucleotides instead of deoxyribonucleotides, repetitive sequences that generate unusual DNA conformations, like hairpins, collision

between replication and transcription machinery, DNA-RNA hybrids, a limiting pool of nucleotides that causes the halting of the replication machinery and the over-expression of oncogenes, such as c-Myc and cyclin E (Gaillard et al., 2015; Mazouzi et al., 2014; Zeman and Cimprich, 2014). This last feature produces premature replication origin firing and re-replication (Jones et al., 2013), as well as nucleotide pool exhaustion (Bester et al., 2011).

ATR is the major actor in the response to replicative stress and is recruited by RPA-bound ssDNA to form a signaling complex on DNA lesions that activates Chk1. This leads to the stabilization of the replication fork, the regulation of recombinatorial repair and the inhibition of new origin of replication firing. On the other hand, ATM is also implicated in the DDR by recognizing DSBs and activating the homology recombination pathway for DNA repair (Mazouzi et al., 2014). Therefore, RPA and Chk1 phosphorylation and ssDNA detection constitute markers of replication stress, but one of the most used markers is phosphorylation of the histone variant H2AX (gamma-H2AX or γ-H2AX). It is not specific of replicative stress, since it can be phosphorylated by other kinases, other than ATR and ATM (Zeman and Cimprich, 2014).

Ependymal cells have been described as postmitotic, but cell cycle regulators seem to be major actors of their differentiation. Furthermore, GemC1 is involved in DNA replication firing, a phenomenon that, in abnormal conditions, could generate replicative stress. We have thus looked for signs of such stress in ependymal differentiation.

3.3. Telomeres and telomerase in cell cycle progression and arrest

3.3.1. The eukaryotic telomere

The genome must be faithfully duplicated at each cell cycle to ensure its stability. In order for this process to succeed, it is imperative that the cell tightly regulates DNA repair mechanisms to correct mistakes in replication or resolve DNA damage. Failure to do so results in genomic instability, a hallmark of cancer (Cesare and Karlseder, 2012; Negrini et al., 2010).

Specific regions of the genome are particularly vulnerable to endure DNA damage, such as repetitive sequences (Mazouzi et al., 2014). The telomeres are among these. They pose a challenge to the replication machinery and are susceptible to be a substrate to the DDR

when deregulated (Giardini et al., 2014; Gomez et al., 2012; Longhese, 2008; Takai et al., 2003). Telomeres are the physical ends of eukaryotic linear chromosomes and consist of a guanine (G)-rich (5'-3') tandemly repeated sequence. It stretches for 4-15 kb in humans and wild-derived mouse species, although it varies among species, like the house mice (*Mus musculus*) used as a model organism in scientific research , which have much longer telomeres (approximately 40-50 kb at birth) (Giardini et al., 2014; Gomez et al., 2012; Hemann and Greider, 2000; Varela et al., 2016).

Telomeres do not end in a blunt double-stranded sequence. They present a long, G-rich, 3' end in the shape of a single-stranded overhang and a shorter, cytosine (C)-rich, 5' end. This overhang is the result of several processes. First, the end of replication problem, rooted in the final RNA primer removal of the lagging strand at the chromosome terminus during semiconservative DNA replication, leaving a gap that cannot be filled by DNA polymerases (Soudet et al., 2014; Wellinger, 2014; Wynford-Thomas and Kipling, 1997). Second, the exonuclease activity that processes the 5'end (Figure 22). Third, the action of the enzyme telomerase, which provides an RNA primer to elongate DNA synthesis at the 3' end of the chromosomes, hence directly controlling telomeric length (see below, Figure 24) (Giardini et al., 2014). The 3' overhang and 5' end resectioning are necessary for binding of protein complexes (described below) and higher-order structure acquisition (t-loops) that are crucial for telomere protection from the DDR, as well as for providing a substrate for telomerase (Wu et al., 2012).

Chromosome termini display, as already mentioned, higher-order structures. The most apparent one is the so-called t-loop, consisting of a 3' overhang invasion of upstream telomeric double-stranded DNA (Figure 23). This structure hides the telomere from the DDR and thus prevent checkpoint activation, non-homologous end joining (NHEJ) or homologous recombination (HR). These conformations also inhibit the loading of the telomerase and thus regulate telomere length (Giardini et al., 2014; De Lange, 2005; Longhese, 2008). Telomeres form G-quadruplexes as well, based on the hydrogen bonds of the telomeric abundant guanine residues, and this has a potential of telomere protection or *capping*, even on the C-rich strand (Smith et al., 2011).

Figure 22. The end-replication problem. Telomeres, the eukaryotic chromosome termini, do not end in blunt double-stranded DNA, but rather in a guanine-rich 3' overhang, this is, a single-stranded extension of the 3' strand over its complementary cytosine-rich 5' end. Upon DNA duplication, the replication machinery faces the so-called end-replication problem. Since DNA polymerases can only read a DNA strand in the 3'→5' sense and synthesize a new one in the 5'→3' direction, on the one hand, the synthesis of the so-called leading strand of the replisome (in light pink, complementary to the parental strand in dark blue) ends in a blunt, double-stranded and fully-copied sequence. On the other hand, the so-called lagging strand (in light blue, complementary to the parental strand in dark red), in order to be synthesized in the 5'→3' as the replication fork is opened and progresses, is generated in segments, called Okazaki fragments. These consist of an RNA primer (dark green on the image) that primes DNA synthesis of each of these segments. Afterwards, the primers are removed and the gaps they leave are filled-in by DNA polymerases that use as primers the Okazaki fragment lying 5' to the gap. However, at the chromosome terminus, the 5'-most Okazaki fragment of the lagging strand does not count on any upstream DNA sequence to fill-in the gap left by the removal of the RNA primer. Hence, the removal of the 5'most primer leaves a gap that cannot be filled by conventional DNA polymerases and creates the telomere 3' overhang on the lagging end. Since telomeres need the 3' overhang to fulfil their function, an exonuclease-mediated resection of the blunt-ended 5' leading strand occurs, which is then filled-in by an Okazaki fragment whose primer removal will leave another 3' overhang in the leading end of the telomere. This leads to a shortening of the daughter telomere with respect to the parental one (dark red arrows). From Wellinger, 2014.

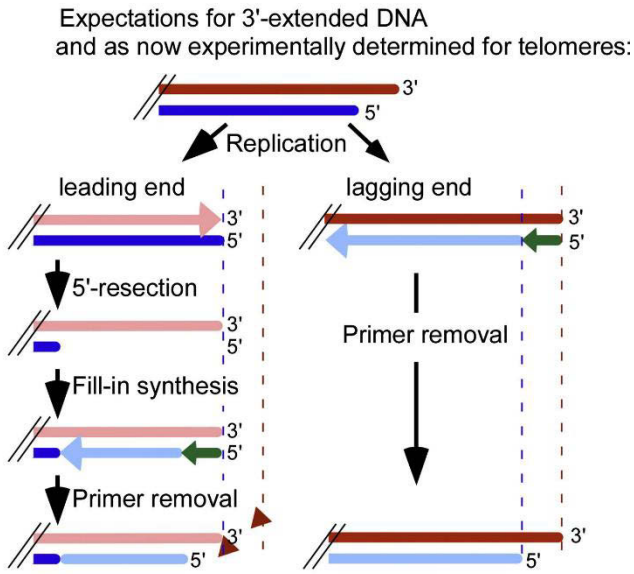

Figure 23. Formation of the t-loop in telomeres. Telomeres can form higher-order structures like t-loops. These are generated by the invasion of the 3' G-rich overhang of the double-stranded telomeric DNA, which lies upstream of it. As a consequence of this invasion, a triple-stranded structure known as a D-loop is formed. The t-loop hides the telomeric end so that it is not recognized by the DNA damage response or the telomerase (hence playing a role in the regulation of telomere length) and its formation is promoted by the shelterin complex (see below). From Giardini et al., 2014.

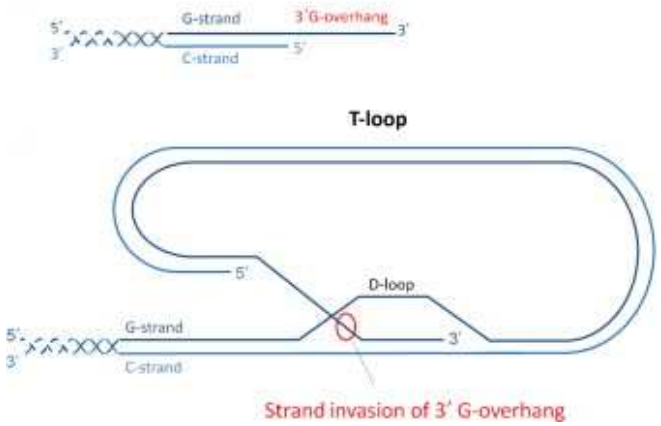

3.3.2. Telomerase-dependent telomere length maintenance and the generation of dysfunctional telomeres

Because of the end of replication problem, after each cell duplication, a loss of telomeric material occurs at the lagging-strand telomere. Furthermore, the resectioning of both telomeric ends by exonucleases contributes to such phenomenon of telomere

shortening (Figure 22). Following many rounds of replication, the reduction of these sequences could reach essential genes and cause deleterious gene deletions. That is why, upon excessive telomeric attrition, a critical threshold known as the Hayflick limit is reached. At this point, telomeres become dysfunctional and trigger the replicative senescence response, a hallmark of ageing in somatic tissues that inhibits further cell division (Giardini et al., 2014; Gomez et al., 2012). Telomere shortening and ageing are not just correlated, but a cause-consequence relationship exists between the two phenomena (Marion and Blasco, 2010).

Critically short telomeres trigger the DDR via ATM and/or ATR kinases, which in turn activate the potent tumor suppressor p53. The expression of this so-called "guardian of the genome" has two possible outcomes: either it promotes a G1/S p21-dependent cell cycle arrest, also known as replicative senescence, or it prompts apoptosis. Both mechanisms act then as potent tumor suppressors, since the DNA reparation machinery could recognize short telomeres, promote NHEJ or HR, and generate genomic instability after mitosis (Giardini et al., 2014; Longhese, 2008; Marion and Blasco, 2010; Roake and Artandi, 2017).

Dysfunctional telomeres are studied via fluorescent staining of chromosome termini and DDR proteins. The co-localization of both markers is indicative of Telomere Dysfunction Induced Foci (TIF), a cytological structure present in cells with damaged telomeres. Telomere fluorescent *in situ* hybridization (FISH) or immunofluorescent staining of telomere-associated proteins (see below) are used to label telomeres, whereas immunostaining of DDR proteins uses antibodies against γH2AX, 53BP1 or phosphorylated ATM or ATR (De Lange, 2005; Longhese, 2008; Takai et al., 2003).

Specific cell types have developed mechanisms to bypass telomere shortening. The most prominent one consists of the expression of an enzyme called telomerase. It is a ribonucleoprotein complex composed of two elements: a non-coding RNA that provides a short template sequence complementary to the telomeric DNA (TERC), and a catalytic unit, a reverse transcriptase that copies the RNA template at the 3' of the telomere, thus elongating it (TERT). This RNA-dependent telomere elongation is executed in several steps. First, the TERC template binds by complementarity to the 3' overhang. Then the TERT enzyme adds nucleotides to complete one telomeric repeat. Once one repeat is added, the enzyme either dissociates from the telomere or translocates along the elongated 3'overhang to add a new

repeat. Finally, the conventional DNA polymerase elongates the C-rich strand, this is, the 5' end of the chromosome (Figure 24) (Giardini et al., 2014; Gomez et al., 2012).

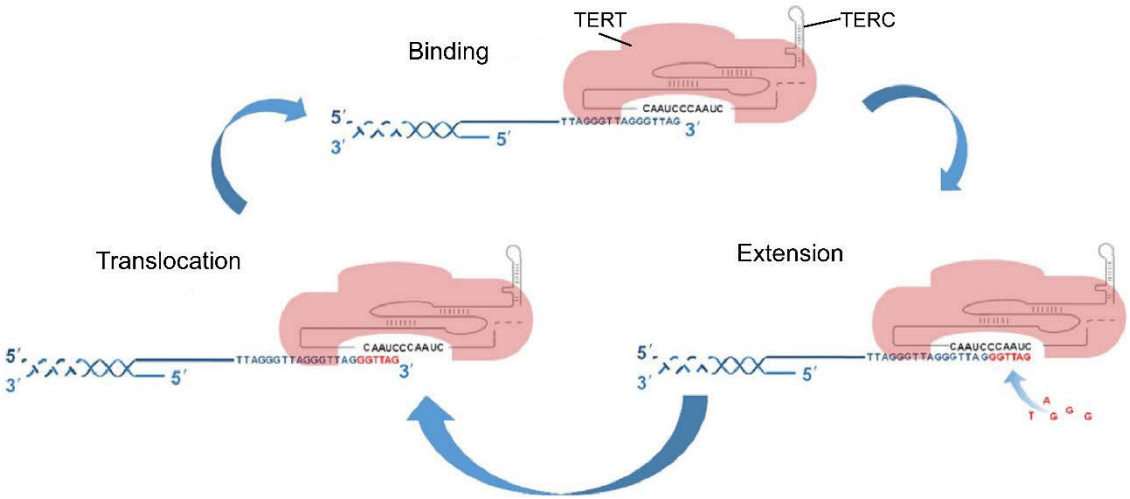

Figure 24. Telomerase-dependent telomere elongation. The enzyme telomerase is able to elongate telomeres by catalyzing the addition of telomeric repeats. The catalytic subunit (TERT) acts as a retrotranscriptase and needs the RNA-component of the telomerase (TERC) to do so, since this molecule contains the RNA template from which telomeric DNA can be replicated. After binding to the 3' overhang and extending its telomeric sequence, telomerase can either dissociate from the telomere or translocate along the now elongated 3'overhang and repeat the process. Adapted from Giardini et al., 2014.

In physiological conditions, telomerase is highly expressed in the germline (gamete precursor cells in the embryonic and adult testis and ovaries) and pluripotent embryonic stem cells (at least up to the blastocyst stage), where it helps maintain a constant telomere length. Its activity is also detected in somatic tissues during development but is extensively decreased by birth (Wright et al., 1996; Zimmermann and Martens, 2008). Adult stem cells also display telomerase activity, but this is insufficient to maintain a constant telomeric length. Consequently, this progressive telomere shortening inhibits the stem cell ability to repair and regenerate tissues with age, since they reach senescence or apoptosis when their telomeres are excessively short. In the case of the rest of the somatic cells, telomerase is completely repressed and hence possess shorter telomeres than their adult stem cell progenitors. The other cell type that expresses high levels of telomerase to elongate telomeres are cancer cells, which present an up-regulation of this enzyme in 85-90% of the cases to be able to divide indefinitely (Figure 25) (Giardini et al., 2014; Harrington, 2004; Marion and Blasco, 2010; Shay and Wright, 2010).

Figure 25. Telomere length and telomerase with the progression of cell divisions in different cell types. The

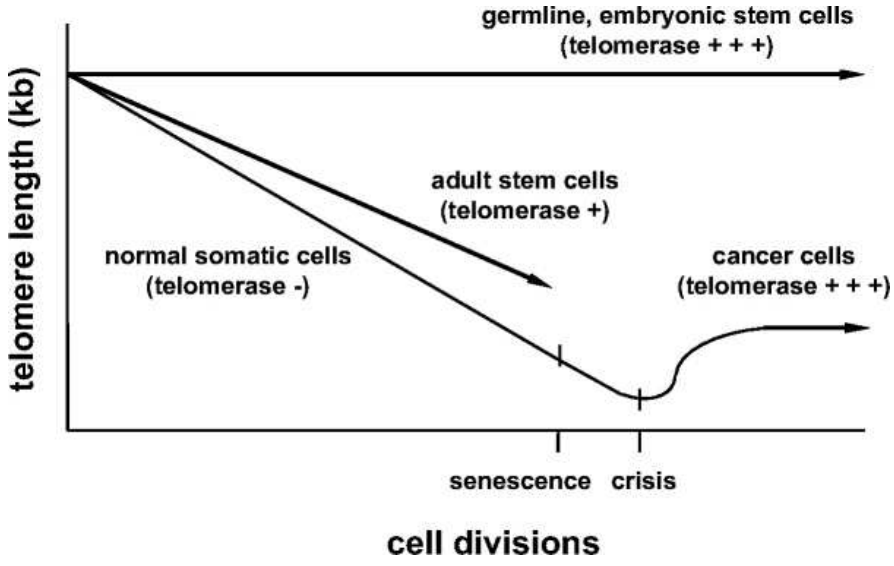

enzyme telomerase is highly activated in the germline and embryonic stem cells, up to the blastocyst stage, so that telomere length is maintained constant. In somatic tissues, however, this activity is either present but insufficient for telomere length maintenance throughout life in adult stem cells of proliferating tissues, or completely repressed in the rest of somatic cells. This leads to a more rapid decline of telomere length in cells of somatic tissues than in the residing adult stem cells (hematopoietic stem cells, epidermal stem cells, adult neural stem cells, etc.). When cells reach a threshold telomere length known as the Hayflick limit, they trigger the process of replicative senescence. It ensures that cells stop dividing and telomere attrition does not lead to genomic instability that could pass on to daughter cells, a hallmark of cancer. If cells continue to divide, they reach a crisis that is resolved in apoptosis or, in case of cancer cells, in an up-regulation of telomerase (in most cases) to stop further telomere shortening and become immortal cell lines. From Zimmermann and Martens, 2008.

Baseline telomerase activity that hinders too rapid telomere shortening is necessary for several rapidly-proliferating tissue homeostasis. Its deficiency is related to a loss of progenitor dividing capacity in the hematopoietic line, upon mitogenic stimulus (Lee et al., 1998; Samper et al., 2002), in epidermal stem cells (Flores et al., 2005) and adult NSCs (Ferrón et al., 2004). Contrary to other publications (Wright et al., 1996), in humans telomerase has been found active in adult rodent brains, particularly in the SVZ and the olfactory bulb (Caporaso et al., 2003).

The need of telomerase to avoid premature senescence in these adult tissues explains some of the most common disease derived from telomerase mutations and loss of activity in humans. Dyskeratosis congenita is characterized by an abnormal pink pigmentation, nail dystrophy, hair loss, developmental delay and bone marrow failure as a cause of premature mortality. Aplastic anemia is a condition whose symptoms are reduced cell blood numbers due to bone marrow failure, as well as liver and lung disease. Hoyeraal-Hreidarsson syndrome

is also accompanied of hematopoietic line deficiencies, rooted in bone marrow failure, such as immunodeficencies. Finally, idiopathic pulmonary fibrosis is a fatal irreversible lung fibrosis linked to telomerase mutations. All these illnesses display shorter telomeres due to mutations in telomerases, linked to premature loss of regeneration capacity (Barnes, 2015; Giardini et al., 2014; Gomez et al., 2012; Roake and Artandi, 2017; Tomás-Loba et al., 2008). In mice, TERC and TERT KO models are directly related to ageing phenotypes and lifespan reduction (Marion and Blasco, 2010). Furthermore, the telomere shortening phenotype worsens in these animals with successive generations concomitantly with aggravation of the premature ageing symptoms, further suggesting a direct role between ageing and telomerase activity (Ferrón et al., 2004; Flores et al., 2005).

Seeing the potential implication of replicative stress in ependymal cell differentiation, as well as their common origin with adult neural stem cells that reside in the neurogenic niche throughout life, we have studied the presence of dysfunctional telomeres in ependymal progenitors and the role of telomerase in the establishment of said niche.

3.3.3. Telomere-associated proteins and capping

Telomeres are more than strands of DNA at the chromosome termini. They are nucleoprotein structures formed by the association of telomeric DNA with protein complexes that protect them against the DDR. Otherwise, it would recognize telomeres as DSB and free ssDNA and, consequently, would trigger repair mechanisms that could result in end-to-end chromosome fusions, inappropriate HR and the resulting genomic instability and telomere length deregulation (Giardini et al., 2014; Gomez et al., 2012; De Lange, 2005).

Shelterin is the main protein complex bound to telomeric DNA and is formed of six proteins: TRF1, TRF2, RAP1, TIN2, TPP1 and POT1. They all play specific roles in hindering specific aspects and actors of the DDR, as well as the action of telomerase. TRF1 and TRF2 are double-stranded telomeric DNA-binding proteins that negatively regulate telomeric length. TRF2 promotes t-loop formation and hence the inaccessibility of telomerase to the 3´overhang. TRF2 blocks the ATM pathway response and, consequently, the formation of TIFs, the activation of p53-dependent premature replicative senescence and NHEJ and HR at chromosome ends (Giardini et al., 2014; Gomez et al., 2012; De Lange, 2005; Longhese, 2008; Marion and Blasco, 2010). RAP1 is recruited by TRF2. It reduces telomere fragility and

telomere HR, which can lead to undesired telomeric sister chromatid exchange and alter telomere length homeostasis. However, it is dispensable for the inhibition of DDR at telomeres and it does not prevent end-to-end chromosome fusions, like TRF2 (Gomez et al., 2012; Martinez et al., 2010; Sfeir et al., 2010). TIN2 is the unifying element of the sheltering complex, binding TRF1 and TRF2 with TPP1/POT1 and its loss is cause for TIF generation (De Lange, 2005; Longhese, 2008). TPP1, one of the less studied subunits seems to have a telomerase recruiting role with its partner POT1, which is recruited by the former, and thus, the phenotypes associated to the loss of either one of them, such as ATR activation, are similar (Diotti and Loayza, 2011). Finally, POT1 is the only protein of the shelterin complex that has single-stranded DNA-binding activity. Its occupation of the 3´overhang avoids the recruitment of RPA to this stretch of single-stranded DNA and thus inhibits the ATR response and TIFs formation. It also regulates telomere length via a negative feedback loop. In long telomeres, POT1 inhibits telomerase action, whereas in short telomeres, there is less POT1 (and less shelterin complex units) on the 3´overhang. Telomerase can then gain access more easily to it and catalyze telomere elongation (De Lange, 2005).

In all, shelterin is implicated in regulation of telomerase-dependent telomere elongation, mostly by preventing the access of such enzyme to the telomeres, but most importantly, it prevents the triggering of a DDR response by protection of the telomeres. This process is called “telomere capping” and is, along telomerase activity, the main inhibitor of premature ageing and decline of adult tissues.

3.4. Objectives and hypotheses

GemC1 has a role in DNA replication firing, as an antagonist to its homolog Geminin. We have wondered whether the role of GemC1 in DNA replication is needed for its role in multiciliated differentiation, and whether this integrates the molecular mechanisms that lead to ependymal cell specification. With that in mind, we have studied the effect of GemC1 expression in cell cycle progression, namely S phase entry. We believe that ependymal specification takes place in cells that have not exited the cell cycle at the onset of differentiation, and whether the presence of replicative stress can drive centriole amplification.

Also, we have asked ourselves whether the difference between cells from the same lineage, one postmitotic (ependymal) and one that can continue to divide (adult NSC), is some sort of damage to the telomeres, due to their shortening or other causes. As such, we have hypothesized as well that telomerase, the enzyme responsible for telomere length maintenance and protection, could favor the stem cell fate, since this cell continues to divide and should not pass on damaged cargoes (such as DNA) onto its descendant cells.

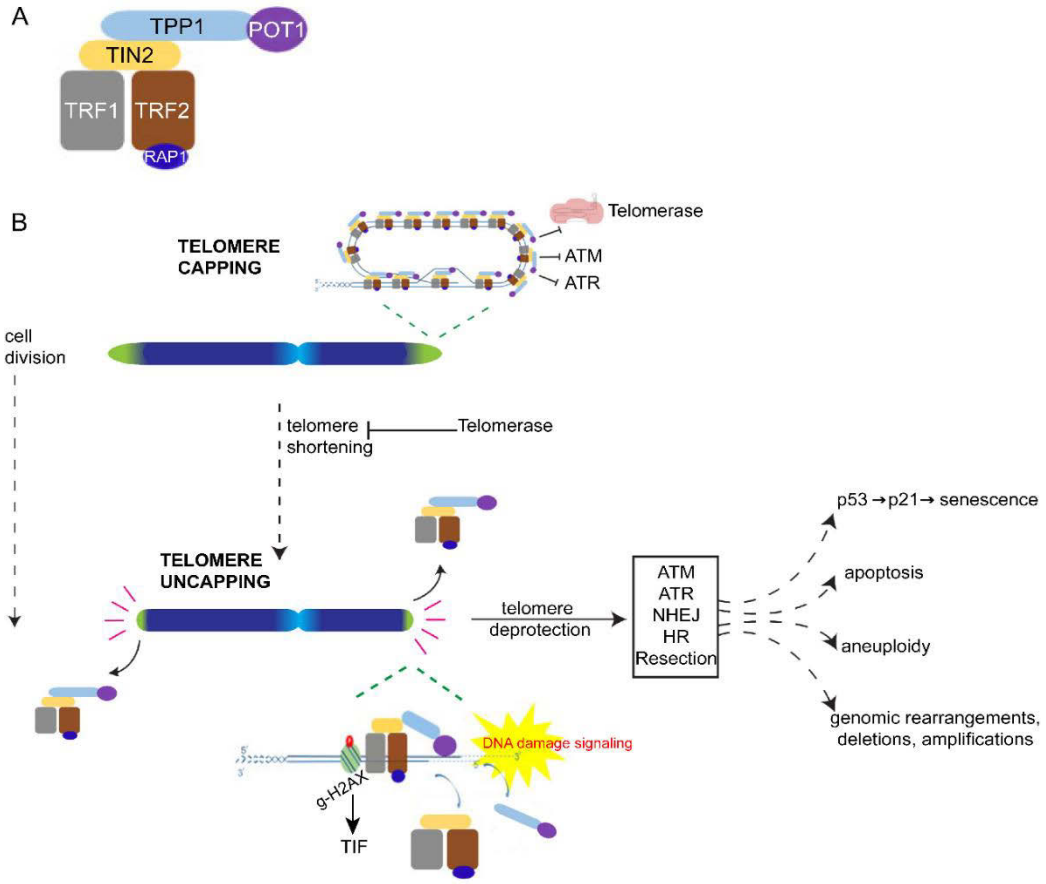

Figure 26. The shelterin complex and the dysfunctional telomere signaling. (A) Shelterin is a protein complex formed by six subunits: TRF1 and TRF2, which are able to bind double-stranded telomeric DNA, RAP1, recruited to the complex by TRF2, PTT1, which forms a heterodimer with POT1, the other protein of the complex with DNA binding activity, in this case to the single-stranded 3' overhang, and, finally, TIN2, which forms a bridge between TRF1/2 and TPP1/POT1. (B) Shelterin subunits promote the formation of t-loops which protects telomere end against telomerase, and the DNA damage response kinases ATM and ATR. This protection by shelterin is known as telomere capping. With successive cell divisions in ageing tissues, telomeres get shorter, a process inhibited by the telomerase in embryonic stem cells, cancer cells or the germline. When telomeres become critically short, telomere uncapping happens, this is, the release of shelterin from the chromosome termini. This leads to the recognition of the telomeres by the DNA damage signaling pathway and the recruitment of its actors, such as phosphorylated gamma-H2AX. As telomeres are deprotected and recognized by ATM and ATR, they can undergo non-homologous end joining (NHEJ), homologous recombination (HR) or resectioning with various possible outcomes. In some cases, the replicative senescence cascade is activated, which involves p53-dependent p21 expression, and hence cell cycle arrest. In other cases, the cell undergoes apoptosis. Finally, aneuploidy and genomic instability can also occur, a hallmark of cancer. Adapted from Giardini et al., 2014 and Jacobs, 2013.

Article 2.

Replicative Stress Response contributes to ependymal versus stem cell specification decision

Ready for submission

Replicative Stress Response contributes to ependymal versus stem cell specification decision

Gonzalo Ortiz-Álvarez[1], Aurélien Fortoul[1]*, Ayush Srivastava[1]*, Marie-Clémence Bouvier[1], Marion Faucourt[1], Mathieu Bahin[1], Corinne Blugeon[1], Vincent Géli[2], Auguste Genovesio[1], Nathalie Delgehyr[1], Alice Meunier[1] and Nathalie Spassky[1]

[1] Institut de Biologie de l'Ecole Normale Supérieure (IBENS), Ecole Normale Supérieure, UMR8197 CNRS, U1024 INSERM, PSL Université Paris, 75005 Paris, France.

[2] Marseille Cancer Research Centre (CRCM), U1068 INSERM, UMR7258 CNRS, UM105 Aix-Marseille University, Institut Paoli-Calmettes, Ligue Nationale Contre le Cancer (équipe labellisée) Marseille, F-13009, France.

Corresponding author: nathalie.spassky@bio.ens.psl.eu

*contributed equally

Abstract

Ependymal cells and Adult Neural Stem Cells (NSC) are cellular components of the adult neurogenic niche, essential for brain homeostasis. These cells share a common lineage of glial cells regulated by the Geminin family antagonists, Geminin and GemC1/Mcidas. Ependymal precursors require GemC1/Mcidas to massively amplify centrioles and become multiciliated cells. Here we show that GemC1-dependent differentiation happens mostly in cycling cells, where it produces a strong replicative stress leading to dysfunctional telomeres and cell cycle arrest concomitant to centriole amplification. Telomerase expression in progenitor cells impairs ependymal differentiation and favors NSC cell fate. In all, we show that ependymal cell specification occurs before exiting the cell cycle, entails cell cycle progression and arrest genes and can be reversed by telomerase expression.

Introduction

Multiciliated ependymal cells and B1 astrocytes are the major glial components of the ventricular-subventricular zone (V-SVZ) adult neurogenic niche in the mammalian brain, where hundreds of new neurons are born every day and migrate to the olfactory bulb (Lim and Alvarez-Buylla, 2016; Ming and Song, 2011). B1 cells, a largely quiescent population (Fuentealba et al., 2015; Furutachi et al., 2015), divides in symmetric proliferative or consumptive divisions, to self-renew or commit to the neuronal lineage, respectively (Obernier et al., 2018). Ependymal cells are essential for cerebrospinal fluid circulation, which carries growth factors during the development of the central nervous system, delivers nutrients, signaling factors and the clears waste and neurotoxic substances (Jiménez et al., 2014; Siyahhan et al., 2014). The coordinated beating of ependymal motile cilia creates flow domains within the ventricle to establish local concentration of substances, according to the needs of different anatomical sections of the ventricular system (Faubel et al., 2016), or even regulate B1 proliferation (Petrik et al., 2018; Silva-Vargas et al., 2016) and guide newborn neurons to the olfactory bulb (Sawamoto et al., 2006).

Ependymal cells are postmitotic (Spassky et al., 2005), unlike their niche stem cell counterparts, which can re-enter the cell cycle during adult neurogenesis (Fuentealba et al., 2015; Obernier et al., 2018). Interestingly, these two highly different cells belong to the same lineage and can arise from a single cell division, as two sister cells in an asymmetric division, but they are also generated through symmetric divisions (Ortiz-Álvarez et al., 2019; Redmond et al., 2019). Furthermore, DNA replication regulators of the Geminin family govern the fate of neurogenic niche cell progenitors (Lalioti et al., 2019a; Ortiz-Álvarez et al., 2019): GemC1 favors ependymal-generating symmetric divisions and Geminin triggers B1-producing symmetric divisions (Ortiz-Álvarez et al., 2019). Interestingly, GemC1 was initially discovered as a part of the DNA pre-replication complex, essential for replication firing (Balestrini et al., 2010), but it is also a master gene of the multiciliogenesis program (Arbi et al., 2016; Terré et al., 2016, 2019). Its antagonist, Geminin, inhibits excessive replication firing by binding to the replication licensing factor Cdt1 (McGarry and Kirschner, 1998; Wohlschlegel et al., 2000) and, upon ablation, cycling cells develop centrosome over-duplication and polyploidy (Tachibana et al., 2005). The over-expression of some components of the pre-replication complex, such

as Cdt1, Cdc6 and Cdc45 has been associated with re-replication and early-stage cancer lesions, which generate replicative stress (Gaillard et al., 2015; Köhler et al., 2016). These factors elicit the DNA damage response (DDR) to signal the cell to stop cell cycle progression and start DNA repair (Mazouzi et al., 2014).

Adult stem cell niches express the enzyme telomerase at higher levels than the rest of somatic cells (Giardini et al., 2014; Marion and Blasco, 2010; Zimmermann and Martens, 2008). It serves to maintain telomere length, repetitive sequences at the eukaryotic chromosome termini that shorten after every round of replication, due to the end of replication problem (Soudet et al., 2014; Wellinger, 2014). However, the levels of telomerase in adult stem cells are far from those in embryonic stem cells and the majority of cancers, so progressive telomere attrition, which leads to the decay and ageing of tissues, is inevitable (Zimmermann and Martens, 2008). B1 cells are not an exception to this rule, whose telomere shortening hinders their proliferative capacity with ageing (Ferrón et al., 2004) and proper differentiation into the neuronal lineage (Ferrón et al., 2009).

Telomeres are normally protected by protein complexes to avoid recognition as double strand breaks or single-stranded DNA and start the DDR (Longhese, 2008). Failure of this protein components to protect the telomeres, due to telomere shortening or other factors, triggers the replicative senescence response, which involves the recognition of telomeres by the DDR actors, such as the Ataxia-telangiectasia mutated (ATM) and Ataxia-telangiectasia and Rad3-related (ATR) kinases. This leads to the activation of the p53/p21 axis, resulting in apoptosis or permanent cell cycle arrest (Gomez et al., 2012; Herbig et al., 2004). This is usually assessed by the presence of cytological structures known as Telomere Dysfunction Induced Foci (TIF), which are seen as telomeres that co-localize with DDR players, like γ-H2AX or 53BP1 (De Lange, 2005; Takai et al., 2003).

We have shown in this study that cell cycle progression and ependymal fate determination are coupled. Indeed, GemC1 expression in ependymal progenitors leads to massive centriole amplification, but only in cycling cells. As GemC1 triggers differentiation, ependymal progenitors enter the S-phase like other cell cycle active cells in the embryonic neuroepithelium. However, GemC1 generates replicative stress, as seen by the increased γ-H2AX signal often associated to EdU staining, which corresponds to sites of DNA replication. Furthermore, in ependymal-differentiation conditions, the presence of replicative stress leads

to an increase of TIFs. Consequently, although GemC1-expressing cells enter the S-phase normally, they slow down their progression through the cell cycle. Although they express the cell cycle progression marker phosphorylated retinoblastoma (PRb), they inhibit mitosis entry and express cell cycle arrest markers, such as p21 and p73. Finally, the presence of a replicative senescence-like response in these cells, with p21 and γ-H2AX expression and a higher frequency of TIFs led us to assess the role of the enzyme telomerase. We observed that it is able to revert the GemC1-dependent differentiation and it can favor the B1 cell fate, in detriment of the ependymal one.

Results

GemC1 induces multiciliated cell differentiation only in cycling cells

GemC1 is a Geminin family protein and a master gene of multiciliogenesis (Arbi et al., 2016; Kyrousi et al., 2015; Terré et al., 2016). It was initially discovered as an essential component of the pre-replication complex, where it promotes DNA replication firing (Balestrini et al., 2010). To decipher the mechanisms of multiciliated cell specification, we tested the link between DNA replication and multiciliogenesis . We electroporated GemC1 and H2B-GFP *in utero* at E14.5 or at P0 (IUE or PE, respectively), in combination with EdU injection (Figure 1A). Two days after the electroporation, the majority of GFP^+ cells in the VZ/SVZ are EdU^+ after IUE but not after PE (Figure 1B-C), suggesting that IUE and PE target cycling and postmitotic cells, respectively (Stancik et al., 2010; Loulier et al., 2014; Ortiz-Alvarez et al., 2019). Ependymal differentiation was massively induced after IUE, albeit very weak after PE, which shows that ependymal cell differentiation induced by GemC1 gain of function is tightly correlated to an EdU^+ active cell cycle state (Figure 1D-E) and suggests a connection between the role of GemC1 in the initiation of DNA replication and centriole amplification.

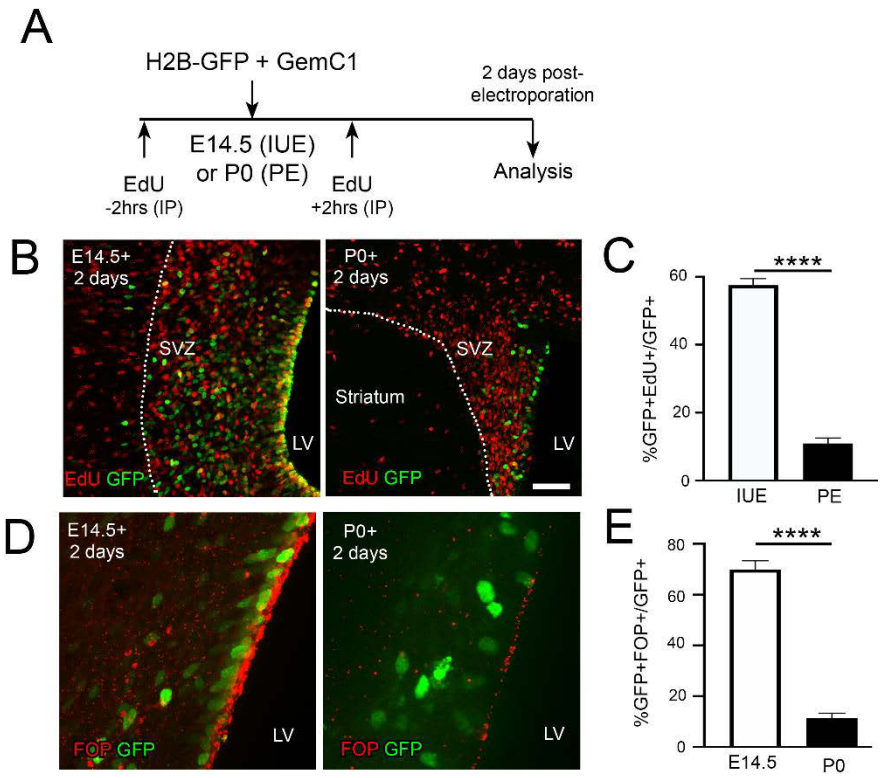

Figure 1. GemC1 induces multiciliated cell differentiation only in cycling cells. (A) Experimental layout depicting the time of electroporation of H2B-GFP + GemC1-expressing plasmids, *in utero* (IUE) or postnatally (PE), as well as the time of EdU intraperitoneal (IP) injection. Coronal sections of electroporated brains were analyzed 48 hours post electroporation. (B, D) Representative images of electroporated brains. A dotted white line indicates the border between the SVZ and the striatum (B). Cells that incorporated EdU (B) or immunostained with the procentriole or centriole-labeling antibody FOP (D) are shown in red. Cells issued from the co-electroporation of H2B-GFP+GemC1 are seen in green. (C, E) Quantification of the mean percentage of GFP+ cells that are EdU+ (C) or multi-FOP+ (E). Error bars indicate the SEM for n=3 animals for the two conditions. A Mann-Whitney test was performed between the two groups to assess the p-value; **** $p \leq 0.0001$. LV: Lateral Ventricle; SVZ: Subventricular Zone. Scale bar 60 µm (B) 20 µm (D).

GemC1 induces replicative stress before centriole amplification

To determine the direct effect of GemC1 upstream of multiciliation, and since genes are expressed from 6 hours after IUE, we studied GemC1GFP$^+$EdU$^+$ cells after EdU administration between 6 and 30 hours post-electroporation (Figure 2A). Most of these cells did not initiate centriole amplification yet and their nuclei were still in the G1-S-G2 phase layers of the VZ (Figure 2B-C). Few GFP$^+$EdU$^-$ cells displayed FOP accumulation in apically migrating G2-M phase, suggesting that these cells had exited S-phase before EdU administration and that S-G2 phase regulatory mechanisms contribute to centriole amplification in these cells (arrows in figure 2B).

Since GemC1 is known to trigger replication firing (Balestrini et al., 2010), we tested if GemC1 gain of function condition altered the S-phase of the cell cycle. No difference in the number of GFP^+EdU^+ double positive cells in controls with respect to GemC1-electroporated brains was observed (Figure 2E-F), showing that GemC1 does not alter the ability of cells to enter the S phase. However, we noticed an increased replicative stress in these cells. We used the initial marker of DNA damage γH2AX (Zeman and Cimprich, 2014), which was only observed in EdU^+ cells both in control and GemC1 conditions, showing that it corresponds to replicative stress. The number and intensities of $\gamma H2AX^+$ foci were strongly increased in $GemC1^+$ cells compared to control cells (Figure 2G-H). Interestingly, we observed similar γH2AX staining in FoxJ1+ cells in controls at E17.5 (Figure 2H-I), suggesting that γH2AX foci could be an early marker of ependymal cell differentiation. In cells with EdU^+ foci, γH2AX foci were often colocalized and around chromocenters (Figure 2J). Since telomeres are localized to the vicinity of chromocenters (Solovei et al., 2009), we quantified telomere dysfunction-induced foci (TIF), characterized by the presence of DNA damage actors at telomeres (D'Adda Di Fagagna et al., 2003; Longhese, 2008; Takai et al., 2003). We performed FISH analysis of telomeric sequences in combination with immunofluorescence of γH2AX (Figure 2K). GemC1 gain of function significantly increased the number of TIFs per cell, as well as the percentage of cells with three or more damaged telomeres (Figure 2L-M). However, apoptosis-like features, such as pyknotic nuclei, were not observed at that stage or later in development (data not shown).

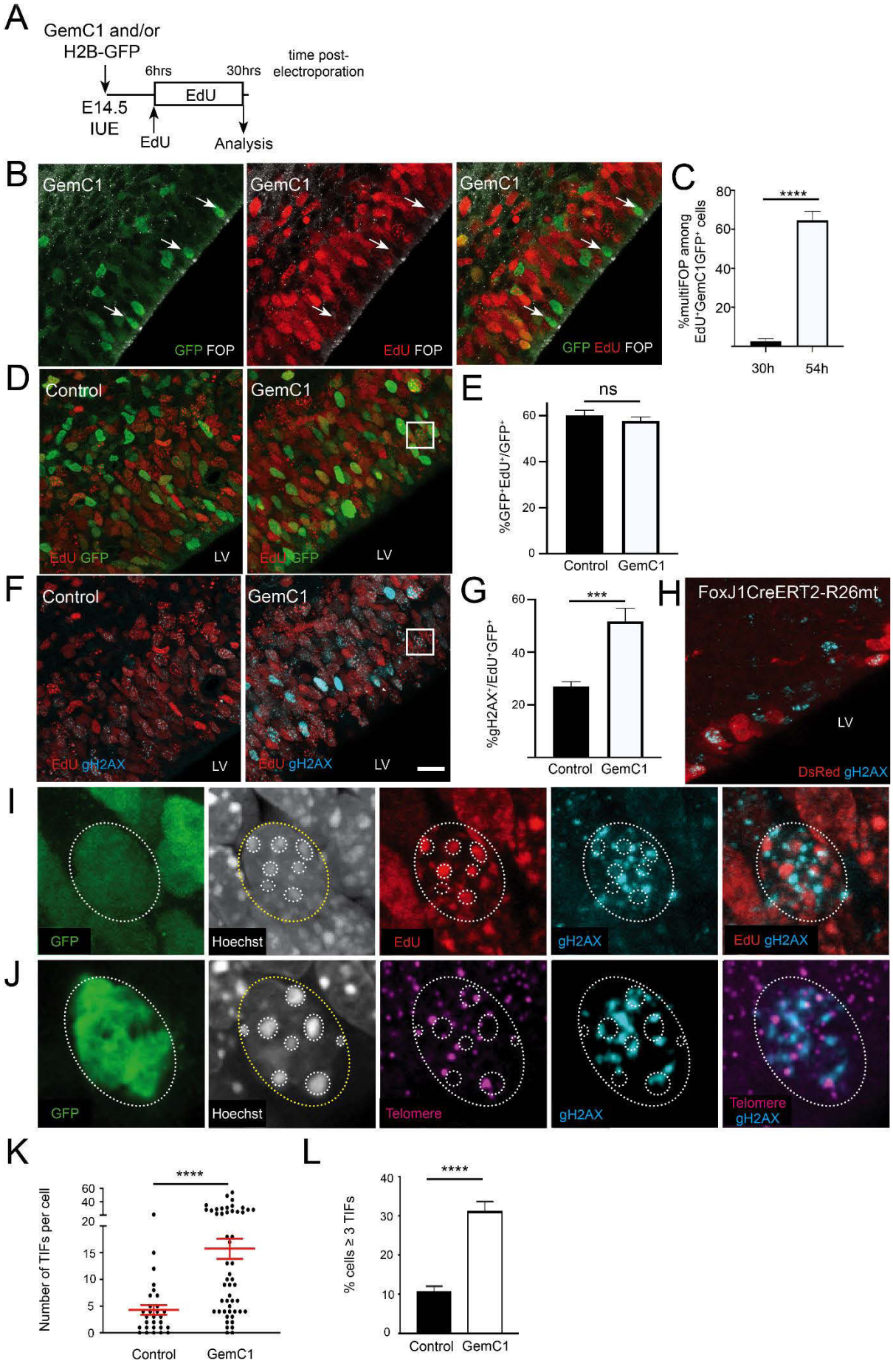
A
GemC1 and/or
H2B-GFP
6hrs
30hrs
time post-
electroporation
E14.5
IUE
EdU
EdU
Analysis
B
GemC1
GFP FOP
GemC1
EdU FOP
GemC1
GFP EdU FOP
C
****
%multiFOP among
EdU+GemC1GFP+ cells
80
60
40
20
30h
54h
D
Control
EdU GFP
LV
GemC1
EdU GFP
LV
E
ns
%GFP+EdU+/GFP+
60
40
20
0
Control
GemC1
F
Control
EdU gH2AX
LV
GemC1
EdU gH2AX
LV
G
***
%gH2AX+/EdU+GFP+
60
40
20
Control
GemC1
H
FoxJ1CreERT2-R26mt
LV
DsRed gH2AX
I
GFP
Hoechst
EdU
gH2AX
EdU gH2AX
J
GFP
Hoechst
Telomere
gH2AX
Telomere
gH2AX
K
****
Number of TIFs per cell
60
40
20
15
10
5
0
Control
GemC1
L
****
% cells ≥ 3 TIFs
40
30
20
10
0
Control
GemC1

Figure 2. GemC1 induces replicative stress before centriole amplification. (A) Schematic representation of the experiment. Control (H2B-GFP) plasmids with or without GemC1 were electroporated *in utero* at E14.5. EdU was intraperitoneally injected in the pregnant females 6 hours later and given in the drinking water for 24 hours. Coronal section analysis was performed at 30 hours post IUE. (B, D, F) Representative images of electroporated cells (GFP^+) are shown in green, EdU labeling in red (B, D, F), FOP in white (B) and γH2AX in blue (F). White arrows indicate cells that are GFP^+EdU^-, and that have started to amplify their centrioles (multi-FOP^+) (B). (C) Quantification of the mean percentage of GemC1GFP^+EdU^+ that are multi FOP^+ at 30 or 54h post IUE (C). (E) Quantification of the mean percentage of GFP^+EdU^+ among all GFP^+ cells in control and GemC1 gain of function conditions. (G) Quantification of the mean percentage of $YH2AX^+$ cells among all GFP^+EdU^+ cells in control and GemC1 gain of function conditions. (H) Representative image of a FoxJ1Cre-ERT2 x R26mT coronal section of the forebrain at E17.5, fed with Tamoxifen at E16.5. The DsRed protein ($FoxJ1^+$ cells) is shown in red and γH2AX in blue. (I) Zoom-in of a cell from panels D, F (same section) depicting the closely-associated EdU (red) and γH2AX (blue) stainings around chromocenters shown with Hoechst (grey). (J) Representative image of a GemC1GFP^+-electroporated cell stained for telomeres (magenta) and γH2AX (blue). Dotted-line depict the nuclei and the chromocenters (seen by Hoechst counterstain, in grey). Note the very frequent association of telomeres and TIFs to chromocenters. (K-L) Quantifications of the mean number of TIFs per cell (considering only $YH2AX^+$ cells, this is, with 3 or more YH2AX foci) (L), and the mean percentage of cells with 3 or more TIFs (L). Error bars indicate the SEM for all graphs, with n=3 animals for the two conditions shown, except for graphs (K-L) (n=4 animals per condition). A Mann-Whitney test was performed between the two groups to assess the p-value; ns (not significant) $p > 0.5$, *** $p \leq 0.001$, **** $p \leq 0.0001$. LV: Lateral Ventricle. Scale bar 20 µm (B, D, F) 15 µm (H) and 3 µm (I-J).

GemC1 delays mitotic progression and arrests cell cycle while amplifying centrioles

We then studied the consequences of GemC1 gain of function and increased gH2AX on cell cycle progression in live explants of GemC1 or control-electroporated V-SVZ wholemounts, using time-lapse microscopy (Figure 3A). We observed that GemC1-electroporated cells displayed a significant decrease in the mitotic frequency, compared to an H2B-GFP control, although we did not observe apoptosis-like features (Figure 3B-C, Supplementary video 1-2). These results suggest that GemC1 prevents the cells from a progression through mitosis.

To further study the link between the cell cycle regulators and centriole amplification, we compared the genetic cascades induced by gain of function of each of the Geminin family members. Two days after IUE at E14.5, the transcriptomes were analyzed by comparing the genes up or down-regulated by Geminin family proteins to control cells (electroporated with GFP only). Geminin did not lead to significant changes in gene expression, although GemC1 and Mcidas induced the up-regulation of more than 500 genes, among which 463 were in common, with a minority of down-regulated genes (Figure 3E-F). Interestingly, a Gene Set Enrichment Analysis performed with the Pathway Studio software (https://www.elsevier.com/solutions/pathway-studio-biological-research) with all the genes differentially expressed revealed a significant presence of G1/S transition genes upon

GemC1/Mcidas expression, as well as G2/M transition genes after Mcidas gain of function electroporations, in the cell cycle regulation category (Figure 3G). A detailed look into the genes that were upregulated revealed that GemC1 triggered Mcidas expression, but the opposite was not true, thus confirming the already established hierarchy between the two Geminin family members (Arbi et al., 2016; Kyrousi et al., 2015). Among the genes upregulated only by Mcidas, there were a number of late cilia motility genes (dnah11, ift22, rsph14), suggesting that, since Mcidas is downstream of GemC1, cells were further down the differentiation cascade. The majority of genes (463) were commonly up-regulated by Mcidas and GemC1, though. Among these, we could find multiciliation-related genes, some of which have been previously described *(foxj1, myb, rfx2, deup1, cep152, foxn4, ccno),* as well as genes that induce cell cycle progression *(cdt1, cav2, dcdc5, usp2, igf2, ccna1)* or that are implicated in cell cycle arrest and stress response *(trp73, pidd1, cdkn1a, e2f7, casp7, aifm3)* (Figure 3H).

Next, we determined the cell cycle status of these cells using immunostainings with well-known markers. Interestingly, we found that GemC1 expression leads to the maintenance of the hyperphosphorylated Rb (pRb), suggesting that most GemC1+ cells are stalled at the G1/S transition, compared to a majority of control cells that are pRb negative (Figure 3D-F). Consistent with this observation, we assessed the presence in the GemC1 condition of the p21, a potent cell cycle arrest inducer (Chen et al., 2002), and p73 proteins, a member of the DNA damage pathway that triggers cell cycle arrest and apoptosis (Urist et al., 2004; Yoon et al., 2015). Both completely absent in controls (not shown), they were significantly up-regulated in GemC1 gain of function condition (Figure 3G-H).

Altogether, these results show that the initiation of ependymal differentiation from neural stem cells and centriole amplification requires an active cell cycle, with concomitant expression of both cell cycle progression (pRb) and cell cycle arrest markers (p21, p73).

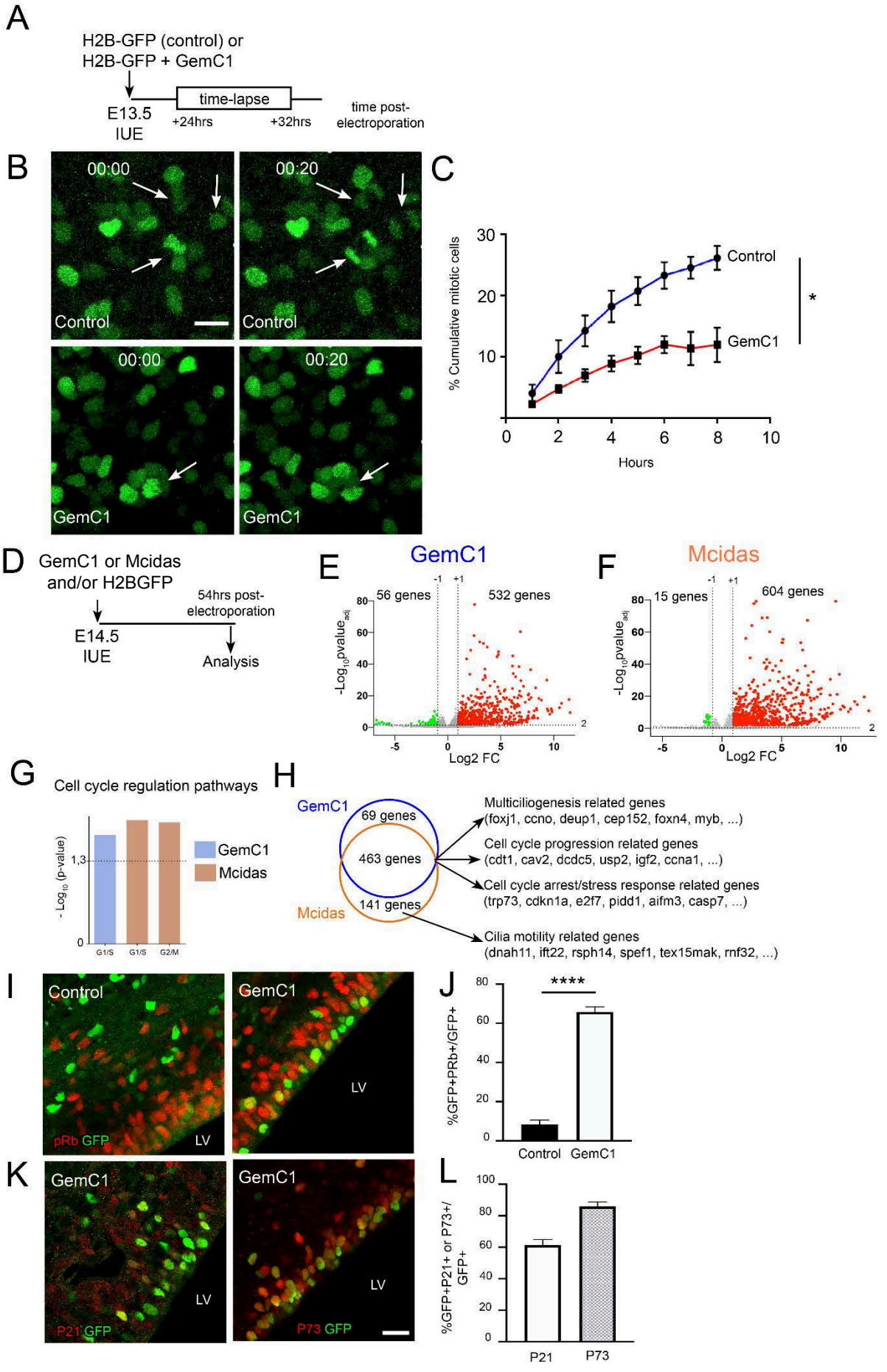
A
H2B-GFP (control) or
H2B-GFP + GemC1
E13.5
IUE
time-lapse
+24hrs
+32hrs
time post-
electroporation
B
00:00
00:20
Control
Control
00:00
00:20
GemC1
GemC1
C
% Cumulative mitotic cells
Control
GemC1
*
Hours
D
GemC1 or Mcidas
and/or H2BGFP
E14.5
IUE
54hrs post-
electroporation
Analysis
E
GemC1
56 genes
532 genes
-Log10pvalueadj
Log2 FC
F
Mcidas
15 genes
604 genes
-Log10pvalueadj
Log2 FC
G
Cell cycle regulation pathways
- Log10 (p-value)
GemC1
Mcidas
G1/S
G1/S
G2/M
H
GemC1
69 genes
463 genes
141 genes
Mcidas
Multiciliogenesis related genes
(foxj1, ccno, deup1, cep152, foxn4, myb, ...)
Cell cycle progression related genes
(cdt1, cav2, dcdc5, usp2, igf2, ccna1, ...)
Cell cycle arrest/stress response related genes
(trp73, cdkn1a, e2f7, pidd1, aifm3, casp7, ...)
Cilia motility related genes
(dnah11, ift22, rsph14, spef1, tex15mak, rnf32, ...)
I
Control
GemC1
pRb GFP
LV
LV
J
****
%GFP+PRb+/GFP+
Control
GemC1
K
GemC1
GemC1
LV
LV
P21 GFP
P73 GFP
L
%GFP+P21+ or P73+/
GFP+
P21
P73

Figure 3. GemC1 slows down cell cycle progression. (A) Schematic representation of the experiment. Control (H2B-GFP) with or without GemC1-expressing plasmids were electroporated at E13.5 and *ex vivo* explants of the V-SVZ were made and filmed for 8 hours, 24 hours after the IUE. (B) Time-selected representative images of the *ex vivo* explant at a time 0 and 20 minutes later. Live electroporated cell nuclei (GFP^+) are seen in green. The arrows indicate cells that undergo mitosis within the selected 20 minutes. (C) Quantification of the mean cumulative frequency of mitosis in electroporated cells. (D) Schematic representation of the experiment. Control (H2B-GFP) plasmids with or without Mcidas or GemC1-expressing plasmids were electroporated *in utero* at E14.5 and FACS-sorted for RNA-sequencing or coronal section analysis, 54 hours post IUE. (E-F) Volcano plots of the differentially expressed genes in and control versus GemC1 (E) or Mcidas (F) expressing conditions *in vivo*. Red dots indicate up-regulated genes and green dots correspond to the down-regulated ones. Genes with a lower than 0.05 p-value and a two-fold change or higher were considered. Three replicates of each condition were used (G) Pathway studio analysis of the significantly enriched gene networks in the conditions just cited. (H) Venn diagram of the Mcidas and GemC1 commonly induced genes or those only induced by each one of them individually. (I, K) Representative images of coronal sections of the forebrain electroporated with H2B-GFP or H2B-GFP + GemC1. The G1/S transition marker phosphorylated retinoblastoma (PRb) is shown in red (E). The cell cycle arrest markers p21 and p73 are also depicted in red (G). (J, L) Quantifications of the mean percentage of pRb^+ (F), $P21^+$ or $P73^+$ (H) electroporated (GFP+) cells. The error bars indicate the SEM for all graphs. In (C) n=3 animals, and 3 positions were filmed in controls and 6 animals and 9 positions were filmed in GemC1. A Kolmogorov-Smirnov test for cumulative distributions was used to calculate the p-value. In (J, L), n=3 animals for all stainings and conditions were analyzed. P-values were calculated using a Mann-Whitney test; * $p \leq 0.05$ and **** $p \leq 0.0001$. Scale bar 10 µm (B) and 20 µm (I, K). LV: Lateral Ventricle.

Telomerase expression rescues the control phenotype in GemC1-expressing conditions and favors a B1 cell fate

To assess the role of replicative stress in ependymal/adult neural stem cell fate decision, we evaluated the effects of telomerase gain of function in GemC1 expressing cells and controls. Telomerase is known for maintenance of telomeric length, thus preventing premature ageing and replicative senescence (Giardini et al., 2014), but also for protecting telomeres against the DNA damage response and chromosome end fusions that are at the source of genomic instability (Chan and Blackburn, 2003; Perera et al., 2019). We electroporated H2B-GFP + GemC1 at E14.5 in mice that express telomerase in a p21-expressing context (heterozygous knockin of telomerase in the p21 locus; p21-mTERT -/+, a gift from the laboratory of V. Géli). Since GemC1 induces p21 expression, it is expected that GemC1 will up-regulate telomerase in these mice. As controls, we used p21 -/+ mice. These animals were generated by crossing p21 -/- mice, which develop normally and were previously generated by targeting a gene-disrupting construct into the exon 2 of the p21 gene to generate a null mutation (Deng et al., 1995) (Figure 4A). Two days later, ependymal-specific p73 expression and centriole amplification significantly diminished in p21-mTERT -/+ mice compared to p21 -/+ controls (Figure 4B-E). This suggests that the enzyme telomerase diminishes the effects of GemC1 on ependymal cell differentiation. To further assess whether

the enzyme telomerase has an impact on the ependymal/adult neural stem cell fate decision, we analyzed at P10 the proportion of ependymal cells (FoxJ1+ Sox9+) or astrocytes (FoxJ1- Sox9+) in telomerase gain of function condition compared to control (Figure 4G-H). Telomerase expression induced a shift in the neurogenic niche cell fate, favoring the generation of adult neural stem cells (astrocytes), in detriment of the terminally differentiated ependymal cells. Indeed, telomerase gain of function resulted in a V-SVZ composed of more of Sox9+FoxJ1- stem cells (astrocytes) compared to controls (Figure 4G-H).

Taken together, these experiments show that telomerase can revert the ependymal phenotype induced by GemC1 and trigger the formation of astrocytes in the neurogenic niche, and suggest that the DNA damage response induced by GemC1 in cycling cells contribute to the terminal differentiation of ependymal cells.

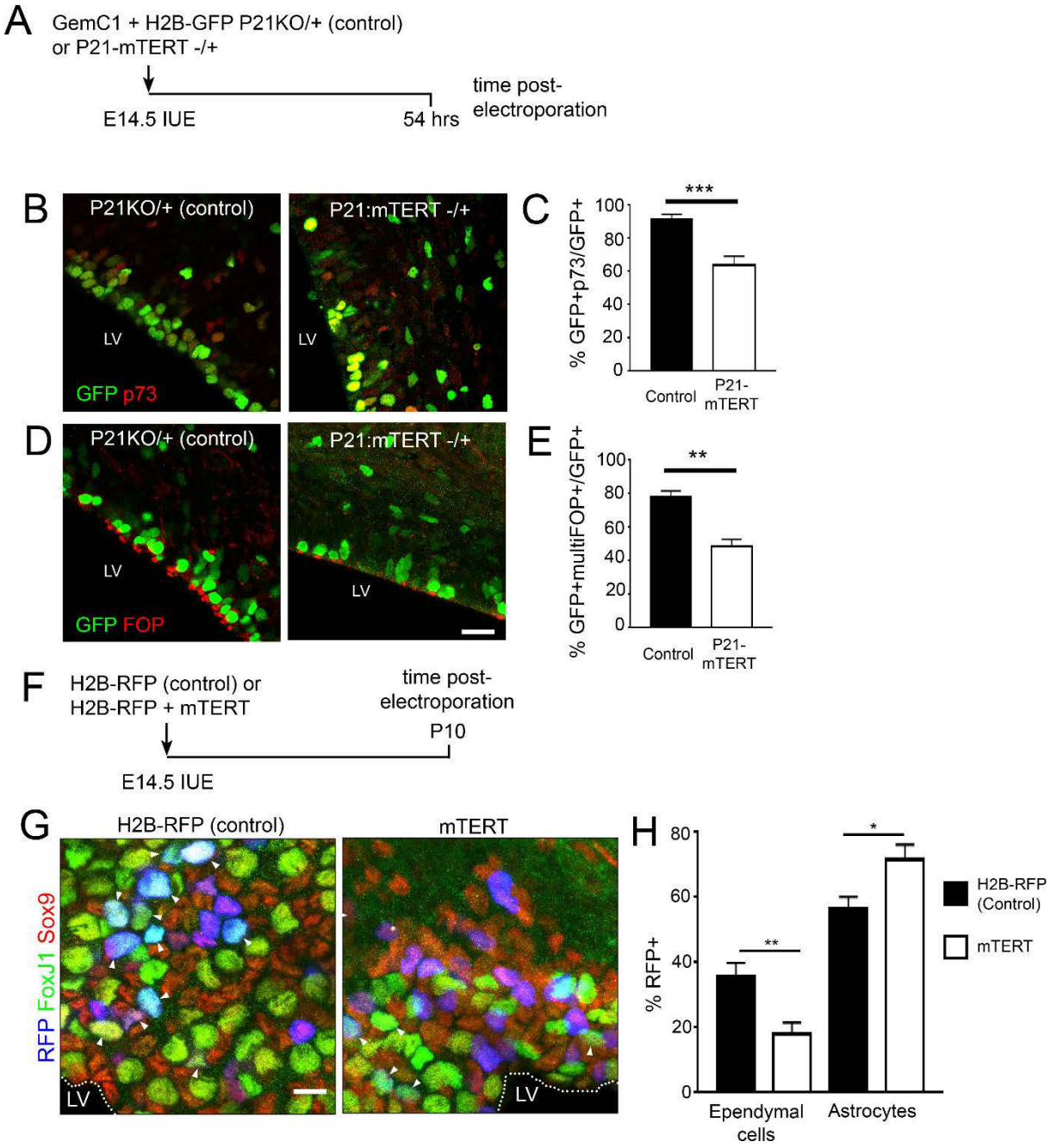

Figure 4. Telomerase attenuates GemC1 effects and reverses ependymal cell differentiation. (A) Schematic representation of the IUE at E14.5 of H2B-GFP + GemC1-expressing plasmids in p21 -/+ (control) or p21-mTERT -/+ mice. Analysis on coronal sections was performed 54 hours after the IUE. (B, D) Representative images of the p21 -/+ or p21-mTERT -/+ neuroepithelium with electroporated cells (GFP^+) shown in green and the different markers tested: p73 (D) and FOP (D, for procentrioles and centrioles), both in red. (C, E) Quantifications of the mean percentage of electroporated cells that are positive for the different markers tested: $p73^+$ GFP^+ (C) or multi FOP^+ GFP^+ (E). (F) Experimental layout showing IUE of either H2B-RFP or H2B-RFP + mTERT performed at E14.5. The cell fate in the neurogenic niche was analyzed in coronal sections at P10. (G) Representative images of electroporated areas of the neurogenic niche, with RFP+ cells shown in blue, immunostained with anti-FoxJ1 and anti-Sox9 antibodies, in green and red, respectively. The arrowheads point at the ependymal cells issued from electroporated cells at E14.5 ($RFP^+FoxJ1^+Sox9^+$). (H) Quantification of the percentage of ependymal cells (FoxJ1+ Sox9+) and astrocytes (FoxJ1- Sox9+) within the electroporated neurogenic niche population (RFP+). In all graphs, the error bars illustrate the SEM for n=3 animals for both genotypes (except for FOP staining, where n=2 in the p21 -/+ group, and the mTERT group, where n=6). P-values were calculated via a Mann-Whitney test in all cases; * $p \leq 0.05$, ** $p \leq 0.01$ and *** $p \leq 0.001$. Scale bar 20 µm (B, D) and 10 µm (G). LV: Lateral Ventricle.

Discussion

GemC1 is a master gene of ciliogenesis and promoter of the multiciliated cell fate (Arbi et al., 2016; Kyrousi et al., 2015; Lalioti et al., 2019a; Ortiz-Álvarez et al., 2019; Terré et al., 2016), but the mechanisms of MCC specification are poorly understood. We have induced ependymal fate via gain-of-function experiments and showed that GemC1 directly induces replicative stress in G1/S cells, which precedes centriole amplification. Replicative stress and damaged telomere responses are concomitant to centriole amplification and reversible as gain-of-function of telomerase increased the B1 astrocyte fate over the ependymal one.

The role of GemC1 in DNA replication firing (Balestrini et al., 2010), led us to assess the presence of replicative stress in gain of function experimental condition. We confirmed the presence of γ-H2AX foci colocalized with EdU staining before the onset of centriole amplification. γ-H2AX is a marker of DNA damage (Zeman and Cimprich, 2014) and also of the presence of an active S/G2 checkpoint, whose expression has been confirmed in unchallenged cycling cells during S and S/G2 transition (Saldivar et al., 2018). We indeed observed significant levels of γ-H2AX in non-electroporated, unharmed embryonic neuroepithelium, which coincided with the layer of proliferating V-SVZ cells (data not shown). The levels of γ-H2AX in GemC1 gain of function condition, though, were much higher than the controls, in cell proportion and signal intensity (Figure 2). Apoptotic traits, such as pyknotic nuclei were rarely observed in fixed slices or the time-lapse movies, suggesting that γ-H2AX^{+} cells did not die. These data indicate that centriole amplification is preceeded by the generation of a GemC1-dependent replicative stress. Since p21 expression and DDR are indicative of telomere-induced replicative senescence (Roake and Artandi, 2017), we evaluated the occurrence of TIFs in our system (Takai et al., 2003). GemC1 induced the formation of TIFs in a higher proportion than control cells (Figure 2). This led us to think that damaged telomeres could be at the onset of the cell cycle arrest phenotype here described and, for that reason, we considered the role of telomerase in neurogenic niche cell specification and differentiation. Telomerase was not only able to rescue a control phenotype in GemC1 expressing conditions, but it also favored the B1 fate over the ependymal one (Figure 4).

RNA-seq analysis of GemC1 or Mcidas-expressing cells in the embryonic neuroepithelium confirmed the specific presence of ciliary growth and centriole amplification genes upon GemC1 or Mcidas expression, as previously described (Terré et al., 2016), as well

as the functional hierarchy of GemC1 and Mcidas, where the former activates the latter (Kyrousi et al., 2015). However, the analysis of the transcriptomes using Pathway Studio software also revealed the presence of active G1/S and G2/M transition gene networks during the GemC1/Mcidas-governed ependymal differentiation (Figure 3G). The presence of active cell cycle markers, such as phosphorylated retinoblastoma (pRb) (Henley and Dick, 2012) or Cenp-F (Loftus et al., 2017) was confirmed via immunofluorescence studies (Figure 3I and data not shown), at the time when most cells were amplifying their centrioles (Figure 1). The potent CDK inhibitor p21 was also rapidly up-regulated in ependymal progenitors (Pack et al., 2019), a cell cycle arrest gene that has been shown to promote quiescence in adult neural stem cells (Kippin et al., 2005; Marqués-Torrejón et al., 2013; Porlan et al., 2013) (Figure 3J). This concomitant expression of cell cycle progression and arrest markers suggests that ependymal cells are in a pseudo-cell cycle state, equivalent to the S/G2 phases, since entry into mitosis is inhibited (Figure 3A-C, Supplementary Movie 1-2). This goes in consonance with our and others previous studies that show that multiciliated cell differentiation requires the activation of cell cycle actors, such as CDK2 and mitotic calibrators, though inhibiting mitotic entry (Al Jord et al., 2017; Vladar et al., 2018).

Altogether our results show that ependymal cell specification occurs when progenitors are still actively cycling. GemC1 gain of function directly induces DNA replication stress that leads to pseudo cell cycle arrest and centriole amplification, which can be reversed by telomerase gain of function.

Materials and Methods

Mouse experimental models

All experiments performed in this work requiring the use of live animals were carried out following French and European Union regulations and guidelines of the local ethics committee (Comité d'éthique en experimentation animal n°005). All mice were healthy, housed under proper conditions in a 12 h light / 12h dark cycle, at a temperature of 22°C, and fed *ad libitum*. None of our individuals was subject to previous experimental procedures.

The day of the vaginal plug was set as embryonic day (E) 0.5 and the birth date as postnatal day (P) 0. Wild type (WT) RjORL:SWISS (Janvier Labs) mice were used in most of the IUE or postnatal electroporations. The knock-in p21-mTERT -/+ line and the line used as

control, p21 -/+ (Deng et al., 1995, JAX stock #016565), both used for IUE experiments, were a gift from the laboratory of V. Géli (Cancer Research Center, Marseille, France). Finally, the FoxJ1Cre-ER^{T2} -/+ (Muthusamy et al., 2014, JAX stock #027012) transgenic animals were bred with the Ai14 (Madisen et al., 2010) (Rosa26mTomato -/-) to obtain heterozygous embryos for the FoxJ1Cre-ER^{T2} and Rosa26mTomato alleles. These embryos express the red fluorescent protein mTomato in FoxJ1+ cells upon treatment with tamoxifen. All animals used in this study were sacrificed at embryonic stages post electroporation or post tamoxifen treatment, at early postnatal stages (P0-P2) after postnatal electroporation or at P10 for cell fate studies. In all cases, it was done following ethical procedures and regulations.

***In utero* or postnatal electroporation and plasmids**

IUE (Briz et al., 2017; Saito and Nakatsuji, 2001) of mouse embryos was performed at E13.5 or E14.5. Pregnant females were injected subcutaneously with buprenorphine (0.1 mg/kg) 15 minutes prior to surgery. They were subsequently anaesthetized by isoflurane (2-2.5%) inhalation, a laparotomy was performed and the uterine horns were exposed. Warm (37°C), sterile PBS was used throughout the procedure to hydrate the exposed embryos. Plasmid solutions were diluted in filtered PBS and stained with FastGreen (0.025%, Sigma) to visualize how the plasmid mix is being injected in the ventricles, using a thin glass capillary (Harvard Apparatus). The final concentration of each plasmid was 1 µg/µl. Immediately after injection of the plasmid solution, four pulses of 50 ms and 35 V were applied to the embryos' telencephalon, with 950 ms intervals between pulses. We used a CUY21 EDIT electroporator from Nepagene to do so. Finally, the embryos were carefully placed back into the abdominal cavity, which was filled with 1 ml of warm sterile PBS.

For postnatal electroporation, the procedure was performed at P0. Pups were anesthetized by placing them in ice for 1 minute and injecting 2-3 mm laterally to the hemisphere midline, still visible in the absence of fur. Plasmids were prepared as described, with a ten-fold higher concentration of FastGreen (0.25%) . The electrodes were never placed directly in contact with the pup's skin, but an electrode gel was applied around its head. We used the Nepagene Super Electroporator NEPA21 with five poring pulses of 100 V and 99 ms each, at 90 ms intervals, and one transfer pulse of 1 V and 1 ms. After electroporation, mice were left on a heating pad to recover.

We used pCAG-H2B-GFP, H2B-RFP as an electroporation reporter (gifts from the laboratory of X. Morin, Institute of Biology of the ENS, Paris, France). The pCAGGS-GemC1 and pCAGGS-Mcidas plasmids were gifts from the laboratory of S. Taraviras (Kyrousi et al., 2015). Finally the pCAG-mTERT plasmid was kindly gifted by the team of L. Harrington (Institute for Research in Immunology and Cancer, Montreal, Canada).

EdU administration and detection

EdU (Thermo Fisher Scientific, A10044) was administered via intraperitoneal injections to pregnant females before and after IUE or subcutaneously to newborn pups before and after postnatal electroporation. A PBS-diluted 8 mg/ml stock at 10 µl/g of body weight was used in both cases. EdU was also diluted in drinking water at a 1mg/ml concentration and given to pregnant females after IUE experiments.

EdU incorporation was detected in tissues using the Click-iT EdU Alexa Fluor imaging kit (Thermo Fisher Scientific for Alexa Fluor 594 or 647 staining), according to manufacturer's instructions. In a few words, fixed coronal sections were permeabilized in blocking solution with 0.1% Triton X-100 and 10% fetal bovine serum in PBS for 1h. Sections were then incubated for 1 hour with the Click-iT reaction mix, in the darkness. Afterwards, we proceeded with the immunostaining method.

Tamoxifen-dependent Cre expression

Tamoxifen (Sigma-Aldrich, T5648) was administered to pregnant females by oral gavage in a corn-oil solution (Sigma-Aldrich, C8267) at 10 mg/ml, feeding 10 µl of solution per gram of body weight.

Tissue collection

Whole brains of embyros were dissected and fixed overnight at 4°C in 4% PFA, previously sacrificing the mother via cervical dislocation. P10 animals were anesthesized with a mixture of 100 mg of ketamine and 10 mg of xylazine per kg of body weight, and then were transcardially perfused with 4% PFA. Their brains were subsequently dissected and fixed as described. All these were afterwards sectioned in a vibratome. 80 µm-thick floating coronal sections were prepared.

Immunohistochemistry

Coronal sections were blocked for at least 30 minutes to 1 hour in 10% FBS, 0.1% Triton X-100. Samples were incubated with the primary antibodies in the blocking solution overnight at 4°C under gentle agitation. The primary antibodies used were: chicken polyclonal anti-GFP (1:1600, Aves Labs, GFP-1020), mouse monoclonal anti-FOP (1:500, Abnova Corporation, H00011116-M01), rabbit monoclonal anti-PRb (1:800, Cell Signaling, 8516S), mouse monoclonal anti-p21 (1:100, Santa Cruz Biotechnology, sc-6246), rabbit monoclonal anti-p73 (1:100, Abcam, ab40658), rabbit monoclonal anti-γ-H2AX (1:400, Cell Signaling, 9718S), mouse monoclonal anti-FoxJ1 (1:400, Thermo Fischer Scientific, 14-9965-82), and rabbit polyclonal anti-Sox9 (1:600, Millipore, AB5535). Species-specific Alexa Fluor fluorophore-conjugated secondary antibodies (Thermo Fischer Scientific) were diluted in blocking solution and incubated for 2 h at room temperature with the samples. In some cases, nuclei were counterstained by adding Hoechst from a 20 mg/ml stock (1:1500, Sigma Aldrich, B2261) into the secondary antibody solution. Brain sections were mounted using Fluoromount-G mounting medium (Southern Biotech, 0100-01).

Fluorescent-activated cell sorting

In order to study GemC1 and Mcidas-triggered gene expression, embryonic brains co-electroporated with H2B-GFP with or without GemC1 or Mcidas-expressing plasmids were dissected and single cell suspensions were prepared. The meninges were removed and brains were cut into small pieces. Then they were incubated for 20 minutes at 37°C in a freshly prepared digestion solution (Collagenase type IV at 0.2 mg/ml and DNAse I at 50 µg/ml in RPMI medium supplemented with 10% FBS). 500 µl per dissected brain were used. Afterwards, the tissue was homogenized doing 5 to 10 “ups and downs” using a syringe and an 18G needle. Then, single cell suspensions were made by passing the homogenized solution through a 70-µm pore size cell strainer, and washing it with FACS buffer (0.5% BSA and 0.074% EDTA in PBS) to a final volume of 15 ml. Finally, cells were centrifuged for 5 minutes at 200xG, washed and resuspended in FACS buffer.

Single cell suspensions from electroporated brains were sorted based on the GFP fluorescence using a S3 cell sorter (Biorad, Curie Institute), previous removal of cell debris and aggregates via appropriate gating.

RNA Extraction for RNA-Seq

For RNA-Seq experiments, GFP+ cells were FACS-sorted 48 hours after IUE of H2B-GFP expressing plasmid alone or together with GemC1 or Mcidas expressing plasmids. Total RNA was extracted from approximately 10000 cells pooled from several embryos for each condition using the RNAqueous®-Micro Total RNA Isolation Kit (Thermofisher, AM1931) following the manufacturer's instructions. RNA was eluted twice in 10 µl elution buffer. Samples were then treated with DNAse I.

cDNA Libraries and RNA-Seq

1 ng of total RNA was amplified and converted to cDNA using the Ovation RNA-Seq kit V2 (NuGEN, 7102). Following amplification, 1 µg of cDNA was fragmented to approximately 200 bps using Covaris S200. The remainder of the library preparation was done using 200 ng of cDNA following TruSeq RNA Sample Prep v2 kit (Illumina, RS-122-2001) from the End Repair step. Libraries were multiplexed by 4 on 1 flow cell lane. A 50 bp read sequencing was performed on a HiSeq 1500 device (Illumina). A mean of 17.3 ± 3.9 million passing Illumina quality filter reads was obtained for each of the four samples. For each biological sample, three technical replicates were done.

Differential expression analysis

The analyses were performed using the Eoulsan pipeline (Jourdren et al., 2012), including read filtering, mapping, alignment filtering, read quantification, normalisation and differential analysis: Before mapping, poly N read tails were trimmed, reads ≤40 bases were removed, and reads with quality mean ≤30 were discarded. Reads were then aligned against the Mus musculus genome from Ensembl version 91, keeping only the uniquely mapping, using STAR (version 2.5.2b) (Dobin et al., 2013). To compute gene expression, Mus musculus GFF3 / GTF genome annotation version 91 from mm10 Ensembl database was used. All overlapping regions between alignments and referenced exons (or genes) were counted with the unstranded option using HTSeq-count 0.5.3 (Anders et al., 2015)

The sample counts were normalized using DESeq2 1.8.1 (Love et al., 2014). Statistical treatments and differential analyses were also performed using DESeq2 1.8.1.

GO analyses

We used the text-mining Pathway Studio ResNetdatabase (Ariadne Genomics, Rockville, MD, USA) and the GSEA tool (Subramanian et al., 2005) in Pathway Studio 12.3.0.16 (Nikitin et al., 2003) to identify overrepresented signaling pathways and biological processes within our differentially expressed data set. As parameters for the GSEA method, we selected the Mann–Whitney U-test, a P-value threshold of 0.05.

Telomere Fluorescent *in situ* hybridization

Tissue from electroporated embryonic brains was processed as described before. When the FISH staining was combined with immunofluorescence, the latter was performed first, as described, then the tissue was post-fixed (30 minutes in 4% PFA at room temperature), FISH-processed and immunostained again, as described, due to the aggressive FISH procedure that compromised the result of the immunofluorescence.

The FISH protocol went as follows. After obtaining floating sections, an essential step for observing telomeres *in vivo* was performed: the demasking of the epitope. Sections were treated with HCl 2N at room temperature for 20 minutes. Slides were then rinsed in water and dehydrated in 95% ethanol for 3 minutes and air-dried. Subsequently, they were incubated with the telomeric probe (TelC-Cy3, Panagene, F1002) at 0.57 ng/µl in 70% formamide in 10 mM Tris pH 7.2 and 10% blocking solution (solution of 10% blocking reagent for nucleic acid hybridization and detection, Roche, 11096176001, in a solution with 100 mM maleic acid and 150 mM NaCl). Hybridization solution was laid on the sections on the slides and covered with a coverslip to avoid evaporation. A brief 3-minute incubation of the slides at 80°C with the solution on a heating block was done to denaturate the telomeric DNA. Slides were incubated overnight, at room temperature, in a humidified, dark chamber. Finally, the telomeric probe was washed twice for 15 minutes with a 70% formamide in 10 mM Tris solution at pH 7.2 and three times for 5 minutes with a 150 mM NaCl, 50 mM Tris, and 0.05% Tween20 solution at pH 7.5.

Time lapse ventricular explant filming

For time-lapse filming, electroporated brains were quickly dissected in ice-cold DMEM/F12 with 2.9 mg/ml glucose, 1% P/S and HEPES 10mM. Ventricular explants were prepared by dissecting the septal portion of the electroporated hemisphere, thus exposing

the ventricular cavity. They were then imaged as previously described (Pilz et al., 2013), except that *en-face* ventricular surfaces were filmed, instead of coronal sections. Explants were placed, ventricular surface down (for inverted microscopy filming) on a filter membrane, inside a 35-mm glass-bottom dish (MatTEK, P35G-0-20-C) with approximately 800 µl of dissection medium, supplemented with N-2 (1:100, Invitrogen, 17502-048), B-27 (1:50, Invitrogen 12587-010), FBS (5%) and normal horse serum (5%). For long-term imaging, the explants were embedded in a collagen matrix consisting of 40% collagen type I and $NaHCO_3$ (0.1%) in the medium just described.

The explants were incubated for 1 hour at 37ºC before starting the time-lapse imaging. They were filmed with a 40x 1.3 NA water objective, which possesses a sufficiently large working distance to enable image acquisition on the system just described. Other immersion objectives would collide with the glass-bottom dish before setting the explant ventricular surface in focus. Since this was a water immersion objective and filming was performed at 37°C, to avoid eventual evaporation, we fashioned a silicon-based support around the objective and filled it with electrode gel and put some of it between the objective lens and the dish. Time lapse acquisition was performed in a 37ºC chamber with 5%CO_2 at 10-minute intervals.

Imaging

3D confocal images of fixed slices or live V-SVZ wholemounts were acquired with a 10X 0.45 NA, a 20x 0.8 NA, a 40x 1.4 NA oil objective, 63x 1.4 NA oil objective or a 40x 1.3 NA water objective on an inverted LSM 880 Airyscan Zeiss microscope.

Statistical analysis and software

At least three independent replicates were chosen for each experiment and condition (unless indicated otherwise). Quantifications and image analysis was done using Fiji (Schindelin et al., 2012), Excel and GraphPad Prism software, for assessment of statistical measures, significance calculations and graph generation. Quantifications represent the mean value with error bars indicating the SEM. P-values were assessed using a Mann-Whitney test or a Kolmogorov-Smirnov test for cumulative distributions. P values in this manuscript present the following star code: ns: $p > 0.05$ (non-significant), *$p \leq 0.05$, **$p \leq 0.01$, ***$p \leq 0.001$, **** $p \leq 0.0001$.

Acknowledgments

We thank all members of the Spassky laboratory for comments and discussions. We thank X. Morin for the pCAAGS-H2B-GFP, H2B-RFP and ZO1-GFP plasmids, as well as the S. Taraviras group for the p-CAAGS-GemC1 and Mcidas plasmids, and the laboratory of L. Harrington for the p-CAG-mTERT plasmid. We thank A.-K. Konate, R. Nagalingum and M. Andrieu for administrative support. We thank the IBENS Animal Facility for animal care. The team received support from Agence Nationale de la Recherche (ANR) Investissements d'Avenir (ANR-10-LABX-54 MEMO LIFE and ANR-11-IDEX-0001-02 PSL* Research University). The Spassky laboratory is supported by INSERM, CNRS, Ecole Normale Supérieure (ENS), ANR (ANR-17-CE12-0021-03), European Research Council (ERC Consolidator grant 647466). G.O.-A. received a fellowship from Labex MEMOLIFE.

References

Anders, S., Pyl, P.T., and Huber, W. (2015). HTSeq-A Python framework to work with high-throughput sequencing data. Bioinformatics *31*, 166–169.

Arbi, M., Pefani, D., Kyrousi, C., Lalioti, M., Kalogeropoulou, A., Papanastasiou, A.D., Taraviras, S., and Lygerou, Z. (2016). GemC1 controls multiciliogenesis in the airway epithelium. EMBO Rep. *17*, 400–413.

Balestrini, A., Cosentino, C., Errico, A., Garner, E., and Costanzo, V. (2010). GEMC1 is a TopBP1-interacting protein required for chromosomal DNA replication. Nat. Cell Biol. *12*, 484–491.

Briz, C.G., Navarrete, M., Esteban, J.A., and Nieto, M. (2017). In utero electroporation approaches to study the excitability of neuronal subpopulations and single-cell connectivity. J. Vis. Exp. *2017*, 55139.

Chan, S.W.L., and Blackburn, E.H. (2003). Telomerase and ATM/Tel1p protect telomeres from nonhomologous end joining. Mol. Cell *11*, 1379–1387.

Chen, X., Zhang, W., Gao, Y.F., Su, X.Q., and Zhai, Z.H. (2002). Senescence-like changes induced by expression of p21Waf1/Cip1 in NIH3T3 cell line. Cell Res. *12*, 229–233.

D'Adda Di Fagagna, F., Reaper, P.M., Clay-Farrace, L., Fiegler, H., Carr, P., Von Zglinicki, T., Saretzki, G., Carter, N.P., and Jackson, S.P. (2003). A DNA damage checkpoint response in telomere-initiated senescence. Nature *426*, 194–198.

Deng, C., Zhang, P., Wade Harper, J., Elledge, S.J., and Leder, P. (1995). Mice Lacking p21 CIP1/WAF1 undergo normal development, but are defective in G1 checkpoint control. Cell *82*, 675–684.

Dobin, A., Davis, C.A., Schlesinger, F., Drenkow, J., Zaleski, C., Jha, S., Batut, P., Chaisson, M., and Gingeras, T.R. (2013). STAR: Ultrafast universal RNA-seq aligner. Bioinformatics *29*, 15–21.

Faubel, R., Westendorf, C., Bodenschatz, E., and Eichele, G. (2016). Cilia-based flow network in the brain ventricles. Science (80-.). *353*, 176–178.

Ferrón, S., Mira, H., Franco, S., Cano-Jimenez, M., Bellmunt, E., Ramírez, C., Fariñas, I., and Blasco, M.A.

(2004). Telomere shortening and chromosomal instability abrogates proliferation of adult but not embryonic neural stem cells. Development *131*, 4059–4070.

Ferrón, S.R., Marqués-Torrejón, M.Á., Mira, H., Flores, I., Taylor, K., Blasco, M.A., and Fariñas, I. (2009). Telomere shortening in neural stem cells disrupts neuronal differentiation and neuritogenesis. J. Neurosci. *29*, 14394–14407.

Fuentealba, L.C., Rompani, S.B., Parraguez, J.I., Obernier, K., Romero, R., Cepko, C.L., and Alvarez-Buylla, A. (2015). Embryonic Origin of Postnatal Neural Stem Cells. Cell *161*, 1644–1655.

Furutachi, S., Miya, H., Watanabe, T., Kawai, H., Yamasaki, N., Harada, Y., Imayoshi, I., Nelson, M., Nakayama, K.I., Hirabayashi, Y., et al. (2015). Slowly dividing neural progenitors are an embryonic origin of adult neural stem cells. Nat. Neurosci. *18*, 657–665.

Gaillard, H., García-Muse, T., and Aguilera, A. (2015). Replication stress and cancer. Nat. Rev. Cancer *15*, 276–280.

Giardini, M.A., Segatto, M., Da Silva, M.S., Nunes, V.S., and Cano, M.I.N. (2014). Telomere and telomerase biology. In Progress in Molecular Biology and Translational Science, (Elsevier B.V.), pp. 1–40.

Gomez, D.E., Armando, R.G., Farina, H.G., Menna, P.L., Cerrudo, C.S., Ghiringhelli, P.D., and Alonso, D.F. (2012). Telomere structure and telomerase in health and disease (Review). Int. J. Oncol. *41*, 1561–1569.

Henley, S.A., and Dick, F.A. (2012). The retinoblastoma family of proteins and their regulatory functions in the mammalian cell division cycle. Cell Div. *7*.

Herbig, U., Jobling, W.A., Chen, B.P.C., Chen, D.J., and Sedivy, J.M. (2004). Telomere shortening triggers senescence of human cells through a pathway involving ATM, p53, and p21CIP1, but not p16INK4a. Mol. Cell *14*, 501–513.

Jiménez, A.J., Domínguez-Pinos, M.D., Guerra, M.M., Fernández-Llebrez, P., and Pérez-Fígares, J.M. (2014). Structure and function of the ependymal barrier and diseases associated with ependyma disruption. Tissue Barriers *2*, 1–14.

Al Jord, A., Shihavuddin, A., Servignat d'Aout, R., Faucourt, M., Genovesio, A., Karaiskou, A., Sobczak-Thépot, J., Spassky, N., and Meunier, A. (2017). Calibrated mitotic oscillator drives motile ciliogenesis. Science (80-.). *358*, 803–806.

Jourdren, L., Bernard, M., Dillies, M.A., and Le Crom, S. (2012). Eoulsan: A cloud computing-based framework facilitating high throughput sequencing analyses. Bioinformatics *28*, 1542–1543.

Kippin, T.E., Martens, D.J., and Van Der Kooy, D. (2005). p21 loss compromises the relative quiescence of forebrain stem cell proliferation leading to exhaustion of their proliferation capacity. Genes Dev. *19*, 756–767.

Köhler, C., Koalick, D., Fabricius, A., Parplys, A.C., Borgmann, K., Pospiech, H., and Grosse, F. (2016). Cdc45 is limiting for replication initiation in humans. Cell Cycle *15*, 974–985.

Kyrousi, C., Arbi, M., Pilz, G.A., Pefani, D.E., Lalioti, M.E., Ninkovic, J., Götz, M., Lygerou, Z., and Taraviras, S. (2015). Mcidas and gemc1 are key regulators for the generation of multiciliated ependymal cells in the adult neurogenic niche. Dev. *142*, 3661–3674.

Lalioti, M.E., Kaplani, K., Lokka, G., Georgomanolis, T., Kyrousi, C., Dong, W., Dunbar, A., Parlapani, E., Damianidou, E., Spassky, N., et al. (2019). GemC1 is a critical switch for neural stem cell generation in the postnatal brain. Glia *67*, 2360–2373.

De Lange, T. (2005). Shelterin: The protein complex that shapes and safeguards human telomeres. Genes Dev. *19*, 2100–2110.

Lim, D.A., and Alvarez-Buylla, A. (2016). The adult ventricular–subventricular zone (V-SVZ) and olfactory bulb (OB) neurogenesis. Cold Spring Harb. Perspect. Biol. *8*.

Loftus, K.M., Cui, H., Coutavas, E., King, D.S., Ceravolo, A., Pereiras, D., and Solmaz, S.R. (2017). Mechanism for G2 phase-specific nuclear export of the kinetochore protein CENP-F. Cell Cycle *16*, 1414–1429.

Longhese, M.P. (2008). DNA damage response at functional and dysfunctional telomeres. Genes Dev. *22*, 125–140.

Love, M.I., Huber, W., and Anders, S. (2014). Moderated estimation of fold change and dispersion for RNA-seq data with DESeq2. Genome Biol. *15*, 550.

Madisen, L., Zwingman, T.A., Sunkin, S.M., Oh, S.W., Zariwala, H.A., Gu, H., Ng, L.L., Palmiter, R.D., Hawrylycz, M.J., Jones, A.R., et al. (2010). A robust and high-throughput Cre reporting and characterization system for the whole mouse brain. Nat. Neurosci. *13*, 133–140.

Marion, R.M., and Blasco, M.A. (2010). Telomeres and telomerase in adult stem cells and pluripotent embryonic stem cells. Adv. Exp. Med. Biol. *695*, 118–131.

Marqués-Torrejón, M.Á., Porlan, E., Banito, A., Gómez-Ibarlucea, E., Lopez-Contreras, A.J., Fernández-Capetillo, Ó., Vidal, A., Gil, J., Torres, J., and Fariñas, I. (2013). Cyclin-dependent kinase inhibitor p21 controls adult neural stem cell expansion by regulating Sox2 gene expression. Cell Stem Cell *12*, 88–100.

Mazouzi, A., Velimezi, G., and Loizou, J.I. (2014). DNA replication stress: Causes, resolution and disease. Exp. Cell Res. *329*, 85–93.

McGarry, T.J., and Kirschner, M.W. (1998). Geminin, an inhibitor of DNA replication, is degraded during mitosis. Cell *93*, 1043–1053.

Ming, G. li, and Song, H. (2011). Adult Neurogenesis in the Mammalian Brain: Significant Answers and Significant Questions. Neuron *70*, 687–702.

Muthusamy, N., Vijayakumar, A., Cheng, G., and Ghashghaei, H.T. (2014). A Knock-in Foxj1CreERT2:: GFP mouse for recombination in epithelial cells with motile cilia. Genesis *52*.

Nikitin, A., Egorov, S., Daraselia, N., and Mazo, I. (2003). Pathway studio - The analysis and navigation of molecular networks. Bioinformatics *19*, 2155–2157.

Obernier, K., Cebrian-Silla, A., Thomson, M., Parraguez, J.I., Anderson, R., Guinto, C., Rodas Rodriguez, J., Garcia-Verdugo, J.M., and Alvarez-Buylla, A. (2018). Adult Neurogenesis Is Sustained by Symmetric Self-Renewal and Differentiation. Cell Stem Cell *22*, 221-234.e8.

Ortiz-Álvarez, G., Daclin, M., Shihavuddin, A., Lansade, P., Fortoul, A., Faucourt, M., Clavreul, S., Lalioti, M.E., Taraviras, S., Hippenmeyer, S., et al. (2019). Adult Neural Stem Cells and Multiciliated Ependymal Cells Share a Common Lineage Regulated by the Geminin Family Members. Neuron *102*, 159-172.e7.

Pack, L.R., Daigh, L.H., and Meyer, T. (2019). Putting the brakes on the cell cycle: mechanisms of cellular growth arrest. Curr. Opin. Cell Biol. *60*, 106–113.

Perera, O.N., Sobinoff, A.P., Teber, E.T., Harman, A., Maritz, M.F., Yang, S.F., Pickett, H.A., Cesare, A.J., Arthur, J.W., MacKenzie, K.L., et al. (2019). Telomerase promotes formation of a telomere protective complex in cancer cells. Sci. Adv. *5*, eaav4409.

Petrik, D., Myoga, M.H., Grade, S., Gerkau, N.J., Pusch, M., Rose, C.R., Grothe, B., and Götz, M. (2018).

Epithelial Sodium Channel Regulates Adult Neural Stem Cell Proliferation in a Flow-Dependent Manner. Cell Stem Cell *22*, 865-878.e8.

Pilz, G.A., Shitamukai, A., Reillo, I., Pacary, E., Schwausch, J., Stahl, R., Ninkovic, J., Snippert, H.J., Clevers, H., Godinho, L., et al. (2013). Amplification of progenitors in the mammalian telencephalon includes a new radial glial cell type. Nat. Commun. *4*, 1–11.

Porlan, E., Morante-Redolat, J.M., Marqués-Torrejón, M.Á., Andreu-Agulló, C., Carneiro, C., Gómez-Ibarlucea, E., Soto, A., Vidal, A., Ferrón, S.R., and Fariñas, I. (2013). Transcriptional repression of Bmp2 by p21 Waf1/Cip1 links quiescence to neural stem cell maintenance. Nat. Neurosci. *16*, 1567–1575.

Redmond, S.A., Figueres-Oñate, M., Obernier, K., Nascimento, M.A., Parraguez, J.I., López-Mascaraque, L., Fuentealba, L.C., and Alvarez-Buylla, A. (2019). Development of Ependymal and Postnatal Neural Stem Cells and Their Origin from a Common Embryonic Progenitor. Cell Rep. *27*, 429-441.e3.

Roake, C.M., and Artandi, S.E. (2017). Control of cellular aging, tissue function, and cancer by p53 downstream of telomeres. Cold Spring Harb. Perspect. Med. *7*.

Saito, T., and Nakatsuji, N. (2001). Efficient gene transfer into the embryonic mouse brain using in vivo electroporation. Dev. Biol. *240*, 237–246.

Saldivar, J.C., Hamperl, S., Bocek, M.J., Chung, M., Bass, T.E., Cisneros-Soberanis, F., Samejima, K., Xie, L., Paulson, J.R., Earnshaw, W.C., et al. (2018). An intrinsic S/G2 checkpoint enforced by ATR. Science (80-.). *361*, 806–810.

Sawamoto, K., Wichterle, H., Gonzalez-Perez, O., Cholfin, J.A., Yamada, M., Spassky, N., Murcia, N.S., Garcia-Verdugo, J.M., Marin, O., Rubenstein, J.L.R., et al. (2006). New neurons follow the flow of cerebrospinal fluid in the adult brain. Science (80-.). *311*, 629–632.

Schindelin, J., Arganda-Carreras, I., Frise, E., Kaynig, V., Longair, M., Pietzsch, T., Preibisch, S., Rueden, C., Saalfeld, S., Schmid, B., et al. (2012). Fiji: an open-source platform for biological-image analysis. Nat. Methods *9*, 676–682.

Silva-Vargas, V., Maldonado-Soto, A.R., Mizrak, D., Codega, P., and Doetsch, F. (2016). Age-Dependent Niche Signals from the Choroid Plexus Regulate Adult Neural Stem Cells. Cell Stem Cell *19*, 643–652.

Siyahhan, B., Knobloch, V., De Zélicourt, D., Asgari, M., Daners, M.S., Poulikakos, D., and Kurtcuoglu, V. (2014). Flow induced by ependymal cilia dominates near-wall cerebrospinal fluid dynamics in the lateral ventricles. J. R. Soc. Interface *11*.

Solovei, I., Kreysing, M., Lanctôt, C., Kösem, S., Peichl, L., Cremer, T., Guck, J., and Joffe, B. (2009). Nuclear Architecture of Rod Photoreceptor Cells Adapts to Vision in Mammalian Evolution. Cell *137*, 356–368.

Soudet, J., Jolivet, P., and Teixeira, M.T. (2014). Elucidation of the DNA end-replication problem in saccharomyces cerevisiae. Mol. Cell *53*, 954–964.

Spassky, N., Merkle, F.T., Flames, N., Tramontin, A.D., García-Verdugo, J.M., and Alvarez-Buylla, A. (2005). Adult ependymal cells are postmitotic and are derived from radial glial cells during embryogenesis. J. Neurosci. *25*, 10–18.

Subramanian, A., Tamayo, P., Mootha, V.K., Mukherjee, S., Ebert, B.L., Gillette, M.A., Paulovich, A., Pomeroy, S.L., Golub, T.R., Lander, E.S., et al. (2005). Gene set enrichment analysis: A knowledge-based approach for interpreting genome-wide expression profiles. Proc. Natl. Acad. Sci. U. S. A. *102*, 15545–15550.

Tachibana, K.K., Gonzalez, M.A., Guarguaglini, G., Nigg, E.A., and Laskey, R.A. (2005). Depletion of

licensing inhibitor geminin causes centrosome overduplication and mitotic defects. EMBO Rep. *6*, 1052–1057.

Takai, H., Smogorzewska, A., and De Lange, T. (2003). DNA damage foci at dysfunctional telomeres. Curr. Biol. *13*, 1549–1556.

Terré, B., Piergiovanni, G., Segura-Bayona, S., Gil-Gómez, G., Youssef, S.A., Attolini, C.S., Wilsch-Bräuninger, M., Jung, C., Rojas, A.M., Marjanović, M., et al. (2016). GEMC 1 is a critical regulator of multiciliated cell differentiation . EMBO J. *35*, 942–960.

Terré, B., Lewis, M., Gil-Gómez, G., Han, Z., Lu, H., Aguilera, M., Prats, N., Roy, S., Zhao, H., and Stracker, T.H. (2019). Defects in efferent duct multiciliogenesis underlie male infertility in GEMC1-, MCIDAS- or CCNO-deficient mice. Dev. *146*.

Urist, M., Tanaka, T., Poyurovsky, M. V., and Prives, C. (2004). p73 induction after DNA damage is regulated by checkpoint kinases Chk1 and Chk2. Genes Dev. *18*, 3041–3054.

Vladar, E.K., Stratton, M.B., Saal, M.L., Salazar-De Simone, G., Wang, X., Wolgemuth, D., Stearns, T., and Axelrod, J.D. (2018). Cyclin-dependent kinase control of motile ciliogenesis. Elife *7*.

Wellinger, R.J. (2014). In the end, what's the problem? Mol. Cell *53*, 855–856.

Wohlschlegel, J.A., Dwyer, B.T., Dhar, S.K., Cvetic, C., Walter, J.C., and Dutta, A. (2000). Inhibition of eukaryotic DNA replication by geminin binding to Cdt1. Science (80-.). *290*, 2309–2312.

Yoon, M.K., Ha, J.H., Lee, M.S., and Chi, S.W. (2015). Structure and apoptotic function of p73. BMB Rep. *48*, 81–90.

Zeman, M.K., and Cimprich, K.A. (2014). Causes and consequences of replication stress. Nat. Cell Biol. *16*, 2–9.

Zimmermann, S., and Martens, U.M. (2008). Telomeres, senescence, and hematopoietic stem cells. Cell Tissue Res. *331*, 79–90.

CHAPTER 4. CONCLUDING REMARKS AND PERSPECTIVES

This doctoral dissertation has for aim the elucidation of the cellular and molecular mechanisms that lead to glial specification and the generation of the mouse neurogenic niche. There are two neurogenic areas in the adult mammalian brain, from which adult neurons are born throughout life: the subgranular zone of the dentate gyrus of the hippocampus and the SVZ that surrounds the lateral ventricles, mainly on the lateral wall (Mirzadeh et al., 2008; Obernier and Alvarez-Buylla, 2019). Our work has been focused on the latter.

Firstly, we have characterized the lineage of multiciliated ependymal cells and adult neural stem cells, or B1 cells, both essential and majority components of said niche. We have used state-of-the art clonal analysis techniques to perform, on the one hand, a high throughput scrutiny of hundreds of clones composed of ependymal and/or B1 cells, using the *Brainbow* technique (Loulier et al., 2014). On the other hand, we have profited from the single-cell resolution power of MADM transgenic animals (Gao et al., 2014) to discern the type of cell division that generates specific clone compositions. Both techniques complement each other and have allowed us to establish that multiciliated ependymal cells and B1 cells share a common lineage. Furthermore, we have proven that proteins from the Geminin family, namely Geminin and GemC1, which bear an important function in DNA replication firing (Balestrini et al., 2010; Wohlschlegel et al., 2000), can tune the fate of RGCs in the embryo. Whereas Geminin favors B1-generating symmetric divisions, GemC1 triggers the production of ependymal cells, also via symmetric divisions. Both cell types can also emerge via a single asymmetric division, thus demonstrating that these two very different cells from the neurogenic niche are indeed sisters.

In the search of the specific mechanisms via which GemC1 induces an ependymal fate, the second part of our work has explored a not very common area in developmental biology: replicative stress and telomere dynamics. Two phenomena usually assessed in malignant transformation and progression (Halazonetis et al., 2008), we have managed to establish a link between them and ependymal differentiation. We have some results suggesting that the separation between cell cycle progression and terminal differentiation is not black and white, but rather a grey area, where some factors that regulate cell cycle progression, and also cell

cycle arrest, are recruited during centriole amplification. Besides, replicative stress, a trait of cycling cells, is indeed present in ependymal differentiation. Ependymal-committed progenitors in the perinatal neuroepithelium display a series of phenotypes that permit us to establish a link between differentiation and senescence, something that is related to ageing tissues, but not embryonic or early postnatal ones. More specifically, replicative senescence-like phenotypes were observed, including the presence of DNA damage signals on telomeres. Since we verified the presence of these dysfunctional chromosome termini, we checked whether telomerase could have an impact on the cell fate specification of the neurogenic niche. In fact, it could both partially rescue the GemC1-dependent ependymal differentiation and promote the generation of B1 astrocytes.

In the next few pages, I will discuss the results obtained during this thesis, and the new insights that we have gained over ependymal differentiation.

4.1. The spatial origin of ependymal cells

The first step before performing a clonal analysis of neurogenic niche cells was to determine the spatial origin of ependymal cells, this is, to answer the question whether ependymal progenitors migrate or if, by the contrary, they remain and differentiate on their site of birth. This was crucial since cell migration would greatly complicate clonal analysis. During the generation of cortical neurons in embryogenesis, extensive radial and tangential migration of neuroblasts is indeed the source of the two most common errors in clonal analysis: the lumping and splitting errors. The former consists of considering one or more cells of a clone as part of another one. The latter entails that one clone that has normally widely spread, is thought as two independent ones (Costa et al., 2009).

We used the Cre-lox fate mapping technique to perform our study. We profited from the spatial compartmentalization of the embryonic neuroepithelium, in terms of the transcription factors they express (Fogarty et al., 2007). The Emx1-Cre (Gorski et al., 2002), Gsh2-Cre (Kessaris et al., 2006) and Nkx2.1-Cre transgenic lines (Xu et al., 2008), which label progenitors of specific areas of the neuroepithelium, have helped us determine that ependymal progenitors do not migrate. The almost absent contribution of ependymal cell populations issued from a specific area to other distant zones in the adult reassured us in this fact (Article 1 – Figure 1). Other data obtained supported this hypothesis, like the fact that

ependymal cells born at a certain time point (seen via EdU birth-dating) usually appeared in closer than random cells (Article 1 – Figure S1).

This permitted us to continue with the clonal analysis without a migration bias. If ependymal migration was the rule, we would have had to envisage other methods of clonal analysis. For instance, labeling of progenitors with low titer retroviruses that would have tagged single progenitors (Ma et al., 2018) or tagging them with retroviral libraries that bear unique identifiers, afterwards revealed via sequencing methods (McCarthy et al., 2001; Walsh and Cepko, 1992). The latter has been already used to establish clonal relationships between B1 cells born during late gestation and their adult descendants, olfactory bulb interneurons (Fuentealba et al., 2015).

Virtually all newborn neurons must migrate to achieve their final destination, which is intrinsically related to its function (Rakic, 2003). However, no specific cellular or molecular particularities have been attributed to distinct ependymal populations throughout the lateral wall. An absence of migration could support this notion: without functional specificities related to ependymal position, an energy-expensive process such as cell migration is not needed. If regional differences exist, these could probably be derived from the positional information of their origin. Thus, ependymal migration would still be unnecessary.

4.2. The lineage of ependymal and B1 cells

Once we ruled out migration, we set out to determine the clonality of neurogenic niche glial cells generated in late gestation and the mode of division of their progenitors. We used the IUE technique (Tabata and Nakajima, 2001) to label RGCs around the time before the last division of most ependymal progenitors, E14.5 (Spassky et al., 2005). We targeted progenitors of both ependymal and B1 cells (Article 1 – Figure 2) and labeled them with almost unique color identifiers using the *Brainbow* technique (Livet et al., 2007; Loulier et al., 2014). We observed that ependymal cells were born via symmetric and asymmetric divisions, in a 1:1 ratio. We confirmed via another clonal analysis technique, MADM (Gao et al., 2014; Zong et al., 2005), the results obtained with *Brainbow* and proved that a single progenitor cell could give birth via one asymmetric cell division to an ependymal cell and a B1 astrocyte (Article 1 – Figure 3-4). This is a highly interesting fact, given that they are very different cell types. The first one is a terminally differentiated postmitotic cell (Spassky et al., 2005). The second one

is an adult stem cell that remains largely quiescent throughout life (Fuentealba et al., 2015; Morizur et al., 2018), which can, however, re-enter the cell cycle in physiological conditions to generate new neurons (Kriegstein and Alvarez-Buylla, 2009).

The IUE of MADM animals at E13 and E14 revealed another fascinating fact: clones born at E13 presented more B1 cells, more mixed (ependymal and B1) clones and higher frequency of B1-generating symmetric divisions, than clones born at E14. This suggests that the bulk of B1 cells is born slightly before the bulk of ependymal cells (Article 1 – Figure 4) and hints at the existence of a hierarchy in the generation of glia. Another hierarchy that seems well established now during the development of the CNS, is that of neurons being born before glia. They are born from bipotent progenitors, rather than neuron-restricted and glial-restricted stem cells (Costa et al., 2009; Rash et al., 2019). Of course, this depends on how restrictive we make the concept of "bipotent progenitor". If by it, we mean a single cell that can generate a neuron and a glial daughter cell in one cell division, bipotent RGCs have not been described in the telencephalon. Interestingly, this has been observed in the rat retina, both *in vitro* and *in vivo*, where a single terminal division can generate a specialized type of photoreceptor neuron or retina interneuron and a glial cell (Müller cell) (Gomes et al., 2011; Turner and Cepko, 1988). However, if by "bipotent progenitor" we mean a stem cell that produces neuroblasts and self-renews and that, at some point, it stops generating neuroblasts to give birth to only glia, RGCs seem indeed bipotent (Gao et al., 2014).

Concerning our results and in the first sense of the concept, we cannot rule out the possibility that an ependymal cell and a neuron could arise from a single progenitor division. The fact that neurogenesis is out of the scope of this work and mostly, that our tissue preparations are wholemounts of the V-SVZ, thus discarding the cortex, leaves this question open. Nonetheless, the fact that a single RGC could generate an ependymal cell and a neuron seems unlikely. It has been ascertained *in vivo* and *in vitro* that clones generated from late embryonic neuroepithelium are glial-restricted, suggesting that after a long enough delay (mid-late gestation), virtually no RGC will yield a neuron and glial cell (Anthony et al., 2004; Costa et al., 2009; Gao et al., 2014; Malatesta et al., 2000). However, a single-cell resolution study of the very last division of RGCs, like the one we have performed, to study the potential clonal relationship between neurogenesis and gliogenesis is missing. Our own analysis reveals that a non-negligible proportion of between 6 and 9% of MADM "clones" are formed by only

one cell (Article 1 – Table S1). This could mean that, on this few occasions, the missing sister cell of the observed ependymal or B1 cell could have undergone apoptosis or left the V-SVZ, becoming a cortical neuron, parenchymal astrocyte or oligodendrocyte.

Some experiments that could be undertaken to answer this question would be to use low-dose tamoxifen-dependent Cre induction in NestinCre^{ERT2}/MADM animals (instead of Cre IUE like in our study), like Gao *et al*., to achieve sparse clone labeling. If this is done at later gestation periods (E14-E15) than what they performed (E10-E13), so that ependymal cells are labeled after the last division of their progenitors, we could observe some two-cell clones, with an ependymal and a cortical cell, if these actually exist. Other clonal analysis techniques, like low-titer retroviral labeling could be useful in this case. The fact that ependymal progenitors do not migrate and that pallial cortical neurons are generated in columnar structures (Magavi et al., 2012) could allow us to confirm or rule out the presence of ependymal/cortical neuron duos, if they happen at all in development. Another possible solution would have been *ex vivo* filming of progenitor divisions and differentiation. However, we have tried to observe ependymal differentiation in these conditions and, for unknown reasons, we failed to find centriole amplification.

4.3. The cellular and molecular mechanisms governing neurogenic niche cell fate

4.3.1. The Geminin family members

IUE is an optimal technique for gene functional studies by delivering DNA molecules that cause a gain or loss of function of these genes (Dixit et al., 2011; Matsui et al., 2011). We thus used said technique to study the role of the Geminin family in the ependymal/B1 lineage. In the MADM transgenic animals we over-expressed Geminin or GemC1 at E13 or E14 and observed that the former favors B1-forming symmetric divisions and the later produces more ependymal-generating symmetric divisions and a final higher output of ependymal cells (Article 1 – Figures 5-6, S7). The mechanisms by which they might do so are discussed in the second part of the this section (corresponding to the second publication).

During the process of revision, we were asked to perform loss-of-function experiments of the same Geminin family members tested: Geminin and GemC1. We electroporated shRNA against Geminin (Origene TR510014A) and GemC1 (Origene TR507275A and TR507275B) at E14.5 in MADM transgenic animals. We observed no significant differences between any of

the tested conditions against a control situation, in clone composition or total cell type output (Figure 27).

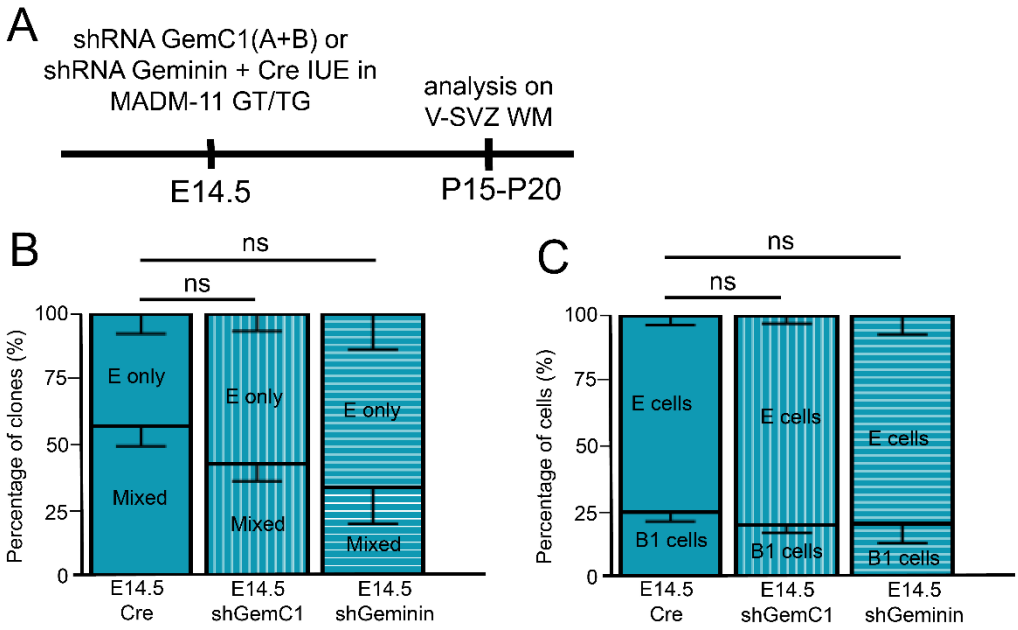

Figure 27. Loss-of-function experiments of Geminin and GemC1 in the neurogenic niche clone composition. (A) We used IUE in MADM animals to knock-down the expression of Geminin and GemC1. ShRNA plasmids for one or the other gene were co-electroporated with the Cre recombinase at E14.5. V-SVZ wholemounts were analyzed between P10 and P15. (B-C) Quantification of the average percentage of clone types, either pure ependymal (E only) or ependymal and B1-containing clones (Mixed) (B), and final percentage of E or B1 electroporated cells in the neurogenic niche (C). Error bars indicate the SEM. P-values were calculated via a two-proportion Z-test; ns $p>0.05$.

Shortly after our work on *Neuron* was published, Lalioti *et al*. confirmed that full GemC1 deletion ($GemC1^{KO/KO}$) and single-cell removal of this gene in RGCs, via *in utero* Cre recombinase electroporation in $GemC1^{Floxed/KO}$ mice resulted in an increase of BLBP+ cells, an adult neural stem cell marker. Proliferation markers such as Ki-67 and cells positive for early neuroblast specification were also up-regulated in the absence of GemC1. They thus concluded that GemC1 acted as a switch of RGC fate and that its absence could favor the B1 fate in detriment of the multiciliated ependymal one (Lalioti et al., 2019a). This was a complimentary approach to the one we followed. In our case, we proved that GemC1 was not expressed at the moment of the electroporation via *in situ* hybridization (Article I – Published work *Neuron*, 2019, Figure S6). Hence, it was likely that GemC1 shRNA was no longer present at the moment that endogenous GemC1 was expressed (we suppose perinatally, around the time of onset of ependymal differentiation) and thus the effect of GemC1 loss could not be observed.

It would be interesting to know whether the lack of GemC1 would increase the number of B1-generating symmetric divisions (like the over-expression of its antagonist, Geminin) or it would just promote direct transformation of RGCs into B1 cells. These two possibilities cannot be discerned in the study of Lalioti *et al*., since it did not entail a lineage analysis like ours. Electroporation of the *Nucbow* plasmids and the Cre recombinase in a GemC1 $^{KO/Floxed}$ mouse line from the study just mentioned could answer the question whether loss of GemC1 in RGCs leads to a higher frequency of B1 pure clones, generated through symmetric divisions.

As for Geminin inhibition in the telencephalon, it has been reported to cause an increase of RGC proliferation and defects in cortical layering (Spella et al., 2011). It would be of great interest to analyze the lineage of Geminin KO cells in clones in the way just described, in order to see if it has the same effect as GemC1 over-expression (induction of ependymal-generating symmetric divisions).

4.3.2. A potential role of Notch and cell cycle length in neurogenic niche progenitor division patterns

Prospective studies into the generation balance of ependymal and B1 cells and the mode of their progenitors' divisions could have, in my opinion, a focus on two very interesting aspects: the role of Notch and the regulation of cell cycle length.

Notch signaling can influence features as dissimilar as cell fate, proliferation and morphology. A highly interesting fact is that it can determinate different cell fates in adjacent cells that end up adopting different morphologies via a cell-cell crosstalk-signaling pathway, where one cell is the ligand expressing and the other, the Notch receptor-expressing one (Chitnis and Bally-Cuif, 2016). This is highly reminiscent of the neuroepithelium, where some cells acquire a B1 cell identity, and others become ependymal cells.

Precisely in this tissue, Notch activity has an important role in the quiescence/division balance of adult NSCs in vertebrates, from zebrafish to mice. In the adult mammalian SVZ neurogenic niche, most neural progenitors are in a quiescent state (Fuentealba et al., 2015). However, Notch inhibition causes massive NSC division and neurogenesis in zebrafish (Alunni et al., 2013; Chapouton et al., 2010) and mice (Kawai et al., 2017; Rieskamp et al., 2018), whereas its induction promotes quiescence maintenance. Curiously, a different notch receptor (notch 1) is also involved in the maintenance of activated, not quiescent, adult NSCs

in mice (Kawai et al., 2017) and Notch inhibition in zebrafish has been shown to promote the aforementioned NSC activation, and it does so via proliferative symmetric divisions (Alunni et al., 2013). This hence suggests that Notch suppression can regulate the mode of division in the neuroepithelium.

Notch displays an essential role in multiciliated epithelia. It inhibits the multiciliation program, as it has been shown in the airway epithelium, *Xenopus* embryonic epidermis and zebrafish pronephros (Liu et al., 2007; Marcet et al., 2011). In the mouse neuroepithelium it has been seen that it actually impedes the role of GemC1 to promote motile ciliogenesis (Kyrousi et al., 2015). It is plausible then that adjacent RGCs express Notch ligand and receptor, respectively, to establish the two main different fates that compose the neurogenic niche, the B1 and the ependymal cell, in a single division. MADM could be an interesting tool to observe the cell division patterns after inhibition or ectopic expression of Notch.

If Notch indeed regulated the mode of division of neurogenic niche cell-committed RGCs, it could be used to answer a difficult question in the specification of these cells: precisely when does this specification occur. The truth is that we do not know what happens between the last division of ependymal-committed RGC and the onset of differentiation. Several days pass between the former (E14.5-E15.5) and the latter (E18.5-P0). If MADM animals were electroporated with the Cre recombinase at the time of the last division (E14.5-E15.5), we could subsequently administer the Notch inhibitor DAPT by oral gavage (Dees et al., 2011), at different time points, between the moment of electroporation and the onset of differentiation. If DAPT had an effect after electroporation, it would suggest that specification takes place right after the last division. It DAPT had an influence, but only later, it would be indicative of a later specification.

Another possible mechanism that influences the mode of division is the cell cycle length. The “cell cycle length” hypothesis establishes that the length of the cell cycle, particularly of the G1 phase, is determinant for differentiation. This fascinating hypothesis states that a prolonged G1 would allow the accumulation of factors that will drive differentiation. Indeed, during mouse corticogenesis, there is a correlation between differentiative neurogenic divisions and cell cycle deceleration due to G1 lengthening. On the other end, a short G1 is associated with proliferative divisions (Dehay and Kennedy, 2007; Hardwick et al., 2015). A cause-consequence relation has been proven when cyclinD1-CDK4/6

was over-expressed or knocked-down via IUE. The former decreased cell cycle length via G1 shortening and maintained basal progenitors in a cycling state, via promotion of self-renewing of proliferative divisions (Pilaz et al., 2009) and inhibited neurogenesis (Lange et al., 2009). The latter had the opposite effect (Lange et al., 2009).

Ependymal cells seem to be the endpoint of RGC proliferation. After our study, we believe that when RGCs extenuate their proliferative potential, they perform one last symmetrical division to generate two ependymal cells. It would be highly interesting to know whether a similar shortening of the cell cycle as the one induced in Lange *et al.* could affect the final output of neurogenic niche cells or alter the mode of division of gliogenic progenitors. This could easily be tested in MADM embryos via over-expression of cell cycle actors, like the ones just mentioned.

Maybe an excessive cell cycle lengthening is at the source of the final symmetric ependymal division. The accumulation of differentiation and/or damage signals could be determinant for this fate acquisition. The presence of cell cycle progression and cell cycle arrest markers in ependymal differentiation, as it is seen on the second part of this work (see below), certainly points this as a hypothesis to be worthy of exploration.

4.3.3. The role of GemC1 in DNA replication and multiciliated program activation

It has been explained before that GemC1, a gene that is necessary and sufficient for MCC differentiation (Arbi et al., 2016; Kyrousi et al., 2015; Terré et al., 2016) plays also an important role in DNA replication firing, as part of the pre-RC (Balestrini et al., 2010). We thought that maybe both GemC1 functions are connected during ependymal differentiation. That is why we tested the role of GemC1 in two very different contexts, in terms of DNA replication: the embryonic and the postnatal neuroepithelium. Whereas during late gestation (E14-E15), the VZ displays extensive cell cycle activity (Article 1 – Figure S2, Article 2 – Figure 1B), the postnatal SVZ is characterized by the presence of a majority of quiescent NSCs, that had endured a progressive slow down of their cycle (Fuentealba et al., 2015; Furutachi et al., 2015; Morales and Mira, 2019). We imagined that cell cycle activity would be much scanter right after cortical neurogenesis is complete (E18-P0) and so we electroporated GemC1 at these two different time points: embryonic (E14.5) and postnatal (P0) and pulse-chased the

electroporated cells with EdU. We found that the number of cells that has undergone S phase after GemC1 electroporation was much higher in the embryonic tissue and, to our surprise, these translated into a massive ependymal differentiation *in utero* and barely present in the postnatal VZ (Article 2 – Figure 1).

These results, which prove that GemC1 promotes centriole amplification in cycling cells, suggest there is indeed a connection between both its roles. However, conclusive proof of the need of GemC1 in the pre-RC for triggering ependymal differentiation is missing. GemC1 loads onto chromatin at origins of replication, but it needs to interact with TopBP1 and to be phosphorylated by Cyclin E-Cdk2 (Balestrini et al., 2010). Roscovitine is a small molecule that inhibits the activity of several CDKs (Cicenas et al., 2015), including CDK2, which promotes G1/S transition and S progression in complex with cyclins E and A, and CDK1 (Henley and Dick, 2012; Poon, 2016). It has been shown in a model of tracheal multiciliated mouse cells *in vitro* that roscovitine-dependent CDK2 inhibition hampers multiciliogenesis (Vladar et al., 2018). We have been able to reproduce such results in our ependymal *in vitro* model, where roscovitine treatment rescued a non-multiciliated phenotype in GemC1-transfected cells (Figure 28).

Nonetheless, Vladar *et al.* maintain that it is CDK2 in complex formation with cyclin A1, and not cyclin E, the one that participates in GemC1 phosphorylation during replication firing according to Balestrini *et al*., that drives motile ciliogenesis. Thus, to conclusively state that the role of GemC1 in DNA replication firing is necessary for its function in multiciliation, we would need to prove that in our culture system, GemC1 is inducing differentiation in cycling cells, like it does *in vivo*. Alternatively, we could treat pregnant mothers with rosocovitine after electroporation with GemC1, via intravenous injection, as it has already been reported (Menn et al., 2010; Nutley et al., 2005).

Other ways to inhibit the loading of GemC1 to the pre-RC or the DNA replication firing altogether could also be tested to prove the link between the two GemC1 functions. Calcein has been shown to inhibit TopBP1 oligomerization and inhibit E2F1-dependent apoptosis and its interaction with mutant p53 in cancer cells (Chowdhury et al., 2014), but nothing was said about its role in the pre-RC. However, there is one study showing that calcein can inhibit formation of a papillomavirus replication complex at its replication origins (Das et al., 2017). This makes calcein an interesting candidate to prove our hypothesis.

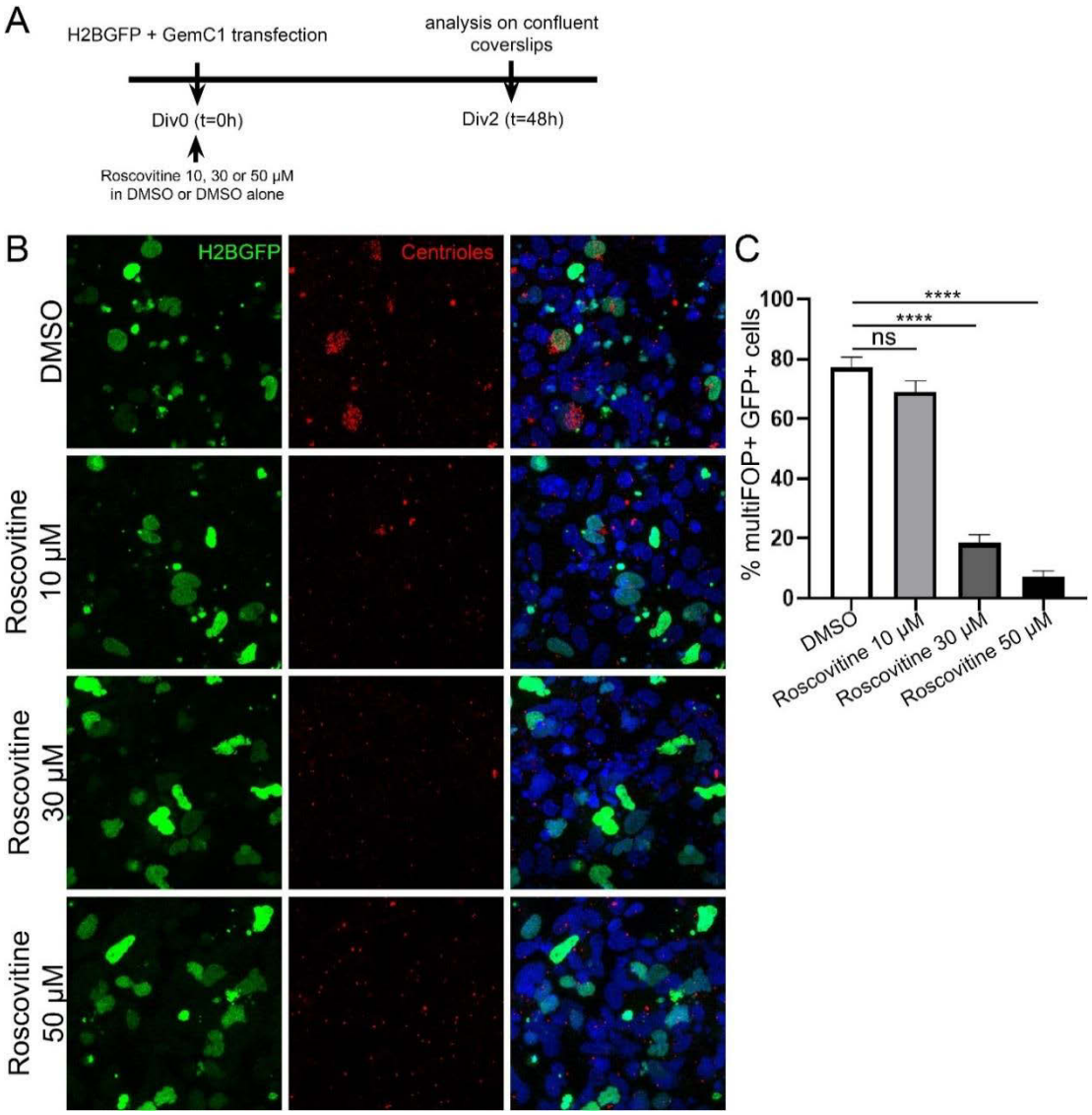

Figure 28. Roscovitine inhibits ependymal differentiation in GemC1-expressing cells. (A) Experimental plan depicting day 0 of highly confluent ependymal culture set-up (see Materials and Methods). Neural progenitor cells grown for 5 days from newborn mice primary cultures were seeded at high confluency to induce differentiation. Besides, these cells were transfected with H2B-GFP and GemC1-expressing plasmids to enhance centriole amplification in transfected cells. At the time of transfection, cells were treated with roscovitine at 10, 30 or 50 µM in DMSO, or its volume equivalent of DMSO as controls. (B) Representative images of the differentiation status (centrioles, in red) of GemC1-transfected cells (green) in culture, treated with either DMSO (controls) or roscovitine. (C) Quantification of the mean percentage of differentiation (multiFOP+) within transfected cells (GFP+). The error bars depict the SEM for at least three independent culture settings. P-values were assessed with a Mann-Whitney test with ns (not significant) $p > 0.5$ and **** $p < 0.0001$.

4.3.4. GemC1 generates replicative stress at the onset of ependymal differentiation

Given that GemC1 induced centriole amplification in cycling cells and that it has a role in DNA replication firing, we studied S phase entry in ependymal progenitors. The rapid and extensive GemC1-induced differentiation did not trigger a rapid cell cycle exit with a decreased number of Edu+ cells in the embryo, as one would expect from differentiation initiation, but rather cells continued to undergo S phase like the highly cycling control cells (Article 2 – Figure 2E-F). We found that GemC1 caused a significant increase of γ-H2AX in cells *in vivo* (Article 2 – Figure 2G-I). Moreover, the occurrence of γ-H2AX+ cells is higher in GemC1+ cells that have undergone S phase (Edu+), than in those that have not. We even observed that γ-H2AX foci often co-localized with Edu+ areas in the cell nucleus, when Edu+ cells did not present an uniform nuclear labeling (Article 2 – Figure 2J). All this indicates that GemC1 produces a replicative stress in differentiating ependymal progenitors.

In order to make sure this DDR is not an artefact of the over-expression of GemC1, we looked for signs of stress in normal differentiating conditions. We indeed found mTomato+ cells in the FoxJ1CreER^{T2} ; R26mTomato embryos that presented signs of replicative stress (γ-H2AX foci) (Article 2 – Figure 2I). Furthermore, we quantified the levels of γ-H2AX in differentiating postnatal V-SVZ wholemounts and confirmed a significant increase in γ-H2AX labeling intensity, concomitant with differentiation (Figure 29). This is somehow reminiscent of recent findings that describe the presence of an S/G2 checkpoint dependent on ATR. As a consequence of this checkpoint, γ-H2AX is present during S and the S/G2 transition in unchallenged cells *in vitro* (Saldivar et al., 2018).

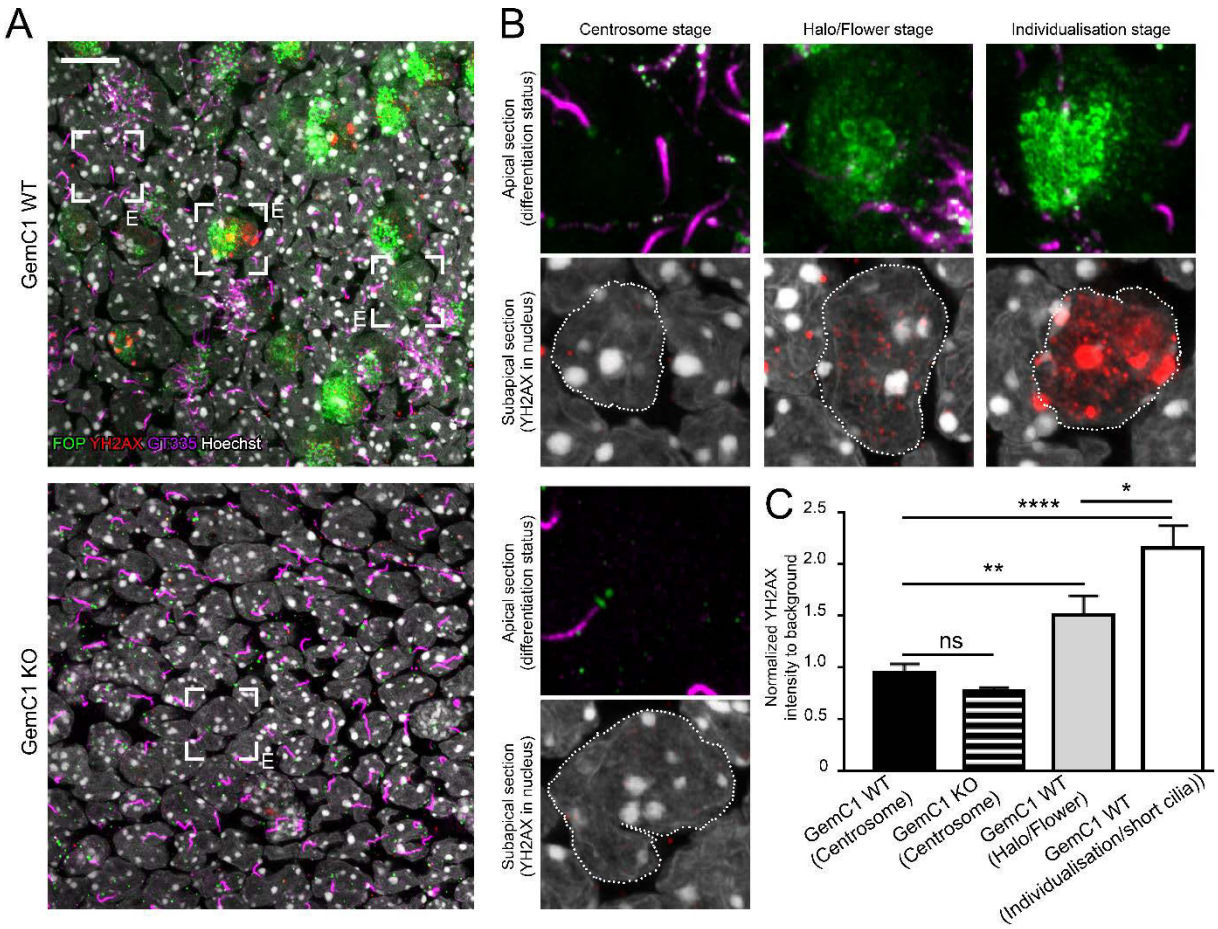

Figure 29. The DNA damage pathway is active in wild type ependymal-differentiating cells. (A-B) Illustrative pictures of P1-P4 V-SVZ wholemounts and zoom-in images (B), during the time of ependymal differentiation in GemC1 WT and GemC1 KO animals. Wholemounts were immunostained with the following antibodies: FOP (procentrioles and centrioels) in green, YH2AX in red and GT335 (cilia) in magenta. Wholemounts were counter-stained with Hoechst (grey) to calculate the YH2AX intensity within nuclei. For the WT condition, examples of cells in the centrosome (two apical centrioles and a cilium), flower (with rings of centrin) and individualization stages (multiple centrioles ready to dock cilia) are illustrated. For the GemC1 KO, only the centrosome stage is present. Cells are shown on its apical (with cilia and centrioles) and subapical planes (with nuclei and YH2AX). (C) Quantification of the mean nuclear YH2AX intensity, normalized to an image background. The error bars show the SEM for n = 3 animals in controls and n = 2 animals in KO. P-values were determined using a Mann-Whitney test; ns (not significant) $p > 0.5$, * $p \leq 0.05$, ** $p \leq 0.01$ and *** $p \leq 0.001$.The scale bar is 10 µm in (A) and 3 µm in (B).

The over-expression of other components of the pre-RC, such as Cdt1, Cdc6 has been associated with re-replication and early-stage cancer lesions (Gaillard et al., 2015). Cdc45, whose loading onto the chromatin at origins of replication is dependent on GemC1 in *Xenopus* egg (Balestrini et al., 2010), causes replicative stress in HeLa cells when over-expressed. It induces disproportionate firing of replication origins and increased replication fork stalling (Köhler et al., 2016). Indeed, potent oncogenes like Myc have been reported to cause early origin of replication firing, which leads to the up-regulation of DDR markers (γ-H2AX, phosphorylated ATM) in mammalian cells, in a Cdc45-dependent manner. These are hallmarks

of genomic instability, which can result in malignant transformation (Srinivasan et al., 2013). It is possible that GemC1 acts, in a certain way, like an oncogene, when it starts to be expressed in the perinatal neuroepithelium. A rise in its expression could generate untimely replication origin firing, which could cause the replicative stress that we have seen in our model.

4.3.5. Ependymal progenitors display dysfunctional telomeres while terminally differentiated ependymal cells have clustered telomeres

Telomeres display DDR markers when they are excessively short or deprotected (Gomez et al., 2012; Takai et al., 2003). What seems increasingly clear is that telomeres, which occupy a minimal fraction of the genome, are favored targets of a random DDR over other genome regions, in ageing tissues where senescence is induced, but also due to other insults, such as oxidative stress (Hewitt et al., 2012). We confirmed the presence of a higher amount of TIFs in GemC1-expressing cells than control cells, as well as a greater percentage of cells with three or more TIFs (Article 2 – Figure 2 K-M).

However, we do not know what is the ultimate cause that generates telomeric damage. We checked for telomere shortening, using manual counting of detectable telomeric foci and semi-automatic quantitative FISH (Q-FISH) analysis per nucleus, which measures the intensity of FISH-detected telomeric sequence (Sharifi-Sanjani et al., 2017). Telomeric signals were detected using an automatic plug-in that identified all pixels (in the telomere FISH channel) in a 3D Z-stack with a certain intensity value above a given threshold (Figure 30A-B). This plug-in used the 3D watershed algorithm implemented in ImageJ and returned, for each detected object (telomere focus) values like its volume, integrated density, mean intensity, and others (Figure 30C). Since the analyzed cell types were located in the same image, this eliminated any possible bias due to image acquisition.

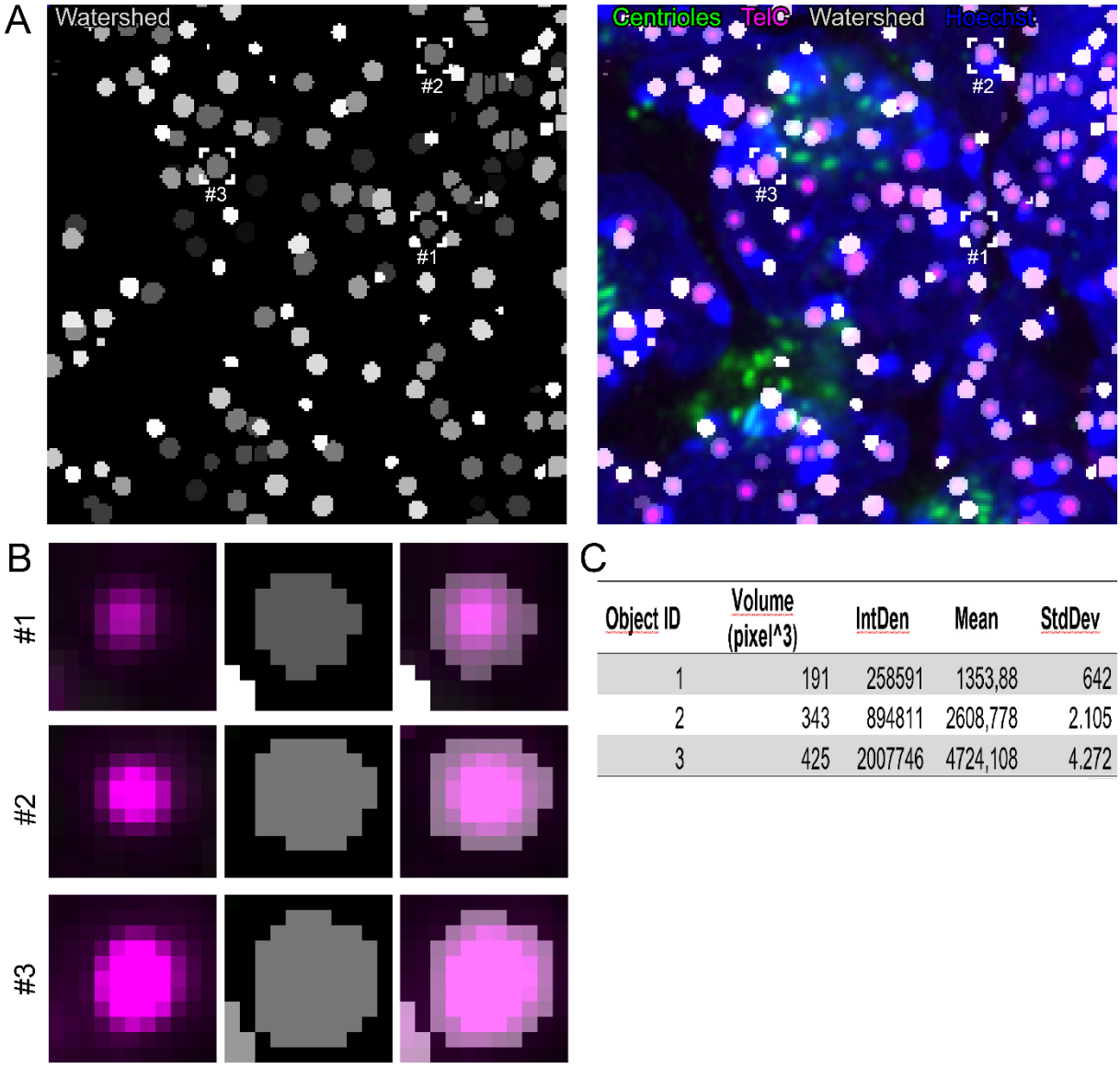

Object ID	Volume (pixel^3)	IntDen	Mean	StdDev
1	191	258591	1353,88	642
2	343	894811	2608,778	2.105
3	425	2007746	4724,108	4.272

Figure 30. Telomere detection and quantitative FISH. (A) Illustrative example of a neurogenic niche area, stained with telomere FISH (magenta) in a Cen2-GFP mouse (transgenic line where Centrin 2, a protein component of the centrioles, is fused to GFP, Higginbotham et al., 2004, seen in green). The used automatic plug-in (see Materials and Methods) detects telomeric foci as individual objects and creates for each of them a mask, in a new channel (Watershed, in grey). It then measures their volume (pixel^3) and fluorescence intensity within the mask. The different grey values of the watershed channel serve as object identifiers (each object/telomere has a distinct grey tonality). It is unrelated to the telomere foci's size or intensity. (B) 2D projections of three examples of three telomeric foci, from smaller and less intense (up) to bigger and more intense (down), labeled as #1, 2 and 3. (C) Calculated values of volume, integrated density, mean intensity and standard deviation using all the pixels from the telomere FISH channel, detected within the mask (watershed).

We observed that overall telomere content per cell was not different in ependymal cells from other non-ependymal SVZ cells (mostly B1 and lineage-related C and A cells). However, we did observe a decrease in total telomere signal per cell in mitotic cells, probably due to the fact that these were the ones that had undergone more cell cycles from all the analyzed cells (Figure 31A-D, F).

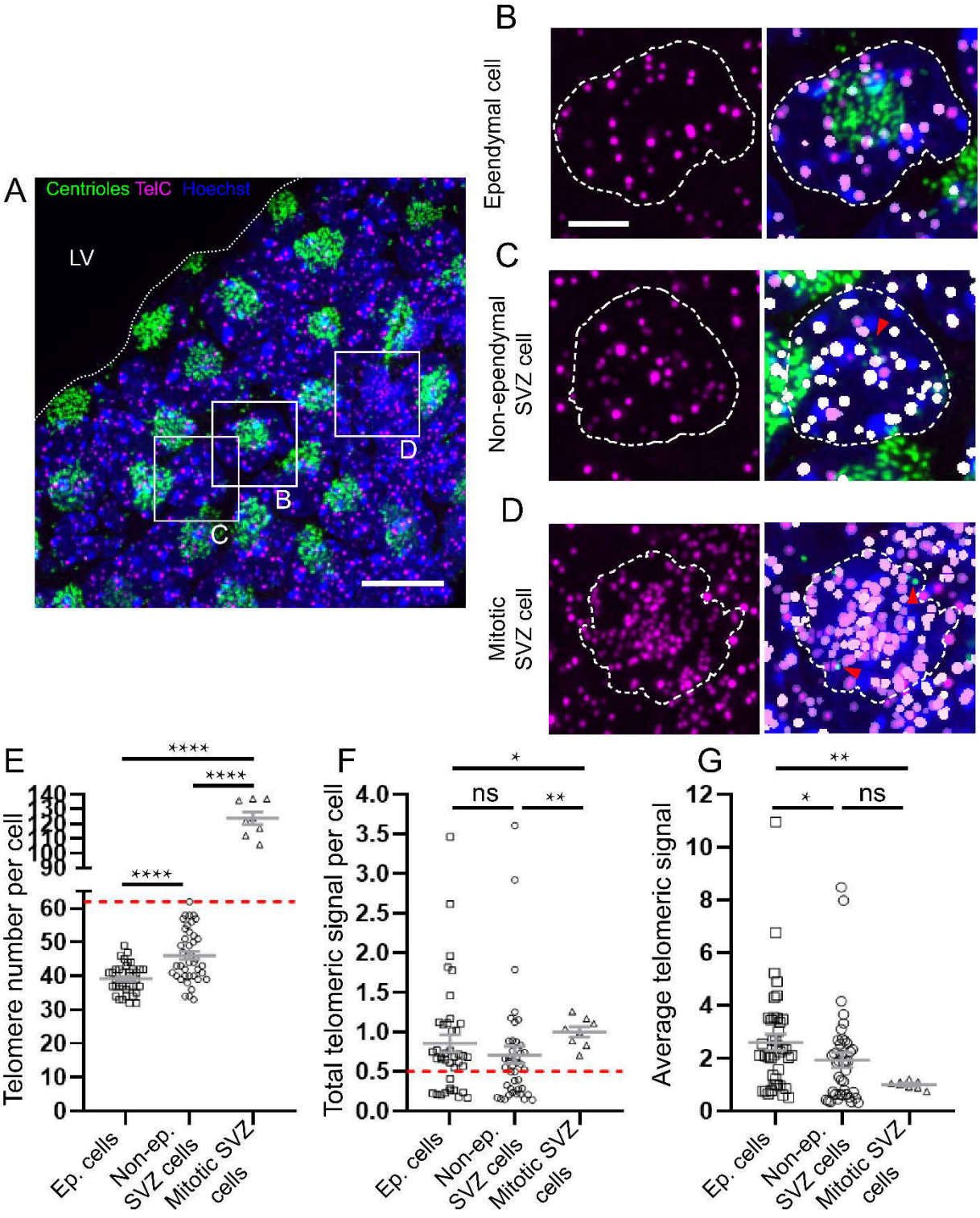

Figure 31. Ependymal cells contain the same amount of telomeric material than other V-SVZ cells in less but denser telomere foci. (A) Example image of a neurogenic niche from a Cen2GFP mouse strain at P10 (coronal section). Centrioles are shown in green and telomere FISH in magenta. Sections were necessarily counterstained with Hoechst to associate telomeric foci to specific nuclei in a highly compacted tissue. (B-D) Examples of an ependymal cell, distinguishable by the presence of an apical patch of centrioles (B), a non-ependymal SVZ cell that shows an apical pair of centrioles (red arrowhead) (C) and a mitotic cell, with characteristic condensed chromatin and two pairs of centrioles (red arrowheads) (D). In slightly transparent or opaque white, the

watershed channel for telomere detection (see Figure S4) is shown. Different levels of transparency in this channel are merely due to different object ID colors attributed by the telomere detection plug-in. (E-G) Quantification of the average telomere number per cell, with the red dotted line on 62 indicating half the value of the average mitotic cell group (E), the total amount of telomeric material per cell, with the red dotted line on 0.5 as half the value of the average mitotic cell group (F), and the average telomeric signal per focus in each cell (G). The bars are representative of the SD for n = 4 animals and n = 40 ependymal, 40 non-ependymal and 8 mitotic cells. Scale bar 10 µm for (A) and 3 µm for (B-D). LV: Lateral Ventricle.

If telomere shortening was not responsible for DNA damage on such regions, it is possible that excessive replication firing, triggered by a sudden increase of GemC1 expression around the time of ependymal differentiation onset, could be the cause of TIFs occurrence. Telomeres are indeed among the "problematic" sequences that the replication fork finds on its way (Gilson and Géli, 2007). Repetitive sequences, such as those that compose telomeres, have provoke replication stalling. The DNA 3D structures formed on chromosome ends, such as t-loops and G-quadruplexes also have this deleterious effect. Finally, the presence of big protein complexes on chromatin, such as the shelterin complex, have been suggested to cause replicative stress (Higa et al., 2017). However, shelterin proteins have actually been found to recruit factors involved in DNA replication and repair that would actually help fork progression (Novo and Londoño-Vallejo, 2013).

Mammalian telomeric replication can start in the subtelomeric region or telomeric repeats themselves (Higa et al., 2017). A chromatin immunoprecipitation analysis to observe whether GemC1 binds to replication origins near the telomeres could also be illustrative. There is also the possibility that excessive replication firing triggers telomeric damage, but in a way that does not implicate GemC1 chromatin binding. In that case a replication timing assay using a single BrdU pulse (around the time of GemC1-induced replicative stress, this is 30 hours post IUE) and BrdU chromatin immunoprecipitation could be a promising experiment (Hasegawa et al., 2019; Katou et al., 2003), to see if GemC1-dependent replication happens on the telomeres.

We have thought of another hypothesis, based on the relation between telomeres and the nuclear envelope. Deep changes in nuclear morphology observed during GemC1-dependent differentiation (Figure 32) could be the cause of telomeric damage. Indeed telomeres do not have a random distribution in mammalian cells (Novo and Londoño-Vallejo, 2013). For instance, later-replicating telomeres assume a more peripheral location in the nucleus, influenced by subtelomeric sequences (Arnoult et al., 2010). Telomeres have also

been found to tether to the nuclear membrane during its reassemby after mitosis (Crabbe et al., 2012). In fact, they are in close contact with lamins, fibrous proteins that line the inner nuclear membrane, as it has been elegantly shown by fusion of an *E. coli* methyltransferase to the lamin B1 protein, which results in detectable methylation of telomere sequences due to physical proximity (Sobecki et al., 2018). Furthermore, the loss of lamins causes an increased presence of TIFs (Gonzalez-Suarez et al., 2009). It could be hypothesized then that the nuclear contorsions we observe could be at the onset of telomeric DNA damage.

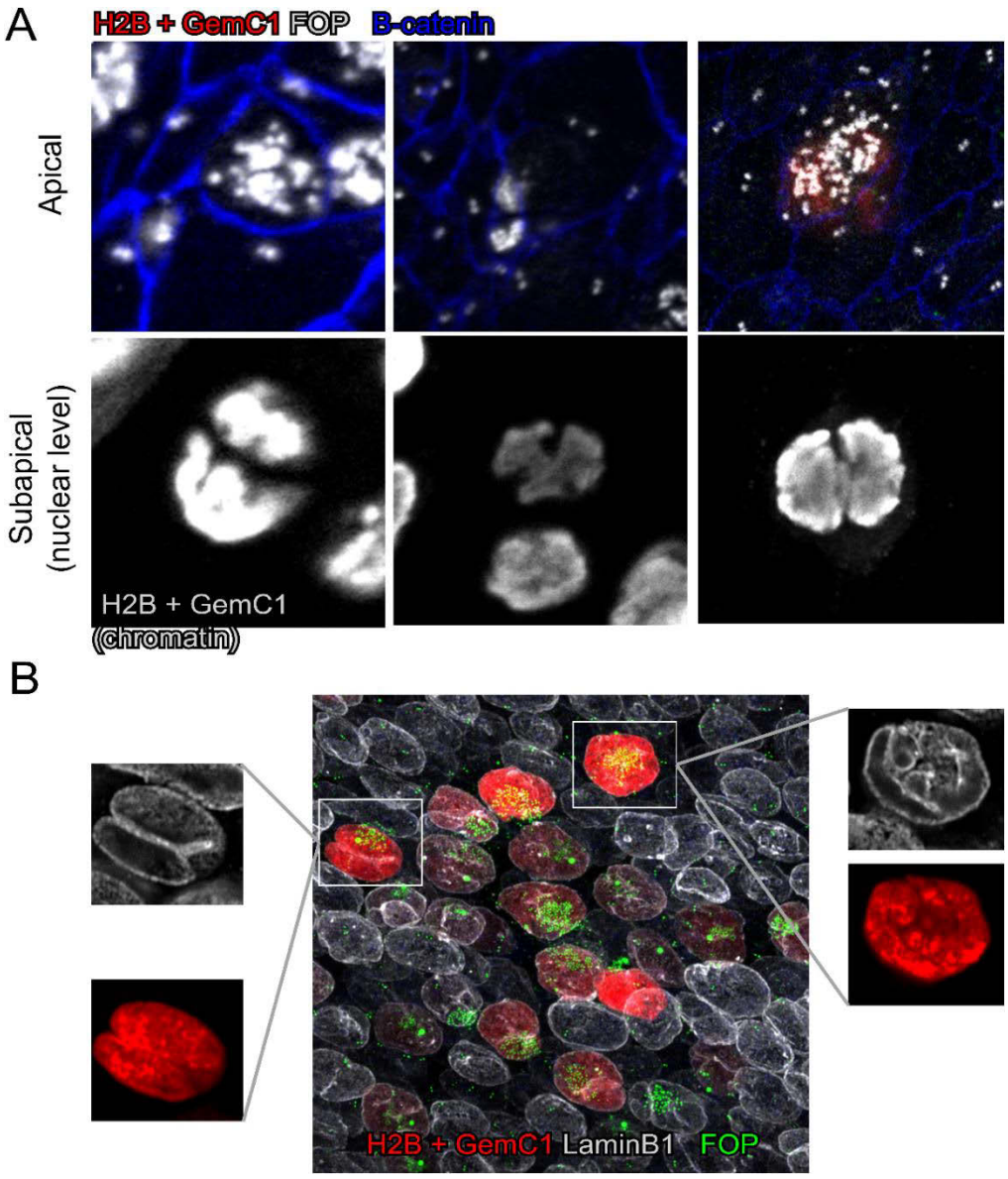

Figure 32. Nuclear deformations during GemC1-dependent ependymal differentiation. (A) Wholemount images of a GemC1 + H2B-RFP-electroporated neuroepithelium, stained with antibodies against β-catenin and FOP, to label apical contacts and centrioles, respectively. Three examples are shown of three independent cells undergoing deep nuclear morphology transformations. For each of the three, an image of the apical contact where amplifying centrioles are seen, and an image of the subapical region, where the nucleus lies, are shown. As a note, the first cell seems as if it were undergoing mitosis. However, the two chromatin accumulations are

connected in a deeper level, making one whole nucleus. (B) Wholemount images of a GemC1 + H2B-RFP electroporated neuroepithelium, showing LaminB1 and centriole staining. LaminB1 reveals the presence of groves on the nuclear envelope.

It is very striking as well the aggregation of telomere foci in ependymal cells, which present significantly less detectable telomeric foci, but these are denser than in other SVZ cells (Figure 31A-D, E, G). Interestingly, induction of senescence in human mesenchymal cells leads to the formation of telomere aggregates that display DNA damage characteristics (TIFs) and associate to lamins (Novo and Londoño-Vallejo, 2013; Raz et al., 2008). Senescence induction in these cells leads to the formation of groves very similar to what we observe in GemC1-electroporated brains (Figure 32B), and senescent, damaged telomeres associate to said grooves in the nuclear envelope (Raz et al., 2008).

The functional implications of these aggregates are unknown. During meiosis, it has been hypothesized that telomeres act as anchors on the nuclear envelope that help pairing of homolog chromosomes and a successful chromosome seggregation (Klutstein and Cooper, 2014). Consequently, telomere clustering is seen in spermatocytes (Marjanović et al., 2015). However, ependymal progenitors do not undergo mitosis, so homolog chromosome pairing does not seem as a functional explanation. Klutstein and Cooper also argue that telomere clustering in meiosis could serve to increase local concentration of telomere-associated factors that are essential in other meiotic functions. It would be tempting to hypothesize that telomere aggregation in ependymal progenitors also serves to create local accumulation of factors, such as those that protect telomeres against DDR and thus prevent NHEJ or HR that could lead to chromosomal instability. In any case, a relationship between senescence, nuclear deformation, nuclear envelope telomere tethering, telomere aggregation and damage seems a exploration-worthy territory although, for the moment, highly unknown. Prospectively, one could claim that assessing this telomere association during ependmal differentiation would be interesting, to see if the time of telomere clustering coincides with the moment of replicative stress induction.

4.3.6. The role of GemC1 in cell cycle progression and arrest during ependymal differentiation

We have observed that, before centriole amplification, GemC1-expressing cells enter S phase like control ones, but they present replicative stress and damaged telomeres. This led us to perform time-lapse tracking of control or GemC1-electroporated nuclei, RNA-sequencing in GemC1 and Mcidas-expressing cells, in search of genes other that those classically involved in ciliogenesis, and immunostaining studies of cell cycle progression and arrest markers.

After gain-of-function experiments of GemC1 and its downstream effector Mcidas via IUE, we obtained a list of genes involved in ciliogenesis and centriole amplification, commonly upregulated by both actors, as expected, that served as proof of concept of our approach (Terré et al., 2016). We also confirmed the functional hierarchy between GemC1 and Mcidas, where the former transactivates the latter, but not vice versa (Arbi et al., 2016; Kyrousi et al., 2015, Article 2 – Figure 3H). Interestingly, cell cycle progression and arrest genes were up-regulated, like cyclin A1, as previously reported (Vladar et al., 2018) and p21, a gene not yet described in ependymal development (Article 2 – Figure 3H, K). Furthermore, a Gene Set Enrichment Analysis performed with the pathway studio software revealed that GemC1 activated the G1/S transition gene network, whereas Mcidas-dependent up-regulated genes were enriched in both G1/S and G2/M. This suggests the existence of an active cell cycle progression transcriptome (Article 2 – Figure 3G).

A highly interesting fact is that GemC1 and Mcidas promoted miR-449c expression, a member of the miR-34/449 family that has been implicated in MCC differentiation in *Xenopus* embryonic epidermis and human airway epithelial cells in culture (Marcet et al., 2011). However, an implication in ependymal differentiation is missing. Our screen is the first one to establish this potential link, and it would suggest the existence of a feedback loop, in which GemC1 and Mcidas activate the expression of these mi-RNAs. These regulatory elements have been described to be most upstream of the multiciliated differentiation cascade, and not downstream or as part of feedback loops. Functional studies (gain or loss-of-function) for these genes in the neuroepithelium could be interesting to perform.

Another fact from the study of Marcet *et al*. that points in a similar direction as our work, is that over-expression of the miR-449 gene in human airway mucociliary epithelial cells leads to the significant enrichment of genes involved in the G2/M checkpoint.

The fact that GemC1-expressing cells quickly differentiated after electroporation (at 54 hours post IUE differentiation is pretty advanced, Article 2 – Figure 1D-E) , but also incorporated EdU like control cells (Article 2 – Figure 2E-F), led us to think there might be a halt in cell cycle between S and mitosis. Indeed, time lapse microscopy of ventricular explants revealed that, despite non-affected S phase entry, mitosis completion was significantly reduced in GemC1-expressing conditions (Article 2 – Figure 3A-C). We also confirmed the presence of the CKI p21 via immunofluorescence and the DNA damage pathway-involved protein p73 (Article 2 – Figure 3G-H). However, even though Ki-67 was downregulated in differentiating conditions (Figure 33), another cell cycle progression marker, like hyperphosphorylated pRb, which is responsible for the G1/S transition, was highly up-regulated (Article 2 – Figure 3E-F). These results were confirmed in early postnatal wholemounts, which bear no Ki-67 expression, but display pRb activity, without GemC1 gain-of-function conditions (Figure 34A-B).

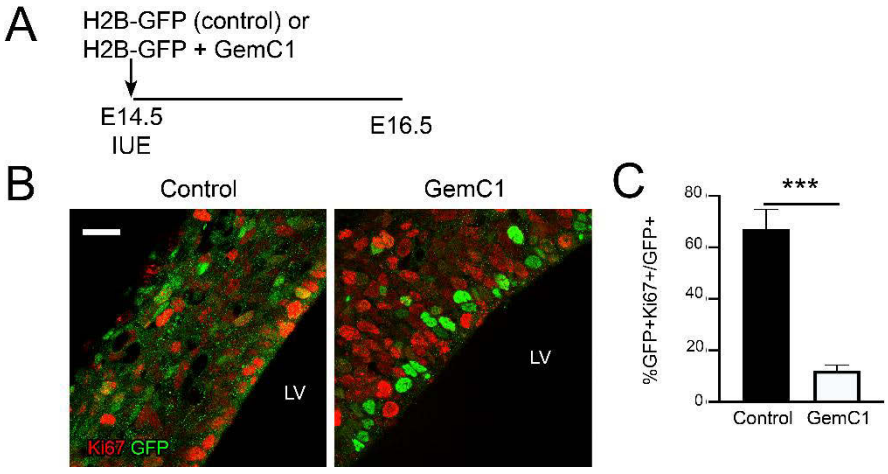

Figure 33. GemC1-expressing cells down-regulate the cell cycle marker Ki-67. (A) Schematic representation of the experiment. Control (H2B-GFP) without or with GemC1 plasmids were electroporated at E14. and coronal sections were analyzed 54 hours later by immunofluorescence. (B) Representative images of coronal sections of embryos electroporated with H2B-GFP or H2B-GFP + GemC1, with electroporated GFP-expressing cells in green and Ki-67 staining shown in red. (C) Quantifications of the mean percentage of Ki-67+ electroporated (GFP+) cells. The error bars indicate the SEM for n = 3 animals for both conditions. The p-value was calculated using a Mann-Whitney test; *** $p \leq 0.001$. Scale bar 20 µm. LV: Lateral Ventricle.

We worked with the hypothesis that cells had not exited the cell cycle before the onset of differentiation, but they slowed down cell cycle progression during centriole amplification. The seeming absence of Ki-67 was an interesting point to focus on. Unlike retinoblastoma, which shows a bistable switch-like nature around the restriction point of G1, this is, it displays an "on or off" response for E2F-dependent G1/S transition (Yao et al., 2008), Ki-67 is a graded marker (Miller et al., 2018). Usually used as a binary marker for cycling versus non-cycling cells, Ki-67 actually displays differential levels of expression that are regulated through cell cycle progression. This protein is actually proteasome-degraded during G1, when it presents its lowest levels, and starts accumulating upon S phase entry and peaks in G2/M (Sobecki et al., 2017). Interestingly, CDK4/6 inhibitors leads to a loss of Ki-67 mRNA levels, and, since it is degraded uniformly during G0 and G1, the longer a cell spends in such phases, the lower the levels of Ki-67 are upon cell cycle or S phase re-entry. This was observed in cancer and non-transformed cell lines (Miller et al., 2018; Sobecki et al., 2017). Curiously, low levels of Ki-67 were detected by Al Jord *et al.* during ependymal centriole amplification (Al Jord et al., 2017), which have also been affirmed to be present in not deeply quiescent cells (Sobecki et al., 2017). It is thus interesting to argue that terminal differentiation is not uncoupled from the cell cycle progression, but rather cells would be in a pseudo-cell cycle state as centriole amplification progresses.

The presence of hyperphsophorylated pRb suggested our cells could be in a S/G2 stage. We sought to detect a protein that has been used as a G2 marker: Cenp-F (Kaida and Miura, 2015). This is a kinetochore-associated protein with an important role in mitotic chromosome seggregation whose expression peaks at G2. Cenp-F remains in the nucleus during most of the cell cycle but it is transiently exported to the cytosol in G2 (Liao et al., 1995; Loftus et al., 2017). We observe an exclusive colocalization of Cenp-F with FoxJ1+ cells in the differentiating (P2), wild type V-SVZ wholemount. Other cells in the nascent neurogenic niche do not seem to have such staining. Besides some of the Cenp-F staining seems to be located on the cytoplasm, apart from the nucleus, which could suggest differentiating cells are in a G2-like state (Figure 34C).

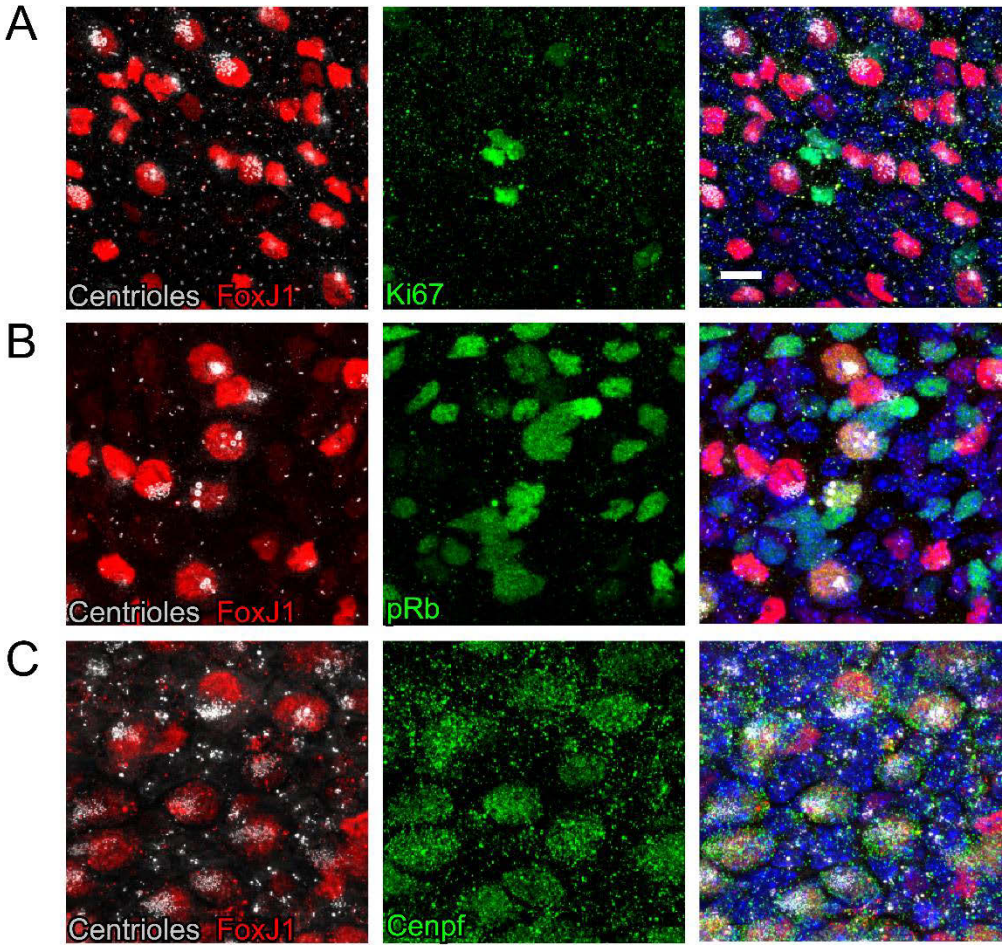

Figure 34. Ependymal differentiation in wild type conditions reproduces the phenotypes observed in GemC1 expressing cells *in utero*. P2 wholemounts of wild type mice present a great number of differentiating ependymal cells (FoxJ1+ and in various stages of centriole amplification: halo, flower and individualization). FoxJ1+ cells were in all cases Ki-67- (A). Many of them in a differentiating stage (halo/flower) were pRb+ (B), as well as Cenp-F+ (C). Scale bar 10 µm (A-C).

As for the cell cycle arrest markers up-regulated by GemC1 (Article 2 – Figure 3G-H), p73 has already been described to be essential for the proper development of the ependyma (Gonzalez-Cano et al., 2016). It was described before though, as a p53 homolog, and the expression of both can be triggered by DNA damage to induce apoptosis in mouse embryonic stem cells and cell cycle arrest in several cancer cell lines (Chen et al., 2001; He et al., 2016; Yoon et al., 2015). Furthermore, it has been shown that effector kinases of the DDR, Chk1 and Chk2 are necessary for the accumulation of p73 (Urist et al., 2004). In the neurogenic niche, p73 is essential to establish many aspects of the proper V-SVZ, such as a correct ependymal specification program, ciliation or translational polarity. Besides, its deletion causes hydrocephalus in mice (Fujitani et al., 2017; Gonzalez-Cano et al., 2016). Its absence is even

deleterious for adult neurogenesis, but this is probably due to non-autonomous cell effects in a completely disrupted neurogenic niche (Gonzalez-Cano et al., 2016). GemC1 is actually an upstream activator of p73, which binds to upstream sequences to its transcription start site and promotes its expression in combination with E2F5 (Lalioti et al., 2019b). However, a connection between its role in activating the multiciliation transcriptional program in the brain or the rest of the multiciliated epithelia in the body (Marshall et al., 2016) and its role as a DNA damage sensor has not been described.

P21 is another cell cycle arrest marker signficantly increased by GemC1 (Article 2 – Figure 3G-H). It is a well known product of p53 transcription during replicative senescence (Roake and Artandi, 2017). Like p73, it has an important role in the neurogenic niche, as it helps maintain the quiescent state of adult NSCs and avoid their excessive proliferation, which ultimately leads to their proliferation capacity exhaustion. It has been postulated that in the absence of p21, the constant and rapid early replication of B1 cells could lead to telomere shortening and, as a consequence, an eventual halt in proliferation (Kippin et al., 2005). Indeed, telomerase has been shown to prevent premature ageing of the proliferative cells in the neurogenic niche (Ferrón et al., 2004). However, p21 also possesses a CKI-independent role in quiescence maintenance in the neurogenic niche. Via the transcriptional repression of morphogenic signaling (BMP), p21 is necessary to avoid excessive progenitor cycling activity, in consonance with ependymal cells, which express the BMP antagonist Noggin (Porlan et al., 2013). A rather interesting phenotype of the p21 full KO, that could be more related to its canonical role as CKI, is that B1 cells present signs of replicative stress (γ-H2AX, 53BP1 and RPA foci), due to increased levels of the pluripotency-related protein Sox2 (Marqués-Torrejón et al., 2013).

4.3.7. Ependymal cells: a matter of ploidy?

The data described so far, this is, the presence of cell cycle progression markers, including S and G2 phases and the mitotic block has led us to the unconfirmed hypothesis that ependymal cells could leave the cell cycle after differentiation in G2. To confirm such hypothesis, a FACS analysis of the DNA content of GemC1-expressing cells will be performed, to check for any aneuploidy. However, it is possible that full-genome replication does not occur, but only some replication firing due to the action of GemC1 that FACS could not detect. To circumvent such lack of resolution, we could perform single-cell whole-genome sequencing

to see if some cells indeed have some stretches of replicated chromosomes (Sladky et al., 2020). This could also reveal if re-replication actually happens near the telomeres and could be at the source of their damage. Interestingly, Sladky *et al*. claim that a multiprotein complex called the PIDDosome impedes excessive ploidy in hepatocytes of the developing or regeneating liver. Polyploidy, which is not rare in the liver, is limited by such complex, which in turn activates the p53-p21 axis, two genes necessary to maintain ploidy below a certain level. A major component of the PIDDosome, the protein Pidd1, is actually one of the top up-regulated genes by GemC1 and Mcidas in our RNA-seq experiments. It would be interesting as well to check the ploidy of ependymal cells in p21 -/- (Deng et al., 1995) mice electroporated with GemC1, since the induction of p21 seen in our model could be the mechanism that puts a halt on excessive DNA replication.

Regarding aneuploidy and centriole amplification, it is indeed intriguing that depletion of Geminin, the antagonist of GemC1 in DNA replication firing, causes supernumerary centrioles and genome over-replication in human normal and cancer cells. Besides, these cells fail to go into mitosis due to G2/M DNA damage checkpoint activation (Tachibana et al., 2005). In some aspects (centriole amplification, G2/M checkpoint activation and mitotic inhibition) these results phenocopy our observations in GemC1-over-expressing cells. Geminin and GemC1 determine the balance of B1 and ependymal cell production (Article 1 – Figure 7). The mechanisms by which they do so could entail their function in DNA replication, namely an induction of replicative stress, or protection against it, which could trigger, or prevent, respectively, a centriole amplification.

Endoreplication, the process of DNA replication without passage through mitosis was previously considered as rare and only functional in plants and insects, like *Drosophila*. However, mammalian endoreplication and polyploidization has increasingly emerged as a not-so-rare event with functional implications in systems like megakaryocytes, hepatocytes, the epithelium of the mammary glands during lactation (Gandarillas et al., 2018), and even, rat cortical neurons, where authors suggest endoreplication could be a potential mechanism to support high metabolic demands of long-range projection neurons (Sigl-Glöckner and Brecht, 2017). Ependymal cells, which contain multiple mitochondria to support the high energy demand of ciliary beating (Doetsch et al., 1997) are certainly good candidates to display endoreplication to support their costly function. Upon GemC1 over-expression, we have

certainly observed the formation of micronuclei (Figure 35) in fully differentiated ependymal cells. Al Jord *et al*. observed it in ependymal differentiating cells, upon pharmacological inhibition of the APC/C complex, which impedes transition into anaphase. Although the number of centromeres they counted was that of diploid mouse cells, this was assesed *in vitro* and does not rule out the presence of partial endoreplication beyond the centromere (Al Jord et al., 2017). The presence of micronuclei could be indicative of endomitosis and polyploidization, which have been described in development (Fox and Duronio, 2013; Ullah et al., 2009).

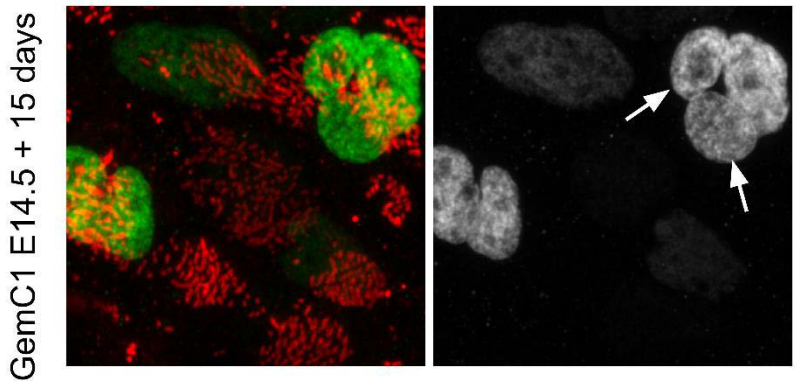

Figure 35. GemC1 expression promotes micronuclei formation. Representative images of the ventricular zone at P10 of animals electroporated at E14.5 with an H2B-GFP + GemC1 plasmid mixture. Nuclei are shown in green and centrioles, in red. The arrows point at the formation of micronuclei in the GemC1-expressing cells.

Finally, something that remains to be elucidated though, is whether GemC1-induced replicative stress is the cause of centriole amplification or if both phenomena are independent. Some examples of DDR-dependent differentiation do exist. Although not replicative stress-related, radiation-induced DNA damage has been shown to be the cause of senescent traits and, most importantly, astrocytic differentiation in adult NSCs *in vitro* and *in vivo* (Schneider et al., 2013). In the *Drosophila* testes, persistent replicative stress due to hydroxyurea treatment leads to the premature differentiation of germ cells, with massive activation of the DDR (Landais et al., 2014). Finally, skin keratinocytes differentiation parallels our observations. In them, Myc expression, which in turn triggers Cyclin E expression, pushes these cells into terminal differentiation with concomitant activation of the p53/p21 pathway, endoreplication and γ-H2AX, which in all trigger a mitotic block and are the cause of differentiation (Gandarillas, 2012). A potential treatment of GemC1-electroporated animals with caffeine, a known inhibitor of the DDR (both ATR and ATM-dependent), could be performed. Thus, we could prove that it is replicative stress and subsequent G2/M checkpoint

activation, combined with mitotic entry inhibition mechanisms (Al Jord et al., 2017) the case that drives ependymal differentiation. The keratynocyte mode of differentiation certainly proves that terminal differentiation is not uncoupled from cell cycle progression, which seems to be the case for ependymal differentiation.

4.3.8. Telomerase favors B1 fate in detriment of the ependymal one

Since telomere damage was present in ependymal progenitors, we wondered whether telomerase, an enzyme known to elongate telomeres, could play a role in ependymal commitment. We confirmed that simultaneous expression of GemC1 and mTERT, the catalytic subunit of the telomerase, in the p21-mTERT mouse significantly decreased ependymal markers (p73 and centriole amplification) (Article 2 – Figure 4A-E). In the same direction, expression of mTERT *in utero* increased the number of B1 cells in detriment of ependymal cells (Article 2 – Figure 4F-H).

Telomerase is indeed expressed in the adult rodent brain and its highest expression is found in the SVZ. Nonetheless, its activity decreases with age (Caporaso et al., 2003), parallel to its expression (Ferrón et al., 2009). This is compatible with the progression exhaustion of the B1 cell pool with age (Obernier et al., 2018). Telomerase KO models (like Terc KO, which lacks the non-coding RNA component of telomerase essential for its activity) display telomere shortening (Flores et al., 2005), which impairs proliferation and self-renewal of B1 cells (Ferrón et al., 2004). But interestingly, telomere shortening over successive generations of Terc -/- inbreeding generates a defect in neuroblast birth and neuronal maturation (as seen by the number of neurites in olfactory bulb neurons). This suggests a role of telomerase in specification and differentiation in the CNS, in a p53/p21 axis-dependent manner, in the absence of apoptosis (Ferrón et al., 2009).

It would be reasonable to hypothesize that telomerase expression increases stem cells' proliferative capacity. Since ependymal cells seem to be the final output of RGCs in one last consumptive symmetrical division (Article 1 – Figure 7), a telomerase increase of expression would lead to a higher production of cells before that last division, like B1 cells (Article 2 – Figure 4), due to the aforementioned increase of proliferative capacity. The other possibility is that telomerase itself would have a cell cycle-independent cell fate specification role in the ependymal/B1 cell lineage.

A prospective experiment could consist of revealing the effect of telomerase deficiency and critical telomere shortening, using a TERC or a TERT KO line, on ependymal differentiation. We tried to produce litters of TERC -/- inbreedings to study the potential implication on ependymal specification. However, we failed to produce any offspring. TERT -/- individuals born over several generations of inbreeding of telomerase-depleted animals (and thus, telomere attrition) have indeed been found to be the cause of infertility, due to aberrant gamete production (Jeffrey Chiang et al., 2010). As an alternative, a telomerase inhibitor known as 3'-azido-2',3'–dideoxythymidine (AZT) has been successfully used to reduce neural progenitors proliferation *in vitro*, with a concomitant increase of neuronal differentiation (Haïk et al., 2000). It would be certainly interesting to use this drug *in vivo* after IUE tagging of RGCs at a specific time point, such as E14.5, to study the balance of neurogenic niche cell production.

Finally, the evaluation of the effect of mTERT expression in the short term could be of high impact for our study. If telomerase can protect cells against replicative stress, or if it is rather a continuation of proliferation of RGCs that promotes B1 fate in detriment of ependymal cells, would help us further understand the molecular mechanisms of neurogenic niche fate specification.

4.4. Final conclusion

This work presents a novel view of the lineage and generation mechanisms of glial cells in the neurogenic niche. The combination of cell fate mapping, precise *in utero* surgery, state-of-the-art clonal analysis techniques and cell cycle progression and stress studies have established a new paradigm of how these cells are born and specified. Ependymal or B1 cell-restricted progenitors are not the norm, much like the existence of neuron and glia-restricted progenitors were discarded to be the rule, almost two decades ago. Instead, two cell types that become highly associated, physically and functionally, but with notable differences in the adult can arise from the same cell division.

In the same groundbreaking way, this work reveals that differentiating and cell cycle progression are not always uncoupled in time. Biology never seems to be black or white. The presence of S-phase traits, such as replicative stress, and senescence-like and cell cycle arrest phenotypes, such as p21 and telomere damage, certainly seem to point in that direction.

Whether these characteristics are necessary for ependymal differentiation or whether they are a secondary effect of its mechanisms, we still do not know. Is replicative stress during multiciliogenesis derived from the role of GemC1 in DNA replication as an accident? Does this necessarily imply telomere damage and senescence? Or is it precisely these stress signals that communicate the cell that it is time to stop dividing and differentiate?

I hope this work, developed over almost five years, has shed some light into the vast and mysterious world that is the development of the Central Nervous System and the specification mechanisms of its cells. I also expect that it has helped bring up as many or more exciting questions to answer in the future, as there were at the beginning. It seems that evolution has created highly intricate biological systems that rarely follow one pathway or another, but recycle the molecules used in one process, to use them in others. That is what makes them both complex and beautiful. A complete understanding of what we are and how we function as living creatures, if it ever comes, seems a long way down the road. So fortunately, many interesting, astonishing discoveries are yet to come.

BIBLIOGRAPHY

Akdemir, E.S., Huang, A.Y.S., and Deneen, B. (2020). Astrocytogenesis: where, when, and how. F1000Research *9*.

Al-Dosari, M.S., Al-Owain, M., Tulbah, M., Kurdi, W., Adly, N., Al-Hemidan, A., Masoodi, T.A., Albash, B., and Alkuraya, F.S. (2013). Mutation in MPDZ causes severe congenital hydrocephalus. J. Med. Genet. *50*, 54–58.

Alfaro-Cervello, C., Soriano-Navarro, M., Mirzadeh, Z., Alvarez-Buylla, A., and Garcia-Verdugo, J.M. (2012). Biciliated ependymal cell proliferation contributes to spinal cord growth. J. Comp. Neurol. *520*, 3528–3552.

Altman, J. (1963). Autoradiographic investigation of cell proliferation in the brains of rats and cats. Anat. Rec. *145*, 573–591.

Altman, J. (1969). Autoradiographic and histological studies of postnatal neurogenesis. IV. Cell proliferation and migration in the anterior forebrain, with special reference to persisting neurogenesis in the olfactory bulb. J. Comp. Neurol. *137*, 433–457.

Alunni, A., Krecsmarik, M., Bosco, A., Galant, S., Pan, L., Moens, C.B., and Bally-Cuif, L. (2013). Notch3 signaling gates cell cycle entry and limits neural stem cell amplification in the adult pallium. Dev. *140*, 3335–3347.

Alvarez-Buylla, A., and Kirn, J.R. (1997). Birth, Migration, Incorporation, and Death of Vocal Control Neurons in Adult Songbirds. J. Neurobiol. *33*, 585–601.

Alvarez-Buylla, A., García-Verdugo, J.M., and Tramontin, A.D. (2001). A unified hypothesis on the lineage of neural stem cells. Nat. Rev. Neurosci. *2*, 287–293.

Anders, S., Pyl, P.T., and Huber, W. (2015). HTSeq-A Python framework to work with high-throughput sequencing data. Bioinformatics *31*, 166–169.

Anthony, T.E., Klein, C., Fishell, G., and Heintz, N. (2004). Radial glia serve as neuronal progenitors in all regions of the central nervous system. Neuron *41*, 881–890.

Arbi, M., Pefani, D., Kyrousi, C., Lalioti, M., Kalogeropoulou, A., Papanastasiou, A.D., Taraviras, S., and Lygerou, Z. (2016). GemC1 controls multiciliogenesis in the airway epithelium. EMBO Rep. *17*, 400–413.

Arnoult, N., Schluth-Bolard, C., Letessier, A., Drascovic, I., Bouarich-Bourimi, R., Campisi, J., Kim, S., Boussouar, A., Ottaviani, A., Magdinier, F., et al. (2010). Replication Timing of Human Telomeres Is Chromosome Arm–Specific, Influenced by Subtelomeric Structures and Connected to Nuclear Localization. PLoS Genet. *6*, e1000920.

Baas, D., Meiniel, A., Benadiba, C., Bonnafe, E., Meiniel, O., Reith, W., and Durand, B. (2006). A deficiency in RFX3 causes hydrocephalus associated with abnormal differentiation of ependymal cells. Eur. J. Neurosci. *24*, 1020–1030.

Backman, M., Machon, O., Mygland, L., Van Den Bout, C.J., Zhong, W., Taketo, M.M., and Krauss, S. (2005). Effects of canonical Wnt signaling on dorso-ventral specification of the mouse telencephalon. Dev. Biol. *279*, 155–168.

Balestrini, A., Cosentino, C., Errico, A., Garner, E., and Costanzo, V. (2010). GEMC1 is a TopBP1-interacting protein required for chromosomal DNA replication. Nat. Cell Biol. *12*, 484–491.

Bandeira, F., Lent, R., and Herculano-Houzel, S. (2009). Changing numbers of neuronal and non-neuronal cells underlie postnatal brain growth in the rat. Proc. Natl. Acad. Sci. U. S. A. *106*, 14108–14113.

Banizs, B., Pike, M.M., Millican, C.L., Ferguson, W.B., Komlosi, P., Sheetz, J., Bell, P.D., Schwiebert, E.M., and Yoder, B.K. (2005). Dysfunctional cilia lead to altered ependyma and choroid plexus function, and result in the formation of hydrocephalus. Development *132*, 5329–5339.

Barnabé-Heider, F., Wasylnka, J.A., Fernandes, K.J.L., Porsche, C., Sendtner, M., Kaplan, D.R., and Miller, F.D. (2005). Evidence that embryonic neurons regulate the onset of cortical gliogenesis via cardiotrophin-1. Neuron *48*, 253–265.

Barnes, P.J. (2015). Mechanisms of development of multimorbidity in the elderly. Eur. Respir. J. *45*, 790–806.

von Bartheld, C.S., Bahney, J., and Herculano-Houzel, S. (2016). The search for true numbers of neurons and glial cells in the human brain: A review of 150 years of cell counting. J. Comp. Neurol. *524*, 3865–3895.

Basak, O., Krieger, T.G., Muraro, M.J., Wiebrands, K., Stange, D.E., Frias-Aldeguer, J., Rivron, N.C., van de Wetering, M., van Es, J.H., van Oudenaarden, A., et al. (2018). Troy+ brain stem cells cycle through quiescence and regulate their number by sensing niche occupancy. Proc. Natl. Acad. Sci. U. S. A. *115*, E610–E619.

Baser, A., Skabkin, M., Kleber, S., Dang, Y., Gülcüler Balta, G.S., Kalamakis, G., Göpferich, M., Ibañez, D.C., Schefzik, R., Lopez, A.S., et al. (2019). Onset of differentiation is post-transcriptionally controlled in adult neural stem cells. Nature *566*, 100–104.

Bejarano, L., Schuhmacher, A.J., Méndez, M., Megías, D., Blanco-Aparicio, C., Martínez, S., Pastor, J., Squatrito, M., and Blasco, M.A. (2017). Inhibition of TRF1 Telomere Protein Impairs Tumor Initiation and Progression in Glioblastoma Mouse Models and Patient-Derived Xenografts. Cancer Cell *32*, 590-607.e4.

Del Bene, F., Wehman, A.M., Link, B.A., and Baier, H. (2008). Regulation of Neurogenesis by Interkinetic Nuclear Migration through an Apical-Basal Notch Gradient. Cell *134*, 1055–1065.

Bergles, D.E., and Richardson, W.D. (2016). Oligodendrocyte development and plasticity. Cold Spring Harb. Perspect. Biol. *8*, a020453.

Bester, A.C., Roniger, M., Oren, Y.S., Im, M.M., Sarni, D., Chaoat, M., Bensimon, A., Zamir, G., Shewach, D.S., and Kerem, B. (2011). Nucleotide deficiency promotes genomic instability in early stages of cancer development. Cell *145*, 435–446.

Del Bigio, M.R. (2010). Ependymal cells: Biology and pathology. Acta Neuropathol. *119*, 55–73.

Bleichert, F. (2019). Mechanisms of replication origin licensing: a structural perspective. Curr. Opin. Struct. Biol. *59*, 195–204.

Blow, J.J., and Hodgson, B. (2002). Replication licensing - Defining the proliferative state? Trends Cell Biol. *12*, 72–78.

De Boer, L., Oakes, V., Beamish, H., Giles, N., Stevens, F., Somodevilla-Torres, M., DeSouza, C., and Gabrielli, B. (2008). Cyclin A/cdk2 coordinates centrosomal and nuclear mitotic events. Oncogene *27*, 4261–4268.

Boldrini, M., Fulmore, C.A., Tartt, A.N., Simeon, L.R., Pavlova, I., Poposka, V., Rosoklija, G.B., Stankov, A., Arango, V., Dwork, A.J., et al. (2018). Human Hippocampal Neurogenesis Persists throughout Aging. Cell Stem Cell *22*, 589-599.e5.

Boon, M., Wallmeier, J., Ma, L., Loges, N.T., Jaspers, M., Olbrich, H., Dougherty, G.W., Raidt, J., Werner, C., Amirav, I., et al. (2014). MCIDAS mutations result in a mucociliary clearance disorder with reduced generation of multiple motile cilia. Nat. Commun. *5*, 1–8.

Branda, C.S., and Dymecki, S.M. (2004). Talking about a revolution: The impact of site-specific recombinases on genetic analyses in mice. Dev. Cell *6*, 7–28.

Brenneis, G., and Beltz, B.S. (2019). Adult neurogenesis in crayfish: Origin, expansion, and migration of neural progenitor lineages in a pseudostratified neuroepithelium. J. Comp. Neurol.

Briz, C.G., Navarrete, M., Esteban, J.A., and Nieto, M. (2017). In utero electroporation approaches to study the excitability of neuronal subpopulations and single-cell connectivity. J. Vis. Exp. *2017*, 55139.

Brooks, E.R., and Wallingford, J.B. (2014). Multiciliated Cells. Curr. Biol. *24*, R973–R982.

Bruni, J. (1998). Ependymal Development, Proliferation, and Functions: A Review. Microsc. Res. Tech. *41*.

Butler, W.E., Agarwalla, P.K., and Codd, P. (2017). CSF in the ventricles of the brain behaves as a relay medium for arteriovenous pulse wave phase coupling. PLoS One *12*, e0181025.

Cai, J., Chen, Y., Cai, W.H., Hurlock, E.C., Wu, H., Kernie, S.G., Parada, L.F., and Lu, Q.R. (2007). A crucial role for Olig2 in white matter astrocyte development. Development *134*, 1887–1899.

Caillat, C., Pefani, D.E., Gillespie, P.J., Taraviras, S., Blow, J.J., Lygerou, Z., and Perrakis, A. (2013). The Geminin and Idas coiled coils preferentially form a heterodimer that Inhibits Geminin function in DNA replication licensing. J. Biol. Chem. *288*, 31624–31634.

Caillat, C., Fish, A., Pefani, D.-E.E., Taraviras, S., Lygerou, Z., and Perrakis, A. (2015). The structure of the GemC1 coiled coil and its interaction with the Geminin family of coiled-coil proteins. *71*, 2278–2286.

Caporaso, G.L., Lim, D.A., Alvarez-Buylla, A., and Chao, M. V. (2003). Telomerase activity in the subventricular zone of adult mice. Mol. Cell. Neurosci. *23*, 693–702.

Carlén, M., Meletis, K., Göritz, C., Darsalia, V., Evergren, E., Tanigaki, K., Amendola, M., Barnabé-Heider, F., Yeung, M.S.Y., Naldini, L., et al. (2009). Forebrain ependymal cells are Notch-dependent and generate neuroblasts and astrocytes after stroke. Nat. Neurosci. *12*, 259–267.

Casper, K.B., Jones, K., and McCarthy, K.D. (2007). Characterization of astrocyte-specific conditional knockouts. Genesis *45*, 292–299.

Catala, M., and Kubis, N. (2013). Gross anatomy and development of the peripheral nervous system. In Handbook of Clinical Neurology, (Elsevier B.V.), pp. 29–41.

Cesare, A.J., and Karlseder, J. (2012). A three-state model of telomere control over human proliferative boundaries. Curr. Opin. Cell Biol. *24*, 731–738.

Chan, S.W.L., and Blackburn, E.H. (2003). Telomerase and ATM/Tel1p protect telomeres from nonhomologous end joining. Mol. Cell *11*, 1379–1387.

Chapouton, P., Skupien, P., Hesl, B., Coolen, M., Moore, J.C., Madelaine, R., Kremmer, E., Faus-Kessler, T., Blader, P., Lawson, N.D., et al. (2010). Notch activity levels control the balance between quiescence and recruitment of adult neural stem cells. J. Neurosci. *30*, 7961–7974.

Chen, R., and Wold, M.S. (2014). Replication protein A: Single-stranded DNA's first responder: Dynamic DNA-interactions allow replication protein A to direct single-strand DNA intermediates into different pathways for synthesis or repair Prospects & Overviews R. Chen and M. S. Wold. BioEssays *36*, 1156–1161.

Chen, J., Knowles, H.J., Hebert, J.L., and Hackett, B.P. (1998). Mutation of the mouse hepatocyte nuclear factor/forkhead homologue 4 gene results in an absence of cilia and random left-right asymmetry. J. Clin. Invest. *102*, 1077–1082.

Chen, V.S., Morrison, J.P., Southwell, M.F., Foley, J.F., Bolon, B., and Elmore, S.A. (2017). Histology Atlas of the Developing Prenatal and Postnatal Mouse Central Nervous System, with Emphasis on Prenatal Days E7.5 to E18.5. Toxicol. Pathol. *45*, 705–744.

Chen, X., Zheng, Y., Zhu, J., Jiang, J., and Wang, J. (2001). p73 is transcriptionally regulated by DNA damage, p53, and p73. Oncogene *20*, 769–774.

Chen, X., Zhang, W., Gao, Y.F., Su, X.Q., and Zhai, Z.H. (2002). Senescence-like changes induced by expression of p21Waf1/Cip1 in NIH3T3 cell line. Cell Res. *12*, 229–233.

De Chevigny, A., Cremer, H., and Coré, N. (2017). miRNAs in Mammalian Adult Olfactory Neurogenesis. In Essentials of Noncoding RNA in Neuroscience: Ontogenetics, Plasticity of the Vertebrate Brain, (Elsevier Inc.), pp. 137–154.

Chitnis, A., and Bally-Cuif, L. (2016). The Notch meeting: An Odyssey from structure to function. Dev. *143*, 547–553.

Chowdhury, P., Lin, G.E., Liu, K., Song, Y., Lin, F.T., and Lin, W.C. (2014). Targeting TopBP1 at a convergent point of multiple oncogenic pathways for cancer therapy. Nat. Commun. *5*, 5476.

Cibois, M., Luxardi, G., Chevalier, B., Thomé, V., Mercey, O., Zaragosi, L.E., Barbry, P., Pasini, A., Marcet, B., and Kodjabachian, L. (2015). BMP signalling controls the construction of vertebrate mucociliary epithelia. Dev. *142*, 2352–2363.

Cicenas, J., Kalyan, K., and Valius, M. (2015). Roscovitine in cancer and other diseases Cellular effects and preclinical tests. Ncbi.Nlm.Nih.Gov *9*, 1–12.

Clark, E., Santiago, F., Deng, L., Chong, S. yen, de la Fuente, C., Wang, L., Fu, P., Stein, D., Denny, T., Lanka, V., et al. (2000). Loss of G1/S Checkpoint in Human Immunodeficiency Virus Type 1-Infected Cells Is Associated with a Lack of Cyclin-Dependent Kinase Inhibitor p21/Waf1. J. Virol. *74*, 5040–5052.

Clavreul, S., Abdeladim, L., Hernández-Garzón, E., Niculescu, D., Durand, J., Ieng, S.H., Barry, R., Bonvento, G., Beaurepaire, E., Livet, J., et al. (2019). Cortical astrocytes develop in a plastic manner at both clonal and cellular levels. Nat. Commun. *10*.

Clément, O., Hemming, I.A., Gladwyn-Ng, I.E., Qu, Z., Li, S.S., Piper, M., and Heng, J.I.T. (2017). Rp58 and p27kip1 coordinate cell cycle exit and neuronal migration within the embryonic mouse cerebral cortex. Neural Dev. *12*, 8.

Costa, M.R., Bucholz, O., Schroeder, T., and Götz, M. (2009). Late origin of glia-restricted progenitors in the developing mouse cerebral cortex. Cereb. Cortex *19 Suppl 1*, i135-43.

Crabbe, L., Cesare, A.J., Kasuboski, J.M., Fitzpatrick, J.A.J., and Karlseder, J. (2012). Human Telomeres Are Tethered to the Nuclear Envelope during Postmitotic Nuclear Assembly. Cell Rep. *2*, 1521–1529.

D'Adda Di Fagagna, F., Reaper, P.M., Clay-Farrace, L., Fiegler, H., Carr, P., Von Zglinicki, T., Saretzki, G., Carter, N.P., and Jackson, S.P. (2003). A DNA damage checkpoint response in telomere-initiated senescence. Nature *426*, 194–198.

Dal Maschio, M., Ghezzi, D., Bony, G., Alabastri, A., Deidda, G., Brondi, M., Sato, S.S., Zaccaria, R.P., Di Fabrizio, E., Ratto, G.M., et al. (2012). High-performance and site-directed in utero electroporation by a triple-electrode probe. Nat. Commun. *3*, 1–11.

Das, D., Smith, N.W., Wang, X., Richardson, S.L., Hartman, M.C.T., and Morgan, I.M. (2017). Calcein represses human papillomavirus 16 E1-E2 mediated DNA replication via blocking their binding to the viral origin of replication. Virology *508*, 180–187.

Dawe, H.R., Farr, H., and Gull, K. (2007). Centriole/basal body morphogenesis and migration during ciliogenesis in animal cells. J. Cell Sci. *120*, 7–15.

Dees, C., Zerr, P., Tomcik, M., Beyer, C., Horn, A., Akhmetshina, A., Palumbo, K., Reich, N., Zwerina, J., Sticherling, M., et al. (2011). Inhibition of Notch signaling prevents experimental fibrosis and induces regression of established fibrosis. Arthritis Rheum. *63*, 1396–1404.

Dehay, C., and Kennedy, H. (2007). Cell-cycle control and cortical development. Nat. Rev. Neurosci. *8*, 438–450.

Delgehyr, N., Meunier, A., Faucourt, M., Grau, M.B., Strehl, L., Janke, C., and Spassky, N. (2015). Ependymal cell differentiation, from monociliated to multiciliated cells. Methods Cell Biol. *127*.

Deng, C., Zhang, P., Wade Harper, J., Elledge, S.J., and Leder, P. (1995). Mice Lacking p21 CIP1/WAF1 undergo normal development, but are defective in G1 checkpoint control. Cell *82*, 675–684.

Dennis, C. V., Suh, L.S., Rodriguez, M.L., Kril, J.J., and Sutherland, G.T. (2016). Human adult neurogenesis across the ages: An immunohistochemical study. Neuropathol. Appl. Neurobiol. *42*, 621–638.

Diotti, R., and Loayza, D. (2011). Shelterin complex and associated factors at human telomeres. Nucleus *2*, 119.

Dixit, R., Lu, F., Cantrup, R., Gruenig, N., Langevin, L.M., Kurrasch, D.M., and Schuurmans, C. (2011). Efficient gene delivery into multiple CNS territories using in utero electroporation. J. Vis. Exp.

Dobin, A., Davis, C.A., Schlesinger, F., Drenkow, J., Zaleski, C., Jha, S., Batut, P., Chaisson, M., and Gingeras, T.R. (2013). STAR: Ultrafast universal RNA-seq aligner. Bioinformatics *29*, 15–21.

Doerflinger, N.H., Macklin, W.B., and Popko, B. (2003). Inducible site-specific recombination in myelinating cells. Genesis *35*, 63–72.

Doetsch, F., García-Verdugo, J.M., and Alvarez-Buylla, A. (1997). Cellular composition and three-dimensional organization of the subventricular germinal zone in the adult mammalian brain. J. Neurosci. *17*, 5046–5061.

Doetsch, F., García-Verdugo, J.M., and Alvarez-Buylla, A. (1999a). Regeneration of a germinal layer in the adult mammalian brain. Proc. Natl. Acad. Sci. U. S. A. *96*, 11619–11624.

Doetsch, F., Caillé, I., Lim, D.A., García-Verdugo, J.M., and Alvarez-Buylla, A. (1999b). Subventricular Zone Astrocytes Are Neural Stem Cells in the Adult Mammalian Brain. Cell *97*, 703–716.

Dragatsis, I., and Zeitlin, S. (2001). A method for the generation of conditional gene repair mutations in mice.

Drielsma, A., Jalas, C., Simonis, N., Désir, J., Simanovsky, N., Pirson, I., Abramowicz, M., and Edvardson, S. (2012). Two novel CCDC88C mutations confirm the role of DAPLE in autosomal recessive congenital hydrocephalus. J. Med. Genet. *49*, 708–712.

Dubois, N.C., Hofmann, D., Kaloulis, K., Bishop, J.M., and Trumpp, A. (2006). Nestin-Cre transgenic mouse line Nes-Cre1 mediates highly efficient Cre/loxP mediated recombination in the nervous system, kidney, and somite-derived tissues. Genesis *44*, 355–360.

Dumas, L., Heitz-Marchaland, C., Fouquet, S., Suter, U., Livet, J., Moreau-Fauvarque, C., and Chédotal, A. (2015). Multicolor analysis of oligodendrocyte morphology, interactions, and development with brainbow. Glia *63*, 699–717.

Emerich, D.F., Skinner, S.J.M., Borlongan, C. V., Vasconcellos, A. V., and Thanos, C.G. (2005). The choroid plexus in the rise, fall and repair of the brain.

Eriksson, P.S., Perfilieva, E., Björk-Eriksson, T., Alborn, A.M., Nordborg, C., Peterson, D.A., and Gage, F.H. (1998). Neurogenesis in the adult human hippocampus. Nat. Med. *4*, 1313–1317.

Faubel, R., Westendorf, C., Bodenschatz, E., and Eichele, G. (2016). Cilia-based flow network in the brain ventricles. Science (80-.). *353*, 176–178.

Ferrón, S., Mira, H., Franco, S., Cano-Jimenez, M., Bellmunt, E., Ramírez, C., Fariñas, I., and Blasco, M.A. (2004). Telomere shortening and chromosomal instability abrogates proliferation of adult but not embryonic neural stem cells. Development *131*, 4059–4070.

Ferrón, S.R., Marqués-Torrejón, M.Á., Mira, H., Flores, I., Taylor, K., Blasco, M.A., and Fariñas, I. (2009). Telomere shortening in neural stem cells disrupts neuronal differentiation and neuritogenesis. J. Neurosci. *29*, 14394–14407.

Flor-García, M., Terreros-Roncal, J., Moreno-Jiménez, E.P., Ávila, J., Rábano, A., and Llorens-Martín, M. (2020). Unraveling human adult hippocampal neurogenesis. Nat. Protoc. *15*, 668–693.

Flores, I., Cayuela, M.L., and Blasco, M.A. (2005). Molecular biology: Effects of telomerase and telomere length on epidermal stem cell behavior. Science (80-.). *309*, 1253–1256.

Florio, M., Borrell, V., and Huttner, W.B. (2017). Human-specific genomic signatures of neocortical expansion. Curr. Opin. Neurobiol. *42*, 33–44.

Foerster, S., Hill, M.F.E., and Franklin, R.J.M. (2019). Diversity in the oligodendrocyte lineage: Plasticity or heterogeneity? Glia *67*, glia.23607.

Fogarty, M., Richardson, W.D., and Kessaris, N. (2005). A subset of oligodendrocytes generated from radial glia in the dorsal spinal cord. Development *132*, 1951–1959.

Fogarty, M., Grist, M., Gelman, D., Marín, O., Pachnis, V., and Kessaris, N. (2007). Spatial genetic patterning of the embryonic neuroepithelium generates GABAergic interneuron diversity in the adult cortex. J. Neurosci. *27*, 10935–10946.

Fox, D.T., and Duronio, R.J. (2013). Endoreplication and polyploidy: Insights into development and disease. Dev. *140*, 3–12.

Frisén, J. (2016). Neurogenesis and Gliogenesis in Nervous System Plasticity and Repair. Annu. Rev. Cell Dev. Biol. *32*, 127–141.

Fuentealba, L.C., Rompani, S.B., Parraguez, J.I., Obernier, K., Romero, R., Cepko, C.L., and Alvarez-Buylla, A. (2015). Embryonic Origin of Postnatal Neural Stem Cells. Cell *161*, 1644–1655.

Fujitani, M., Sato, R., and Yamashita, T. (2017). Loss of p73 in ependymal cells during the perinatal period leads to aqueductal stenosis. Sci. Rep. *7*, 1–9.

Funk, M.C., Bera, A.N., Menchen, T., Kuales, G., Thriene, K., Lienkamp, S.S., Dengjel, J., Omran, H., Frank, M., and Arnold, S.J. (2015). Cyclin O (Ccno) functions during deuterosome-mediated centriole amplification of multiciliated cells . EMBO J. *34*, 1078–1089.

Furube, E., Ishii, H., Nambu, Y., Kurganov, E., Nagaoka, S., Morita, M., and Miyata, S. (2020). Neural stem cell phenotype of tanycyte-like ependymal cells in the circumventricular organs and central canal of adult mouse brain. Sci. Rep. *10*.

Furutachi, S., Miya, H., Watanabe, T., Kawai, H., Yamasaki, N., Harada, Y., Imayoshi, I., Nelson, M., Nakayama, K.I., Hirabayashi, Y., et al. (2015). Slowly dividing neural progenitors are an embryonic origin of adult neural stem cells. Nat. Neurosci. *18*, 657–665.

Gaiano, N., Nye, J.S., and Fishell, G. (2000). Radial glial identity is promoted by Notch1 signaling in the murine forebrain. Neuron *26*, 395–404.

Gaillard, H., García-Muse, T., and Aguilera, A. (2015). Replication stress and cancer. Nat. Rev.

Cancer *15*, 276–280.

Galderisi, U., Jori, F.P., and Giordano, A. (2003). Cell cycle regulation and neural differentiation. Oncogene *22*, 5208–5219.

Gammill, L.S., and Bronner-Fraser, M. (2003). Neural crest specification: Migrating into genomics. Nat. Rev. Neurosci. *4*, 795–805.

Gandarillas, A. (2012). The mysterious human epidermal cell cycle, or an oncogene-induced differentiation checkpoint. Cell Cycle *11*, 4507–4516.

Gandarillas, A., Molinuevo, R., and Sanz-Gómez, N. (2018). Mammalian endoreplication emerges to reveal a potential developmental timer. Cell Death Differ. *25*, 471–476.

Gao, P., Postiglione, M.P., Krieger, T.G., Hernandez, L., Wang, C., Han, Z., Streicher, C., Papusheva, E., Insolera, R., Chugh, K., et al. (2014). Deterministic progenitor behavior and unitary production of neurons in the neocortex. Cell *159*, 775–788.

Garcia, G., and Reiter, J.F. (2016). A primer on the mouse basal body. Cilia *5*.

Gavériaux-Ruff, C., and Kieffer, B.L. (2007). Conditional gene targeting in the mouse nervous system: Insights into brain function and diseases. Pharmacol. Ther. *113*, 619–634.

Giardini, M.A., Segatto, M., Da Silva, M.S., Nunes, V.S., and Cano, M.I.N. (2014). Telomere and telomerase biology. In Progress in Molecular Biology and Translational Science, (Elsevier B.V.), pp. 1–40.

Gilbert, S.F. (2000). Developmental Biology (Sinauer Associates).

Gilson, E., and Géli, V. (2007). How telomeres are replicated. Nat. Rev. Mol. Cell Biol. *8*, 825–838.

Gomes, F.L.A.F., Zhang, G., Carbonell, F., Correa, J.A., Harris, W.A., Simons, B.D., and Cayouette, M. (2011). Reconstruction of rat retinal progenitor cell lineages in vitro reveals a surprising degree of stochasticity in cell fate decisions. Development *138*, 227–235.

Gomez, D.E., Armando, R.G., Farina, H.G., Menna, P.L., Cerrudo, C.S., Ghiringhelli, P.D., and Alonso, D.F. (2012). Telomere structure and telomerase in health and disease (Review). Int. J. Oncol. *41*, 1561–1569.

Gonzalez-Cano, L., Fuertes-Alvarez, S., Robledinos-Anton, N., Bizy, A., Villena-Cortes, A., Fariñas, I., Marques, M.M., and Marin, M.C. (2016). p73 is required for ependymal cell maturation and neurogenic SVZ cytoarchitecture. Dev. Neurobiol. *76*, 730–747.

Gonzalez-Suarez, I., Redwood, A.B., Perkins, S.M., Vermolen, B., Lichtensztejin, D., Grotsky, D.A., Morgado-Palacin, L., Gapud, E.J., Sleckman, B.P., Sullivan, T., et al. (2009). Novel roles for A-type lamins in telomere biology and the DNA damage response pathway. EMBO J. *28*, 2414–2427.

Gonzalez, M.A., Tachibana, K.E.K., Adams, D.J., Van Der Weyden, L., Hemberger, M., Coleman, N., Bradley, A., and Laskey, R.A. (2006). Geminin is essential to prevent endoreduplication and to form pluripotent cells during mammalian development. Genes Dev. *20*, 1880–1884.

Gorski, J.A., Talley, T., Qiu, M., Puelles, L., Rubenstein, J.L.R., and Jones, K.R. (2002). Cortical

excitatory neurons and glia, but not GABAergic neurons, are produced in the Emx1-expressing lineage. J. Neurosci. *22*, 6309–6314.

Greene, N.D.E., and Copp, A.J. (2009). Development of the vertebrate central nervous system: Formation of the neural tube. Prenat. Diagn. *29*, 303–311.

Gross, J.B., and Hanken, J. (2008). Review of fate-mapping studies of osteogenic cranial neural crest in vertebrates. Dev. Biol. *317*, 389–400.

Guemez-Gamboa, A., Coufal, N.G., and Gleeson, J.G. (2014). Primary Cilia in the Developing and Mature Brain. Neuron *82*, 511–521.

Guirao, B., Meunier, A., Mortaud, S., Aguilar, A., Corsi, J.M., Strehl, L., Hirota, Y., Desoeuvre, A., Boutin, C., Han, Y.G., et al. (2010). Coupling between hydrodynamic forces and planar cell polarity orients mammalian motile cilia. Nat. Cell Biol. *12*, 341–350.

Guruharsha, K.G., Kankel, M.W., and Artavanis-Tsakonas, S. (2012). The Notch signalling system: Recent insights into the complexity of a conserved pathway. Nat. Rev. Genet. *13*, 654–666.

Hadjieconomou, D., Rotkopf, S., Alexandre, C., Bell, D.M., Dickson, B.J., and Salecker, I. (2011). Flybow: Genetic multicolor cell labeling for neural circuit analysis in Drosophila melanogaster. Nat. Methods *8*, 260–266.

Haïk, S., Gauthier, L.R., Granotier, C., Peyrin, J.M., Lages, C.S., Dormont, D., and Boussin, F.D. (2000). Fibroblast growth factor 2 up regulates telomerase activity in neural precursor cells. Oncogene *19*, 2957–2966.

Halazonetis, T.D., Gorgoulis, V.G., and Bartek, J. (2008). An oncogene-induced DNA damage model for cancer development. Science (80-.). *319*, 1352–1355.

Hamilton, M., Gruen, J.P., and Luciano, M.G. (2016). Adult hydrocephalus. Neurosurg. Focus *41*.

Hardwick, L.J.A., Ali, F.R., Azzarelli, R., and Philpott, A. (2015). Cell cycle regulation of proliferation versus differentiation in the central nervous system. Cell Tissue Res. *359*, 187–200.

Harrington, L. (2004). Does the reservoir for self-renewal stem from the ends? Oncogene *23*, 7283–7289.

Hartwell, L.H., and Weinert, T.A. (1989). Checkpoints: Controls that ensure the order of cell cycle events. Science (80-.). *246*, 629–634.

Hasegawa, Y., Yamamoto, M., Miyamori, J., and Kanoh, J. (2019). Telomere DNA length-dependent regulation of DNA replication timing at internal late replication origins. Sci. Rep. *9*, 1–9.

Haubensak, W., Attardo, A., Denk, W., and Huttner, W.B. (2004). Neurons arise in the basal neuroepithelium of the early mammalian telencephalon: A major site of neurogenesis. Proc. Natl. Acad. Sci. U. S. A. *101*, 3196–3201.

Hauke, C., Ackermann, I., and Korr, H. (1995). Cell proliferation in the subependymal layer of the adult mouse in vivo and in vitro. Cell Prolif. *28*, 595–607.

He, H., Wang, C., Dai, Q., Li, F., Bergholz, J., Li, Z., Li, Q., and Xiao, Z.X. (2016). p53 and p73 Regulate Apoptosis but Not Cell-Cycle Progression in Mouse Embryonic Stem Cells upon DNA Damage and Differentiation. Stem Cell Reports *7*, 1087–1098.

Hemann, M.T., and Greider, C.W. (2000). Wild-derived inbred mouse strains have short telomeres. Nucleic Acids Res. *28*, 4474–4478.

Henley, S.A., and Dick, F.A. (2012). The retinoblastoma family of proteins and their regulatory functions in the mammalian cell division cycle. Cell Div. *7*.

Herbig, U., Jobling, W.A., Chen, B.P.C., Chen, D.J., and Sedivy, J.M. (2004). Telomere shortening triggers senescence of human cells through a pathway involving ATM, p53, and p21CIP1, but not p16INK4a. Mol. Cell *14*, 501–513.

Hermanson, O., Jepsen, K., and Rosenfeld, M.G. (2002). N-CoR controls differentiation of neural stem cells into astrocytes. Nature *419*, 934–939.

Hewitt, G., Jurk, D., Marques, F.D.M., Correia-Melo, C., Hardy, T., Gackowska, A., Anderson, R., Taschuk, M., Mann, J., and Passos, J.F. (2012). Telomeres are favoured targets of a persistent DNA damage response in ageing and stress-induced senescence. Nat. Commun. *3*.

Higa, M., Fujita, M., and Yoshida, K. (2017). DNA replication origins and fork progression at mammalian telomeres. Genes (Basel). *8*.

Higginbotham, H., Bielas, S., Tanaka, T., and Gleeson, J.G. (2004). Transgenic mouse line with green-fluorescent protein-labeled Centrin 2 allows visualization of the centrosome in living cells. Transgenic Res. *13*, 155–164.

Hippenmeyer, S., Youn, Y.H., Moon, H.M., Miyamichi, K., Zong, H., Wynshaw-Boris, A., and Luo, L. (2010). Genetic mosaic dissection of Lis1 and Ndel1 in neuronal migration. Neuron *68*, 695–709.

Hirota, Y., Meunier, A., Huang, S., Shimozawa, T., Yamada, O., Kida, Y.S., Inoue, M., Ito, T., Kato, H., Sakaguchi, M., et al. (2010). Planar polarity of multiciliated ependymal cells involves the anterior migration of basal bodies regulated by non-muscle myosin II. Development *137*, 3037–3046.

Hosogane, M., Bosu, L., Fukumoto, E., Yamada, H., Sato, S., and Nakayama, K. (2017). Geminin is an indispensable inhibitor of Cdt1 in mouse embryonic stem cells. Genes to Cells *22*, 360–375.

Ibañez-Tallon, I., Gorokhova, S., and Heintz, N. (2002). Loss of function of axonemal dynein Mdnah5 causes primary ciliary dyskinesia and hydrocephalus. Hum. Mol. Genet. *11*, 715–721.

Jacobs, J.J.L. (2013). Loss of Telomere Protection: Consequences and Opportunities. Front. Oncol. *3*, 88.

Jeffrey Chiang, Y., Calado, R.T., Hathcock, K.S., Lansdorp, P.M., Young, N.S., and Hodes, R.J. (2010). Telomere length is inherited with resetting of the telomere set-point. Proc. Natl. Acad. Sci. U. S. A. *107*, 10148–10153.

Jiménez, A.J., Domínguez-Pinos, M.D., Guerra, M.M., Fernández-Llebrez, P., and Pérez-Fígares, J.M. (2014). Structure and function of the ependymal barrier and diseases

associated with ependyma disruption. Tissue Barriers *2*, 1–14.

Johansson, C.B., Momma, S., Clarke, D.L., Risling, M., Lendahl, U., and Frisén, J. (1999). Identification of a neural stem cell in the adult mammalian central nervous system. Cell *96*, 25–34.

Jones, R.M., Mortusewicz, O., Afzal, I., Lorvellec, M., García, P., Helleday, T., and Petermann, E. (2013). Increased replication initiation and conflicts with transcription underlie Cyclin E-induced replication stress. Oncogene *32*, 3744–3753.

Al Jord, A., Lemaître, A.-I., Delgehyr, N., Faucourt, M., Spassky, N., and Meunier, A. (2014). Centriole amplification by mother and daughter centrioles differs in multiciliated cells. Nature *516*, 104–107.

Al Jord, A., Shihavuddin, A., Servignat d'Aout, R., Faucourt, M., Genovesio, A., Karaiskou, A., Sobczak-Thépot, J., Spassky, N., and Meunier, A. (2017). Calibrated mitotic oscillator drives motile ciliogenesis. Science (80-.). *358*, 803–806.

Jourdren, L., Bernard, M., Dillies, M.A., and Le Crom, S. (2012). Eoulsan: A cloud computing-based framework facilitating high throughput sequencing analyses. Bioinformatics *28*, 1542–1543.

Kahle, K.T., Kulkarni, A. V., Limbrick, D.D., and Warf, B.C. (2016). Hydrocephalus in children. In The Lancet, (Lancet Publishing Group), pp. 788–799.

Kaida, A., and Miura, M. (2015). Unusual prolongation of radiation-induced G2 arrest in tumor xenografts derived from HeLa cells. Cancer Sci. *106*, 1370–1376.

Katou, Y., Kanoh, Y., Bando, M., Noguchi, H., Tanaka, H., Ashikari, T., Sugimoto, K., and Shirahige, K. (2003). S-phase checkpoint proteins Tof1 and Mrc1 form a stable replication-pausing complex. Nature *424*, 1078–1083.

Kawai, H., Kawaguchi, D., Kuebrich, B.D., Kitamoto, T., Yamaguchi, M., Gotoh, Y., and Furutachi, S. (2017). Area-specific regulation of quiescent neural stem cells by Notch3 in the adult mouse subependymal zone. J. Neurosci. *37*, 11867–11880.

Kessaris, N., Fogarty, M., Iannarelli, P., Grist, M., Wegner, M., and Richardson, W.D. (2006). Competing waves of oligodendrocytes in the forebrain and postnatal elimination of an embryonic lineage. Nat. Neurosci. *9*, 173–179.

Kim, H., Kim, M., Im, S.-K., and Fang, S. (2018). Mouse Cre-LoxP system: general principles to determine tissue-specific roles of target genes. Lab. Anim. Res. *34*, 147.

Kippin, T.E., Martens, D.J., and Van Der Kooy, D. (2005). p21 loss compromises the relative quiescence of forebrain stem cell proliferation leading to exhaustion of their proliferation capacity. Genes Dev. *19*, 756–767.

Kizil, C., Kaslin, J., Kroehne, V., and Brand, M. (2012). Adult neurogenesis and brain regeneration in zebrafish. Dev. Neurobiol. *72*, 429–461.

Klutstein, M., and Cooper, J.P. (2014). The chromosomal courtship dance-homolog pairing in early meiosis. Curr. Opin. Cell Biol. *26*, 123–131.

Köhler, C., Koalick, D., Fabricius, A., Parplys, A.C., Borgmann, K., Pospiech, H., and Grosse, F.

(2016). Cdc45 is limiting for replication initiation in humans. Cell Cycle *15*, 974–985.

Kosodo, Y., Suetsugu, T., Suda, M., Mimori-Kiyosue, Y., Toida, K., Baba, S.A., Kimura, A., and Matsuzaki, F. (2011). Regulation of interkinetic nuclear migration by cell cycle-coupled active and passive mechanisms in the developing brain. EMBO J. *30*, 1690–1704.

Kriegstein, A., and Alvarez-Buylla, A. (2009). The Glial Nature of Embryonic and Adult Neural Stem Cells. Annu. Rev. Neurosci. *32*, 149–184.

Kroll, K.L. (2007). Geminin in embryonic development: Coordinating transcription and the cell cycle during differentiation. Front. Biosci. *12*, 1395–1409.

Kroll, K.L., Salic, A.N., Evans, L.M., and Kirschner, M.W. (1998). Geminin, a neuralizing molecule that demarcates the future neural plate at the onset of gastrulation. Development *125*, 3247–3258.

Kulikova, S., Abatis, M., Heng, C., and Lelievre, V. (2011). Interkinetic nuclear migration: Reciprocal activities of dynein and kinesin. Cell Adhes. Migr. *5*, 277.

Kumar, A., Pareek, V., Faiq, M.A., Ghosh, S.K., and Kumari, C. (2019). ADULT NEUROGENESIS IN HUMANS: A Review of Basic Concepts, History, Current Research, and Clinical Implications. Innov. Clin. Neurosci. *16*, 30–37.

Kyrousi, C., Arbi, M., Pilz, G.A., Pefani, D.E., Lalioti, M.E., Ninkovic, J., Götz, M., Lygerou, Z., and Taraviras, S. (2015). Mcidas and gemc1 are key regulators for the generation of multiciliated ependymal cells in the adult neurogenic niche. Dev. *142*, 3661–3674.

Lalioti, M.E., Kaplani, K., Lokka, G., Georgomanolis, T., Kyrousi, C., Dong, W., Dunbar, A., Parlapani, E., Damianidou, E., Spassky, N., et al. (2019a). GemC1 is a critical switch for neural stem cell generation in the postnatal brain. Glia *67*, 2360–2373.

Lalioti, M.E., Arbi, M., Loukas, I., Kaplani, K., Kalogeropoulou, A., Lokka, G., Kyrousi, C., Mizi, A., Georgomanolis, T., Josipovic, N., et al. (2019b). GemC1 governs multiciliogenesis through direct interaction with and transcriptional regulation of p73. J. Cell Sci. *132*.

Landais, S., D'Alterio, C., and Jones, D.L. (2014). Persistent Replicative Stress Alters Polycomb Phenotypes and Tissue Homeostasis in Drosophila melanogaster. Cell Rep. *7*, 859–870.

Lange, C., Huttner, W.B., and Calegari, F. (2009). Cdk4/CyclinD1 Overexpression in Neural Stem Cells Shortens G1, Delays Neurogenesis, and Promotes the Generation and Expansion of Basal Progenitors. Cell Stem Cell *5*, 320–331.

De Lange, T. (2005). Shelterin: The protein complex that shapes and safeguards human telomeres. Genes Dev. *19*, 2100–2110.

Lechtreck, K.-F., Delmotte, P., Robinson, M.L., Sanderson, M.J., and Witman, G.B. (2008). Mutations in Hydin impair ciliary motility in mice. J. Cell Biol. *180*, 633–643.

Lee, L. (2013). Riding the wave of ependymal cilia: Genetic susceptibility to hydrocephalus in primary ciliary dyskinesia. J. Neurosci. Res. *91*, 1117–1132.

Lee, H.W., Blasco, M.A., Gottlieb, G.J., Horner, J.W., Greider, C.W., and DePinho, R.A. (1998). Essential role of mouse telomerase in highly proliferative organs. Nature *392*, 569–574.

Lemonnier, T., Dupré, A., and Jessus, C. (2020). The G2-to-M transition from a phosphatase

perspective: A new vision of the meiotic division. Cell Div. *15*.

Levine, M., and Holland, A. (2017). Cell cycle proteins moonlight in multiciliogenesis. Science (80-.). *358*, 716–718.

Liao, H., Winkfein, R.J., Mack, G., Rattner, J.B., and Yen, T.J. (1995). CENP-F is a protein of the nuclear matrix that assembles onto kinetochores at late G2 and is rapidly degraded after mitosis. J. Cell Biol. *130*, 507–518.

Lim, D.A., and Alvarez-Buylla, A. (2016). The adult ventricular–subventricular zone (V-SVZ) and olfactory bulb (OB) neurogenesis. Cold Spring Harb. Perspect. Biol. *8*.

Lim, S., and Kaldis, P. (2013). Cdks, cyclins and CKIs: Roles beyond cell cycle regulation. Dev. *140*, 3079–3093.

Liu, B., Chen, S., Johnson, C., and Helms, J.A. (2014). A ciliopathy with hydrocephalus, isolated craniosynostosis, hypertelorism, and clefting caused by deletion of Kif3a. Reprod. Toxicol. *48*, 88–97.

Liu, B., Ma, A., Zhang, F., Wang, Y., Li, Z., Li, Q., Xu, Z., and Zheng, Y. (2016). MAZ mediates the cross-talk between CT-1 and NOTCH1 signaling during gliogenesis. Sci. Rep. *6*.

Liu, Y., Pathak, N., Kramer-Zucker, A., and Drummond, I.A. (2007). Notch signaling controls the differentiation of transporting epithelia and multiciliated cells in the zebrafish pronephros. Development *134*, 1111–1122.

Livet, J., Weissman, T.A., Kang, H., Draft, R.W., Lu, J., Bennis, R.A., Sanes, J.R., and Lichtman, J.W. (2007). Transgenic strategies for combinatorial expression of fluorescent proteins in the nervous system. Nature *450*, 56–62.

Llorens-Bobadilla, E., Zhao, S., Baser, A., Saiz-Castro, G., Zwadlo, K., and Martin-Villalba, A. (2015). Single-Cell Transcriptomics Reveals a Population of Dormant Neural Stem Cells that Become Activated upon Brain Injury. Cell Stem Cell *17*, 329–340.

Loftus, K.M., Cui, H., Coutavas, E., King, D.S., Ceravolo, A., Pereiras, D., and Solmaz, S.R. (2017). Mechanism for G2 phase-specific nuclear export of the kinetochore protein CENP-F. Cell Cycle *16*, 1414–1429.

Lois, C., and Alvarez-Buylla, A. (1994). Long-distance neuronal migration in the adult mammalian brain. Science (80-.). *264*, 1145–1148.

Longhese, M.P. (2008). DNA damage response at functional and dysfunctional telomeres. Genes Dev. *22*, 125–140.

Loulier, K., Barry, R., Mahou, P., Franc, Y. Le, Supatto, W., Matho, K.S., Ieng, S., Fouquet, S., Dupin, E., Benosman, R., et al. (2014). Multiplex Cell and Lineage Tracking with Combinatorial Labels. Neuron *81*, 505–520.

Love, M.I., Huber, W., and Anders, S. (2014). Moderated estimation of fold change and dispersion for RNA-seq data with DESeq2. Genome Biol. *15*, 550.

Lun, M.P., Johnson, M.B., Broadbelt, K.G., Watanabe, M., Kang, Y.J., Chau, K.F., Springel, M.W., Malesz, A., Sousa, A.M.M., Pletikos, M., et al. (2015). Spatially heterogeneous choroid plexus transcriptomes encode positional identity and contribute to regional CSF production.

J. Neurosci. *35*, 4903–4916.

Ma, J., Shen, Z., Yu, Y.C., and Shi, S.H. (2018). Neural lineage tracing in the mammalian brain. Curr. Opin. Neurobiol. *50*, 7–16.

Ma, L., Quigley, I., Omran, H., and Kintner, C. (2014). Multicilin drives centriole biogenesis via E2f proteins. *28*, 1461–1471.

Madisen, L., Zwingman, T.A., Sunkin, S.M., Oh, S.W., Zariwala, H.A., Gu, H., Ng, L.L., Palmiter, R.D., Hawrylycz, M.J., Jones, A.R., et al. (2010). A robust and high-throughput Cre reporting and characterization system for the whole mouse brain. Nat. Neurosci. *13*, 133–140.

Magavi, S., Friedmann, D., Banks, G., Stolfi, A., and Lois, C. (2012). Coincident generation of pyramidal neurons and protoplasmic astrocytes in neocortical columns. J. Neurosci. *32*, 4762–4772.

Magnusson, J.P., Zamboni, M., Santopolo, G., Mold, J.E., Barrientos-Somarribas, M., Talavera-Lopez, C., Andersson, B., and Frisén, J. (2020). Activation of a neural stem cell transcriptional program in parenchymal astrocytes. Elife *9*.

Mahuzier, A., Shihavuddin, A., Fournier, C., Lansade, P., Faucourt, M., Menezes, N., Meunier, A., Garfa-Traoré, M., Carlier, M.-F.F., Voituriez, R., et al. (2018). Ependymal cilia beating induces an actin network to protect centrioles against shear stress. Nat. Commun. *9*.

Malatesta, P., Hartfuss, E., and Götz, M. (2000). Isolation of radial glial cells by fluorescent-activated cell sorting reveals a neural lineage. Development *127*, 5253–5263.

Marcet, B., Chevalier, B., Luxardi, G., Coraux, C., Zaragosi, L.E., Cibois, M., Robbe-Sermesant, K., Jolly, T., Cardinaud, B., Moreilhon, C., et al. (2011). Control of vertebrate multiciliogenesis by miR-449 through direct repression of the Delta/Notch pathway. Nat. Cell Biol. *13*, 693–701.

Marín, O., and Müller, U. (2014). Lineage origins of GABAergic versus glutamatergic neurons in the neocortex. Curr. Opin. Neurobiol. *26*, 132–141.

Marion, R.M., and Blasco, M.A. (2010). Telomeres and telomerase in adult stem cells and pluripotent embryonic stem cells. Adv. Exp. Med. Biol. *695*, 118–131.

Marjanović, M., Sánchez-Huertas, C., Terré, B., Gómez, R., Scheel, J.F., Pacheco, S., Knobel, P.A., Martínez-Marchal, A., Aivio, S., Palenzuela, L., et al. (2015). CEP63 deficiency promotes p53-dependent microcephaly and reveals a role for the centrosome in meiotic recombination. Nat. Commun. *6*, 1–14.

Marqués-Torrejón, M.Á., Porlan, E., Banito, A., Gómez-Ibarlucea, E., Lopez-Contreras, A.J., Fernández-Capetillo, Ó., Vidal, A., Gil, J., Torres, J., and Fariñas, I. (2013). Cyclin-dependent kinase inhibitor p21 controls adult neural stem cell expansion by regulating Sox2 gene expression. Cell Stem Cell *12*, 88–100.

Marshall, C.B., Mays, D.J., Beeler, J.S., Rosenbluth, J.M., Boyd, K.L., Santos Guasch, G.L., Shaver, T.M., Tang, L.J., Liu, Q., Shyr, Y., et al. (2016). P73 Is Required for Multiciliogenesis and Regulates the Foxj1-Associated Gene Network. Cell Rep. *14*, 2289–2300.

Martinez, P., Thanasoula, M., Carlos, A.R., Gómez-López, G., Tejera, A.M., Schoeftner, S., Dominguez, O., Pisano, D.G., Tarsounas, M., and Blasco, M.A. (2010). Mammalian Rap1

controls telomere function and gene expression through binding to telomeric and extratelomeric sites. Nat. Cell Biol. *12*, 768–780.

Martynoga, B., Drechsel, D., and Guillemot, F. (2012). Molecular control of neurogenesis: A view from the mammalian cerebral cortex. Cold Spring Harb. Perspect. Biol. *4*, a008359.

Massagué, J. (2004). G1 cell-cycle control and cancer. Nature *432*, 298–306.

Matsui, A., Yoshida, A.C., Kubota, M., Ogawa, M., and Shimogori, T. (2011). Mouse in utero electroporation: Controlled spatiotemporal gene transfection. J. Vis. Exp. 3024.

Mazouzi, A., Velimezi, G., and Loizou, J.I. (2014). DNA replication stress: Causes, resolution and disease. Exp. Cell Res. *329*, 85–93.

McCarthy, M., Turnbull, D.H., Walsh, C.A., and Fishell, G. (2001). Telencephalic neural progenitors appear to be restricted to regional and glial fates before the onset of neurogenesis. J. Neurosci. *21*, 6772–6781.

McGarry, T.J., and Kirschner, M.W. (1998). Geminin, an inhibitor of DNA replication, is degraded during mitosis. Cell *93*, 1043–1053.

Menn, B., Bach, S., Blevins, T.L., Campbell, M., Meijer, L., and Timsit, S. (2010). Delayed Treatment with Systemic (S)-Roscovitine Provides Neuroprotection and Inhibits In Vivo CDK5 Activity Increase in Animal Stroke Models. PLoS One *5*, e12117.

Mercey, O., Al Jord, A., Rostaing, P., Mahuzier, A., Fortoul, A., Boudjema, A.R., Faucourt, M., Spassky, N., and Meunier, A. (2019a). Dynamics of centriole amplification in centrosome-depleted brain multiciliated progenitors. Sci. Rep. *9*, 1–11.

Mercey, O., Levine, M.S., LoMastro, G.M., Rostaing, P., Brotslaw, E., Gomez, V., Kumar, A., Spassky, N., Mitchell, B.J., Meunier, A., et al. (2019b). Massive centriole production can occur in the absence of deuterosomes in multiciliated cells. Nat. Cell Biol. *21*, 1544–1552.

Merkle, F.T., Tramontin, A.D., García-Verdugo, J.M., and Alvarez-Buylla, A. (2004). Radial glia give rise to adult neural stem cells in the subventricular zone. Proc. Natl. Acad. Sci. U. S. A. *101*, 17528–17532.

Merkle, F.T., Fuentealba, L.C., Sanders, T. a, Magno, L., Kessaris, N., and Alvarez-Buylla, A. (2014). Adult neural stem cells in distinct microdomains generate previously unknown interneuron types. Nat. Neurosci. *17*.

Miller, F.D., and Gauthier, A.S. (2007). Timing Is Everything: Making Neurons versus Glia in the Developing Cortex. Neuron *54*, 357–369.

Miller, I., Min, M., Yang, C., Tian, C., Gookin, S., and Spence, S.L. (2018). Ki67 is a Graded Rather than a Binary Marker of Proliferation versus Quiescence. *24*, 1105–1112.

Ming, G. li, and Song, H. (2011). Adult Neurogenesis in the Mammalian Brain: Significant Answers and Significant Questions. Neuron *70*, 687–702.

Mirzadeh, Z., Merkle, F.T., Soriano-Navarro, M., Garcia-Verdugo, J.M., and Alvarez-Buylla, A. (2008). Neural stem cells confer unique pinwheel architecture to the ventricular surface in neurogenic regions of the adult brain. Cell Stem Cell *3*, 265–278.

Mirzadeh, Z., Han, Y.G., Soriano-Navarro, M., García-Verdugo, J.M., and Alvarez-Buylla, A.

(2010). Cilia organize ependymal planar polarity. J. Neurosci. *30*, 2600–2610.

Mishra, P.K., and Teale, J.M. (2012). Transcriptome analysis of the ependymal barrier during murine neurocysticercosis. J. Neuroinflammation *9*, 733.

Mitra, J., and Enders, G.H. (2004). Cyclin A/Cdk2 complexes regulate activation of Cdk1 and Cdc25 phosphatases in human cells. Oncogene *23*, 3361–3367.

Miyata, T., Kawaguchi, A., Okano, H., and Ogawa, M. (2001). Asymmetric inheritance of radial glial fibers by cortical neurons. Neuron *31*, 727–741.

Miyata, T., Okamoto, M., Shinoda, T., and Kawaguchi, A. (2015). Interkinetic nuclear migration generates and opposes ventricular-zone crowding: Insight into tissue mechanics. Front. Cell. Neurosci. *8*, 473.

Mizutani, K.I., Yoon, K., Dang, L., Tokunaga, A., and Gaiano, N. (2007). Differential Notch signalling distinguishes neural stem cells from intermediate progenitors. Nature *449*, 351–355.

Molofsky, A.V., and Deneen, B. (2015). Astrocyte development: A Guide for the Perplexed. Glia *63*, 1320–1329.

Moore, D.L., and Jessberger, S. (2017). Creating Age Asymmetry: Consequences of Inheriting Damaged Goods in Mammalian Cells. Trends Cell Biol. *27*, 82–92.

Moore, D.L., Pilz, G.A., Arauzo-Bravo, M.J., Barral, Y., and Jessberger, S. (2015). A mechanism for the segregation of age in mammalian neural stem cells. Science (80-.). *349*, 1334–1338.

Morales, A. V., and Mira, H. (2019). Adult Neural Stem Cells: Born to Last. Front. Cell Dev. Biol. *7*, 96.

Moreno-Jiménez, E.P., Flor-García, M., Terreros-Roncal, J., Rábano, A., Cafini, F., Pallas-Bazarra, N., Ávila, J., and Llorens-Martín, M. (2019). Adult hippocampal neurogenesis is abundant in neurologically healthy subjects and drops sharply in patients with Alzheimer's disease. Nat. Med. *25*, 554–560.

Morizur, L., Chicheportiche, A., Gauthier, L.R., Daynac, M., Boussin, F.D., and Mouthon, M.A. (2018). Distinct Molecular Signatures of Quiescent and Activated Adult Neural Stem Cells Reveal Specific Interactions with Their Microenvironment. Stem Cell Reports *11*, 565–577.

MuhChyi, C., Juliandi, B., Matsuda, T., and Nakashima, K. (2013). Epigenetic regulation of neural stem cell fate during corticogenesis. Int. J. Dev. Neurosci. *31*, 424–433.

Muhr, J., and Ackerman, K.M. (2020). Embryology, Gastrulation (StatPearls Publishing).

Muthusamy, N., Vijayakumar, A., Cheng, G., and Ghashghaei, H.T. (2014). A Knock-in Foxj1CreERT2:: GFP mouse for recombination in epithelial cells with motile cilia. Genesis *52*.

Muthusamy, N., Brumm, A., Zhang, X., Carmichael, S.T., and Ghashghaei, H.T. (2018). Foxj1 expressing ependymal cells do not contribute new cells to sites of injury or stroke in the mouse forebrain. Sci. Rep. *8*, 1–9.

Myster, D.L., and Duronio, R.J. (2000). Cell cycle: To differentiate or not to differentiate? Curr. Biol. *10*, R302–R304.

Nagy, A. (2000). Cre recombinase: The universal reagent for genome tailoring. Genesis *26*, 99–109.

Nakashima, K., Yanagisawa, M., Arakawa, H., Kimura, N., Hisatsune, T., Kawabata, M., Miyazono, K., and Taga, T. (1999). Synergistic signaling in fetal brain by STAT3-Smad1 complex bridged by p300. Science *284*, 479–482.

Nakazawa, Y., Hiraki, M., Kamiya, R., and Hirono, M. (2007). SAS-6 is a Cartwheel Protein that Establishes the 9-Fold Symmetry of the Centriole. Curr. Biol. *17*, 2169–2174.

Namba, T., and Huttner, W.B. (2017). Neural progenitor cells and their role in the development and evolutionary expansion of the neocortex (John Wiley and Sons Inc.).

Negrini, S., Gorgoulis, V.G., and Halazonetis, T.D. (2010). Genomic instability an evolving hallmark of cancer. Nat. Rev. Mol. Cell Biol. *11*, 220–228.

Nery, S., Wichterle, H., and Fishell, G. (2001). Sonic hedgehog contributes to oligodendrocyte specification in the mammalian forebrain. Development *128*, 527–540.

Nieuwenhuys, R., Voogd, J., and Huijzen, C. (2008). The Human Central Nervous System. A Synopsis and Atlas (Springer Berlin Heidelberg).

Nikitin, A., Egorov, S., Daraselia, N., and Mazo, I. (2003). Pathway studio - The analysis and navigation of molecular networks. Bioinformatics *19*, 2155–2157.

Nikolopoulou, E., Galea, G.L., Rolo, A., Greene, N.D.E., and Copp, A.J. (2017). Neural tube closure: Cellular, molecular and biomechanical mechanisms. Dev. *144*, 552–566.

Nishimura, Y. V., Shinoda, T., Inaguma, Y., Ito, H., and Nagata, K.I. (2012). Application of in utero electroporation and live imaging in the analyses of neuronal migration during mouse brain development. Med. Mol. Morphol. *45*, 1–6.

Noctor, S.C., Flint, A.C., Weissman, T.A., Dammerman, R.S., and Kriegstein, A.R. (2001). Neurons derived from radial glial cells establish radial units in neocortex. Nature *409*, 714–720.

Nord, A.S., Pattabiraman, K., Visel, A., and Rubenstein, J.L.R. (2015). Genomic Perspectives of Transcriptional Regulation in Forebrain Development. Neuron *85*, 27–47.

Norden, C. (2017). Pseudostratified epithelia - cell biology, diversity and roles in organ formation at a glance. J. Cell Sci. *130*, 1859–1863.

Novo, C.L., and Londoño-Vallejo, J.A. (2013). Telomeres and the nucleus. Semin. Cancer Biol. *23*, 116–124.

Nutley, B.P., Raynaud, F.I., Wilson, S.C., Fischer, P.M., Hayes, A., Goddard, P.M., McClue, S.J., Jarman, M., Lane, D.P., and Workman, P. (2005). Metabolism and pharmacokinetics of the cyclin-dependent kinase inhibitor R-roscovitine in the mouse. Mol. Cancer Ther. *4*.

Obernier, K., and Alvarez-Buylla, A. (2019). Neural stem cells: Origin, heterogeneity and regulation in the adult mammalian brain. Dev. *146*.

Obernier, K., Cebrian-Silla, A., Thomson, M., Parraguez, J.I., Anderson, R., Guinto, C., Rodas Rodriguez, J., Garcia-Verdugo, J.M., and Alvarez-Buylla, A. (2018). Adult Neurogenesis Is Sustained by Symmetric Self-Renewal and Differentiation. Cell Stem Cell *22*, 221-234.e8.

Ogino, T., Sawada, M., Takase, H., Nakai, C., Herranz-Pérez, V., Cebrián-Silla, A., Kaneko, N., García-Verdugo, J.M., and Sawamoto, K. (2016). Characterization of multiciliated ependymal cells that emerge in the neurogenic niche of the aged zebrafish brain. J. Comp. Neurol. *524*, 2982–2992.

Ohata, S., Nakatani, J., Herranz-Pérez, V., Cheng, J.G., Belinson, H., Inubushi, T., Snider, W.D., García-Verdugo, J.M., Wynshaw-Boris, A., and Álvarez-Buylla, A. (2014). Loss of Dishevelleds Disrupts Planar Polarity in Ependymal Motile Cilia and Results in Hydrocephalus. Neuron *83*, 558–571.

Olstad, E.W., Ringers, C., Hansen, J.N., Wens, A., Brandt, C., Wachten, D., Yaksi, E., and Jurisch-Yaksi, N. (2019). Ciliary Beating Compartmentalizes Cerebrospinal Fluid Flow in the Brain and Regulates Ventricular Development. Curr. Biol. *29*, 229-241.e6.

Ortiz-Álvarez, G., Daclin, M., Shihavuddin, A., Lansade, P., Fortoul, A., Faucourt, M., Clavreul, S., Lalioti, M.E., Taraviras, S., Hippenmeyer, S., et al. (2019). Adult Neural Stem Cells and Multiciliated Ependymal Cells Share a Common Lineage Regulated by the Geminin Family Members. Neuron *102*, 159-172.e7.

Otto, T., Candido, S. V., Pilarz, M.S., Sicinska, E., Bronson, R.T., Bowden, M., Lachowicz, I.A., Mulry, K., Fassl, A., Han, R.C., et al. (2017). Cell cycle-targeting microRNAs promote differentiation by enforcing cell-cycle exit. Proc. Natl. Acad. Sci. U. S. A. *114*, 10660–10665.

Pack, L.R., Daigh, L.H., and Meyer, T. (2019). Putting the brakes on the cell cycle: mechanisms of cellular growth arrest. Curr. Opin. Cell Biol. *60*, 106–113.

Pan, Y.A., Livet, J., Sanes, J.R., Lichtman, J.W., and Schier, A.F. (2011). Multicolor brainbow imaging in Zebrafish. Cold Spring Harb. Protoc. *6*, pdb.prot5546.

Pardee, A.B. (1974). A restriction point for control of normal animal cell proliferation. Proc. Natl. Acad. Sci. U. S. A. *71*, 1286–1290.

Paridaen, J.T.M.L., Wilsch-Bräuninger, M., and Huttner, W.B. (2013). Asymmetric inheritance of centrosome-associated primary cilium membrane directs ciliogenesis after cell division. Cell *155*, 333.

Park, T.J., Mitchell, B.J., Abitua, P.B., Kintner, C., and Wallingford, J.B. (2008). Dishevelled controls apical docking and planar polarization of basal bodies in ciliated epithelial cells. Nat. Genet. *40*, 871–879.

Patmanidi, A.L., Champeris Tsaniras, S., Karamitros, D., Kyrousi, C., Lygerou, Z., and Taraviras, S. (2017). Concise Review: Geminin—A Tale of Two Tails: DNA Replication and Transcriptional/Epigenetic Regulation in Stem Cells. Stem Cells *35*, 299–310.

Patterson, E.S., Waller, L.E., and Kroll, K.L. (2014). Geminin loss causes neural tube defects through disrupted progenitor specification and neuronal differentiation. Dev. Biol. *393*, 44–56.

Pechnick, R.N., Zonis, S., Wawrowsky, K., Pourmorady, J., and Chesnokova, V. (2008). p21Cip1 restricts neuronal proliferation in the subgranular zone of the dentate gyrus of the hippocampus. Proc. Natl. Acad. Sci. U. S. A. *105*, 1358–1363.

Pefani, D.E., Dimaki, M., Spella, M., Karantzelis, N., Mitsiki, E., Kyrousi, C., Symeonidou, I.E.,

Perrakis, A., Taraviras, S., and Lygerou, Z. (2011). Idas, a novel phylogenetically conserved geminin-related protein, binds to geminin and is required for cell cycle progression. J. Biol. Chem. *286*, 23234–23246.

Perera, O.N., Sobinoff, A.P., Teber, E.T., Harman, A., Maritz, M.F., Yang, S.F., Pickett, H.A., Cesare, A.J., Arthur, J.W., MacKenzie, K.L., et al. (2019). Telomerase promotes formation of a telomere protective complex in cancer cells. Sci. Adv. *5*, eaav4409.

Petrik, D., Myoga, M.H., Grade, S., Gerkau, N.J., Pusch, M., Rose, C.R., Grothe, B., and Götz, M. (2018). Epithelial Sodium Channel Regulates Adult Neural Stem Cell Proliferation in a Flow-Dependent Manner. Cell Stem Cell *22*, 865-878.e8.

Pilaz, L.J., Patti, D., Marcy, G., Ollier, E., Pfister, S., Douglas, R.J., Betizeau, M., Gautier, E., Cortay, V., Doerflinger, N., et al. (2009). Forced G1-phase reduction alters mode of division, neuron number, and laminar phenotype in the cerebral cortex. Proc. Natl. Acad. Sci. U. S. A. *106*, 21924–21929.

Pilz, G.A., Shitamukai, A., Reillo, I., Pacary, E., Schwausch, J., Stahl, R., Ninkovic, J., Snippert, H.J., Clevers, H., Godinho, L., et al. (2013). Amplification of progenitors in the mammalian telencephalon includes a new radial glial cell type. Nat. Commun. *4*, 1–11.

Platel, J.C., and Bordey, A. (2016). The multifaceted subventricular zone astrocyte: From a metabolic and pro-neurogenic role to acting as a neural stem cell. Neuroscience *323*, 20–28.

Ponti, G., Obernier, K., Guinto, C., Jose, L., Bonfanti, L., and Alvarez-Buylla, A. (2013). Cell cycle and lineage progression of neural progenitors in the ventricular-subventricular zones of adult mice. Proc. Natl. Acad. Sci. U. S. A. *110*, E1045.

Poon, R.Y.C. (2016). Cell cycle control: A system of interlinking oscillators. Methods Mol. Biol. *1342*, 3–19.

Porlan, E., Morante-Redolat, J.M., Marqués-Torrejón, M.Á., Andreu-Agulló, C., Carneiro, C., Gómez-Ibarlucea, E., Soto, A., Vidal, A., Ferrón, S.R., and Fariñas, I. (2013). Transcriptional repression of Bmp2 by p21 Waf1/Cip1 links quiescence to neural stem cell maintenance. Nat. Neurosci. *16*, 1567–1575.

Pozo, P., and Cook, J. (2016). Regulation and Function of Cdt1; A Key Factor in Cell Proliferation and Genome Stability. Genes (Basel). *8*, 2.

Quinn, L.M., Herr, A., McGarry, T.J., and Richardson, H. (2001). The Drosophila Geminin homolog: Roles for Geminin in limiting DNA replication, in anaphase and in neurogenesis. Genes Dev. *15*, 2741–2754.

Raha, R., and Amon, A. (2008). Mitotic CDKs control the metaphase-anaphase transition and trigger spindle elongation. Genes Dev. *22*, 1534–1548.

Rakic, P. (2003). Developmental and Evolutionary Adaptations of Cortical Radial Glia Title. Cereb. Cortex *13*, 541–549.

Rallu, M., Corbin, J.G., and Fishell, G. (2002a). Parsing the prosencephalon. Nat. Rev. Neurosci. *3*, 943–951.

Rallu, M., Machold, R., Gaiano, N., Corbin, J.G., McMahon, A.P., and Fishell, G. (2002b). Dorsoventral patterning is established in the telencephalon of mutants lacking both Gli3 and

hedgehog signaling. Development *129*, 4963–4974.

Ramón y Cajal, S. (1928). Degeneration & Regeneration of the Nervous System (Oxford University Press (OUP)).

Rash, B.G., Duque, A., Morozov, Y.M., Arellano, J.I., Micali, N., and Rakic, P. (2019). Gliogenesis in the outer subventricular zone promotes enlargement and gyrification of the primate cerebrum. Proc. Natl. Acad. Sci. U. S. A. *116*, 7089–7094.

Raz, V., Vermolen, B.J., Garini, Y., Onderwater, J.J.M., Mommaas-Kienhuis, M.A., Koster, A.J., Young, I.T., Tanke, H., and Dirks, R.W. (2008). The nuclear lamina promotes telomere aggregation and centromere peripheral localization during senescence of human mesenchymal stem cells. J. Cell Sci. *121*, 4018–4028.

Redmond, S.A., Figueres-Oñate, M., Obernier, K., Nascimento, M.A., Parraguez, J.I., López-Mascaraque, L., Fuentealba, L.C., and Alvarez-Buylla, A. (2019). Development of Ependymal and Postnatal Neural Stem Cells and Their Origin from a Common Embryonic Progenitor. Cell Rep. *27*, 429-441.e3.

Rhind, N., and Russell, P. (2012). Signaling pathways that regulate cell division. Cold Spring Harb. Perspect. Biol. *4*.

Rieskamp, J.D., Denninger, J.K., and Dause, T.J. (2018). Identifying the unique role of notch3 in adult neural stem cell maintenance. J. Neurosci. *38*, 3157–3159.

Roake, C.M., and Artandi, S.E. (2017). Control of cellular aging, tissue function, and cancer by p53 downstream of telomeres. Cold Spring Harb. Perspect. Med. *7*.

Rowitch, D.H., and Kriegstein, A.R. (2010). Developmental genetics of vertebrate glial–cell specification. Nature *468*, 214–222.

Saade, M., Gonzalez-Gobartt, E., Escalona, R., Usieto, S., and Martí, E. (2017). Shh-mediated centrosomal recruitment of PKA promotes symmetric proliferative neuroepithelial cell division. Nat. Cell Biol. *19*, 493–503.

Saade, M., Blanco-Ameijeiras, J., Gonzalez-Gobartt, E., and Martı, E. (2018). A centrosomal view of cns growth. Dev. *145*.

Saito, T., and Nakatsuji, N. (2001). Efficient gene transfer into the embryonic mouse brain using in vivo electroporation. Dev. Biol. *240*, 237–246.

Sakamoto, M., Hirata, H., Ohtsuka, T., Bessho, Y., and Kageyama, R. (2003). The Basic Helix-Loop-Helix Genes Hesr1/Hey1 and Hesr2/Hey2 Regulate Maintenance of Neural Precursor Cells in the Brain. J. Biol. Chem. *278*, 44808–44815.

Saldivar, J.C., Hamperl, S., Bocek, M.J., Chung, M., Bass, T.E., Cisneros-Soberanis, F., Samejima, K., Xie, L., Paulson, J.R., Earnshaw, W.C., et al. (2018). An intrinsic S/G2 checkpoint enforced by ATR. Science (80-.). *361*, 806–810.

Samper, E., Fernández, P., Eguía, R., Martín-Rivera, L., Bernad, A., Blasco, M.A., and Aracil, M. (2002). Long-term repopulating ability of telomerase-deficient murine hematopoietic stem cells. Blood *99*, 2767–2775.

Sanai, N., Nguyen, T., Ihrie, R.A., Mirzadeh, Z., Tsai, H.H., Wong, M., Gupta, N., Berger, M.S.,

Huang, E., Garcia-Verdugo, J.M., et al. (2011). Corridors of migrating neurons in the human brain and their decline during infancy. Nature *478*, 382–386.

Sauer, F.C. (1935). Mitosis in the neural tube. J. Comp. Neurol. *62*, 377–405.

Sawamoto, K., Wichterle, H., Gonzalez-Perez, O., Cholfin, J.A., Yamada, M., Spassky, N., Murcia, N.S., Garcia-Verdugo, J.M., Marin, O., Rubenstein, J.L.R., et al. (2006). New neurons follow the flow of cerebrospinal fluid in the adult brain. Science (80-.). *311*, 629–632.

Schenk, J., Wilsch-Bräuninger, M., Calegari, F., and Huttner, W.B. (2009). Myosin II is required for interkinetic nuclear migration of neural progenitors. Proc. Natl. Acad. Sci. U. S. A. *106*, 16487–16492.

Schille, C., and Schambony, A. (2017). Signaling pathways and tissue interactions in neural plate border formation. Neurogenesis *4*, e1292783.

Schindelin, J., Arganda-Carreras, I., Frise, E., Kaynig, V., Longair, M., Pietzsch, T., Preibisch, S., Rueden, C., Saalfeld, S., Schmid, B., et al. (2012). Fiji: an open-source platform for biological-image analysis. Nat. Methods *9*, 676–682.

Schmidt, M., Rohe, A., Platzer, C., Najjar, A., Erdmann, F., and Sippl, W. (2017). Regulation of G2/M transition by inhibition of WEE1 and PKMYT1 Kinases. Molecules *22*.

Schneider, L., Pellegatta, S., Favaro, R., Pisati, F., Roncaglia, P., Testa, G., Nicolis, S.K., Finocchiaro, G., and D'Adda Di Fagagna, F. (2013). DNA damage in mammalian neural stem cells leads to astrocytic differentiation mediated by BMP2 signaling through JAK-STAT. Stem Cell Reports *1*, 123–138.

Selleck, M.A., and Stern, C.D. (1991). Fate mapping and cell lineage analysis of Hensen's node in the chick embryo. Development *112*.

Sfeir, A., Kabir, S., Van Overbeek, M., Celli, G.B., and De Lange, T. (2010). Loss of Rap1 induces telomere recombination in the absence of NHEJ or a DNA damage signal. Science (80-.). *327*, 1657–1661.

Shah, P.T., Stratton, J.A., Stykel, M.G., Abbasi, S., Sharma, S., Mayr, K.A., Koblinger, K., Whelan, P.J., and Biernaskie, J. (2018). Single-Cell Transcriptomics and Fate Mapping of Ependymal Cells Reveals an Absence of Neural Stem Cell Function. Cell *173*, 1045-1057.e9.

Shaheen, R., Sebai, M.A., Patel, N., Ewida, N., Kurdi, W., Altweijri, I., Sogaty, S., Almardawi, E., Seidahmed, M.Z., Alnemri, A., et al. (2017). The genetic landscape of familial congenital hydrocephalus. Ann. Neurol. *81*, 890–897.

Sharifi-Sanjani, M., Meeker, A.K., and Mourkioti, F. (2017). Evaluation of telomere length in human cardiac tissues using cardiac quantitative FISH. Nat. Protoc. *12*, 1855–1870.

Shay, J.W., and Wright, W.E. (2010). Telomeres and telomerase in normal and cancer stem cells. FEBS Lett. *584*, 3819–3825.

Shparberg, R., Glover, H., and Morris, M.B. (2019). Modelling mammalian commitment to the neural lineage using embryos and embryonic stem cells. Front. Physiol. *10*.

Sigl-Glöckner, J., and Brecht, M. (2017). Polyploidy and the Cellular and Areal Diversity of Rat Cortical Layer 5 Pyramidal Neurons. Cell Rep. *20*, 2575–2583.

Silbereis, J.C., Pochareddy, S., Zhu, Y., Li, M., and Sestan, N. (2016). The Cellular and Molecular Landscapes of the Developing Human Central Nervous System. Neuron *89*, 248.

Silva-Vargas, V., Maldonado-Soto, A.R., Mizrak, D., Codega, P., and Doetsch, F. (2016). Age-Dependent Niche Signals from the Choroid Plexus Regulate Adult Neural Stem Cells. Cell Stem Cell *19*, 643–652.

Siyahhan, B., Knobloch, V., De Zélicourt, D., Asgari, M., Daners, M.S., Poulikakos, D., and Kurtcuoglu, V. (2014). Flow induced by ependymal cilia dominates near-wall cerebrospinal fluid dynamics in the lateral ventricles. J. R. Soc. Interface *11*.

Sladky, V.C., Knapp, K., Soratroi, C., Heppke, J., Eichin, F., Rocamora-Reverte, L., Szabo, T.G., Bongiovanni, L., Westendorp, B., Moreno, E., et al. (2020). E2F-Family Members Engage the PIDDosome to Limit Hepatocyte Ploidy in Liver Development and Regeneration. Dev. Cell *52*, 335-349.e7.

Smith, J.S., Chen, Q., Yatsunyk, L.A., Nicoludis, J.M., Garcia, M.S., Kranaster, R., Balasubramanian, S., Monchaud, D., Teulade-Fichou, M.P., Abramowitz, L., et al. (2011). Rudimentary G-quadruplex-based telomere capping in Saccharomyces cerevisiae. Nat. Struct. Mol. Biol. *18*, 478–486.

Sobecki, M., Mrouj, K., Colinge, J., Gerbe, F., Jay, P., Krasinska, L., Dulic, V., and Fisher, D. (2017). Cell-cycle regulation accounts for variability in Ki-67 expression levels. Cancer Res. *77*, 2722–2734.

Sobecki, M., Souaid, C., Boulay, J., Guerineau, V., Noordermeer, D., and Crabbe, L. (2018). MadID, a Versatile Approach to Map Protein-DNA Interactions, Highlights Telomere-Nuclear Envelope Contact Sites in Human Cells. Cell Rep. *25*, 2891-2903.e5.

Solovei, I., Kreysing, M., Lanctôt, C., Kösem, S., Peichl, L., Cremer, T., Guck, J., and Joffe, B. (2009). Nuclear Architecture of Rod Photoreceptor Cells Adapts to Vision in Mammalian Evolution. Cell *137*, 356–368.

Song, R., Walentek, P., Sponer, N., Klimke, A., Lee, J.S., Dixon, G., Harland, R., Wan, Y., Lishko, P., Lize, M., et al. (2014). MiR-34/449 miRNAs are required for motile ciliogenesis by repressing cp110. Nature *510*, 115–120.

Sonnen, K.F., Gabryjonczyk, A.M., Anselm, E., Nigg, E.A., and Stierhof, Y.D. (2013). Human cep192 and cep152 cooperate in plk4 recruitment and centriole duplication. J. Cell Sci. *126*, 3223–3233.

Sorokin, S.P. (1968). Reconstructions of Centriole Formation and Ciliogenesis in Mammalian Lungs. J. Cell Sci. *3*.

Sorrells, S.F., Paredes, M.F., Cebrian-Silla, A., Sandoval, K., Qi, D., Kelley, K.W., James, D., Mayer, S., Chang, J., Auguste, K.I., et al. (2018). Human hippocampal neurogenesis drops sharply in children to undetectable levels in adults. Nature *555*, 377–381.

Soudet, J., Jolivet, P., and Teixeira, M.T. (2014). Elucidation of the DNA end-replication problem in saccharomyces cerevisiae. Mol. Cell *53*, 954–964.

Sousa, A.M.M., Meyer, K.A., Santpere, G., Gulden, F.O., and Sestan, N. (2017). Evolution of the Human Nervous System Function, Structure, and Development. Cell *170*, 226–247.

Spassky, N., and Meunier, A. (2017). The development and functions of multiciliated epithelia. Nat. Rev. Mol. Cell Biol. *18*, 423–436.

Spassky, N., Heydon, K., Mangatal, A., Jankovski, A., Olivier, C., Queraud-Lesaux, F., Goujet-Zalc, C., Thomas, J.L., and Zalc, B. (2001). Sonic hedgehog-dependent emergence of oligodendrocytes in the telencephalon: evidence for a source of oligodendrocytes in the olfactory bulb that is independent of PDGFRalpha signaling. Development *128*, 4993–5004.

Spassky, N., Merkle, F.T., Flames, N., Tramontin, A.D., García-Verdugo, J.M., and Alvarez-Buylla, A. (2005). Adult ependymal cells are postmitotic and are derived from radial glial cells during embryogenesis. J. Neurosci. *25*, 10–18.

Spella, M., Kyrousi, C., Kritikou, E., Stathopoulou, A., Guillemot, F., Kioussis, D., Pachnis, V., Lygerou, Z., and Taraviras, S. (2011). Geminin Regulates Cortical Progenitor Proliferation and Differentiation. Stem Cells *29*, 1269–1282.

Srinivasan, S. V., Dominguez-Sola, D., Wang, L.C., Hyrien, O., and Gautier, J. (2013). Cdc45 Is a Critical Effector of Myc-Dependent DNA Replication Stress. Cell Rep. *3*, 1629–1639.

Strzyz, P.J., Lee, H.O., Sidhaye, J., Weber, I.P., Leung, L.C., and Norden, C. (2015). Interkinetic Nuclear Migration Is Centrosome Independent and Ensures Apical Cell Division to Maintain Tissue Integrity. Dev. Cell *32*, 203–219.

Stubbs, J.L., Vladar, E.K., Axelrod, J.D., and Kintner, C. (2012). Multicilin promotes centriole assembly and ciliogenesis during multiciliate cell differentiation. Nat. Cell Biol. *14*, 140–147.

Subramanian, A., Tamayo, P., Mootha, V.K., Mukherjee, S., Ebert, B.L., Gillette, M.A., Paulovich, A., Pomeroy, S.L., Golub, T.R., Lander, E.S., et al. (2005). Gene set enrichment analysis: A knowledge-based approach for interpreting genome-wide expression profiles. Proc. Natl. Acad. Sci. U. S. A. *102*, 15545–15550.

Tabansky, I., Lenarcic, A., Draft, R.W., Loulier, K., Keskin, D.B., Rosains, J., Rivera-Feliciano, J., Lichtman, J.W., Livet, J., Stern, J.N.H., et al. (2013). Developmental bias in cleavage-stage mouse blastomeres. Curr. Biol. *23*, 21–31.

Tabata, H. (2015). Diverse subtypes of astrocytes and their development during corticogenesis. Front. Neurosci. *9*, 114.

Tabata, H., and Nakajima, K. (2001). Efficient in utero gene transfer system to the developing mouse brain using electroporation: Visualization of neuronal migration in the developing cortex. Neuroscience *103*, 865–872.

Tachibana, K.K., Gonzalez, M.A., Guarguaglini, G., Nigg, E.A., and Laskey, R.A. (2005). Depletion of licensing inhibitor geminin causes centrosome overduplication and mitotic defects. EMBO Rep. *6*, 1052–1057.

Takai, H., Smogorzewska, A., and De Lange, T. (2003). DNA damage foci at dysfunctional telomeres. Curr. Biol. *13*, 1549–1556.

Tamamaki, N., Nakamura, K., Okamoto, K., and Kaneko, T. (2001). Radial glia is a progenitor of neocortical neurons in the developing cerebral cortex. Neurosci. Res. *41*, 51–60.

Tatsumi, K., Isonishi, A., Yamasaki, M., Kawabe, Y., Morita-Takemura, S., Nakahara, K., Terada, Y., Shinjo, T., Okuda, H., Tanaka, T., et al. (2018). Olig2-Lineage astrocytes: A distinct

subtype of astrocytes that differs from GFAP astrocytes. Front. Neuroanat. *12*.

Taulman, P.D., Haycraft, C.J., Balkovetz, D.F., and Yoder, B.K. (2001). Polaris, a protein involved in left-right axis patterning, localizes to basal bodies and cilia. Mol. Biol. Cell *12*, 589–599.

Taverna, E., Götz, M., and Huttner, W.B. (2014). The Cell Biology of Neurogenesis: Toward an Understanding of the Development and Evolution of the Neocortex. Annu. Rev. Cell Dev. Biol. *30*, 465–502.

Tekki-Kessaris, N., Woodruff, R., Hall, A.C., Gaffield, W., Kimura, S., Stiles, C.D., Rowitch, D.H., and Richardson, W.D. (2001). Hedgehog-dependent oligodendrocyte lineage specification in the telencephalon. Development *128*, 2545–2554.

Terré, B., Piergiovanni, G., Segura-Bayona, S., Gil-Gómez, G., Youssef, S.A., Attolini, C.S., Wilsch-Bräuninger, M., Jung, C., Rojas, A.M., Marjanović, M., et al. (2016). GEMC 1 is a critical regulator of multiciliated cell differentiation . EMBO J. *35*, 942–960.

Terré, B., Lewis, M., Gil-Gómez, G., Han, Z., Lu, H., Aguilera, M., Prats, N., Roy, S., Zhao, H., and Stracker, T.H. (2019). Defects in efferent duct multiciliogenesis underlie male infertility in GEMC1-, MCIDAS- or CCNO-deficient mice. Dev. *146*.

Tien, A.C., Tsai, H.H., Molofsky, A. V., McMahon, M., Foo, L.C., Kaul, A., Dougherty, J.D., Heintz, N., Gutmann, D.H., Barres, B.A., et al. (2012). Regulated temporal-spatial astrocyte precursor cell proliferation involves BRAF signalling in mammalian spinal cord. Dev. *139*, 2477–2487.

Tomás-Loba, A., Flores, I., Fernández-Marcos, P.J., Cayuela, M.L., Maraver, A., Tejera, A., Borrás, C., Matheu, A., Klatt, P., Flores, J.M., et al. (2008). Telomerase Reverse Transcriptase Delays Aging in Cancer-Resistant Mice. Cell *135*, 609–622.

Tramontin, A.D., García-Verdugo, J.M., Lim, D.A., and Álvarez-Buylla, A. (2003). Postnatal Development of Radial Glia and the Ventricular Zone (VZ): a Continuum of the Neural Stem Cell Compartment. Cereb. Cortex *13*, 580–587.

Tsai, H.-H., Li, H., Fuentealba, L.C., Molofsky, A. V, Taveira-Marques, R., Zhuang, H., Tenney, A., Murnen, A.T., Fancy, S.P.J., Merkle, F., et al. (2012). Regional astrocyte allocation regulates CNS synaptogenesis and repair. Science *337*, 358–362.

Tsai, J.W., Lian, W.N., Kemal, S., Kriegstein, A.R., and Vallee, R.B. (2010). Kinesin 3 and cytoplasmic dynein mediate interkinetic nuclear migration in neural stem cells. Nat. Neurosci. *13*, 1463–1472.

Turner, D.L., and Cepko, C.L. (1988). A common progenitor for neurons and glia persists in rat retina late in development. Nature *328*, 131–136.

Ullah, Z., Lee, C.Y., Lilly, M.A., and DePamphilis, M.L. (2009). Developmentally programmed endoreduplication in animals. Cell Cycle *8*, 1501–1509.

Urist, M., Tanaka, T., Poyurovsky, M. V., and Prives, C. (2004). p73 induction after DNA damage is regulated by checkpoint kinases Chk1 and Chk2. Genes Dev. *18*, 3041–3054.

Valny, M., Honsa, P., Kirdajova, D., Kamenik, Z., and Anderova, M. (2016). Tamoxifen in the mouse brain: Implications for fate-mapping studies using the tamoxifen-inducible cre-loxP

system. Front. Cell. Neurosci. *10*.

Varela, E., Muñoz-Lorente, M.A., Tejera, A.M., Ortega, S., and Blasco, M.A. (2016). Generation of mice with longer and better preserved telomeres in the absence of genetic manipulations. Nat. Commun. *7*, 1–16.

Vazquez-Villaseñor, I., Garwood, C.J., Heath, P.R., Simpson, J.E., Ince, P.G., and Wharton, S.B. (2020). Expression of p16 and p21 in the frontal association cortex of ALS/MND brains suggests neuronal cell cycle dysregulation and astrocyte senescence in early stages of the disease. Neuropathol. Appl. Neurobiol. *46*, 171–185.

Venkei, Z.G., and Yamashita, Y.M. (2018). Emerging mechanisms of asymmetric stem cell division. J. Cell Biol. *217*, 3785–3795.

Verkhratsky, A., Rodríguez, J.J., and Parpura, V. (2014). Neuroglia in ageing and disease. Cell Tissue Res. *357*, 493–503.

Viñals, F., Reiriz, J., Ambrosio, S., Bartrons, R., Rosa, J.L., and Ventura, F. (2004). BMP-2 decreases Mash1 stability by increasing Id1 expression. EMBO J. *23*, 3527–3537.

Vinchon, M., Rekate, H., and Kulkarni, A. V. (2012). Pediatric hydrocephalus outcomes: a review. Fluids Barriers CNS *9*, 18.

Vladar, E.K., Stratton, M.B., Saal, M.L., Salazar-De Simone, G., Wang, X., Wolgemuth, D., Stearns, T., and Axelrod, J.D. (2018). Cyclin-dependent kinase control of motile ciliogenesis. Elife *7*.

Voronina, V.A., Takemaru, K.I., Treuting, P., Love, D., Grubb, B.R., Hajjar, A.M., Adams, A., Li, F.Q., and Moon, R.T. (2009). Inactivation of Chibby affects function of motile airway cilia. J. Cell Biol. *185*, 225–233.

Wahid, F., Shehzad, A., Khan, T., and Kim, Y.Y. (2010). MicroRNAs: Synthesis, mechanism, function, and recent clinical trials. Biochim. Biophys. Acta - Mol. Cell Res. *1803*, 1231–1243.

Wallingford, J.B. (2010). Planar cell polarity signaling, cilia and polarized ciliary beating. Curr. Opin. Cell Biol. *22*, 597–604.

Walsh, C., and Cepko, C.L. (1992). Widespread dispersion of neuronal clones across functional regions of the cerebral cortex. Science (80-.). *255*, 434–440.

Wang, C., and Mei, L. (2013). In Utero Electroporation in Mice. In Methods in Molecular Biology (Clifton, N.J.), (Methods Mol Biol), pp. 151–163.

Wang, D.D., and Bordey, A. (2008). The astrocyte odyssey. Prog. Neurobiol. *86*, 342–367.

Weisblat, D.A., Sawyer, R.T., and Stent, G.S. (1978). Cell lineage analysis by intracellular injection of a tracer enzyme. Science (80-.). *202*, 1295–1298.

Wellinger, R.J. (2014). In the end, what's the problem? Mol. Cell *53*, 855–856.

Wilsch-Bräuninger, M., Florio, M., and Huttner, W.B. (2016). Neocortex expansion in development and evolution - from cell biology to single genes. Curr. Opin. Neurobiol. *39*, 122–132.

Winey, M., and O'Toole, E. (2014). Centriole structure. Philos. Trans. R. Soc. B Biol. Sci. *369*.

Wohlschlegel, J.A., Dwyer, B.T., Dhar, S.K., Cvetic, C., Walter, J.C., and Dutta, A. (2000). Inhibition of eukaryotic DNA replication by geminin binding to Cdt1. Science (80-.). *290*, 2309–2312.

Woodruff, J.B., Wueseke, O., and Hyman, A.A. (2014). Pericentriolar material structure and dynamics. Philos. Trans. R. Soc. B Biol. Sci. *369*.

Worthington, W.C., and Cathcart, R.S. (1963). Ependymal cilia: Distribution and activity in the adult human brain. Science (80-.). *139*, 221–222.

Wright, W., Piatyszek, M., Rainey, W., Byrd, W., and Shay, J. (1996). Telomerase Activity in Human Germline and Embryonic Tissues and Cells. Dev. Genet. *18*.

Wu, J., Bao, J., Kim, M., Yuan, S., Tang, C., Zheng, H., Mastick, G.S., Xu, C., and Yan, W. (2014). Two miRNA clusters, miR-34b/c and miR-449, are essential for normal brain development, motile ciliogenesis, and spermatogenesis. Proc. Natl. Acad. Sci. U. S. A. *111*.

Wu, P., Takai, H., and De Lange, T. (2012). Telomeric 3' overhangs derive from resection by Exo1 and apollo and fill-in by POT1b-associated CST. Cell *150*, 39–52.

Wynford-Thomas, D., and Kipling, D. (1997). The end-replication problem. Nature *389*, 551–551.

Xu, Q., Tam, M., and Anderson, S.A. (2008). Fate mapping Nkx2.1-lineage cells in the mouse telencephalon. J. Comp. Neurol. *506*, 16–29.

Yanagisawa, M., Takizawa, T., Ochiai, W., Uemura, A., Nakashima, K., and Taga, T. (2001). Fate alteration of neuroepithelial cells from neurogenesis to astrocytogenesis by bone morphogenetic proteins. Neurosci. Res. *41*, 391–396.

Yao, G., Lee, T.J., Mori, S., Nevins, J.R., and You, L. (2008). A bistable Rb-E2F switch underlies the restriction point. Nat. Cell Biol. *10*, 476–482.

Yoon, M.K., Ha, J.H., Lee, M.S., and Chi, S.W. (2015). Structure and apoptotic function of p73. BMB Rep. *48*, 81–90.

Young, K.M., Fogarty, M., Kessaris, N., and Richardson, W.D. (2007). Subventricular zone stem cells are heterogeneous with respect to their embryonic origins and neurogenic fates in the adult olfactory bulb. J. Neurosci. *27*, 8286–8296.

Zambrowicz, B.P., Imamoto, A., Fiering, S., Herzenberg, L.A., Kerr, W.G., and Soriano, P. (1997). Disruption of overlapping transcripts in the ROSA βgeo 26 gene trap strain leads to widespread expression of β-galactosidase in mouse embryos and hematopoietic cells. Proc. Natl. Acad. Sci. U. S. A. *94*, 3789–3794.

Zeman, M.K., and Cimprich, K.A. (2014). Causes and consequences of replication stress. Nat. Cell Biol. *16*, 2–9.

Zhang, S., and Mitchell, B.J. (2015). Centriole biogenesis and function in multiciliated cells. Methods Cell Biol. *129*, 103–127.

Zhang, P., Wong, C., Liu, D., Finegold, M., Harper, J.W., and Elledge, S.J. (1999). p21(CIP1) and p57(KIP2) control muscle differentiation at the myogenin step. Genes Dev. *13*, 213–224.

Zhao, C., Suh, H., and Gage, F.H. (2009). Notch keeps ependymal cells in line. Nat. Neurosci.

12, 243–245.

Zhao, H., Zhu, L., Zhu, Y., Cao, J., Li, S., Huang, Q., Xu, T., Huang, X., Yan, X., and Zhu, X. (2013). The cep63 paralogue deup1 enables massive de novo centriole biogenesis for vertebrate multiciliogenesis. Nat. Cell Biol. *15*, 1434–1444.

Zhou, F., Narasimhan, V., Shboul, M., Chong, Y.L., Reversade, B., and Roy, S. (2015). Gmnc Is a Master Regulator of the Multiciliated Cell Differentiation Program. Curr. Biol. *25*, 3267–3273.

Zhu, L., Liu, H., Chen, Y., Yan, X., and Zhu, X. (2019). Rsph9 is critical for ciliary radial spoke assembly and central pair microtubule stability. Biol. Cell *111*, 29–38.

Zimmermann, S., and Martens, U.M. (2008). Telomeres, senescence, and hematopoietic stem cells. Cell Tissue Res. *331*, 79–90.

Zong, H., Espinosa, J.S., Su, H.H., Muzumdar, M.D., and Luo, L. (2005). Mosaic analysis with double markers in mice. Cell *121*, 479–492.

Annex I - Invited review for

Current Opinion in Neurobiology:

One progenitor to generate them all: plasticity in the glial lineage

Submitted. Revision pending.

Issue 66 - Expected publication date: February 2021

One progenitor to generate them all: plasticity in the glial lineage

Gonzalo Ortiz-Álvarez[1] and Nathalie Spassky[1]*

[1] Institut de Biologie de l'Ecole Normale Supérieure (IBENS), Ecole Normale Supérieure, CNRS UMR8197, INSERM U1024, PSL Université Paris, 75005 Paris, France

*Corresponding author:

Nathalie Spassky

Cilia biology and neurogenesis

Ecole Normale Supérieure

46, rue d'Ulm – 75005

Paris, FRANCE

nathalie.spassky@bio.ens.psl.eu

Abstract

The past two decades have allowed to leave behind the old conception of early fate-restricted glial progenitors. The new paradigm is that of a more plastic brain, where common progenitors undergo a process of progressive competence restriction, in the neurogenesis to gliogenesis switch, but also in the generation of different glial cells and adult neurogenesis. The mechanisms that establish brain cell diversity, or the heterogeneity within a single population, are starting to be elucidated. The role of cell cycle regulators and dynamics and asymmetric repartition of cell cargoes during cell division are gaining more and more attention. The unraveling of such mechanisms could have a big impact on therapeutic solutions for brain malignancies, from amyotrophic lateral sclerosis to neurodegenerative disorders.

Highlights

- Adult NSCs are transcriptionally heterogeneous, ranging from quiescent to activated.
- Proof of human adult neurogenesis has been found, but remains a subject of debate.
- CNS glial progenitors are plastic and not cell-type specific.
- Cell cycle progression and arrest actors regulate fate determination.
- Asymmetric inheritance of cellular components can control cell fate.

Keywords: Glia, Adult neural stem cell, Multiciliated ependymal cell, Plasticity, Cell division

Abbreviations

SVZ: Subventricular Zone; **OB**: Olfactory Bulb; **NSC**: Neural Stem Cell; **RGC**: Radial Glial Cell; **CNS**: Central Nervous System; **SGZ:** Subgranular Zone; **aNSC**: Active Neural Stem Cell; **qNSC**: Quiescent Neural Stem Cell; **DCX**: Doublecortin; **MADM**: Mosaic Analysis with Double Markers; **GFAP**: Glial Fibrillary Acidic Protein; **CKI**: Cyclin-dependent Kinase Inhibitors.

INTRODUCTION

The adult mammalian brain was long considered devoid of neuronal regeneration (Ramón y Cajal, 1928), until the 1960s, when a migratory stream of cells from the subventricular zone (SVZ) of the lateral ventricle to the olfactory bulb (OB) was observed in rodents (Altman, 1969). This was the first milestone of adult neurogenesis, this is, the formation of neurons *de novo*. However, it was not until the end of the 1990s that the identity of the adult neural stem cell (NSC) was revealed. These, which are now called B1 cells, form an astroglial population that were from then on appointed as the primary adult NSCs of the SVZ neurogenic niche (Doetsch et al., 1999a, 1999b). In 1998, human cancer patients that had received BrdU for diagnostic purposes provided the first proof for adult human neurogenesis (Eriksson et al., 1998). These discoveries led to a paradigm shift: the adult brain is now considered much more plastic than it was a hundred years ago.

Radial Glial Cells (RGCs) generate both neurons and glia (Malatesta et al., 2000). At the turn of this century, neuron and glia-restricted progenitors were thought to exist. Since gliogenesis follows neurogenesis, glial progenitors were thought to remain inactive during neurogenesis, until the time came to generate glial cells (Costa et al., 2009). Nonetheless, we will discuss here that cell type-restricted progenitors are not the rule in the developing central nervous system (CNS). Instead, plastic progenitors progressively acquire more limited potential until they differentiate in one cell type. We will take a particular focus on the generation of neurons from a particular set of glia, adult NSCs, their heterogeneity and controversial existence of this process in the adult human. We will then discuss the plastic glial cell lineage and the mechanisms that specify it.

Glial cell lineage. Plasticity of glial progenitors

During embryogenesis, firstly only neurons are formed from one progenitor in “quanta” of 8 to 9 neurons through asymmetric divisions. Then, at the end of these rounds of divisions, one in six RGCs generate glia [8●●]. Furthermore, this study confirmed using Mosaic Analysis with Double Markers (MADM) that glia were contained within neurogenic clones, implying that the first were born after a series of neurogenic divisions (Figure 1A) [8●●]. This work helps to settle, since the discovery that RGCs generate both neurons and glia, that some forebrain progenitors are plastic, as opposed to the previous paradigm that stated there are

neuron and glia-restricted progenitors. In order to find glia-restricted RGCs, later developmental stages must be assessed. However, these come from the asymmetric self-renewing cell divisions that earlier on generated neuron precursors (Costa et al., 2009).

Retroviral bar-coding has revealed that B1 cell-precursors diverge from the other forebrain cell lineages during mid-gestation (E13-E15). Then remain largely quiescent until their reactivation during the adult life [9●]. This is also roughly the time when most ependymal progenitors divide for the last time (Spassky et al., 2005). State-of-the art clonal analysis techniques, such as *Brainbow*, MADM and StarTrack have shown that adult NSCs and multiciliated ependymal cells belong to the same lineage and can arise from either symmetrical divisions or asymmetrical divisions yielding an ependymal and a B1 sister cells (Figure 1A) [11●●], [12].

Oligodendrocytes and astrocytes other than B1 cells come from a rather plastic group of progenitors. Astrocytes are classified in two groups: protoplasmic astrocytes of the grey matter with highly branched bushy processes and low or absent expression of glial fibrillary acidic protein (GFAP), and fibrous astrocytes with straight long processes, mainly located in the white matter and higher expression of GFAP (Tabata, 2015). Interestingly, neonatal birth of both types of astrocytes has been associated to Olig2-expressing precursors (Figure 1A) [14●], [15]. Olig2 is a transcription factor expressed in glial progenitors and, although downregulated in mature astrocytes, it is present in differentiated oligodendrocytes. Therefore, oligodendrocytes and, seemingly, both kinds of astrocytes, share a common lineage in the neonatal brain (Tabata, 2015). An apparently contradictory study showed that fibrous astrocytes arise from progenitors different from protoplasmic astrocyte Olig2+ progenitors. They show how GFAP+ and Olig2+-derived astrocytes colonize mutually exclusive brain territories. However, they observe this from the eleventh postnatal week (Tatsumi et al., 2018). Protoplasmic and fibrous astrocytes, along with oligodendrocytes, could share a common lineage in neonatal stages, but in the adult, both lineages diverge, into a fibrous astrocyte precursor lineage and a protoplasmic astrocyte/oligodendrocyte lineage. To contribute even further to the hypothesis of plastic glial precursors, *Brainbow* labeling of RGCs *in utero* revealed that most GFAP+ pial astrocytes derive from the same progenitor as protoplasmic astrocytes (Figure 1A) [14●]. Furthermore, single-cell transcriptomics and fate mapping have demonstrated that striatal parenchymal astrocytes act as a reservoir of

neuroblasts upon stroke-mimicking Notch inhibition and mitogen activation, following a neurogenesis activation program that closely resembles that of adult NSCs in the SVZ (Magnusson et al., 2020).

The mammalian neurogenic niche and adult neurogenesis

Ependymal and B1 cells, along with its related lineage of neuronal-committed transit-amplifying cells (C cells) and migrating neuroblasts (A cells), form one of the two neurogenic niches of the adult mammalian brain. Ependymal cells project several dozens of motile cilia, nucleated by one basal body each, a modified centriole. B1 cells present small apical contacts from which they project a single primary cilium (Mirzadeh et al., 2008), a necessary component of adult neurogenesis and cognitive functions, as it was shown in the subgranular zone (SGZ) of the dentate gyrus of the hippocampus, the other neurogenic niche in the adult brain (Guemez-Gamboa et al., 2014). In the SVZ, these two very different cell types are tightly associated physically (Mirzadeh et al., 2008) and functionally (Petrik et al., 2018; Sawamoto et al., 2006). Ependymal cell ciliary beating directly contributes to adult neurogenesis, for instance, by either increasing the cerebrospinal fluid circulation, which enhances B1 cell proliferation by opening epithelium sodium channels expressed on their surface (Petrik et al., 2018) or by guiding newborn neurons to the OB (Sawamoto et al., 2006).

The current consensus is that ependymal cells are postmitotic (Spassky et al., 2005), although it was claimed that they can generate neuroblasts, upon a stroke, or inhibition of their constitutive Notch expression (Carlén et al., 2009). A more recent report has assessed different models of stroke induction and found, via fate mapping, some contribution of ependymal-derived neurons to the OB. However, they claim this contribution to be very low and attribute the extensive presence of ependymal-derived neurons in other studies to ectopic expression from the used ependymal promoter-driving Cre transgenic line (Muthusamy et al., 2018). Other current findings determine that they do not proliferate *in vitro*, or *in vivo*, after induction of a hemorrhagic stroke. Furthermore, single-cell RNA-sequencing establishes a very distinct transcriptome that clusters ependymal cells away from the adult NSC lineage (Shah et al., 2018). Thus, the plasticity of ependymal cells upon brain injury remains debated.

Adult neurogenesis seems then, mostly maintained by B1 cells (reviewed in (Lim and Alvarez-Buylla, 2016)). Recently, it was described that 80% of B1 cells undergo symmetric consumptive divisions to generate two C cells, whereas the other cells perform symmetric proliferative divisions to maintain the stem cell pool (Figure 1B) (Basak et al., 2018). Consequently, B1 cell density and adult neurogenesis decrease significantly with age [27●●]. The exact mechanisms that exhaust this proliferative capacity are not yet fully understood, but interesting reports suggest that telomerase expression decline with age and consequent telomere shortening lead to the impairment of B1 cell proliferation, as well as improper neuronal differentiation (Ferrón et al., 2004, 2009).

Molecular heterogeneity of adult NSCs

Interestingly, B1 cells do not form a homogeneous population (Merkle et al., 2014; Obernier and Alvarez-Buylla, 2019). RNA-sequencing has evidenced that they exist as active or quiescent cells (aNSCs and qNSCs, respectively). Actually, in the quiescence to the activation and differentiation continuum, four subtypes of NSCs exist based on their different transcriptome, from a dormant quiescent to a primed quiescent state, followed by two aNSCs states, which primarily differ in the expression of mitotic genes [26], [32●●]. The transition from dormancy to differentiation is characterized by a shift in cell metabolism. In this way, B1 cells are enriched in lipid synthesis, compared to neuroblasts, glycolysis genes are more highly expressed in qNSCs than aNSCs and neuroblasts, and protein anabolism is more active in aNSCs than qNSCs (Figure 1B) [32●●]. Another group has confirmed that the latter is a key activity in dormancy exit. Besides, it seems that the regulation of the transition from aNSC to a neuroblast is regulated at the protein translation level, rather than the transcriptional one. Consequently, neuroblasts and mature neurons display high levels of post-transcriptional repression of stemness factors such as Sox2. This transcription factor, for instance, displays similar levels of mRNA expression in NSCs and neuroblasts, but the Sox2 protein is absent in the latter. In this post-transcriptional regulation, mTORC1 signaling plays a crucial role and it is necessary to enter the primed qNSC state and differentiate (Baser et al., 2019).

Adult neurogenesis in humans

Migrating immature neurons have been recently identified with cell markers like doublecortin (DCX) and the proliferation marker Ki67 was observed in the SVZ and SGZ of

infants. However, these were undetectable in older children [34], [35●],[36] Nonetheless, others have reported the presence of unchanged adult neurogenesis in the SGZ until the tenth decade of life, using the same marker DCX, among others [37], [38●●].

These publications evidence the difficulty of performing studies in human adult tissues, due to the rare optimum brain tissue availability, the handling of post-mortem samples and the lack of noninvasive research methods (Kumar et al., 2019). A thorough report that evaluates the impact of fixation and pre-immunostaining treatments insists on the importance of assessing differences in antibody sensitivity in immunohistochemistry studies, tissue handling or post-mortem delay to produce robust data (Flor-García et al., 2020).

Mechanisms of glial and neuronal cell specification

The balance between B1 and ependymal glial cells is controlled by Geminin and GemC1 (Figure 1A) [11●●]. The former favors a B1 fate and its loss has been linked to the presence of supernumerary centrioles (Tachibana et al., 2005), whereas the later induces an ependymal fate [11●●], [42], characterized by massive centriole amplification, in the presence of a dampened mitotic machinery (Al Jord et al., 2017). GemC1 knockout rodent models display hydrocephalus due to the complete lack of multiciliated ependymal cells and die prematurely (Arbi et al., 2016; Terré et al., 2016). The mechanisms by which Geminin and GemC1 favor one fate or the other remain unsolved but, interestingly, both have a well-defined role in DNA replication licensing. Whereas Geminin acts as a halt to replication firing to avoid endoreplication (Wohlschlegel et al., 2000), GemC1 has been described as a necessary factor to initiate DNA replication (Balestrini et al., 2010). It is intriguing, however, that DNA replication regulators would have a role in cell fate choice, and it is possible that both functions are related. After all, cell cycle progression markers have been implicated in multiciliated cell differentiation (Al Jord et al., 2017; Vladar et al., 2018) and neuronal differentiation (Hardwick et al., 2015).

GemC1 upstream mechanisms remain partially unknown in the brain. It has been shown that Notch can impede the GemC1-dependent multiciliation program (Kyrousi et al., 2015) and neuronal differentiation, helping maintain the RGC state (Gaiano et al., 2000; Kyrousi et al., 2015). The family of micro-RNAs miR-34/449 is involved in Notch inhibition and, consequently, multiciliation promotion, in human airway mucociliary epithelial cell culture or

Xenopus embryonic epidermis (Figure 1A) (Marcet et al., 2011). Furthermore, although not yet implicated in embryonic B1 cell specification, Notch signaling is necessary for both qNSC maintenance and aNSC proliferation (Figure 1B) (Kawai et al., 2017; Rieskamp et al., 2018). Notch can determinate different cell fates in adjacent cells that end up adopting different morphologies via this cell-cell crosstalk-signaling pathway, where one cell expresses the ligand and, the other, the Notch receptor (Chitnis and Bally-Cuif, 2016). Hence, the idea that it could play a role in the determination of the B1 versus ependymal fate, two physically contacting cells in the neuroepithelium, is certainly appealing (Figure 1A).

The elucidation of the balance of these two cell types could certainly shed some light into the disease mechanisms of neurodegenerative disorders or CNS aggressive tumors. Ependymal cells seem to be the proliferative endpoint of a subset of RGCs, since the bulk of ependymal cells is born after the bulk of B1 cells, and symmetric B1-generating divisions precede ependymal-generating ones [11●●]. The fate divergence between two such distinct cell types, one postmitotic, one proliferative, could be related to a difference in telomere maintenance or damage (Figure 1A). Curiously, telomere attrition or protection have been related to the decrease in adult NSC proliferation observed with age, or the proliferation of glioblastomas, respectively (Bejarano et al., 2017; Ferrón et al., 2004).

Cyclin-dependent kinase inhibitors (CKI) play a pivotal role in development. B1 cell progenitors slow down their cell cycle via upregulation of p57 in the embryo to enter quiescence (Figure 1A) [57●]. Other CKIs, like p27 and p21 have also been implicated in the regulation of neuronal progenitor cell cycle exit, during embryonic corticogenesis or adult neurogenesis (Clément et al., 2017; Pechnick et al., 2008). It is thus an interesting idea that a specific combination of CKIs could drive glial specification in the neurogenic niche, or other regions of the brain (Figure 1A). The mechanisms and consequences of CKI expression are of high interest, not only because they can determine fate during development (Zhang et al., 1999), but also because proteins like p16 or p21 cause cell cycle dysregulation in response to DNA damage in early stages of CNS diseases, like amyotrophic lateral sclerosis (Vazquez-Villaseñor et al., 2020).

In relation to cell division pattern and cell cycle regulation, the “cell cycle length” hypothesis is an interesting theory. It establishes that the length of the cell cycle, particularly of the G1 phase, is determinant for differentiation. According to it, a prolonged G1 would

allow the accumulation of differentiation-driving factors. Indeed, during mouse corticogenesis, there is a correlation between differentiative neurogenic divisions and cell cycle deceleration due to G1 lengthening. On the other end, a short G1 is associated with proliferative divisions (Dehay and Kennedy, 2007; Hardwick et al., 2015). CyclinD1-CDK4/6 was over-expressed or knocked-down via *in utero* electroporation. The former decreased cell cycle length through G1 shortening and maintained basal progenitors in a cycling state, via promotion of self-renewing proliferative divisions (Pilaz et al., 2009) and inhibited neurogenesis (Lange et al., 2009). The latter had the opposite effect (Figure 1A) (Lange et al., 2009). The relation between cell cycle length and gliogenesis has not been as extensively studied as in neurogenesis. Nonetheless, it is plausible that gliogenic divisions are also affected by cell cycle dynamics (Figure 1A).

The precise balance between symmetric and asymmetric divisions is crucial for the correct development of an organ, including the brain. A neurodevelopmental disorder known as microcephaly, characterized by a small CNS at birth and intellectual disability, is a direct consequence of the deregulation of the correct amount and type of cell divisions during embryogenesis and, among the disease-associated mutations, there are genes involved in DNA damage and repair or centrosomal proteins (Marjanović et al., 2015). The asymmetric repartition of certain fate determinants between the two daughter cells is an area of intense research. For instance, the centrosome has gained significant interest in this respect. The semiconservative duplication of the centrosome leads to one cell inheriting the older “mother” centriole, whereas the other receives the younger “daughter” centriole, each of which paired with a newly-synthetized centriole. It has been shown in the developing mouse cortex and chick neural tube that the cell bearing the mother centriole is the one that keeps the stem cell characteristics, whereas the one that receives the daughter one become a prospective neuron and differentiates (Saade et al., 2018). This is due to the presence of an asymmetry of centriole-associated proteins between mother and daughter centrioles, which has consequences in cell signaling or primary cilium assembly, both key factors for RGC division (Figure 1A) (Paridaen et al., 2013; Saade et al., 2017).

Other cellular components that have been implicated in asymmetric divisions are the genome, mitochondria or damaged or misfolded proteins. The immortal strand hypothesis is an interesting theory that suggests that DNA sister chromatids are not segregated randomly.

The older (immortal) strand is preferentially passed on to the self-renewing daughter cell, to avoid the inheritance of replication errors in the cell that further divides and, thus, circumvent genomic instability. However, this might not be true for all stem cells and it is not devoid of controversy (Moore and Jessberger, 2017; Venkei and Yamashita, 2018). Finally, segregation of misfolded or damaged proteins into the differentiating daughter cell has been thought to improve fitness of the self-renewing cell. Interestingly, ubiquitinated proteins, a marker for damaged peptides targeted for degradation, are distributed asymmetrically upon cell division in adult NSCs, due to the presence of a diffusion barrier, whose existence has also been confirmed in RGCs (Figure 1B) [71●●]. Although asymmetric cell divisions are highly common in the developing CNS, B1 cells divide symmetrically in consuming or proliferative divisions [27●●]. It would be of great value to assess whether segregation of damaged proteins during B1 cell-generating symmetric divisions primes the one with the damaged cargo to perform successive consumptive divisions.

Conclusion

Plastic embryonic and adult brain progenitors can be of potential impact in regenerative therapeutic approaches to treat brain diseases characterized by the decay of specific cell types. Recent studies showing physiological and sustained adult neurogenesis give hope to future treatments against neurodegenerative diseases. It is then that the research of the mechanisms leading to the specification of one cell lineage or another becomes crucial. Much has been described about neurogenesis, but glia, which some reports claim to be as numerous as neurons (von Bartheld et al., 2016), are responsible for key brain functions. Thus, their replacement in diseased brains is a matter of great importance and it could benefit from the study of its lineage and specification mechanisms. However, plasticity in the brain is not incompatible with spatial restriction of progenitors. For instance, during adult neurogenesis, distinct spatially-allocated progenitors along the SVZ generate specific OB neurons (Merkle et al., 2014), and during corticogenesis functionally different neurons derive from anatomoically-distinct areas (Marín and Müller, 2014). These facts will also have to be taken into consideration when developing therapeutic strategies to replace certain CNS populations.

Figure 1

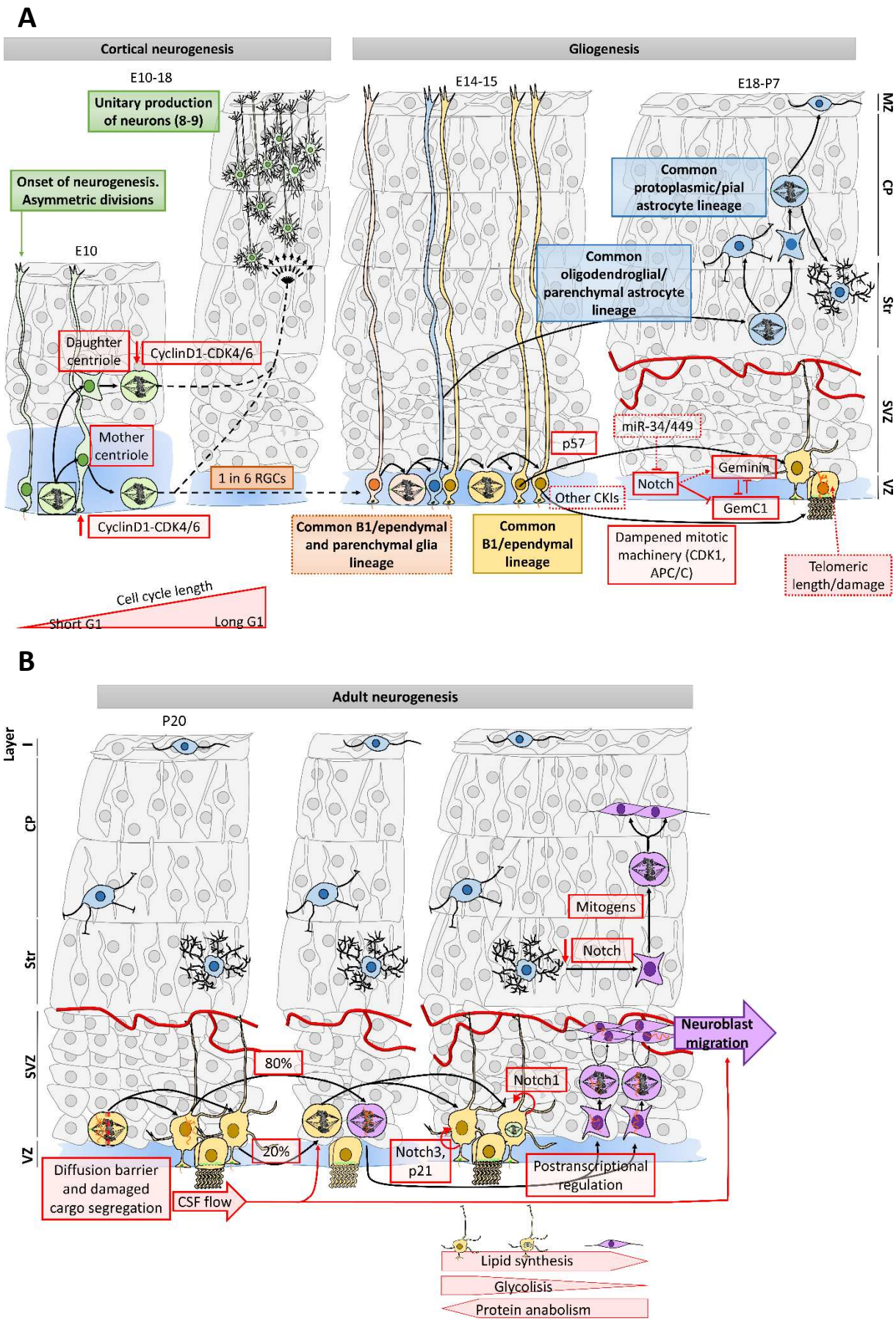
A
Cortical neurogenesis
Gliogenesis
E10-18
Unitary production of neurons (8-9)
Onset of neurogenesis. Asymmetric divisions
E10
E14-15
E18-P7
MZ
CP
Str
SVZ
VZ
Common protoplasmic/pial astrocyte lineage
Common oligodendroglial/ parenchymal astrocyte lineage
Daughter centriole
CyclinD1-CDK4/6
Mother centriole
1 in 6 RGCs
CyclinD1-CDK4/6
p57
miR-34/449
Notch
Geminin
GemC1
Other CKIs
Common B1/ependymal and parenchymal glia lineage
Common B1/ependymal lineage
Dampened mitotic machinery (CDK1, APC/C)
Telomeric length/damage
Cell cycle length
Short G1
Long G1
B
Adult neurogenesis
P20
Layer
I
CP
Str
SVZ
VZ
Mitogens
Notch
Neuroblast migration
80%
20%
Notch1
Notch3, p21
Postranscriptional regulation
Diffusion barrier and damaged cargo segregation
CSF flow
Lipid synthesis
Glycolisis
Protein anabolism

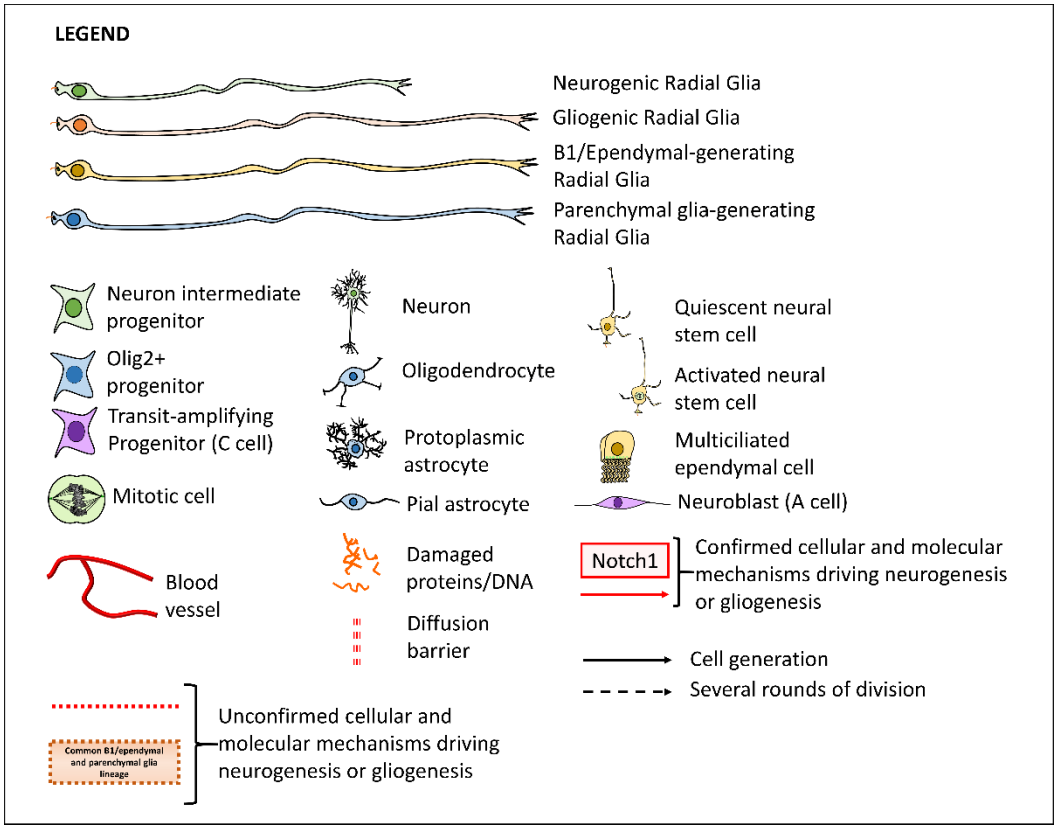

Figure 1. Continuity of plastic neuron/glia progenitors in the developing brain.

(A) During cortical neurogenesis (E10-E18 in mice), RGCs divide asymmetrically to self-renew and generate neurons or neuron-committed intermediate progenitors. From the onset of neurogenesis, a single RGC produces 8-9 neurons in a deterministic way. Among the mechanisms that drive cell fate and division pattern are the asymmetric segregation of centriolar proteins and cell cycle length. In the first case, proteins associated to the mother centriole promote self-renewal of the daughter cell. Thus, the daughter centriole-inheriting cell commits to the neural lineage. In the second case, cell cycle lengthening is linked to symmetric consumptive divisions and neurogenesis. Consequently, G1 phase lengthening (via cyclin D1-CDK4/6 expression knock-down) promotes neurogenesis, whereas the opposite effect enhances self-renewal. At the end of neurogenesis, 1 in 6 RGCs become gliogenic.

During gliogenesis (E14-P7), plastic progenitors emerge. The first to perform their last division are ependymal and B1-committed RGCs. These two cells belong to the same lineage. P57 and Geminin promote B1 cell generation, whereas a dampened mitotic machinery and GemC1, whose action can be inhibited by Notch, favors the ependymal fate. Notch has been described to be inhibited by the miR-34/449 family of microRNAs to enhance multiciliation in other systems, but this has not been described in the brain. It would be interesting to assess whether the difference between postmitotic ependymal cells and their sister B1 cells, could be generated by the asymmetric inheritance of damaged proteins or DNA by the former, like it has been shown in adult dividing B1 cells (see below). It is unknown whether ependymal cells, B1 astrocytes, oligodendrocytes and parenchymal astrocytes have a common progenitor. However, at neonatal stages, Olig2+ progenitors exist that can give rise to oligodendrocytes, protoplasmic astrocytes and GFAP+ pial astrocytes. Striatal astrocytes can

also start the neurogenic program and become transit-amplifying progenitors in the adult, via Notch inhibition. Then, upon mitogen stimulation, they continue to divide and generate neuroblasts.

(B) During adult neurogenesis (from young adults at P20, on), B1 cells divide symmetrically. 80% of them generate transit amplifying progenitors (C cells), whereas 20% of them self-renew. Ependymal-generated cerebrospinal fluid (CSF) flow promotes B1 cell division and guides neuroblast migration. A diffusion barrier has been described in adult B1 miotic cells, which promote an asymmetric inheritance of damaged proteins. These usually segregate into the more committed line (prospective neurons). B1 cell quiescence is maintained via mechanisms such as Notch3 or p21 expression, whereas Notch 1 keeps activated B1 cells. The transition from quiescence to differentiation entails a change in cellular metabolism that affects lipid synthesis, protein generation or glycolysis and posttranscriptional regulation.

VZ: Ventricular Zone, SVZ: Subventricular Zone, Str: Striatum, CP: Cortical Plate, MZ: Marginal Zone, RGCs: Radial Glial Cells.

Acknowledgments

The team received support from Agence Nationale de la Recherche (ANR) Investissements d'Avenir (ANR-10-LABX-54 MEMO LIFE and ANR-11-IDEX-0001-02 PSL* Research University). The Spassky laboratory is supported by INSERM, CNRS, Ecole Normale Supérieure (ENS), ANR (ANR-17-CE12-0021-03), European Research Council (ERC Consolidator grant 647466) and fellowships from the Labex MEMOLIFE program.

Conflict of interest

The authors declare no competing interests.

References and recommended reading

Papers of particular interest have been highlighted as:

• of special interest

•• of outstanding interest

References

[1] S. Ramón y Cajal, *Degeneration & Regeneration of the Nervous System*. Oxford University Press (OUP), 1928.

[2] J. Altman, “Autoradiographic and histological studies of postnatal neurogenesis. IV. Cell proliferation and migration in the anterior forebrain, with special reference to persisting neurogenesis in the olfactory bulb,” *J. Comp. Neurol.*, vol. 137, no. 4, pp. 433–457, 1969.

[3] F. Doetsch, I. Caillé, D. A. Lim, J. M. García-Verdugo, and A. Alvarez-Buylla, “Subventricular Zone Astrocytes Are Neural Stem Cells in the Adult Mammalian Brain,” *Cell*, vol. 97, no. 6, pp. 703–716, 1999.

[4] F. Doetsch, J. M. García-Verdugo, and A. Alvarez-Buylla, “Regeneration of a germinal layer in the adult mammalian brain,” *Proc. Natl. Acad. Sci. U. S. A.*, vol. 96, no. 20, pp. 11619–11624, 1999.

[5] P. S. Eriksson, E. Perfilieva, T. Björk-Eriksson, A. M. Alborn, C. Nordborg, D. A. Peterson, and F. H. Gage, “Neurogenesis in the adult human hippocampus,” *Nat. Med.*, vol. 4, no. 11, pp. 1313–1317, 1998.

[6] P. Malatesta, E. Hartfuss, and M. Götz, “Isolation of radial glial cells by fluorescent-activated cell sorting reveals a neural lineage,” *Development*, vol. 127, no. 24, pp. 5253–5263, 2000.

[7] M. R. Costa, O. Bucholz, T. Schroeder, and M. Götz, “Late origin of glia-restricted progenitors in the developing mouse cerebral cortex.,” *Cereb. Cortex*, vol. 19 Suppl 1, pp. i135-43, 2009.

[8] P. Gao, M. P. Postiglione, T. G. Krieger, L. Hernandez, C. Wang, Z. Han, C. Streicher, E. Papusheva, R. Insolera, K. Chugh, O. Kodish, *et al.*, “Deterministic progenitor behavior and unitary production of neurons in the neocortex,” *Cell*, vol. 159, no. 4, pp. 775–788, 2014. (••)

Mosaic Analysis with Double Markers proves in this study that a single RGC produces 8 to 9 neurons from the neurogenic onset (start of asymmetric division mode), in a deterministic manner. Besides, no layer-specific progenitors exist at the onset of neurogenesis. Finally, they confirm *in vivo* that 1 in 6 RGCs proceed to generate glia at the end of neurogenesis.

[9] L. C. Fuentealba, S. B. Rompani, J. I. Parraguez, K. Obernier, R. Romero, C. L. Cepko, and A. Alvarez-Buylla, “Embryonic Origin of Postnatal Neural Stem Cells,” *Cell*, vol. 161, no. 7, pp. 1644–1655, 2015. (•)

The authors use retroviral bar coding to affirm the adult NSC lineage diverges around mid-gestation (E15) from the rest of forebrain cells and remains quiescent until the young adult stage. Furthermore, different NSCs along the walls of the ventricles give different kinds of olfactory bulb neurons.

[10] N. Spassky, F. T. Merkle, N. Flames, A. D. Tramontin, J. M. García-Verdugo, and A. Alvarez-Buylla, “Adult ependymal cells are postmitotic and are derived from radial glial cells during embryogenesis.,” *J. Neurosci.*, vol. 25, no. 1, pp. 10–8, 2005.

[11] G. Ortiz-Álvarez, M. Daclin, A. Shihavuddin, P. Lansade, A. Fortoul, M. Faucourt, S. Clavreul, M. E. Lalioti, S. Taraviras, S. Hippenmeyer, J. Livet, *et al.*, “Adult Neural Stem Cells and Multiciliated Ependymal Cells Share a Common Lineage Regulated by the Geminin Family Members,” *Neuron*, vol. 102, no. 1, pp. 159-172.e7, 2019. (••)

A combination of *Brainbow* and Mosaic Analysis with Double Markers clonal analysis evidences that adult NSCs and ependymal cells, which are physically and functionally associated in the adult neurogenic niche, belong to the same lineage. They are generated through symmetric or asymmetric divisions and their proportions are controlled by DNA replication regulators: Geminin and GemC1.

[12] S. A. Redmond, M. Figueres-Oñate, K. Obernier, M. A. Nascimento, J. I. Parraguez, L. López-Mascaraque, L. C. Fuentealba, and A. Alvarez-Buylla, “Development of Ependymal and

Postnatal Neural Stem Cells and Their Origin from a Common Embryonic Progenitor," *Cell Rep.*, vol. 27, no. 2, pp. 429-441.e3, 2019.

[13] H. Tabata, "Diverse subtypes of astrocytes and their development during corticogenesis," *Frontiers in Neuroscience*, vol. 9, no. APR. Frontiers Research Foundation, p. 114, 2015.

[14] S. Clavreul, L. Abdeladim, E. Hernández-Garzón, D. Niculescu, J. Durand, S. H. Ieng, R. Barry, G. Bonvento, E. Beaurepaire, J. Livet, and K. Loulier, "Cortical astrocytes develop in a plastic manner at both clonal and cellular levels," *Nat. Commun.*, vol. 10, no. 1, 2019. (•)

The use of Magic Markers (*Brainbow*) exposes the mode of colonization and expansion of parenchymal astrocytes in neonatal mice. They migrate to the cortex, where they proliferate and mature. Besides, they prove protoplasmic astrocytes belong to the Olig2 lineage of glial cells, and that different kinds of astrocytes, like protoplasmic and pial astrocytes, derive from a common progenitor.

[15] J. Cai, Y. Chen, W. H. Cai, E. C. Hurlock, H. Wu, S. G. Kernie, L. F. Parada, and Q. R. Lu, "A crucial role for Olig2 in white matter astrocyte development," *Development*, vol. 134, no. 10, pp. 1887–1899, 2007.

[16] K. Tatsumi, A. Isonishi, M. Yamasaki, Y. Kawabe, S. Morita-Takemura, K. Nakahara, Y. Terada, T. Shinjo, H. Okuda, T. Tanaka, and A. Wanaka, "Olig2-Lineage astrocytes: A distinct subtype of astrocytes that differs from GFAP astrocytes," *Front. Neuroanat.*, vol. 12, no. 8, 2018.

[17] J. P. Magnusson, M. Zamboni, G. Santopolo, J. E. Mold, M. Barrientos-Somarribas, C. Talavera-Lopez, B. Andersson, and J. Frisén, "Activation of a neural stem cell transcriptional program in parenchymal astrocytes," *Elife*, vol. 9, 2020.

[18] Z. Mirzadeh, F. T. Merkle, M. Soriano-Navarro, J. M. Garcia-Verdugo, and A. Alvarez-Buylla, "Neural stem cells confer unique pinwheel architecture to the ventricular surface in neurogenic regions of the adult brain.," *Cell Stem Cell*, vol. 3, no. 3, pp. 265–78, 2008.

[19] A. Guemez-Gamboa, N. G. Coufal, and J. G. Gleeson, "Primary Cilia in the Developing and Mature Brain," *Neuron*, vol. 82, no. 3. Cell Press, pp. 511–521, 2014.

[20] K. Sawamoto, H. Wichterle, O. Gonzalez-Perez, J. A. Cholfin, M. Yamada, N. Spassky, N. S. Murcia, J. M. Garcia-Verdugo, O. Marin, J. L. R. Rubenstein, M. Tessier-Lavigne, *et al.*, "New neurons follow the flow of cerebrospinal fluid in the adult brain," *Science (80-.).*, vol. 311, no. 5761, pp. 629–632, 2006.

[21] D. Petrik, M. H. Myoga, S. Grade, N. J. Gerkau, M. Pusch, C. R. Rose, B. Grothe, and M. Götz, "Epithelial Sodium Channel Regulates Adult Neural Stem Cell Proliferation in a Flow-Dependent Manner," *Cell Stem Cell*, vol. 22, no. 6, pp. 865-878.e8, 2018.

[22] M. Carlén, K. Meletis, C. Göritz, V. Darsalia, E. Evergren, K. Tanigaki, M. Amendola, F. Barnabé-Heider, M. S. Y. Yeung, L. Naldini, T. Honjo, *et al.*, "Forebrain ependymal cells are Notch-dependent and generate neuroblasts and astrocytes after stroke," *Nat. Neurosci.*, vol. 12, no. 3, pp. 259–267, 2009.

[23] N. Muthusamy, A. Brumm, X. Zhang, S. T. Carmichael, and H. T. Ghashghaei, "Foxj1 expressing ependymal cells do not contribute new cells to sites of injury or stroke in the mouse forebrain," *Sci. Rep.*, vol. 8, no. 1, pp. 1–9, 2018.

[24] P. T. Shah, J. A. Stratton, M. G. Stykel, S. Abbasi, S. Sharma, K. A. Mayr, K. Koblinger, P. J. Whelan, and J. Biernaskie, "Single-Cell Transcriptomics and Fate Mapping of Ependymal Cells Reveals an Absence of Neural Stem Cell Function," *Cell*, vol. 173, no. 4, pp. 1045-1057.e9, 2018.

[25] D. A. Lim and A. Alvarez-Buylla, "The adult ventricular–subventricular zone (V-SVZ) and olfactory bulb (OB) neurogenesis," *Cold Spring Harb. Perspect. Biol.*, vol. 8, no. 5, 2016.

[26] O. Basak, T. G. Krieger, M. J. Muraro, K. Wiebrands, D. E. Stange, J. Frias-Aldeguer, N. C. Rivron, M. van de Wetering, J. H. van Es, A. van Oudenaarden, B. D. Simons, *et al.*, "Troy+ brain stem cells cycle through quiescence and regulate their number by sensing niche occupancy," *Proc. Natl. Acad. Sci. U. S. A.*, vol. 115, no. 4, pp. E610–E619, 2018.

[27] K. Obernier, A. Cebrian-Silla, M. Thomson, J. I. Parraguez, R. Anderson, C. Guinto, J. Rodas Rodriguez, J. M. Garcia-Verdugo, and A. Alvarez-Buylla, "Adult Neurogenesis Is Sustained by Symmetric Self-Renewal and Differentiation," *Cell Stem Cell*, vol. 22, no. 2, pp. 221-234.e8, 2018. (●●)

This study unveils the mode of division that governs adult neurogenesis and causes the progressive decline of the stem cell reservoir with age. Viral short-term lineage tracing, fate mapping using a stochastic multicolor Cre reporter line and *ex vivo* explant filming established that 80% of adult NSCs undergo consumptive symmetric divisions, whereas only 20% of these self renew via proliferative symmetric divisions. The latter can remain quiescent for months and give progeny later in life.

[28] S. Ferrón, H. Mira, S. Franco, M. Cano-Jimenez, E. Bellmunt, C. Ramírez, I. Fariñas, and M. A. Blasco, "Telomere shortening and chromosomal instability abrogates proliferation of adult but not embryonic neural stem cells," *Development*, vol. 131, no. 16, pp. 4059–4070, 2004.

[29] S. R. Ferrón, M. Á. Marqués-Torrejón, H. Mira, I. Flores, K. Taylor, M. A. Blasco, and I. Fariñas, "Telomere shortening in neural stem cells disrupts neuronal differentiation and neuritogenesis," *J. Neurosci.*, vol. 29, no. 46, pp. 14394–14407, 2009.

[30] K. Obernier and A. Alvarez-Buylla, "Neural stem cells: Origin, heterogeneity and regulation in the adult mammalian brain," *Development (Cambridge)*, vol. 146, no. 4. Company of Biologists Ltd, 2019.

[31] F. T. Merkle, L. C. Fuentealba, T. a Sanders, L. Magno, N. Kessaris, and A. Alvarez-Buylla, "Adult neural stem cells in distinct microdomains generate previously unknown interneuron types.," *Nat. Neurosci.*, vol. 17, no. 2, 2014.

[32] E. Llorens-Bobadilla, S. Zhao, A. Baser, G. Saiz-Castro, K. Zwadlo, and A. Martin-Villalba, "Single-Cell Transcriptomics Reveals a Population of Dormant Neural Stem Cells that Become Activated upon Brain Injury," *Cell Stem Cell*, vol. 17, no. 3, pp. 329–340, 2015. (●●)

RNA-sequencing reveals the heterogeneity of the adult NSC population. Their analysis establishes the existence of a pseudo-time continuum, between the non-primed quiescent NSCs to the mitotic activated NSCs and neuroblats, during which a drastic transcriptomic change related to cellular metabolism takes place.

[33] A. Baser, M. Skabkin, S. Kleber, Y. Dang, G. S. Gülcüler Balta, G. Kalamakis, M. Göpferich, D. C. Ibañez, R. Schefzik, A. S. Lopez, E. L. Bobadilla, *et al.*, "Onset of differentiation is post-transcriptionally controlled in adult neural stem cells," *Nature*, vol. 566, no. 7742, pp. 100–104, 2019.

[34] N. Sanai, T. Nguyen, R. A. Ihrie, Z. Mirzadeh, H. H. Tsai, M. Wong, N. Gupta, M. S. Berger, E. Huang, J. M. Garcia-Verdugo, D. H. Rowitch, *et al.*, "Corridors of migrating neurons in the human brain and their decline during infancy," *Nature*, vol. 478, no. 7369, pp. 382–386, 2011.

[35] S. F. Sorrells, M. F. Paredes, A. Cebrian-Silla, K. Sandoval, D. Qi, K. W. Kelley, D. James, S. Mayer, J. Chang, K. I. Auguste, E. F. Chang, *et al.*, "Human hippocampal neurogenesis drops

sharply in children to undetectable levels in adults," ***Nature*****, vol. 555, no. 7696, pp. 377–381, 2018. (•)**

The authors use a combination of proliferation and stem cell markers, as well as young neuron markers to assess adult neurogenesis in the SGZ of the dentate gyrus of human post-mortem samples. They claim that hippocampal adult neurogenesis drops sharply during infancy until undetectable levels in the human adult.

[36] C. V. Dennis, L. S. Suh, M. L. Rodriguez, J. J. Kril, and G. T. Sutherland, "Human adult neurogenesis across the ages: An immunohistochemical study," *Neuropathol. Appl. Neurobiol.*, vol. 42, no. 7, pp. 621–638, 2016.

[37] M. Boldrini, C. A. Fulmore, A. N. Tartt, L. R. Simeon, I. Pavlova, V. Poposka, G. B. Rosoklija, A. Stankov, V. Arango, A. J. Dwork, R. Hen, *et al.*, "Human Hippocampal Neurogenesis Persists throughout Aging," *Cell Stem Cell*, vol. 22, no. 4, pp. 589-599.e5, 2018.

[38] E. P. Moreno-Jiménez, M. Flor-García, J. Terreros-Roncal, A. Rábano, F. Cafini, N. Pallas-Bazarra, J. Ávila, and M. Llorens-Martín, "Adult hippocampal neurogenesis is abundant in neurologically healthy subjects and drops sharply in patients with Alzheimer's disease," ***Nat. Med.*****, vol. 25, no. 4, pp. 554–560, 2019. (••)**

This work combines immature and mature neuronal markers to identify a robust presence of several neuronal maturation stages in the dentate gyrus of the adult human hippocampus of healthy patients, up to the ninth decade of life. They reach the opposite conclusion to the study by Sorrels et al., but they claim that adequate tissue processing and exclusion of patients with any neurological disorders. In fact, they find a substantial decrease of neurogenesis that correlates with the progress of Alzheimer's disease.

[39] A. Kumar, V. Pareek, M. A. Faiq, S. K. Ghosh, and C. Kumari, "ADULT NEUROGENESIS IN HUMANS: A Review of Basic Concepts, History, Current Research, and Clinical Implications.," *Innov. Clin. Neurosci.*, vol. 16, no. 5–6, pp. 30–37, 2019.

[40] M. Flor-García, J. Terreros-Roncal, E. P. Moreno-Jiménez, J. Ávila, A. Rábano, and M. Llorens-Martín, "Unraveling human adult hippocampal neurogenesis," *Nat. Protoc.*, vol. 15, no. 2, pp. 668–693, 2020.

[41] K. K. Tachibana, M. A. Gonzalez, G. Guarguaglini, E. A. Nigg, and R. A. Laskey, "Depletion of licensing inhibitor geminin causes centrosome overduplication and mitotic defects," *EMBO Rep.*, vol. 6, no. 11, pp. 1052–1057, 2005.

[42] M. E. Lalioti, K. Kaplani, G. Lokka, T. Georgomanolis, C. Kyrousi, W. Dong, A. Dunbar, E. Parlapani, E. Damianidou, N. Spassky, K. T. Kahle, *et al.*, "GemC1 is a critical switch for neural stem cell generation in the postnatal brain," *Glia*, vol. 67, no. 12, pp. 2360–2373, 2019.

[43] A. Al Jord, A. Shihavuddin, R. Servignat d'Aout, M. Faucourt, A. Genovesio, A. Karaiskou, J. Sobczak-Thépot, N. Spassky, and A. Meunier, "Calibrated mitotic oscillator drives motile ciliogenesis," *Science (80-.).*, vol. 358, no. 6364, pp. 803–806, 2017.

[44] M. Arbi, D. Pefani, C. Kyrousi, M. Lalioti, A. Kalogeropoulou, A. D. Papanastasiou, S. Taraviras, and Z. Lygerou, "GemC1 controls multiciliogenesis in the airway epithelium," *EMBO Rep.*, vol. 17, no. 3, pp. 400–413, 2016.

[45] B. Terré, G. Piergiovanni, S. Segura-Bayona, G. Gil-Gómez, S. A. Youssef, C. S. Attolini, M. Wilsch-Bräuninger, C. Jung, A. M. Rojas, M. Marjanović, P. A. Knobel, *et al.*, " GEMC 1 is a critical regulator of multiciliated cell differentiation ," *EMBO J.*, vol. 35, no. 9, pp. 942–960, 2016.

[46] J. A. Wohlschlegel, B. T. Dwyer, S. K. Dhar, C. Cvetic, J. C. Walter, and A. Dutta, "Inhibition of

eukaryotic DNA replication by geminin binding to Cdt1," *Science (80-.).*, vol. 290, no. 5500, pp. 2309–2312, 2000.

[47] A. Balestrini, C. Cosentino, A. Errico, E. Garner, and V. Costanzo, "GEMC1 is a TopBP1-interacting protein required for chromosomal DNA replication," *Nat. Cell Biol.*, vol. 12, no. 5, pp. 484–491, 2010.

[48] E. K. Vladar, M. B. Stratton, M. L. Saal, G. Salazar-De Simone, X. Wang, D. Wolgemuth, T. Stearns, and J. D. Axelrod, "Cyclin-dependent kinase control of motile ciliogenesis," *Elife*, vol. 7, 2018.

[49] L. J. A. Hardwick, F. R. Ali, R. Azzarelli, and A. Philpott, "Cell cycle regulation of proliferation versus differentiation in the central nervous system," *Cell Tissue Res.*, vol. 359, no. 1, pp. 187–200, 2015.

[50] C. Kyrousi, M. Arbi, G. A. Pilz, D. E. Pefani, M. E. Lalioti, J. Ninkovic, M. Götz, Z. Lygerou, and S. Taraviras, "Mcidas and gemc1 are key regulators for the generation of multiciliated ependymal cells in the adult neurogenic niche," *Dev.*, vol. 142, no. 21, pp. 3661–3674, 2015.

[51] N. Gaiano, J. S. Nye, and G. Fishell, "Radial glial identity is promoted by Notch1 signaling in the murine forebrain," *Neuron*, vol. 26, no. 2, pp. 395–404, 2000.

[52] B. Marcet, B. Chevalier, G. Luxardi, C. Coraux, L. E. Zaragosi, M. Cibois, K. Robbe-Sermesant, T. Jolly, B. Cardinaud, C. Moreilhon, L. Giovannini-Chami, *et al.*, "Control of vertebrate multiciliogenesis by miR-449 through direct repression of the Delta/Notch pathway," *Nat. Cell Biol.*, vol. 13, no. 6, pp. 693–701, 2011.

[53] H. Kawai, D. Kawaguchi, B. D. Kuebrich, T. Kitamoto, M. Yamaguchi, Y. Gotoh, and S. Furutachi, "Area-specific regulation of quiescent neural stem cells by Notch3 in the adult mouse subependymal zone," *J. Neurosci.*, vol. 37, no. 49, pp. 11867–11880, 2017.

[54] J. D. Rieskamp, J. K. Denninger, and T. J. Dause, "Identifying the unique role of notch3 in adult neural stem cell maintenance," *Journal of Neuroscience*, vol. 38, no. 13. Society for Neuroscience, pp. 3157–3159, 2018.

[55] A. Chitnis and L. Bally-Cuif, "The Notch meeting: An Odyssey from structure to function," *Development (Cambridge)*, vol. 143, no. 4. Company of Biologists Ltd, pp. 547–553, 2016.

[56] L. Bejarano, A. J. Schuhmacher, M. Méndez, D. Megías, C. Blanco-Aparicio, S. Martínez, J. Pastor, M. Squatrito, and M. A. Blasco, "Inhibition of TRF1 Telomere Protein Impairs Tumor Initiation and Progression in Glioblastoma Mouse Models and Patient-Derived Xenografts," *Cancer Cell*, vol. 32, no. 5, pp. 590-607.e4, 2017.

[57] S. Furutachi, H. Miya, T. Watanabe, H. Kawai, N. Yamasaki, Y. Harada, I. Imayoshi, M. Nelson, K. I. Nakayama, Y. Hirabayashi, and Y. Gotoh, "Slowly dividing neural progenitors are an embryonic origin of adult neural stem cells," *Nat. Neurosci.*, vol. 18, no. 5, pp. 657–665, 2015. (•)

Analysis of label-retaining cells establishes that adult NSCs derive at mid-gestation from a subpopulation of RGCs that slow down their cell cycle via p57 upregulation. This cell cycle brake is necessary the specification of the adult NSC fate.

[58] R. N. Pechnick, S. Zonis, K. Wawrowsky, J. Pourmorady, and V. Chesnokova, "p21Cip1 restricts neuronal proliferation in the subgranular zone of the dentate gyrus of the hippocampus," *Proc. Natl. Acad. Sci. U. S. A.*, vol. 105, no. 4, pp. 1358–1363, 2008.

[59] O. Clément, I. A. Hemming, I. E. Gladwyn-Ng, Z. Qu, S. S. Li, M. Piper, and J. I. T. Heng, "Rp58 and p27kip1 coordinate cell cycle exit and neuronal migration within the embryonic mouse

cerebral cortex," *Neural Dev.*, vol. 12, no. 1, p. 8, 2017.

[60] P. Zhang, C. Wong, D. Liu, M. Finegold, J. W. Harper, and S. J. Elledge, "p21(CIP1) and p57(KIP2) control muscle differentiation at the myogenin step.," *Genes Dev.*, vol. 13, no. 2, pp. 213–24, 1999.

[61] I. Vazquez-Villaseñor, C. J. Garwood, P. R. Heath, J. E. Simpson, P. G. Ince, and S. B. Wharton, "Expression of p16 and p21 in the frontal association cortex of ALS/MND brains suggests neuronal cell cycle dysregulation and astrocyte senescence in early stages of the disease," *Neuropathol. Appl. Neurobiol.*, vol. 46, no. 2, pp. 171–185, 2020.

[62] C. Dehay and H. Kennedy, "Cell-cycle control and cortical development," *Nat. Rev. Neurosci.*, vol. 8, no. 6, pp. 438–450, 2007.

[63] L. J. Pilaz, D. Patti, G. Marcy, E. Ollier, S. Pfister, R. J. Douglas, M. Betizeau, E. Gautier, V. Cortay, N. Doerflinger, H. Kennedy, *et al.*, "Forced G1-phase reduction alters mode of division, neuron number, and laminar phenotype in the cerebral cortex," *Proc. Natl. Acad. Sci. U. S. A.*, vol. 106, no. 51, pp. 21924–21929, 2009.

[64] C. Lange, W. B. Huttner, and F. Calegari, "Cdk4/CyclinD1 Overexpression in Neural Stem Cells Shortens G1, Delays Neurogenesis, and Promotes the Generation and Expansion of Basal Progenitors," *Cell Stem Cell*, vol. 5, no. 3, pp. 320–331, 2009.

[65] M. Marjanović, C. Sánchez-Huertas, B. Terré, R. Gómez, J. F. Scheel, S. Pacheco, P. A. Knobel, A. Martínez-Marchal, S. Aivio, L. Palenzuela, U. Wolfrum, *et al.*, "CEP63 deficiency promotes p53-dependent microcephaly and reveals a role for the centrosome in meiotic recombination," *Nat. Commun.*, vol. 6, p. 7676, 2015.

[66] M. Saade, J. Blanco-Ameijeiras, E. Gonzalez-Gobartt, and E. Martı, "A centrosomal view of cns growth," *Dev.*, vol. 145, no. 21, 2018.

[67] J. T. M. L. Paridaen, M. Wilsch-Bräuninger, and W. B. Huttner, "Asymmetric inheritance of centrosome-associated primary cilium membrane directs ciliogenesis after cell division," *Cell*, vol. 155, no. 2, p. 333, 2013.

[68] M. Saade, E. Gonzalez-Gobartt, R. Escalona, S. Usieto, and E. Martí, "Shh-mediated centrosomal recruitment of PKA promotes symmetric proliferative neuroepithelial cell division," *Nat. Cell Biol.*, vol. 19, no. 5, pp. 493–503, 2017.

[69] D. L. Moore and S. Jessberger, "Creating Age Asymmetry: Consequences of Inheriting Damaged Goods in Mammalian Cells," *Trends in Cell Biology*, vol. 27, no. 1. Elsevier Ltd, pp. 82–92, 2017.

[70] Z. G. Venkei and Y. M. Yamashita, "Emerging mechanisms of asymmetric stem cell division," *Journal of Cell Biology*, vol. 217, no. 11. Rockefeller University Press, pp. 3785–3795, 2018.

[71] D. L. Moore, G. A. Pilz, M. J. Arauzo-Bravo, Y. Barral, and S. Jessberger, "A mechanism for the segregation of age in mammalian neural stem cells," *Science (80-.).*, vol. 349, no. 6254, 2015. (••)

This study describes using fluorescent loss in photobleaching the presence of a diffusion barrier along the cleavage plane of a dividing cell. This barrier, which decreases with age, acts to distribute damaged proteins to the more committed progeny during asymmetric cell divisions. The authors suggest it would be a mechanism to increase the fitness of the self-renewing cell.

[72] C. S. von Bartheld, J. Bahney, and S. Herculano-Houzel, "The search for true numbers of neurons and glial cells in the human brain: A review of 150 years of cell counting," *Journal of Comparative Neurology*, vol. 524, no. 18. Wiley-Liss Inc., pp. 3865–3895, 2016.

[73] O. Marín and U. Müller, “Lineage origins of GABAergic versus glutamatergic neurons in the neocortex,” *Current Opinion in Neurobiology*, vol. 26. NIH Public Access, pp. 132–141, 2014.

ABSTRACT

The adult mouse brain retains a capability to produce new neurons from discrete neurogenic regions throughout life. One of them is localized in the subventricular zone of the lateral ventricle and is composed of two types of glial cells: astrocytes (adult neural stem cells) and multiciliated ependymal cells. The latter are highly specialized cells that present an apical patch of centrioles that nucleate motile cilia, whose coordinated beating is at the root of functions key to adult neurogenesis, in particular, and brain homeostasis in general. Among these, the cerebrospinal fluid circulation for trophic support, waste removal and neuronal migration guidance are of high importance. Therefore, understanding the processes that establish the neurogenic niche composition is of high value to tackle some of the most severe brain malignancies, such as hydrocephalus, neurodegenerative diseases or even tumors generated in the germinal regions.

In the present doctoral research, we have used a fate mapping technique to determine that ependymal progenitors do not migrate. This knowledge was necessary to use state-of-the-art clonal analysis techniques. Thus, a high-throughput analysis of large cohorts of neurogenic niche clones visualized with the *Brainbow* technique, as well as single-cell resolution of the ependymal progenitor division patterns via the Mosaic Analysis with Double Markers transgenic animals, has revealed that: (i) ependymal and adult neural stem cells share a common lineage, (ii) they can both arise through symmetric or asymmetrical cell divisions and (iii) their fate is modulated by DNA replication regulators, Geminin and GemC1, which favor a stem or an ependymal cell fate, respectively.

We have consequently elucidated the cellular and molecular mechanisms by which GemC1 triggers an ependymal fate. This protein, initially discovered as being a DNA replication-licensing factor, generates an arrested cell cycle-like phenotype at the same time that it promotes centriole amplification. Ependymal progenitors that express GemC1 halt their cell cycle and thus inhibit entry into mitosis. Upon looking at the specific mechanisms that could trigger such an arrest, we found that GemC1 generates the simultaneous expression of centriole amplification, ciliary growth, cell cycle progression and arrest genes, as well as the induction of a replicative stress, although strikingly, all this only in cycling cells. The occurrence of such stress translates to a higher presence of telomere dysfunction induced foci, this is, telomeres that co-localize with DNA damage signals. Furthermore, when we over-expressed the telomerase, the enzyme responsible for telomere length maintenance, we observed a bias towards the neural stem cell fate. This suggests that damage to the telomeres or its protection could be at the source of the terminal ependymal differentiation or the stem cell fate, respectively.

Together, this work sheds some light into the specific mechanisms that lead to an ependymal fate against the stem cell one, with some unexpected roles of cell cycle actors, damage pathways and telomere dynamics, that are usually associated to cycling or quiescent cells, but rarely to differentiation.

KEYWORDS

Multiciliated Ependymal Cell
Neural Stem Cell
Clonal Analysis
Replicative Stress
Geminin Family
Telomeres

RÉSUMÉ

Le cerveau adulte des souris conserve une capacité à produire de nouveaux neurones tout au long de la vie, à partir de niches neurogéniques. Une d'entre elles est localisée dans la zone sous-ventriculaire et est composée de deux types de cellules gliales : les astrocytes (cellules souches neurales) et les cellules épendymaires multiciliées. Celles-ci sont des cellules fortement spécialisées qui présentent un groupe apical de centrioles à la base des cils motiles, dont le battement coordonné est à l'origine de fonctions indispensables pour la neurogenèse adulte, en particulier, et l'homéostase du cerveau, de façon générale. Parmi ces fonctions essentielles, la circulation du liquide céphalorachidien pour support trophique, l'enlèvement des déchets ou guider la migration des neurones sont d'une grande importance. Donc, la compréhension des procès qui établissent la niche neurogénique est d'une grande valeur pour aborder quelques maladies du cerveau d'entre les plus sévères, comme l'hydrocéphalie, les affections neurodégénératives ou même les tumeurs engendrées dans les régions germinales.

Mon travail de recherche doctorale a consisté à utiliser une technique de suivi du destin cellulaire et à déterminer que les progéniteurs épendymaires ne migrent pas. Cette connaissance était nécessaire pour l'utilisation de techniques de pointe d'analyse clonal. Alors, l'analyse à haute résolution d'un grand nombre de clones de la niche neurogénique visualisés avec la technique *Brainbow*, ainsi que la résolution au niveau cellulaire des modes de division des progéniteurs épendymaires, en utilisant les animaux transgéniques *Mosaic Analysis with Double Markers*, nous a révélé que : (i) les cellules épendymaires et les cellules souches neurales adultes appartiennent à un même lignage, (ii) elle sont nées via des divisions symétriques ou asymétriques, (iii) leur destin est modulé par des facteurs de la réplication de l'ADN, Geminin et GemC1, qui favorisent le destin souche ou épendymaire, respectivement.

Nous avons ensuite élucidé les mécanismes cellulaires et moléculaires par lesquels GemC1 déclenche le destin épendymaire. Cette protéine, initialement décrite comme un facteur de promotion de la réplication de l'ADN, génère un phénotype d'arrêt de cycle au même temps que l'amplification centriolaire. Les progéniteurs épendymaires qui expriment GemC1 pausent leur cycle et inhibent ainsi leur entrée en mitose. Lors de la recherche d'un mécanisme qui pourrait déclencher cet arrêt, nous avons décrit comment GemC1 génère l'expression simultanée de gènes d'amplification centriolaire et croissance ciliaire, de progression et arrêt de cycle, et aussi un stress réplicatif mais, étonnamment, tout ça uniquement dans des cellules cyclantes. La présence de ce stress se traduit dans une plus haute fréquence de télomères dysfonctionnels, c'est-à-dire, des télomères colocalisés avec des signaux de dommage à l'ADN. De plus, lorsque nous avons surexprimé la télomérase, l'enzyme responsable du maintien de la longueur des télomères, nous avons observé un biais vers le destin de cellule souche adulte. Cela suggère que le dommage aux télomères ou leur protection pourrait être à la source de la différentiation terminal épendymaire ou un destin de cellule souche, respectivement.

Ce travail permet de clarifier les mécanismes qui mènent à un destin épendymaire ou de cellules souches, avec des rôles inattendus des acteurs du cycle, les voies de signalisation de dommage cellulaire et la dynamique des télomères, qui sont habituellement associés aux cellules en cycle ou quiescentes, mais rarement à la différentiation.

MOTS CLÉS

Cellule Ependymaire Multiciliée
Cellule Souche Neurale
Analyse Clonale
Stress Réplicatif
Famille Geminine
Télomère